WESTINGHOUSE CLASS 3 (Non-Proprietary)

WCAP-14066

Analysis of the 137° Capsule from the Arizona Public Service Company Palo Verde Unit No. 1 Reactor Vessel Radiation Surveillance Program

J. M. Chicots
E. P. Lippincott
A. Madeyski

May 1994

Work Performed Under Shop Order MFYP-106B

Prepared by Westinghouse Electric Corporation
for the Arizona Public Service Company

Approved by: R. D. Rishel
R. D. Rishel, Manager
Metallurgical & NDE Analysis

WESTINGHOUSE ELECTRIC CORPORATION
Nuclear and Advanced Technology Division
P.O. Box 355
Pittsburgh, Pennsylvania 15230-0355

PREFACE

This report has been technically reviewed and verified.

	Reviewer:	
Sections 1 through 5, 7, 8, and Appendix A	E. Terek	Ed Terek
Section 6	S. L. Anderson	S. L. Anderson

TABLE OF CONTENTS

LIST OF TABLES

LIST OF TABLES (continued)

LIST OF TABLES (continued)

LIST OF TABLES (continued)

LIST OF ILLUSTRATIONS

LIST OF ILLUSTRATIONS

LIST OF ILLUSTRATIONS

LIST OF ILLUSTRATIONS

SECTION 1.0
SUMMARY OF RESULTS

The analysis of the reactor vessel materials contained in the surveillance capsule removed from the 137° location, the first capsule to be removed from the Palo Verde Unit 1 reactor pressure vessel, led to the following conclusions:

- The capsule received an average fast neutron fluence (E > 1.0 MeV) of 3.453×10^{18} n/cm^2 after 4.53 effective full power years (EFPY) of plant operation.

- Irradiation of the reactor vessel intermediate shell plate M-6701-2 Charpy specimens, oriented with the longitudinal axis of the specimen parallel to the major rolling direction of the plate (longitudinal orientation), to 3.453×10^{18} n/cm^2 (E > 1.0 MeV) resulted in a 30 ft-lb transition temperature increase of 33°F and a 50 ft-lb transition temperature increase of 33°F. This results in an irradiated 30 ft-lb transition temperature of 40°F and an irradiated 50 ft-lb transition temperature of 70°F for the longitudinally oriented specimens.

- Irradiation of the reactor vessel intermediate shell plate M-6701-2 Charpy specimens, oriented with the longitudinal axis of the specimen normal to the major rolling direction of the plate (transverse orientation), to 3.453×10^{18} n/cm^2 (E > 1.0 MeV) resulted in a 30 ft-lb transition temperature increase of 8°F and a 50 ft-lb transition temperature increase of 28°F. This results in an irradiated 30 ft-lb transition temperature of 40°F and an irradiated 50 ft-lb transition temperature of 100°F for transversely oriented specimens.

- Irradiation of the weld metal Charpy specimens to 3.453×10^{18} n/cm^2 (E > 1.0 MeV) resulted in a 30 ft-lb transition temperature increase of 9°F and a 50 ft-lb transition temperature increase of 13°F. This results in an irradiated 30 ft-lb transition temperature of -45°F and an irradiated 50 ft-lb transition temperature of -20°F.

- Irradiation of the weld Heat-Affected-Zone (HAZ) metal Charpy specimens to 3.453×10^{18} n/cm^2 (E > 1.0 MeV) resulted in a no increases in the 30 and 50 ft-lb transition temperatures. This results in an unchanged irradiated 30 ft-lb transition temperature of -62°F and an unchanged irradiated 50 ft-lb transition temperature of -25°F.

- The average upper shelf energy of the intermediate shell plate M-6701-2 Charpy specimens (longitudinal orientation) resulted in an average energy decrease of 22 ft-lbs after irradiation to 3.453 x 10^{18} n/cm^2 (E > 1.0 MeV). This results in an irradiated average upper shelf energy of 129 ft-lbs for the longitudinally oriented specimens.

- The average upper shelf energy of the intermediate shell plate M-6701-2 Charpy specimens (transverse orientation) resulted in an average energy decrease of 11 ft-lbs after irradiation to 3.453 x 10^{18} n/cm^2 (E > 1.0 MeV). This results in an irradiated average upper shelf energy of 87 ft-lbs for the transversely oriented specimens.

- The average upper shelf energy of the weld metal Charpy specimens resulted in an average energy decrease of 2 ft-lbs after irradiation to 3.453 x 10^{18} n/cm^2 (E > 1.0 MeV). This results in an irradiated average upper shelf energy of 162 ft-lbs for the weld metal specimens.

- The average upper shelf energy of the weld HAZ metal Charpy specimens decreased 11 ft-lbs after irradiation to 3.453 x 10^{18} n/cm^2 (E > 1.0 MeV). This results in an irradiated average upper shelf energy of 124 ft-lbs for the weld HAZ metal.

- A comparison of the Palo Verde Unit 1 surveillance material 30 ft-lb transition temperature shifts and upper shelf energy decreases with Regulatory Guide 1.99, Revision 2[1], lead to the following conclusions:

  - The 30 ft-lb transition temperature increases of the surveillance weld metal and the transversely oriented intermediate shell plate M-6701-2 Charpy test results are less than the Regulatory Guide 1.99, Revision 2[1], predictions.

  - The 30 ft-lb transition temperature increase of the longitudinally oriented intermediate shell plate M-6701-2 Charpy test results is 7°F higher than the Regulatory Guide 1.99, Revision 2[1], prediction. Regulatory Guide 1.99, Revision 2, requires a 2 sigma allowance of 34°F (for base metal) be added to the predicted reference transition temperature to obtain a conservative upper bound value. Thus, the reference transition temperature increase for the intermediate shell plate M-6701-2 (longitudinal orientation) is bounded by the 2 sigma allowance for shift prediction.

- The measured average upper shelf energy decrease of the weld metal and intermediate shell plate M-6701-2 (longitudinal and transeverse) Charpy test results are equal to or less than the Regulatory Guide 1.99, Revision 2[1], predictions.

o The precracked Charpy specimen test results are in good agreement with the unirradiated test results[2]. The data are bounded by the K_{IR} curve, which provides a lower bound estimate for the fracture toughness.

o The calculated end-of-life (EOL) 32 effective full power years (EFPY) maximum neutron fluence (E > 1.0 MeV) for the Palo Verde Unit 1 reactor vessel is as follows:

Vessel inner radius* = 1.725×10^{19} n/cm^2
Vessel 1/4 thickness = 9.032×10^{18} n/cm^2
Vessel 3/4 thickness = 1.736×10^{18} n/cm^2

* Clad/base metal interface

SECTION 2.0
INTRODUCTION

This report presents the results of the examination of the Palo Verde Unit 1 surveillance capsule removed from the 137° location. This is the first capsule to be removed from the reactor in the continuing surveillance program which monitors the effects of neutron irradiation on the Arizona Public Service Company Palo Verde Unit 1 reactor pressure vessel materials under actual operating conditions.

The surveillance program for the Arizona Public Service Company Palo Verde Unit 1 reactor pressure vessel materials was designed and recommended by ABB Combustion Engineering. A description of the preirradiation mechanical properties of the reactor vessel materials is presented in TR-V-MCM-013, "Arizona Public Service Company Palo Verde Unit 1 Evaluation of Baseline Specimens Reactor Vessel Materials Irradiation Surveillance Program"[2]. The surveillance program was planned to cover the 40-year design life of the reactor pressure vessel and was based on ASTM E185-82, "Standard Practice for Conducting Surveillance Tests for Light-Water Cooled Nuclear Power Reactor Vessels". The 137° capsule was removed from the reactor after less than 5 EFPY of exposure and shipped to the Westinghouse Science and Technology Center Hot Cell Facility, where the postirradiation mechanical testing of the Charpy V-notch impact, tensile and precracked Charpy V-notch surveillance specimens was performed.

This report summarizes the testing of and the post irradiation data obtained from the surveillance capsule removed from the 137° location of the Arizona Public Service Company Palo Verde Unit 1 reactor vessel and discusses the analysis of the data.

SECTION 3.0
BACKGROUND

The ability of the large steel pressure vessel containing the reactor core and its primary coolant to resist fracture constitutes an important factor in ensuring safety in the nuclear industry. The beltline region of the reactor pressure vessel is the most critical region of the vessel because it is subjected to significant fast neutron bombardment. The overall effects of fast neutron irradiation on the mechanical properties of low alloy, ferritic pressure vessel steels such as SA533 Grade B Class 1 (base material of the Palo Verde Unit 1 reactor pressure vessel) are well documented in the literature. Generally, low alloy ferritic materials show an increase in hardness and tensile properties and a decrease in ductility and toughness during high-energy irradiation.

A method for performing analyses to guard against fast fracture in reactor pressure vessels has been presented in "Protection Against Nonductile Failure," Appendix G to Section III of the ASME Boiler and Pressure Vessel Code[3]. The method uses fracture mechanics concepts and is based on the reference nil-ductility transition temperature (RT_{NDT}).

RT_{NDT} is defined as the greater of either the drop weight nil-ductility transition temperature (NDTT per ASTM E-208[4]) or the temperature 60°F less than the 50 ft-lb (and 35-mil lateral expansion) temperature as determined from Charpy specimens oriented normal (transverse) to the major working direction of the plate. The RT_{NDT} of a given material is used to index that material to a reference stress intensity factor curve (K_{IR} curve) which appears in Appendix G to the ASME Code[3]. The K_{IR} curve is a lower bound of dynamic, crack arrest, and static fracture toughness results obtained from several heats of pressure vessel steel. When a given material is indexed to the K_{IR} curve, allowable stress intensity factors can be obtained for this material as a function of temperature. Allowable operating limits can then be determined using these allowable stress intensity factors.

RT_{NDT} and, in turn, the operating limits of nuclear power plants can be adjusted to account for the effects of radiation on the reactor vessel material properties. The changes in mechanical properties of a given reactor pressure vessel steel, due to irradiation, can be monitored by a reactor vessel surveillance program, such as the Palo Verde Unit 1 reactor vessel materials irradiation surveillance program[2], in which a surveillance capsule is periodically removed from the operating nuclear reactor and the encapsulated specimens tested.

The increase in the average Charpy V-notch 30 ft-lb temperature (ΔRT_{NDT}) due to irradiation is added to the initial RT_{NDT} to adjust the RT_{NDT} (ART) for radiation embrittlement. The ART (RT_{NDT} initial + ΔRT_{NDT}) is used to index the material to the K_{IR} curve and, in turn, to set operating limits for the nuclear power plant that take into account the effects of irradiation on the reactor vessel materials.

SECTION 4.0
DESCRIPTION OF PROGRAM

Six surveillance capsules for monitoring the effects of neutron exposure on the Palo Verde Unit 1 reactor pressure vessel core region materials were inserted in the reactor vessel prior to initial plant start-up. The six capsules were positioned in the reactor vessel between the core support barrel and the vessel wall as shown in Figure 4-1. The vertical center of the capsules is opposite the vertical center of the core. The capsule, removed from the 137° location, consisted of three compartments (Figure 4-2). Each compartment consisted of two sections attached by a connecting spacer. The top and bottom compartments of the capsule (Figure 4-3) contained Charpy V-notch and precracked Charpy V-notch specimens along with flux monitors. The middle compartment of the capsule (Figure 4-4) contained tension and Charpy V-notch specimens along with flux and temperature monitors. The test specimens contained in the capsule were made from intermediate shell plate M-6701-2 and weld metal and are representative of the reactor vessel beltline region materials. The capsule was removed after 4.53 EFPY of plant operation. This capsule contained Charpy V-notch, tensile, and precracked Charpy V-notch specimens made from intermediate shell plate M-6701-2 and weld metal representative of the reactor vessel beltline welds. In addition, this capsule contained Charpy V-notch specimens from the Heavy Section Steel Technology (HSST) plate 01MY and the weld HAZ metal from lower shell plate M-4311-1 and M-4311-2.

The Palo Verde Unit 1 reactor vessel intermediate shell plate M-6701-2 was fabricated from steel plate produced according to ASME Specification SA-533 Grade B Class 1 mechanical properties. The Palo Verde Unit 1 surveillance plate material was taken from sections of intermediate shell plate M-6701-2. Weld metal material was fabricated by welding together lower shell plates M-4311-1 and M-4311-2. Weld HAZ test material was fabricated by welding together lower shell plates M-4311-1 and M-4311-2. Test specimens were machined from approximately the 1/4 thickness (1/4T) location. Specimens from the weld metal were machined from a weldment joining lower shell plate M-4311-2 and adjacent lower shell plate M-4311-3. All heat-affected-zone specimens were obtained from the weld heat-affected-zone of either lower shell plate M-4311-1or lower shell plate M-4311-2. The Palo Verde Unit 1 surveillance capsule also contained Charpy V-notch specimens from a standard heat of ASTM A 533 Grade B Class 1 manganese-molybdenum-nickel steel made available by the NRC sponsored HSST Program. This reference material has been fully processed and characterized and was used for Charpy impact specimen correlation monitors.

Charpy V-notch impact specimens were machined from intermediate shell plate M-6701-2 in both the longitudinal orientation (longitudinal axis of the specimen parallel to the major rolling direction of the plate) and transverse orientation (longitudinal axis of the specimen normal to the major rolling direction of the plate). Tensile specimens were machined from intermediate shell plate M-6701-2 in the transverse orientation. Charpy V-notch and tensile specimens from the weld metal were oriented such that the long dimension of the specimen was normal to the welding direction. The notch of the weld metal Charpy specimens was machined such that the direction of crack propagation in the specimen is in the welding direction. Precracked Charpy V-notch test specimens from intermediate shell plate M-6701-2 were machined in both the longitudinal and transverse orientations and precracked Charpy V-notch specimens from the weld metal were machined such that the simulated crack in the specimen would propagate in the direction of welding.

The chemical composition and heat treatment of the surveillance material is presented in Tables 4-1 and 4-2. The chemical analysis reported in Table 4-1 was obtained from unirradiated material used in the surveillance program[2].

The capsule contained flux monitors made of sulfur, titanium, iron, nickel (cadmium shielded), copper (cadmium shielded), cobalt (cadmium shielded and unshielded) and uranium (cadmium shielded and unshielded).

The capsule contained thermal monitors made from four low-melting-point eutectic alloys sealed in glass tubes. These thermal monitors were used to define the maximum temperature attained by the test specimens during irradiation. The composition of the four eutectic alloys and their melting points are as follows:

80% Au, 20% Sn	Melting Point: 536°F (280°C)
90% Pb, 5% Sn, 5% Ag	Melting Point: 558°F (292°C)
2.5% Ag, 97.5% Pb	Melting Point: 580°F (304°C)
1.75% Ag, 0.75% Sn, 97.5% Pb	Melting Point: 590°F (310°C)

TABLE 4-1

Chemical Composition (wt%) of the Palo Verde Unit 1 Reactor Vessel Surveillance Materials[2]

Element	Plate M-6701-2	Weld Metal M-4311-2/M-4311-3
C	0.24	0.16
Mn	1.33	1.08
P	0.004	0.005
S	0.010	0.005
Si	0.28	0.24
Ni	0.60	0.06
Cr	0.04	0.06
Mo	0.53	0.58
V	0.003	0.006
Cb	<0.01	0.01
Ti	<0.01	0.01
Co	0.013	0.018
Cu	0.06	0.04
Al	0.029	0.005
B	<0.001	0.001
W	<0.01	0.02
Sb	0.0015	0.0014
As	<0.001	0.006
Sn	0.003	0.004
Zr	<0.001	0.001
Pb	<0.001	0.001
N	0.009	0.007

TABLE 4-2

Heat Treatment of the Palo Verde Unit 1 Reactor Vessel Surveillance Materials[2]

Material	Temperature (°F)	Time (hr)	Coolant
Surveillance Program Test Plate M-6701-2	Austenitizing: 1600 ± 25	4	Water quenched
	Tempered: 1225 ± 25	4	Air cooled
	Stress Relief: 1150 ± 50	40	Furnace cooled to 600°F
Weldment	Stress Relief: 1125 ± 25	41 hr. & 45 min.	

TABLE 4-3

Summary of Unirradiated Surveillance Material Data[2]

Material and Code	C_V Upper Shelf (ft-lb)	30 ft-lb Index (°F)	50 ft-lb Index (°F)	35 Mils Lat. Exp. Index (°F)	NDTT (°F)	RT_{NDT} (°F)	RT Yield Strength (ksi)	
							Static	Dynamic
Base Metal Plate M-6701-2 (WR) (Transverse)	98	32	72	70	-50	25	65.6/65.1	83.5
Base Metal Plate M-6701-2 (RW) (Longitudinal)	151	7	37	35	-50	0	-	89.9
Weld Metal M-4311-2/ M-4311-3	164	-54	-33	-30	-40	-40	68.7/65.8	103.1
HAZ Metal M-4311-1/ M-4311-2	135	-62	-25	-30	0	0	-	-
SRM HSST Plate 01MY (RW) (Longitudinal)	129	23	50	45	0	-	-	-

TABLE 4-4

Arrangement of Encapsulated Test Specimens by Code Number within the Palo Verde Unit 1 137° Capsule[5]

Compartment Position	Compartment Number	Specimen Numbers		
1	1A31Y	1AY2Y	1AY1C	1AY4Y
		1AY17	1AY32	1AY4J
		1AY5J	1AY1D	1AY1T
		1AY2L	1AY3M	1AY4P
		1AY4B	1AY4U	1AY53
2	1A32Y-U	1AYA7	1AY13	1AY16
		1AY3B	1AY1E	1AY2M
		1AY27	1AY4T	1AY34
		1AU2P	1AU2Y	1AU2E
		1AU3P	1AU24	1AU3P
		1AU26	1AU4P	1AU2B
3	1A33Y-4	1AYJ3	1AYJD	1AYJ1
		1A42C	1A447	1A445
		1A45D	1A44B	1A434
		1A42D	1A41A	1A43P
		1A456	1A45K	1A42T
4	1A34B-3	1AB6C	1AB63	1AB5P
		1AB4J	1AB55	1AB5J
		1AB54	1AB4P	1AB4L
		1A3J1	1A3JA	1A3JD
5	1A353	1A33C	1A33U	1A34M
		1A337	1A33T	1A32J
		1A36C	1A32E	1A34Y
		1A32A	1A345	1A3A4
		1A36D	1A36U	1A37K
6	1A363-U	1A32B	1A33J	1A316
		1A37D	1A35T	1A36L
		1A376	1A31C	1A32C
		1AU27	1AU3T	1AU2C
		1AU44	1AU4L	1AU1Y
		1AU1P	1AU3J	1AU32

CODE:

Specimen ID.	Material
1AUXX	Intermediate Shell Plate M-6701-2 (Longitudinal Orientation)
1AYXX	Intermediate Shell Plate M-6701-2 (Transverse Orientation)
1A3XX	Weld Metal
1A4XX	Heat-Affected-Zone Material
1ABXX	SRM HSST 01MY Material (Longitudinal Orientation)

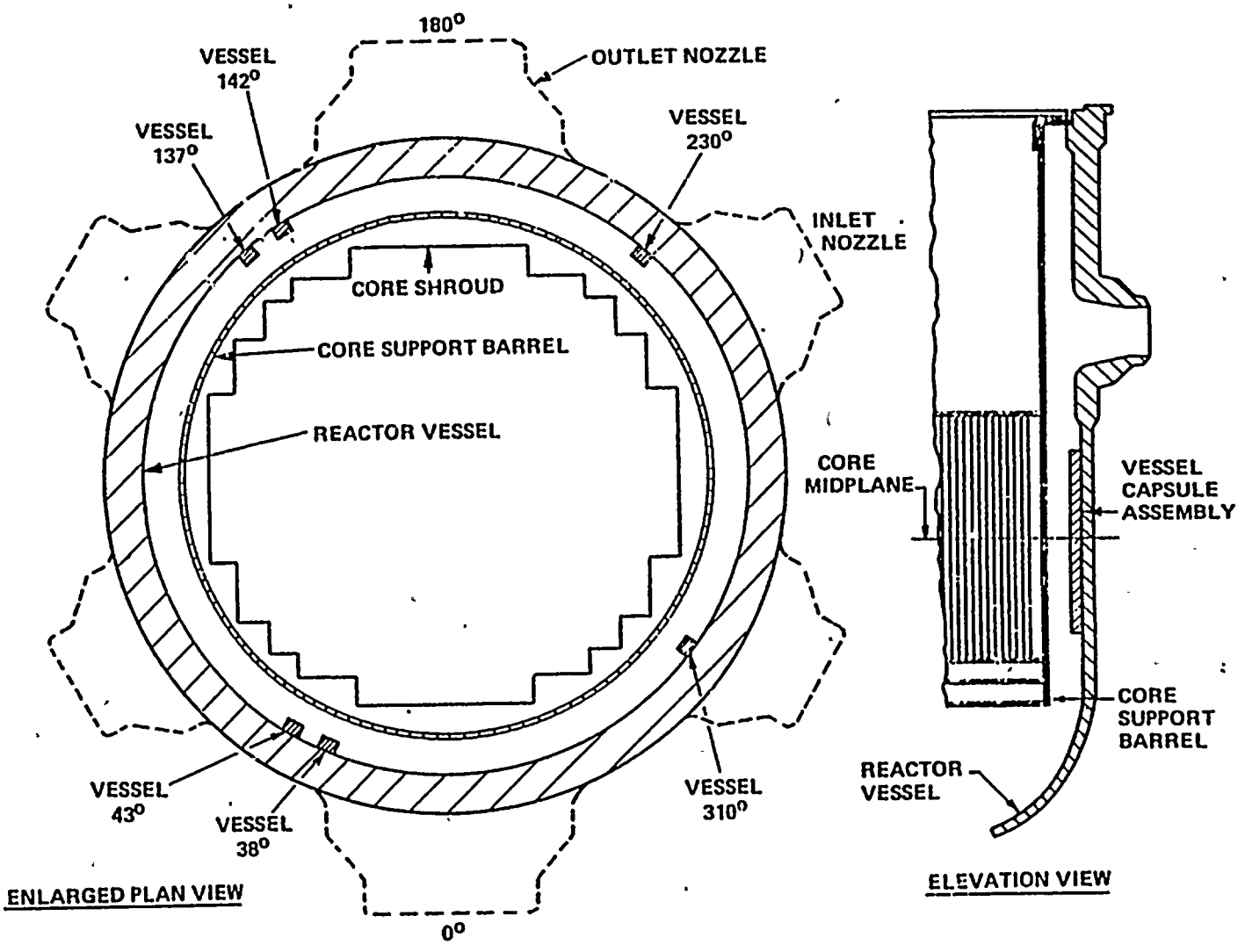

Figure 4-1. Arrangement of Surveillance Capsules in the Palo Verde Unit 1 Reactor Vessel

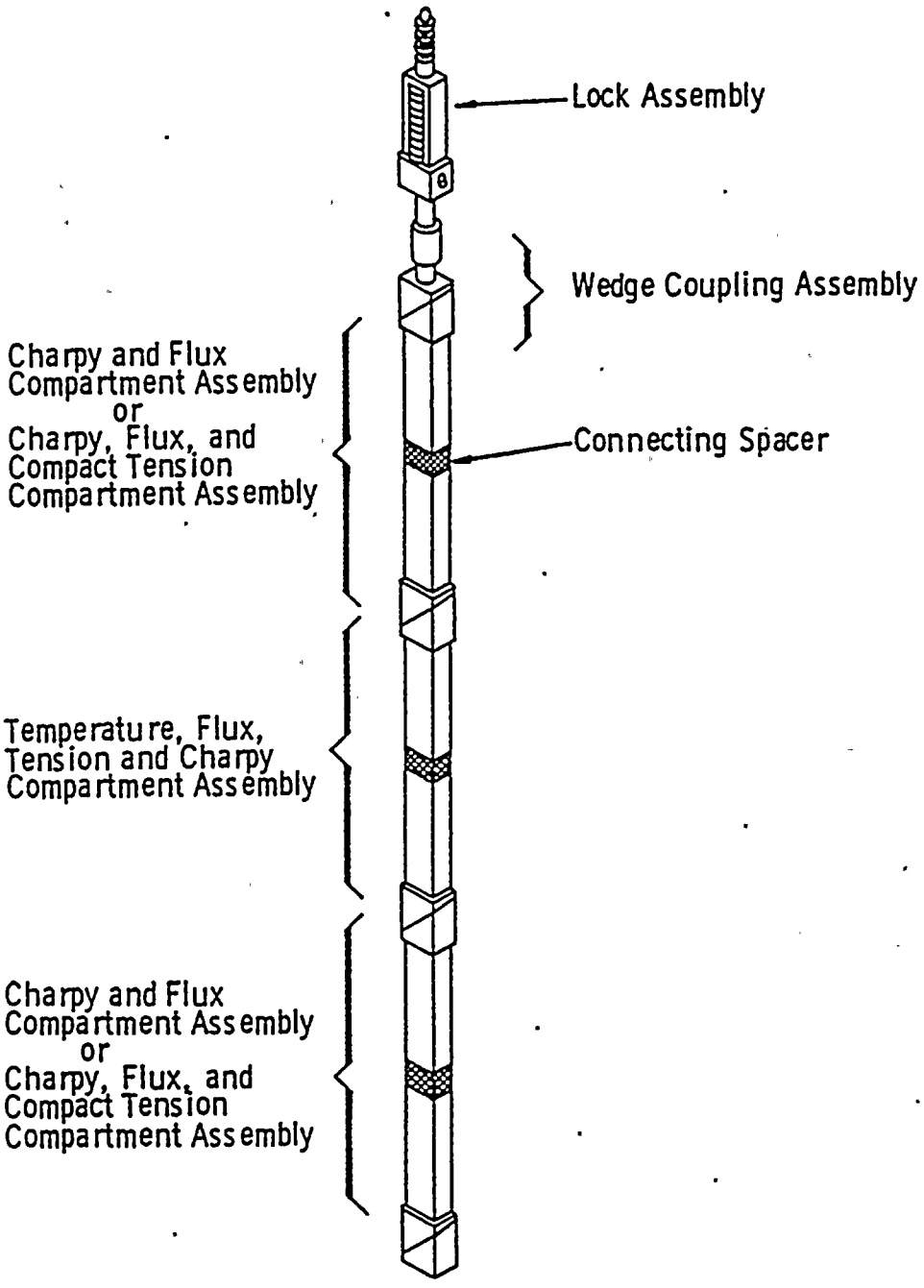

Figure 4-2. Typical Palo Verde Unit 1 Surveillance Capsule Assembly

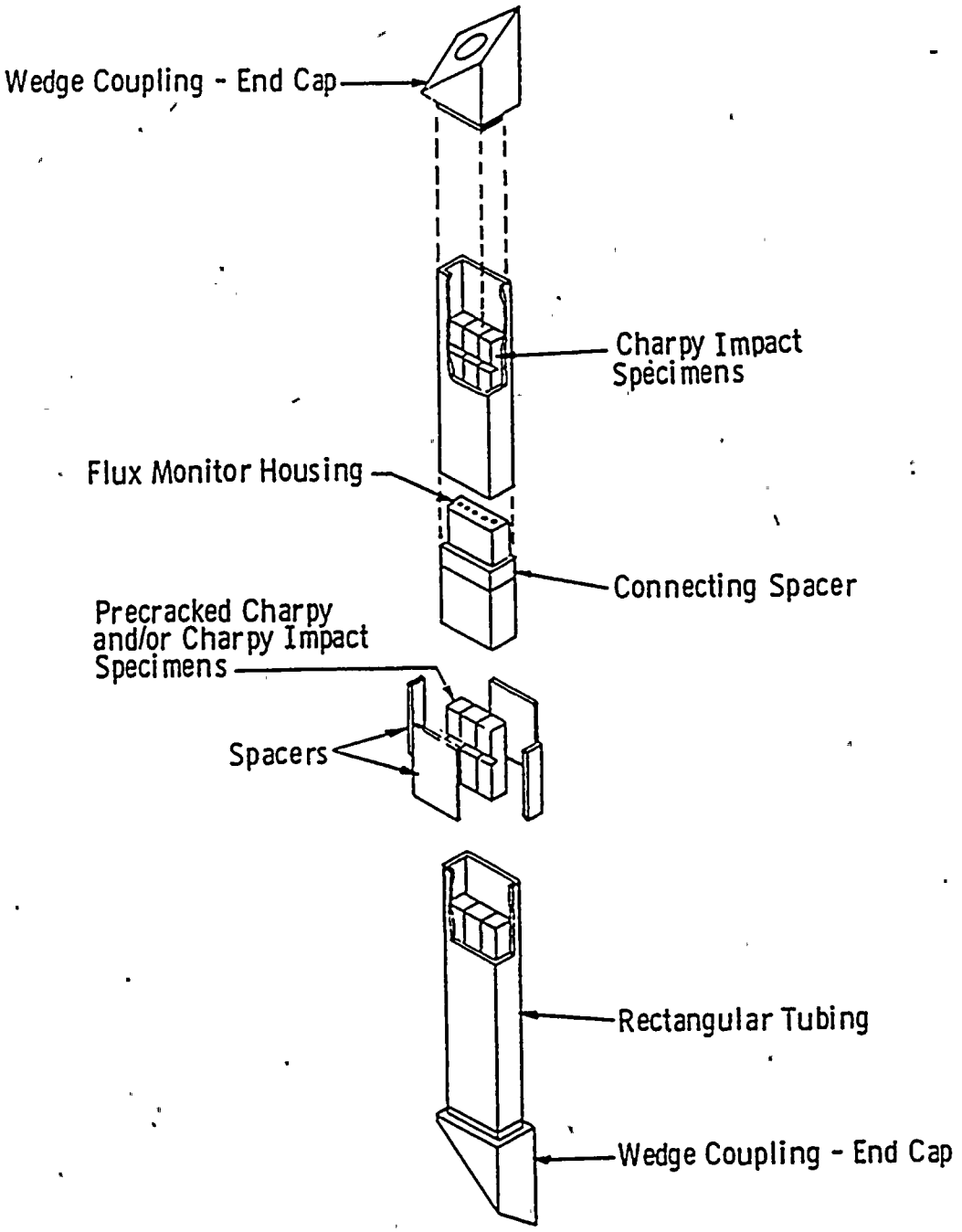

Figure 4-3. Typical Palo Verde Unit 1 Surveillance Capsule Charpy Impact Compartment Assembly

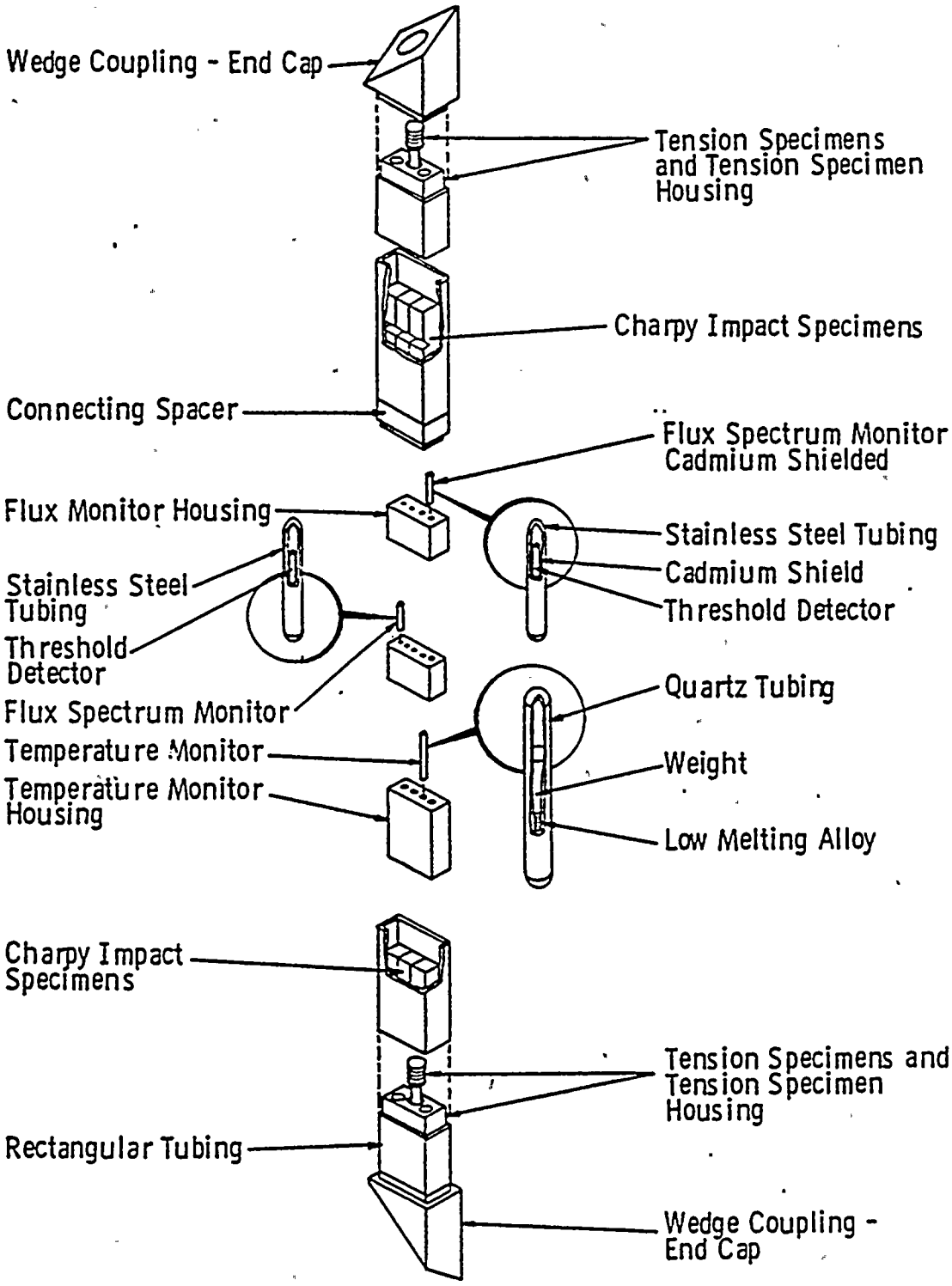

Figure 4-4. Typical Palo Verde Unit 1 Surveillance Capsule Tensile-Monitor Compartment Assembly

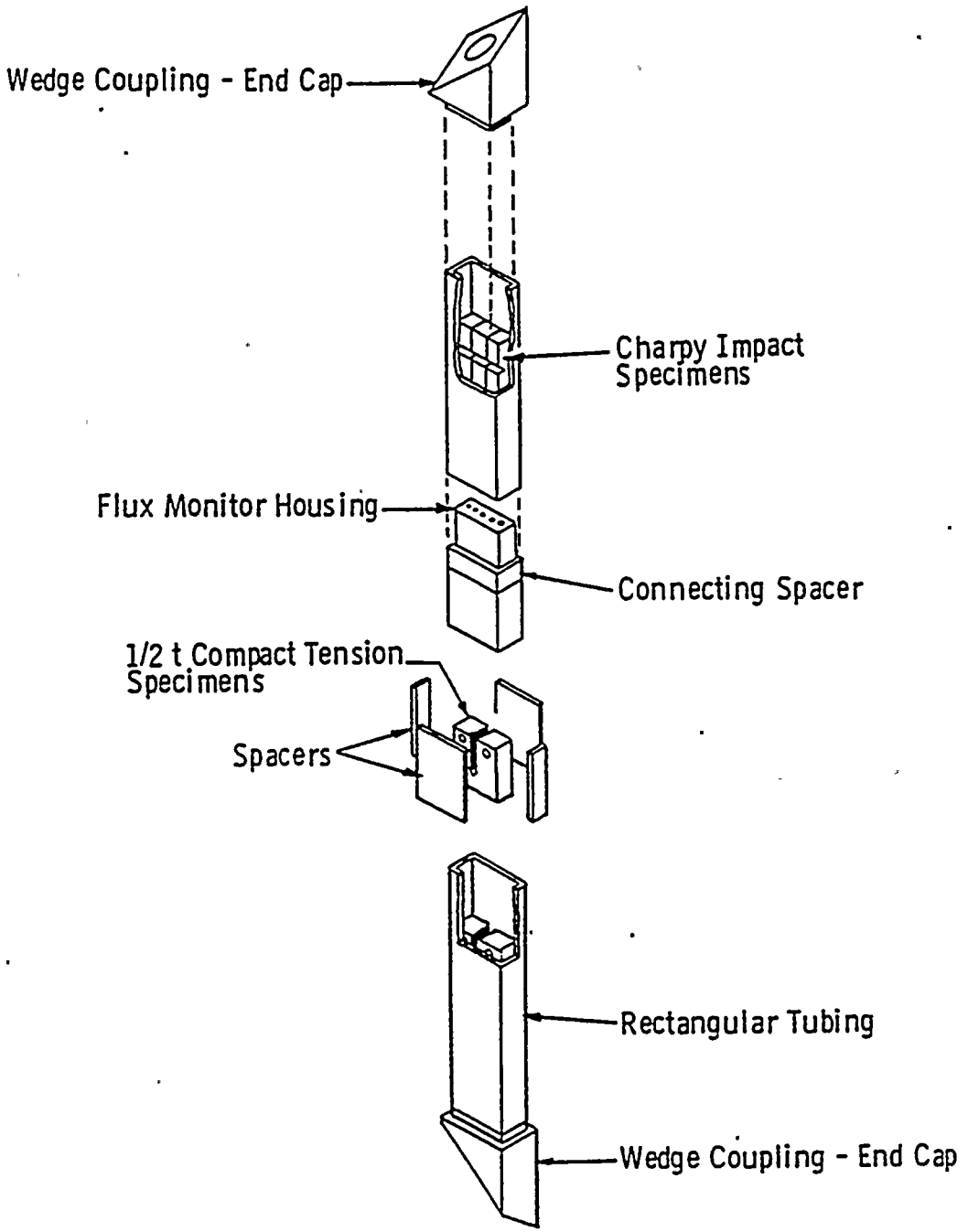

Figure 4-5. Typical Palo Verde Unit 1 Surveillance Capsule Charpy Flux and Compact Tension Compartment Assembly

SECTION 5.0
TESTING OF SPECIMENS FROM CAPSULE W137

5.1 Overview

The post-irradiation mechanical testing of the Charpy V-notch impact, precracked Charpy and tensile specimens was performed in the Remote Metalograhpic Facility (RMF) at the Westinghouse Science and Technology Center. Testing was performed in accordance with 10CFR50, Appendices G and H[6] and ASTM Specification E185-82[7] and Westinghouse Procedure RMF 8402, Revision 2 as modified by Westinghouse RMF Procedure 8102, Revision 1, and 8103, Revision 1.

Upon receipt of the capsule at the hot cell laboratory, the specimens and spacer blocks were carefully removed, inspected for identification number, and checked against the master list in Reference 5. Per Reference 5, the capsule should have had thermal monitors with melting temperatures of 536°F (280°C), 558°F (292°C), 580°F (304°C) and 590°F (310°C). When the capsule was disassembled the 536°F (280°C) thermal monitor was missing. Examination of the three remaining thermal monitors, Figure 5-1, indicated that the 558°F (292°C) thermal monitor melted. Thus, the missing 536°F (280°C) thermal monitor will have no impact on the results of this analysis. Based on the examination of the thermal monitors, the maximum temperature to which the test specimens were exposed to was less than 580°F (304°C).

The Charpy impact tests were performed per ASTM Specification E23-92[8] and RMF Procedure 8103, Revision 1, and NSMT Procedure 9306, on a Tinius-Olsen Model 74, 358J machine. The tup (striker) of the Charpy impact test machine is instrumented with a GRC 830-I instrumentation system, feeding information into an IBM PC Computer. With this system, load-time and energy-time signals can be recorded in addition to the standard measurement of Charpy energy (E_D). From the load-time curve, the load of general yielding (P_{GY}), the time to general yielding (t_{GY}), the maximum load (P_M), and the time to maximum load (t_M) can be determined. Under some test conditions, a sharp drop in load indicative of fast fracture was observed. The load at which fast fracture was initiated is identified as the fast fracture load (P_F), and the load at which fast fracture terminated is identified as the arrest load (P_A). The energy at maximum load (E_M) was determined by comparing the energy-time record and the load-time record. The energy at maximum load is approximately equivalent to the energy required to initiate a crack in the specimen. Therefore, the propagation energy for the crack (E_p) is the difference between the total energy to fracture (E_D) and the energy at maximum load (E_M).

The yield stress (σ_Y) was calculated from the three-point bend formula having the following expression:

$$\sigma_Y = [P_{GY} * L] / [B * (W - a)^2 * C] \quad (1)$$

where: L = distance between the specimen supports in the impact machine
B = the width of the specimen measured parallel to the notch
W = height of the specimen, measured perpendicularly to the notch
a = notch depth

The constant C is dependent on the notch flank angle (ϕ), notch root radius (ρ) and the type of loading (ie. pure bending or three-point bending). In three-point bending, for a Charpy specimen in which $\phi = 45°$ and $\rho = 0.010"$, Equation 1 is valid with C = 1.21. Therefore, (for L = 4W),

$$\sigma_Y = [P_{GY} * L] / [B * (W - a)^2 * 1.21] = [3.3 * P_{GY} * W] / [B * (W - a)^2] \quad (2)$$

For the Charpy specimen, B = 0.394", W = 0.394" and a = 0.079" Equation 2 then reduces to:

$$\sigma_Y = 33.3 * P_{GY} \quad (3)$$

where σ_Y is in units of psi and P_{GY} is in units of lbs. The flow stress was calculated from the average of the yield and maximum loads, also using the three-point bend formula.

The symbol A in columns 4, 5 and 6 of Tables 5-6 through 5-10 is the cross-section area under the notch of the charpy specimen:

$$A = B (W - a) = 0.1241 \text{ sq. in.}$$

Percent shear was determined from post-fracture photographs using the ratio-of-areas methods in compliance with ASTM Specification A370-92[9]. The lateral expansion was measured using a dial gage rig similar to that shown in the same specification.

In addition to the standard Charpy test specimens, the capsule also contained precracked Charpy specimens. Testing of the precracked Charpy specimens provides estimates of the dynamic fracture

toughness of the irradiated materials contained in the capsule using small specimens, rather than much larger ones used in Fracture Mechanics.

Although the Charpy specimens are too small to allow valid determinations of the fracture toughness, the testing of sub-sized specimens, makes it feasible to test multiple irradiated specimens.

The precracked Charpy test offers the further advantage of being simple to perform. The test requires an instrumented Charpy impact machine and the ability to adjust the drop height of the impact hammer. The load-time data for each test is recorded using high speed data acquisition equipment. The tests in this program were conducted using the same system as for standard Charpy specimens, ie., a Tinius-Olsen Model 74 Charpy impact machine equipped with a Dynatup Products Model 830-I data acquisition system. The adjustable drop height capability is required to allow proper analysis of the test records. The early portion of the test record is dominated by oscillations in the load signal caused by the inertial loading that occurs when the hammer impacts the specimen. The Charpy hammer must be lowered to reduce the inertial effects and to increase the length of the test. In general, the primary points of analysis (general yielding, etc.) should occur at least 100 msec after the initial impact.

The load time records must be analyzed to determine fracture toughness values. The initial velocity of the Charpy hammer was determined using the Dynatup instrumentation system. The velocity measurement was then used to interpret the load-time record in terms of load and displacement. This data was then analyzed to provide an energy versus time curve. The analysis of the instrumented data was performed using the standard Dynatup system software. At low temperatures, the specimens fail in a brittle manner, with no evidence of yielding in the test record. Specimens that failed in a brittle manner were analyzed using standard linear-elastic techniques to determine a dynamic fracture toughness, K_{Id}. The determination of K_{Id} requires only a knowledge of the precrack length, which was determined from post test photos, and the maximum load, which was determined from the test record. At higher temperatures, the test records indicate that general yielding of the specimens occurs prior to failure. Elastic-plastic analysis was required to estimate a dynamic fracture toughness value, K_{Jd}, in the higher temperature specimens. In small specimens, maximum load generally occurs at the onset of crack growth. The determination of K_{Jd} requires a knowledge of the energy absorbed in the specimen at maximum load, and the crack length. The energy calculated by the instrumentation system includes both the energy absorbed in the specimen and the energy absorbed by the elastic deformation of the Charpy system. The total system

compliance was determined and the Charpy specimen compliance was calculated to allow correction of the measured energy values. The corrected value of energy absorbed at maximum load, E_I, was then used to calculate K_{Jd} according to the formula:

$$K_{Jd} = [(2*E_I*E)/(b*B)]^{1/2} \quad (4)$$

where,

E = Young's Modulus

b = Remaining ligament (specimen depth less crack length)

B = Specimen thickness

The test records were also analyzed to determine the dynamic yield strength, σ_{yd}. The general formula for the determination of general yielding for a member in three point bending is (in analogy to equation 2):

$$\sigma_{yd} = [(3.3 * P_{gy} * W)/(b * B)^2] \quad (5)$$

where,

W = Specimen depth

P_{gy} = Load at general yielding

Three sets of precracked Charpy specimens were contained in the surveillance capsule. These sets included specimens from intermediate shell plate M-6701-2 (both transverse and longitudinal orientations) and from the surveillance weld metal.

Tensile tests were performed on a 20,000-pound Instron, split-console test machine (Model 1115) per ASTM Specification E8-93[10] and E21-92[11], and RMF Procedure 8102, Revision 1. All pull rods, grips, and pins were made of Inconel 718. The upper pull rod was connected through a universal joint to improve axiality of loading. The tests were conducted at a constant crosshead speed of 0.05 inches per minute throughout the test.

Extension measurements were made with a linear variable displacement transducer extensometer. The extensometer knife edges were spring-loaded to the specimen and operated through specimen failure. The extensometer gage length was 1.00 inch. The extensometer is rated as Class B-2 per ASTM E83-93[12].

Elevated test temperatures were obtained with a three-zone electric resistance split-tube furnace with a 9-inch hot zone. All tests were conducted in air. Because of the difficulty in remotely attaching a thermocouple directly to the specimen, the following procedure was used to monitor specimen temperatures. Chromel-alumel thermocouples were positioned at center and each end of the gage section of a dummy specimen and in each grip. In the test configuration, with a slight load on the specimen, a plot of specimen temperature versus upper and lower grip and controller temperatures was developed over the range from room temperature to 550°F (288°C). During the actual testing, the grip temperatures were used to obtain desired specimen temperatures. Experiments indicated that this method is accurate to $\pm$2°F.

The yield load, ultimate load, fracture load, total elongation, and uniform elongation were determined directly from the load-extension curve. The yield strength, ultimate strength, and fracture strength were calculated using the original cross-sectional area. The final diameter and final gage length were determined from post-fracture photographs. The fracture area used to calculate the fracture stress (true stress at fracture) and percent reduction in area was computed using the final diameter measurement.

5.2 Charpy V-Notch Impact Test Results

The results of the Charpy V-notch impact tests performed on the various materials contained in the capsule, which was irradiated to 3.453 x 10^{18} n/cm^2 (E > 1.0 MeV), are presented in Tables 5-1 through 5-10 and are compared with unirradiated results[2] as shown in Figures 5-2 through 5-6. The transition temperature increases and upper shelf energy decreases for the surveillance materials are summarized in Table 5-11.

Irradiation of the reactor vessel intermediate shell plate M-6701-2 Charpy specimens oriented with the longitudinal axis of the specimen parallel to the major rolling direction of the plate (longitudinal orientation) to 3.453 x 10^{18} n/cm^2 (E > 1.0 MeV) (Figure 5-2) resulted in a 30 ft-lb transition temperature increase of 33°F and a 50 ft-lb transition temperature increase of 33°F. This resulted in an irradiated 30 ft-lb transition temperature of 40°F and an irradiated 50 ft-lb transition temperature of 70°F (longitudinal orientation).

The average upper shelf energy (USE) of the intermediate shell plate M-6701-2 Charpy specimens (longitudinal orientation) resulted in an energy decrease of 22 ft-lb after irradiation to 3.453 x 10^{18} n/cm^2 (E > 1.0 MeV). This results in an irradiated average USE of 129 ft-lb (Figure 5-2).

Irradiation of the reactor vessel intermediate shell plate M-6701-2 Charpy specimens oriented with the longitudinal axis of the specimen normal to the major rolling direction of the plate (transverse orientation) to 3.453 x 10^{18} n/cm^2 (E > 1.0 MeV) (Figure 5-3) resulted in a 30 ft-lb transition temperature increase of 8°F and a 50 ft-lb transition temperature increase of 28°F. This results in an irradiated 30 ft-lb transition temperature of 40°F and an irradiated 50 ft-lb transition temperature of 100°F (transverse orientation).

The average USE of the intermediate shell plate M-6701-2 Charpy specimens (transverse orientation) resulted in an average energy decrease of 11 ft-lbs after irradiation to 3.453 x 10^{18} n/cm^2 (E > 1.0 MeV). This results in an irradiated average USE of 87 ft-lb (Figure 5-3).

Irradiation of the surveillance weld metal Charpy specimens to 3.453 x 10^{18} n/cm^2 (E > 1.0 MeV) (Figure 5-4) resulted in a 30 ft-lb transition temperature increase of 9°F and a 50 ft-lb transition temperature increase of 13°F. This results in an irradiated 30 ft-lb transition temperature of -45°F and an irradiated 50 ft-lb transition temperature of -20°F.

The average USE of the surveillance weld metal resulted in an energy decrease of 2 ft-lbs after irradiation to 3.453 x 10^{18} n/cm^2 (E > 1.0 MeV). This resulted in an irradiated average USE of 162 ft-lb (Figure 5-4).

Irradiation of the reactor vessel weld HAZ metal Charpy specimens to 3.453 x 10^{18} n/cm^2 (E > 1.0 MeV) (Figure 5-5) resulted in no increase in the 30 ft-lb transition temperature and no increase in the 50 ft-lb transition temperature. This results in an unchanged irradiated 30 ft-lb transition temperature of -62°F and an unchanged irradiated 50 ft-lb transition temperature of -25°F.

The average USE of the weld HAZ metal resulted in an energy decrease of 11 ft-lbs after irradiation to 3.453 x 10^{18} n/cm^2 (E > 1.0 MeV). This resulted in an irradiated average USE of 124 ft-lb (Figure 5-5).

Irradiation of the HSST plate 01MY Charpy specimens to 3.453 x 10^{18} n/cm^2 (E > 1.0 MeV) (Figure 5-6) resulted in a 30 ft-lb transition temperature increase of 107°F and a 50 ft-lb transition temperature increase of 110°F. This results in an irradiated 30 ft-lb transition temperature of 130°F and an irradiated 50 ft-lb transition temperature of 160°F.

The average USE of the HSST plate 01MY Charpy specimens resulted in an energy decrease of 24

ft-lbs after irradiation to 3.453 x 10^{18} n/cm^2 (E > 1.0 MeV). This resulted in an irradiated average USE of 105 ft-lb (Figure 5-6).

The fracture appearance of each irradiated Charpy specimen from the various materials is shown in Figures 5-7 through 5-11 and show an increasingly ductile or tougher appearance with increasing test temperature.

A comparison of the 30 ft-lb transition temperature increases and upper shelf energy decreases for the various Palo Verde Unit 1 surveillance materials with predicted values using the methods of NRC Regulatory Guide 1.99, Revision 2[1] is presented in Table 5-12 and led to the following conclusions:

- The 30 ft-lb transition temperature increases for the surveillance weld metal and the transversely oriented intermediate shell plate M-6701-2 Charpy test results are less than the Regulatory Guide 1.99, Revision 2, predictions.

- The 30 ft-lb transition temperature increase of the longitudinally oriented intermediate shell plate M-6701-2 Charpy test results is 7°F higher than the Regulatory Guide 1.99, Revision 2[1], prediction. Regulatory Guide 1.99, Revision 2, requires a 2 sigma allowance of 34°F (for base metal) be added to the predicted reference transition temperature to obtain a conservative upper bound value. Thus, the reference transition temperature increase for the intermediate shell plate M-6701-2 (longitudinal orientation) is bounded by the 2 sigma allowance for shift prediction.

- The measured average USE decrease of the weld metal and intermediate shell plate M-6701-2 (longitudinal and transverse) Charpy test results are equal to or less than the Regulatory Guide 1.99, Revision 2, predictions.

The load-time records for the Charpy impact tests are provided in Figures A-2 through A-31 in Appendix A.

5.3 Precracked Charpy Specimen Test Results

The results of the precracked Charpy specimen tests are reported in Tables 5-13 through 5-15 and in Figures 5-12 through 5-14. Data for the unirradiated materials was reported in the original ABB-Combustion Engineering report[2]. The unirradiated and irradiated precrack Charpy data are

both included in Figures 5-12 through 5-14. The data is plotted on the basis of the RT_{NDT} value to eliminate the effects of the relatively small shifts in the ductile-to-brittle temperature. These figures indicate good agreement between the irradiated and unirradiated test results. The K_I reference (K_{IR}) curve is also shown in Figures 5-12 through 5-14. The data is bounded by the K_{IR} curve, which should provide a lower bound estimate for the fracture toughness. The low temperature unirradiated and irradiated data, which was determined using linear-elastic procedures (K_{Id}), approaches the bounding curve. The low fracture toughness values may be attributed to the sub-sized specimens, which do not meet standard validity requirements.

The load-time records of the irradiated precracked Charpy specimen tests are provided in Figures A-32 through A-58 in Appendix A.

The fracture appearance of each precracked charpy specimen from the various materials is shown in Figures 5-15 through 5-17.

5.4 Tension Test Results

The results of the tension tests performed on the various materials contained in the capsule irradiated to 3.453×10^{18} n/cm^2 (E > 1.0 MeV) are presented in Table 5-16 and are compared with unirradiated results[2] as shown in Figures 5-18 and 5-19.

The results of the tension tests performed on the intermediate shell plate M-6701-2 (transverse orientation) indicated that irradiation to 3.453×10^{18} n/cm^2 (E > 1.0 MeV) caused a 2 to 4 ksi increase in the ultimate tensile strength and a 0 to 4 ksi increase in 0.2% offset yield strength when compared to unirradiated data[2] (Figure 5-18).

The results of the tension tests performed on the surveillance weld metal indicated that irradiation to 3.453×10^{18} n/cm^2 (E > 1.0 MeV) caused a 0 to 4 ksi increase in the ultimate tensile strength and a 0 to 4 ksi increase in 0.2% offset yield strength when compared to unirradiated data[2] (Figure 5-19).

The fractured tension specimens for the intermediate shell plate M-6701-2 material are shown in Figure 5-20, while the fractured specimens for the surveillance weld metal are shown in Figure 5-21.

The engineering Stress-strain curves for the tension tests are shown in Figures 5-22 through 5-25.

TABLE 5-1

Charpy V-notch Data for the Palo Verde Unit 1 Intermediate Shell Plate M-6701-2 Irradiated to a Fluence of 3.453 X 10^{18} n/cm^2 (E > 1.0 MeV) (Longitudinal Orientation)

Sample	Temperature		Impact Energy		Lateral Expansion		Shear
Number	(°F)	(°C)	(ft-lb)	(J)	(mils)	(mm)	(%)
1AU2C	-25	-32	9	12	9	0.23	10
1AU27	25	-4	24	33	22	0.56	15
1AU44	45	7	28	37	24	0.61	20
1AU3J	65	18	49	67	38	0.97	25
1AU3T	100	38	86	117	71	1.80	40
1AU1Y	150	66	118	160	81	2.06	70
1AU32	200	93	125	169	79	2.01	100
1AU4L	250	121	136	184	94	2.39	100
1AU1P	300	149	126	171	90	2.29	100

TABLE 5-2

Charpy V-notch Data for the Palo Verde Unit 1 Intermediate Shell Plate M-6701-2 Irradiated to a Fluence of 3.453 X 10^{18} n/cm^2 (E > 1.0 MeV) (Transverse Orientation)

Sample	Temperature		Impact Energy		Lateral Expansion		Shear
Number	(°F)	(°C)	(ft-lb)	(J)	(mils)	(mm)	(%)
1AY4J	-25	-32	9	13	10	0.25	15
1AY2Y	5	-15	23	31	24	0.61	10
1AY3M	35	2	24	32	24	0.61	10
1AY4P	50	10	27	37	26	0.66	15
1AY17	65	18	35	47	32	0.81	20
1AY53	75	24	47	64	40	1.02	20
1AY5J	85	29	52	70	43	1.09	20
1AY1C	100	38	56	76	46	1.17	25
1AY2L	125	52	53	72	50	1.27	25
1AY4U	150	66	68	92	56	1.42	30
1AY4Y	185	85	63	85	54	1.37	40
1AY32	225	107	86	117	70	1.78	100
1AY1T	265	129	87	118	74	1.88	100
1AY4B	300	149	90	122	78	1.98	100
1AY1D	350	177	85	115	79	2.01	100

TABLE 5-3

Charpy V-notch Data for the Palo Verde Unit 1 Surveillance Weld Metal Irradiated to a Fluence of 3.453 X 10^{18} n/cm^2 (E > 1.0 MeV)

Sample	Temperature		Impact Energy		Lateral Expansion		Shear
Number	(°F)	(°C)	(ft-lb)	(J)	(mils)	(mm)	(%)
1A32J	-95	-71	7	10	5	0.13	10
1A33C	-70	-57	21	29	18	0.46	15
1A33U	-50	-46	28	39	26	0.66	15
1A36D	-35	-37	36	49	27	0.69	20
1A337	-25	-32	55	75	42	1.07	30
1A36U	-5	-21	67	91	50	1.27	45
1A37K	0	-18	79	107	58	1.47	50
1A34Y	5	-15	97	132	72	1.83	70
1A36C	15	-9	109	148	70	1.78	80
1A34M	60	16	123	167	90	2.29	95
1A3A4	75	24	124	169	82	2.08	90
1A33T	100	38	147	199	92	2.34	100
1A32E	225	107	155	210	93	2.36	100
1A32A	300	149	162	219	84	2.13	100
1A345	350	177	182	246	75	1.91	100

TABLE 5-4

Charpy V-notch Data for the Palo Verde Unit 1 Heat-Affected-Zone (HAZ) Metal Irradiated to a Fluence of 3.453 X 10^{18} n/cm^2 (E > 1.0 MeV)

Sample Number	Temperature		Impact Energy		Lateral Expansion		Shear
	(°F)	(°C)	(ft-lb)	(J)	(mils)	(mm)	(%)
1A42C	-70	-57	27	37	21	0.53	15
1A447	-45	-43	89	121	53	1.35	60
1A43P	-35	-37	56	76	35	0.89	50
1A45D	-20	-29	25	34	26	0.66	40
1A44B	5	-15	44	60	37	0.94	50
1A42T	20	-7	118	160	79	2.01	80
1A42D	35	2	85	116	63	1.60	60
1A434	100	38	138	187	83	2.11	100
1A445	150	66	137	185	82	2.08	100
1A41A	225	107	118	161	84	2.13	100
1A456	300	149	108	146	85	2.16	100
1A45K	350	177	120	163	86	2.18	100

TABLE 5-5

Charpy V-notch Data for the Palo Verde Unit 1 Correlation Monitor
Standard Reference Material HSST 01MY Irradiated to a
Fluence of 3.453 X 10^{18} n/cm^2 (E > 1.0 MeV) (Longitudinal Orientation)

Sample	Temperature		Impact Energy		Lateral Expansion		Shear
Number	(°F)	(°C)	(ft-lb)	(J)	(mils)	(mm)	(%)
1AB63	25	-4	8	11	8	0.20	10
1AB5J	70	21	9	12	11	0.28	15
1AB6C	100	38	32	43	24	0.61	20
1AB4L	125	52	22	30	26	0.66	25
1AB55	150	66	47	63	41	1.04	30
1AB4J	200	93	74	101	57	1.45	60
1AB5P	250	121	105	142	82	2.08	100
1AB54	300	149	110	149	84	2.13	100
1AB4P	350	177	100	136	76	1.93	100

TABLE 5-6

Instrumented Charpy Impact Test Results for the Palo Verde Unit 1 Intermediate Shell Plate M-6701-2 Irradiated to a Fluence of 3.453 X 10^{18} n/cm^2 (E > 1.0 MeV) (Longitudinal Orientation)

Sample No.	Test Temp. (°F)	Charpy Energy E_D (ft-lb)	Normalized Energies (ft-lb/in^2)			Yield Load P_{GY} (lbs)	Time to Yield t_{GY} (μsec)	Max. Load P_M (lbs)	Time to Max. t_M (μsec)	Fast Fract. Load P_F (lbs)	Arrest Load P_A (lbs)	Yield Stress σ_Y (ksi)	Flow Stress (ksi)
			Charpy E_D/A	Max. E_M/A	Prop. E_P/A								
1AU2C	-25	9	74	49	25	3129	0.33	3129	0.33	3129	87	104	104
1AU27	25	24	196	127	70	3158	0.16	3803	0.36	3803	523	105	116
1AU44	45	28	222	139	83	3115	0.17	3726	0.40	3726	922	103	114
1AU3J	65	49	397	287	109	3045	0.16	4145	0.69	4145	1511	101	119
1AU3T	100	86	694	353	341	3100	0.39	4231	0.98	4041	2377	103	122
1AU1Y	150	118	949	350	599	2760	0.15	3988	0.84	2558	1882	92	112
1AU32	200	125	1006	340	666	2646	0.17	3846	0.86	*	*	88	108
1AU4L	250	136	1091	333	758	2635	0.17	3911	0.83	*	*	88	109
1AU1P	300	126	1012	320	692	2497	0.15	3678	0.83	*	*	83	103

* Fully ductile fracture.

TABLE 5-7

Instrumented Charpy Impact Test Results for the Palo Verde Unit 1 Intermediate Shell Plate M-6701-2 Irradiated to a Fluence of 3.453×10^{18} n/cm^2 (E > 1.0 MeV) (Transverse Orientation)

Sample No.	Test Temp. (°F)	Charpy Energy E_D (ft-lb)	Normalized Energies (ft-lb/in^2)			Yield Load P_{GY} (lbs)	Time to Yield t_{GY} (μsec)	Max. Load P_M (lbs)	Time to Max. t_M (μsec)	Fast Fract. Load P_F (lbs)	Arrest Load P_A (lbs)	Yield Stress σ_Y (ksi)	Flow Stress (ksi)
			Charpy E_D/A	Max. E_M/A	Prop. E_P/A								
1AY4J	-25	9	75	46	29	3524	0.20	3524	0.20	3524	93	117	100
1AY2Y	5	23	186	109	77	3452	0.17	3860	0.31	3860	431	115	121
1AY3M	35	24	190	125	65	3145	0.15	3825	0.35	3825	388	104	116
1AY4P	50	27	219	138	81	3154	0.16	3824	0.38	3842	733	105	116
1AY17	65	35	281	183	98	3258	0.17	4058	0.47	4058	829	108	122
1AY53	75	47	379	282	97	3072	0.14	4128	0.65	4128	992	102	120
1AY5J	85	52	416	267	149	3303	0.16	4038	0.64	4009	1291	101	117
1AY1C	100	56	450	282	168	3040	0.16	4044	0.67	3900	1544	101	118
1AY2L	125	53	426	237	189	2963	0.19	3880	0.62	3800	1581	98	114
1AY4U	150	68	546	277	269	2932	0.17	3927	0.69	3721	2273	97	114
1AY4Y	185	63	507	185	322	2668	0.15	3596	0.52	3591	2774	89	104
1AY32	225	86	693	262	432	2729	0.16	3786	0.68	*	*	91	108
1AY1T	265	87	704	257	447	2732	0.18	3732	0.67	*	*	91,	107
1AY4B	300	90	722	254	468	2527	0.15	2527	0.69	*	*	84	84
1AY1D	350	85	682	251	431	2596	0.15	2596	0.66	*	*	86	86

* Fully ductile fracture.

TABLE 5-8

Instrumented Charpy Impact Test Results for the Palo Verde Unit 1 Surveillance Weld Metal Irradiated to a Fluence of 3.453 X 10^{18} n/cm^2 (E > 1.0 MeV)

Sample No.	Test Temp. (°F)	Charpy Energy E_D (ft-lb)	Normalized Energies (ft-lb/in^2)			Yield Load P_{GY} (lbs)	Time to Yield t_{GY} (μsec)	Max. Load P_M (lbs)	Time to Max. t_M (μsec)	Fast Fract. Load P_F (lbs)	Arrest Load P_A (lbs)	Yield Stress σ_Y (ksi)	Flow Stress (ksi)
			Charpy E_D/A	Max. E_M/A	Prop. E_P/A								
1A32J	-95	7	58	32	26	3462	0.16	3462	0.16	3462	145	115	115
1A33C	-70	21	173	87	86	3678	0.17	3913	0.27	3913	1154	122	126
1A33U	-50	28	229	148	81	3808	0.19	4208	0.38	4208	1196	126	133
1A36D	-35	36	290	213	76	3713	0.19	4263	0.51	4263	1184	123	132
1A337**	-25	55	443	--	--	--	--	--	--	--	--	--	--
1A36U	-5	67	540	280	260	3590	0.17	4181	0.63	3969	1712	119	129
1A37K	0	79	635	310	325	3580	0.16	4200	0.69	3776	2115	119	129
1A34Y	5.	97	784	304	481	3499	0.16	4180	0.68	3194	1626	116	128
1A36C	15	109	882	312	569	3566	0.17	4242	0.69	2835	1642	118	130
1A34M	60	123	991	325	665	3269	0.18	4056	0.76	2139	1435	109	122
1A3A4	75	124	.1001	288	712	3221	0.16	3977	0.69	2633	1903	107	120
1A33T	100	147	1180	298	882	3195	0.16	4047	0.70	*	*	106	120
1A32E	225	155	1250	323	927	2511	0.14	3553	0.86	*	*	83	101
1A32A	300	162	1302	321	981	2491	0.15	3518	0.86	*	*	83	100
1A345	350	182	1463	308	1155	2465	0.15	3417	0.84	*	*	82	98

* Fully ductile fracture.

** Data not [illegible] due to computer system malfunction.

TABLE 5-9

Instrumented Charpy Impact Test Results for the Palo Vede Unit 1 Surveillance Heat-Affected-Zone (HAZ) Metal Irradiated to a Fluence of 3.453 X 10^{18} n/cm^2 (E > 1.0 MeV)

Sample No.	Test Temp. (°F)	Charpy Energy E_D (ft-lb)	Normalized Energies (ft-lb/in^2)			Yield Load P_{GY} (lbs)	Time to Yield t_{GY} (μsec)	Max. Load P_M (lbs)	Time to Max. t_M (μsec)	Fast Fract. Load P_F (lbs)	Arrest Load P_A (lbs)	Yield Stress σ_Y (ksi)	Flow Stress (ksi)
			Charpy E_D/A	Max. E_M/A	Prop. E_P/A								
1A42C	-70	27	219	155	64	3741	0.18	4098	0.40	4098	491	124	130
1A447	-45	89	717	333	384	3862	0.17	4577	0.69	3566	1031	128	140
1A43P	-35	56	453	236	216	3955	0.17	4630	0.51	4630	3132	131	143
1A45D	-20	25	202	98	104	3603	0.17	3722	0.29	3722	1095	120	122
1A44B	5	44	355	190	165	3388	0.15	3944	0.47	3944	1814	113	122
1A42T	20	118	952	325	628	3550	0.16	4542	0.69	1738	919	118	134
1A42D	35	85	687	277	411	3263	0.15	3978	0.65	3003	1832	108	120
1A434	100	138	1113	310	803	3228	0.15	4309	0.69	*	*	107	125
1A445	150	137	1101	308	793	3049	0.16	4108	0.72	*	*	101	119
1A41A	225	118	954	263	690	2663	0.14	3688	0.69	*	*	88	105
1A456	300	108	870	295	575	2480	0.16	3397	0.82	*	*	82	98
1A45K	350	120	967	244	723	2315	0.23	3363	0.79	*	*	77	94

* Fully ductile fracture

TABLE 5-10

Instrumented Charpy Impact Test Results for the Palo Verde Unit 1 Surveillance Standard Reference Material HSST 01MY Irradiated to a Fluence of 3.453×10^{18} n/cm^2 (E > 1.0 MeV) (Longitudinal Orientation).

Sample No.	Test Temp. (°F)	Charpy Energy E_D (ft-lb)	Normalized Energies (ft-lb/in^2)			Yield Load P_{GY} (lbs)	Time to Yield t_{GY} (μsec)	Max. Load P_M (lbs)	Time to Max. t_M (μsec)	Fast Fract. Load P_F (lbs)	Arrest Load P_A (lbs)	Yield Stress σ_Y (ksi)	Flow Stress (ksi)
			Charpy E_D/A	Max. E_M/A	Prop. E_P/A								
1AB63	25	8	65	35	30	3285	0.17	3285	0.17	3285	196	109	109
1AB5J	70	9	72	20	52	2526	0.13	2526	0.13	2526	774	84	84
1AB6C	100	32	257	189	68	3152	0.16	4122	0.48	4122	498	105	121
1AB4L	125	22	177	78	98	3215	0.19	3491	0.27	3491	1391	107	111
1AB55	150	47	375	265	110	2991	0.17	4116	0.65	4074	1667	99	118
1AB4J	200	74	597	307	290	2997	0.31	4176	0.84	3797	2445	100	119
1AB5P	250	105	846	277	569	2816	0.16	3961	0.69	*	*	94	113
1AB54	300	110	883	276	607	2699	0.16	3952	0.69	*	*	90	110
1AB4P	350	100	806	267	539	2687	0.15	3834	0.67	*	*	89	108

* Fully ductile fracture.

TABLE 5-11

Effect of Irradiation to 3.453 X 10^{18} n/cm^2 (E > 1.0 MeV) on the Notch Toughness Properties of the Palo Verde Unit 1 Reactor Vessel Surveillance Materials

Material	Average 30 (ft-lb) [a,b] Transition Temperature (°F)			Average 35 mil Lateral [a,b] Expansion Temperature (°F)			Average 50 ft-lb [a,b] Transition Temperature (°F)			Average Energy Absorption [a,b] at Full Shear (ft-lb)		
	Unirradiated	Irradiated	ΔT	Unirradiated	Irradiated	ΔT	Unirradiated	Irradiated	ΔT	Unirradiated	Irradiated	ΔE
Inter. Plate M-6701-2 (longitudinal)	7	40	33	35	60	25	37	70	33	151	129	-22
Inter. Plate M-6701-2 (transverse)	32	40	8	70	75	5	72	100	28	98	87	-11
Weld Metal	-54	-45	9	-30	-30	0	-33	-20	13	164	162	-2
HAZ Metal	-62	-62	0	-30	-30	0	-25	-25	0	135	124	-11
SRM 01MY	23	130	107	45	150	105	50	160	110	129	105	-24

(a) "Average" is defined as the value read from the curve fit through the data points of the Charpy tests (see Figures 5-1 through 5-5)

(b) Unirradiated data is from Reference 2.

TABLE 5-12

Comparison of the Palo Verde Unit 1 Surveillance Material 30 ft-lb Transition Temperature Shifts and Upper Shelf Energy Decreases with Regulatory Guide 1.99 Revision 2 Predictions

Material	Fluence (E > 1.0 MeV) (X 10^{18} n/cm^2)	30 ft-lb Transition Temperature Shift		Upper Shelf Energy Decrease	
		Predicted [a] (°F)	Measured (°F)	Predicted [a] (%)	Measured (%)
Intermediate Shell Plate M-6701-2 (longitudinal)	3.453	26	33	15	15
Intermediate Shell Plate M-6701-2 (transverse)	3.453	26	8	15	11
Weld Metal	3.453	21	9	15	1
HAZ Metal	3.453	--	0	--	8
SRM HSST Plate 01MY (longitudinal)	3.453	--	107	--	19

(a) Based on Regulatory Guide 1.99, Revision 2 methodology using wt. % values of Cu and Ni from Reference 2.

TABLE 5-13

Precracked Instrumented Charpy Impact Test Results for the Palo Verde Unit 1 Intermediate Shell Plate M-6701-2
Irradiated to a Fluence of 3.453 X 10^{18} n/cm^2 (E > 1.0 MeV)
(Longitudinal Orientation)

Sample No.	Test Temp. (°F)	Specimem Comp.	Initial Velocity (in/sec)	Time to Yield (μsec)	Yield Load (lbs)	Time to Max. (μsec)	Max. Load (lbs)	Energy at Initiation (in-lbs)	Available Energy (in-lbs)	Crack Length (in.)	a/W	K_{Id} (ksi√in)	K_{Jd} (ksi√in)	Yield Stress (ksi)
1AU3P	-25	51.1	61.0	--	--	210	1440	--	289	0.188	0.477	57.5	--	112.0
1AU2Y	25	54.8	61.3	--	--	185	1286	--	291	0.195	0.495	54.3	--	107.2
1AU3Y	50	54.2	80.6	--	--	140	1056	--	504	0.194	0.492	44.2	--	87.0
1AU26	75	52.1	80.2	190	1285	505	1439	41.3	499	0.190	0.482	--	158	101.9
1AU2E	100	54.2	100.3	140	1225	225	1244	17.6	781	0.194	0.492	--	96.4	101.1
1AU4P	125	49.6	80.8	170	1250	715	1508	65.4	507	0.185	0.470	--	203.8	94.4
1AU2B	175	49.6	99.5	160	1260	900	1689	115.7	768	0.185	0.470	--	272.2	95.2
1AU2P	225	51.6	99.7	120	1105	1190	1755	158.4	772	0.189	0.480	--	327.6	86.8
1AU24	275	58.3	100.1	110	960	1185	1562	142.4	778	0.201	0.510	--	320.0	85.0

TABLE 5-14

Precracked Instrumented Charpy Impact Test Results for the Palo Verde Unit 1 Intermediate Shell Plate M-6701-2
Irradiated to a Fluence of 3.453 X 10^{18} n/cm^2 (E > 1.0 MeV)
(Transverse Orientation)

Sample No.	Test Temp. (°F)	Specimem Comp.	Initial Velocity (in/sec)	Time to Yield (μsec)	Yield Load (lbs)	Time to Max. (μsec)	Max. Load (lbs)	Energy at Initiation (in-lbs)	Available Energy (in-lbs)	Crack Length (in.)	a/W	K_{Id} (ksi√in)	K_{Jd} (ksi√in)	Yield Stress (ksi)
1AY2M	-25	51.6	60.9	--	--	165	1098	--	288	0.189	0.48	44.2	--	86.2
1AY27	25	49.6	61.3	--	--	275	1468	--	291	0.185	0.470	57.3	--	110.8
1AY1E	75	51.1	61.6	--	--	170	1163	--	295	0.188	0.477	46.4	--	90.2
1AY4T	125	52.1	80.2	170	1205	510	1374	40.2	500	0.190	0.482	--	157.6	95.6
1AY3B	150	53.7	100.5	155	1295	480	1519	52.8	785	0.193	0.490	--	181.5	105.8
1AY13	175	52.6	99.8	165	1230	730	1563	85.5	773	0.191	0.485	--	234.3	98.5
1AY47	225	52.1	100.0	140	1300	1050	1758	143.9	777	0.190	0.482	--	312.1	103.1
1AY1B	275	52.6	100.4	110	1160	860	1643	110.6	782	0.191	0.485	--	271.4	92.9
1AY34	325	47.8	100.2	110	1120	805	1722	104.3	780	0.181	0.459	--	256.3	81.56

TABLE 5-15

Precracked Instrumented Charpy Impact Test Results for the Palo Verde Unit 1 Surveillance Weld Metal Irradiated to a Fluence of 3.453 X 10^{18} n/cm^2 (E > 1.0 MeV)

Sample No.	Test Temp. (°F)	Specimem Comp.	Initial Velocity (in/sec)	Time to Yield (μsec)	Yield Load (lbs)	Time to Max. (μsec)	Max. Load (lbs)	Energy at Initiation (in-lbs)	Available Energy (in-lbs)	Crack Length (in.)	a/W	K_{Id} (ksi√in)	K_{Jd} (ksi√in)	Yield Stress (ksi)
1A35T	-50	60.2	60.8	--	--	265	1030	--	287	0.204	0.518	46.8	--	94.2
1A33J	-25	51.1	61.0	--	--	225	1738	--	289	0.188	0.477	69.4	--	134.9
1A32B	0	57.7	61.0	210	1395	215	1398	10.1	289	0.200	0.508	--	68.4	122.3
1A37D	25	51.1	80.6	180	1475	485	1542	44.9	504	0.188	0.477	--	168.7	114.7
1A32C	50	62.8	79.8	135	1285	370	1377	33.0	495	0.208	0.528	--	157.0	122.6
1A316	75	51.6	79.9	225	1500	755	1689	78.0	495	0.189	0.480	--	222.7	117.8
1A376	100	53.7	99.4	150	1360	720	1568	87.5	767	0.193	0.490	--	244.6	111.1
1A31C	150	60.8	100.0	160	1150	1150	1383	129.7	777	0.205	0.520	--	310.1	106.2
1A36L	200	48.7	99.8	180	1420	1055	1712	143.3	773	0.183	0.464	--	303.7	105.3

TABLE 5-16

Tensile Properties of the Palo Verde Unit 1 Reactor Vessel Surveillance Materials Irradiated to 3.453 X 10^{18} n/cm^2 (E > 1.0 MeV)

Material	Sample Number	Test Temp. (°F)	0.2% Yield Strength (ksi)	Ultimate Strength (ksi)	Fracture Load (kip)	Fracture Stress (ksi)	Fracture Strength (ksi)	Uniform Elongation (%)	Total Elongation (%)	Reduction in Area (%)
Plate M-6701-2 (transverse)	1AYJ1	85	66.7	89.0	2.95	172.6	60.1	11.3	24.3	65
Plate M-6701-2 (transverse)	1AYJD	190	63.2	83.5	2.78	168.4	56.6	10.5	24.0	66
Plate M-6701-2 (transverse)	1AYJ3	550	60.6	86.0	3.05	151.7	62.1	11.6	22.4	59
Weld Metal	1A3JA	10	72.3	86.2	2.70	195.8	55.0	13.5	27.6	72
Weld Metal	1A3J1	100	70.8	81.5	2.45	171.2	49.9	11.3	25.8	71
Weld Metal	1A3JD	550	54.0	75.8	2.30	144.2	46.9	12.8	26.4	68

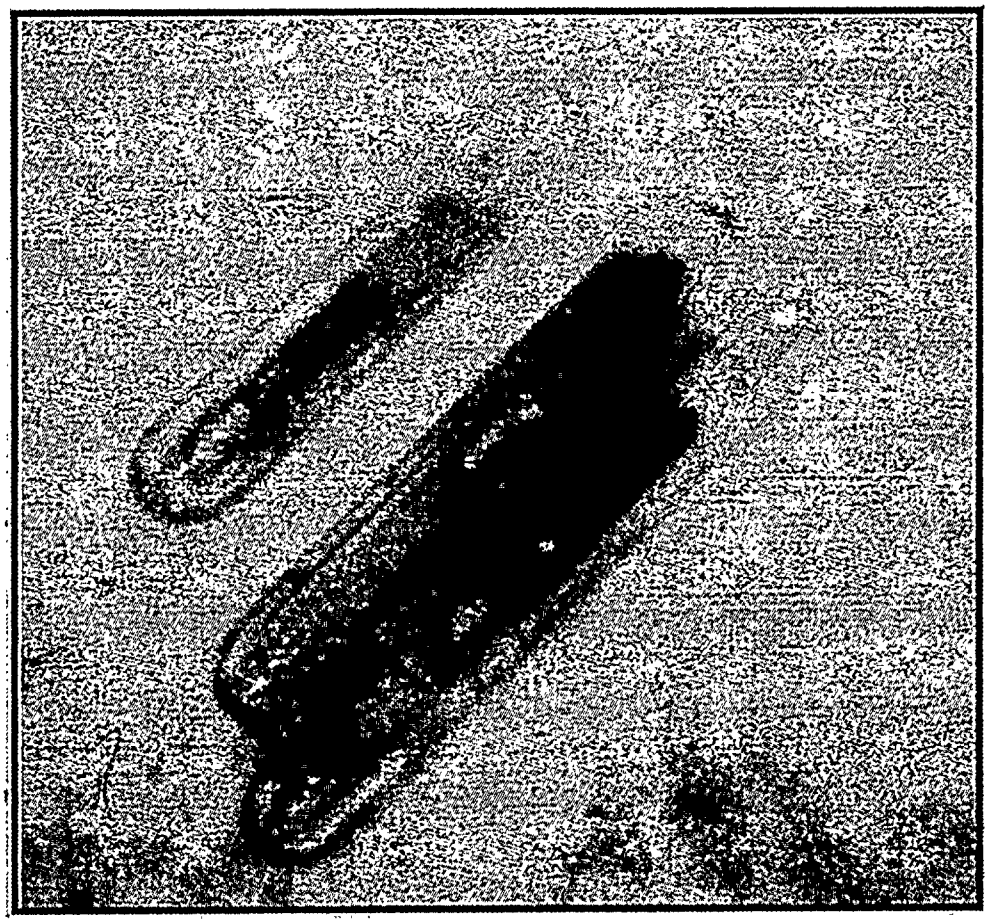

Figure 5-1 Palo Verde Unit 1 Capsule W-137 Thermal Monitors

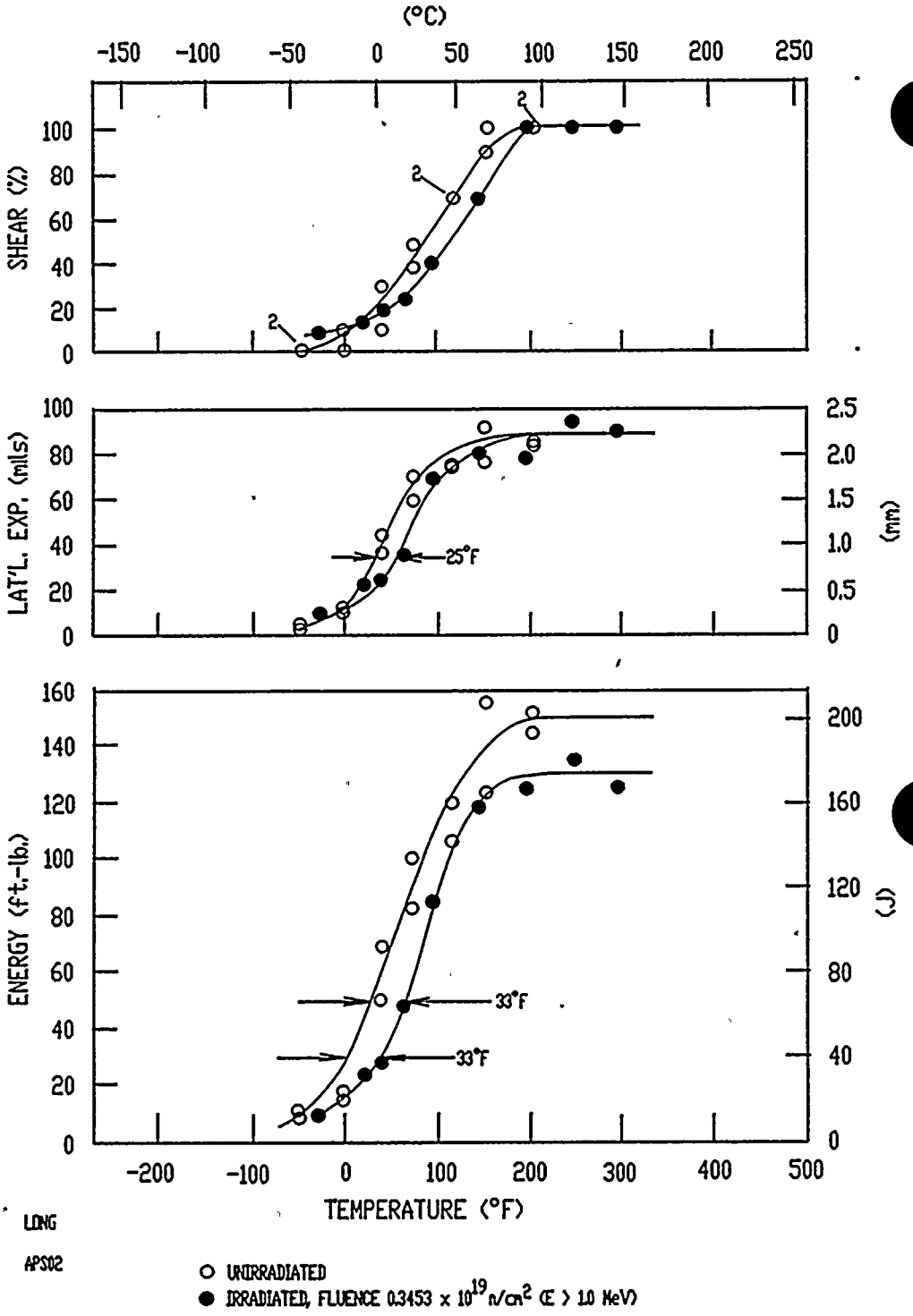

Figure 5-2 Charpy V-Notch Impact Properties for Palo Vedre Unit 1 Reactor Vessel Intermediate Shell Plate M-6701-2 (Longitudinal Orientation)

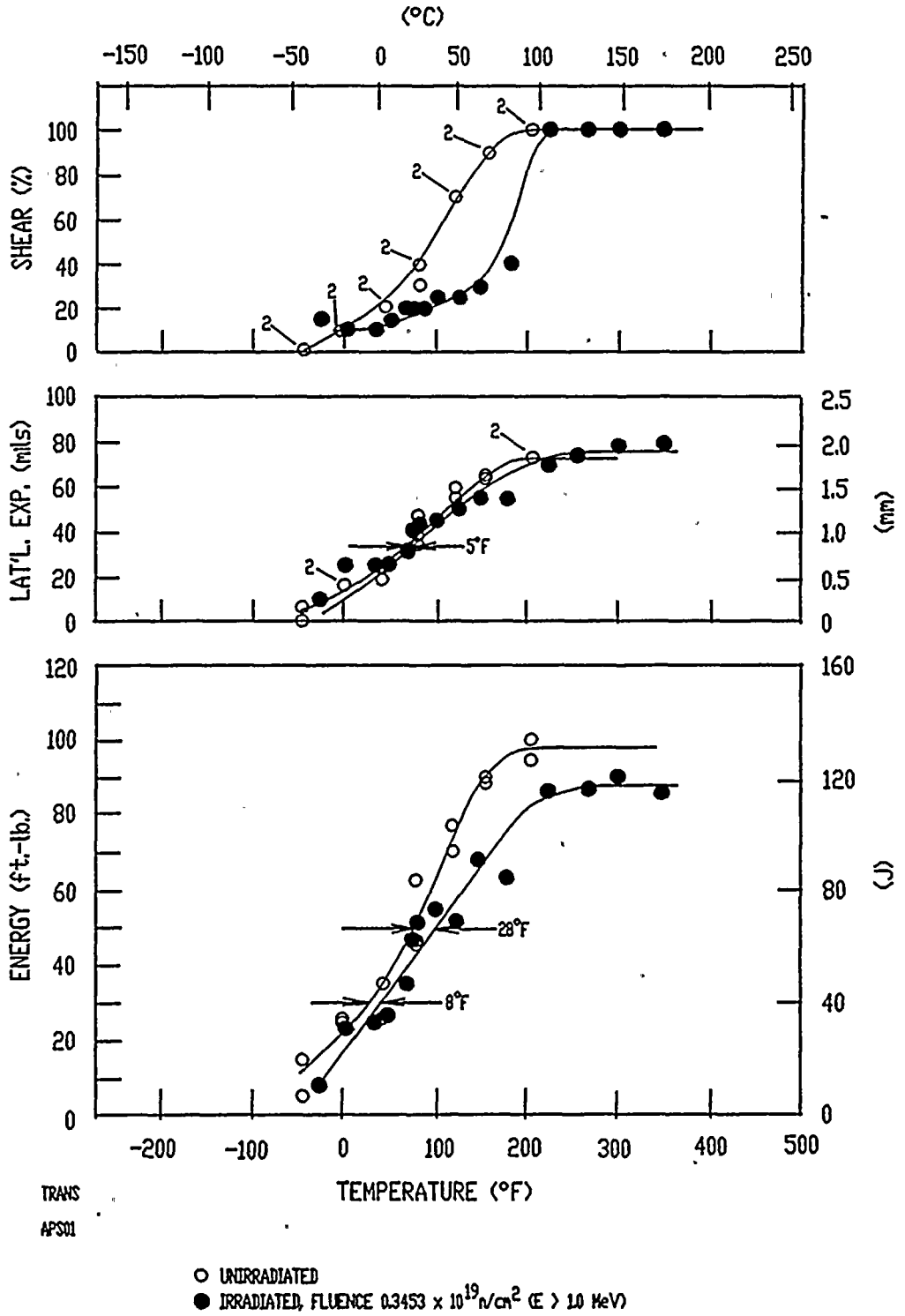

Figure 5-3 Charpy V-Notch Impact Properties for Palo Verde Unit 1 Reactor Vessel Intermediate Shell Plate M-6701-2 (Transverse Orientation)

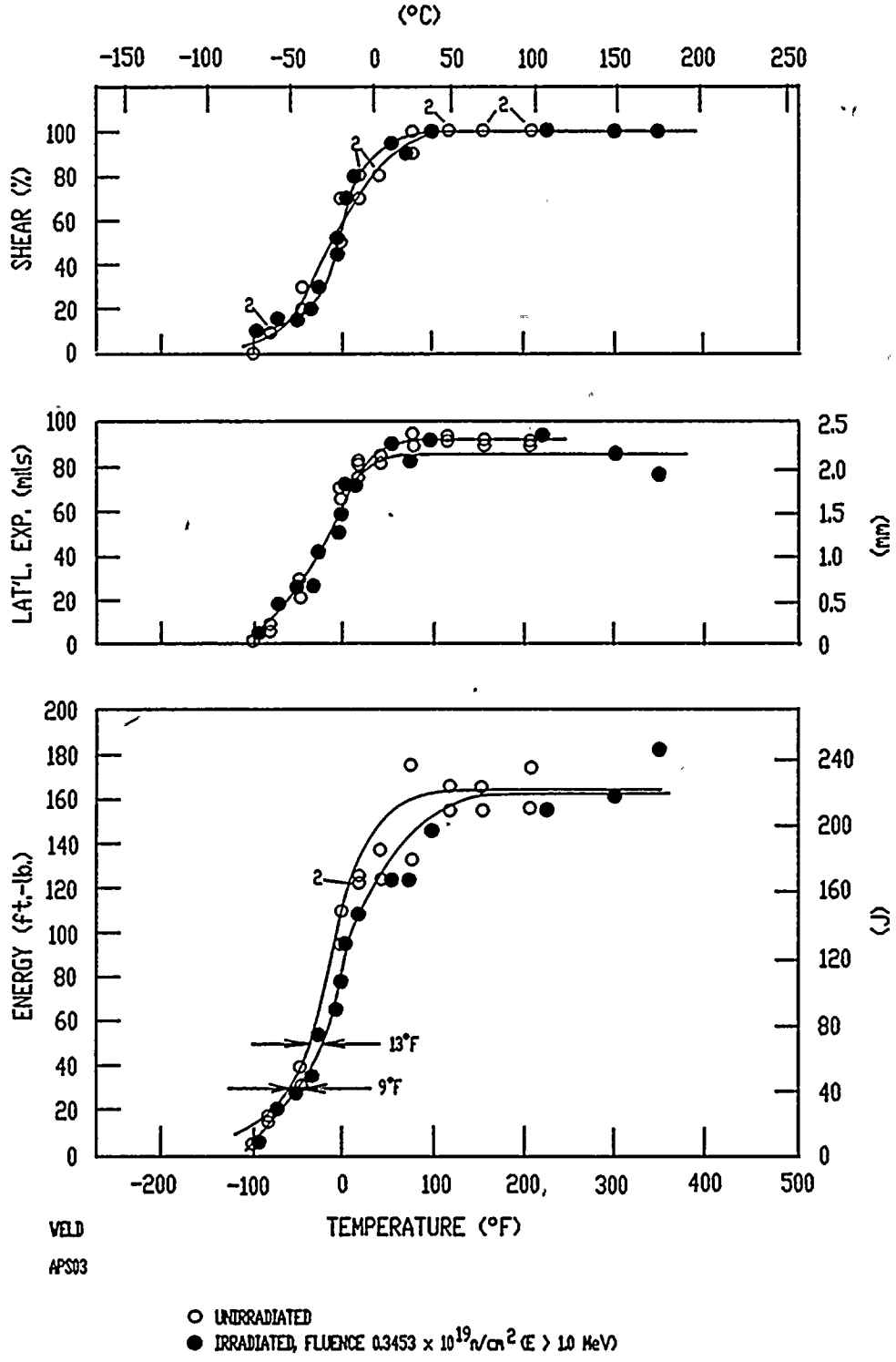

Figure 5-4 Charpy V-Notch Impact Properties for Palo Verde Unit 1 Reactor Vessel Surveillance Weld Metal (M-4311-2/M-4311-3)

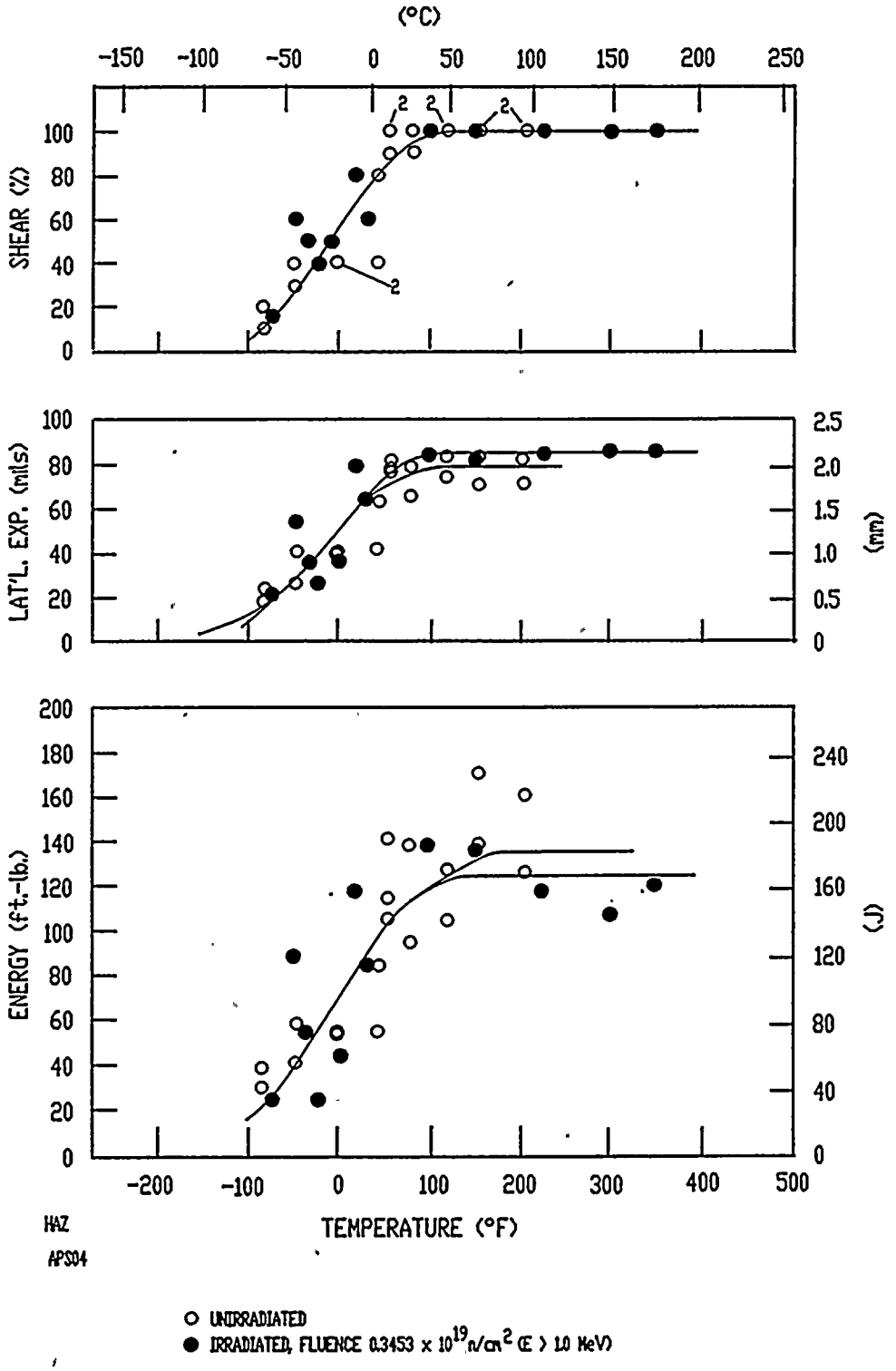

Figure 5-5 Charpy V-Notch Impact Properties for Palo Verde Unit 1 Reactor Vessel Weld Heat-Affected-Zone Metal

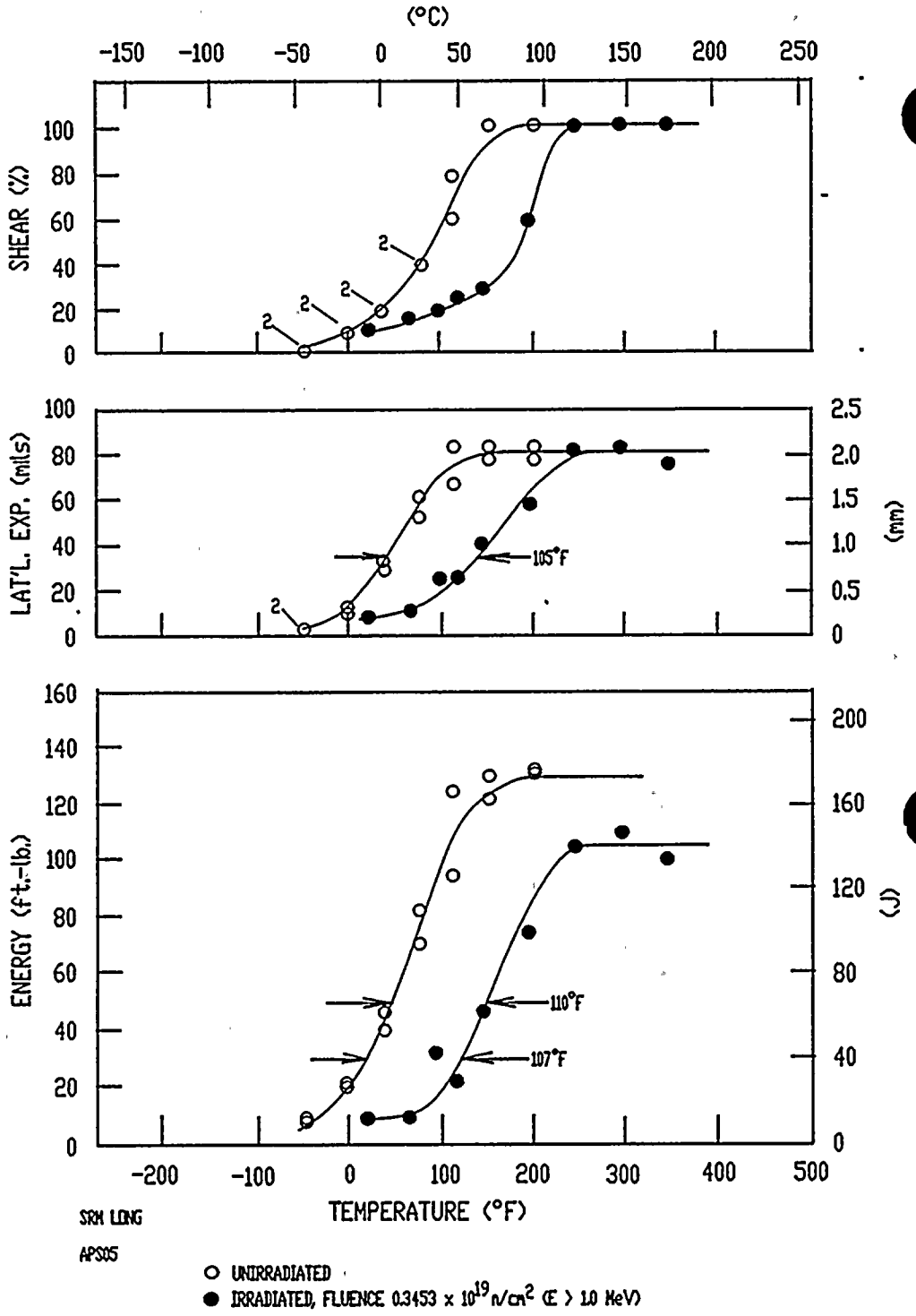

Figure 5-6 Charpy V-Notch Impact Properties for Palo Verde Unit 1 SRM HSST 01MY (Longitudinal Orientation)

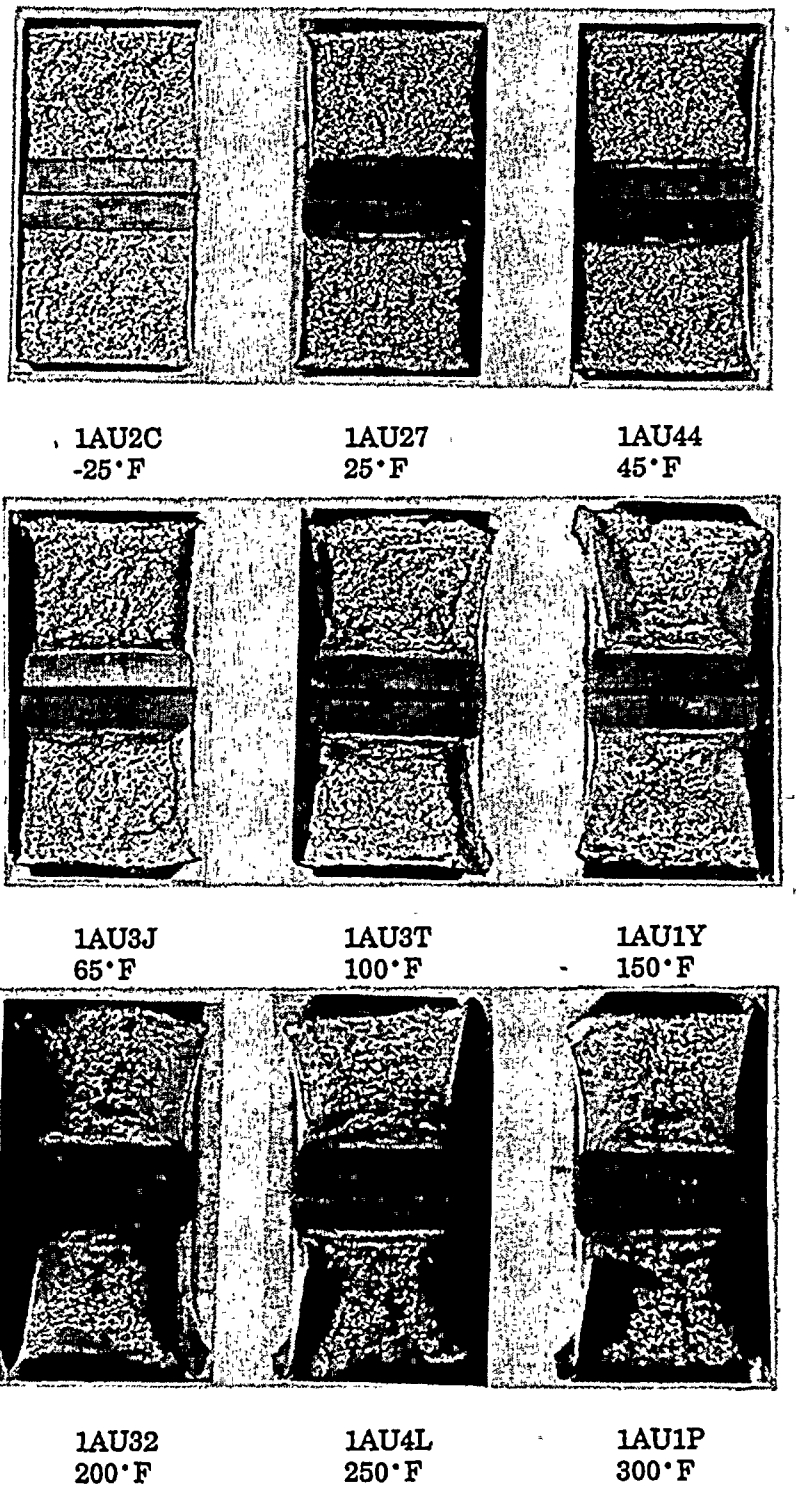

Figure 5-7 Charpy Impact Specimen Fracture Surfaces for Palo Verde Unit 1 Reactor Vessel Intermediate Shell Plate M-6701-2 (Longitudinal Orientation)

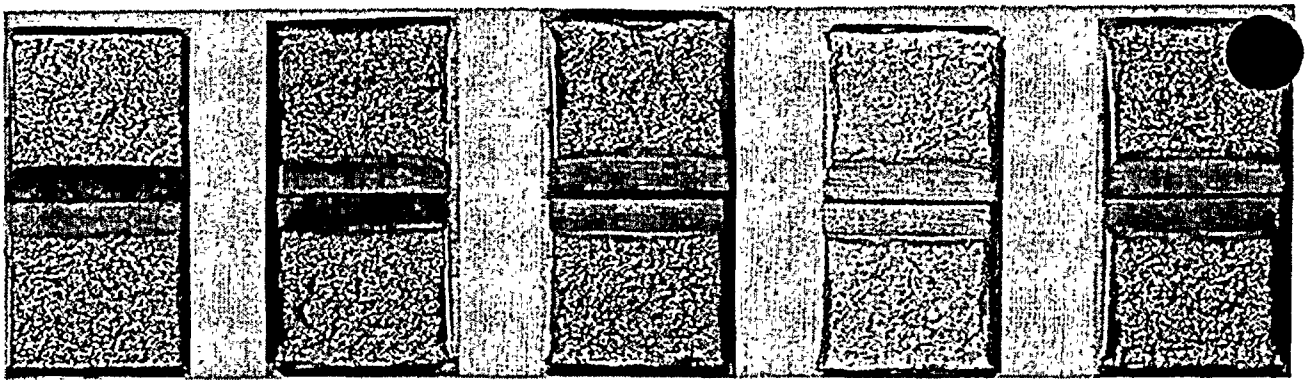

1AY4J -25°F | 1AY2Y 5°F | 1AY3M 35°F | 1AY4P 50°F | 1AY17 65°F

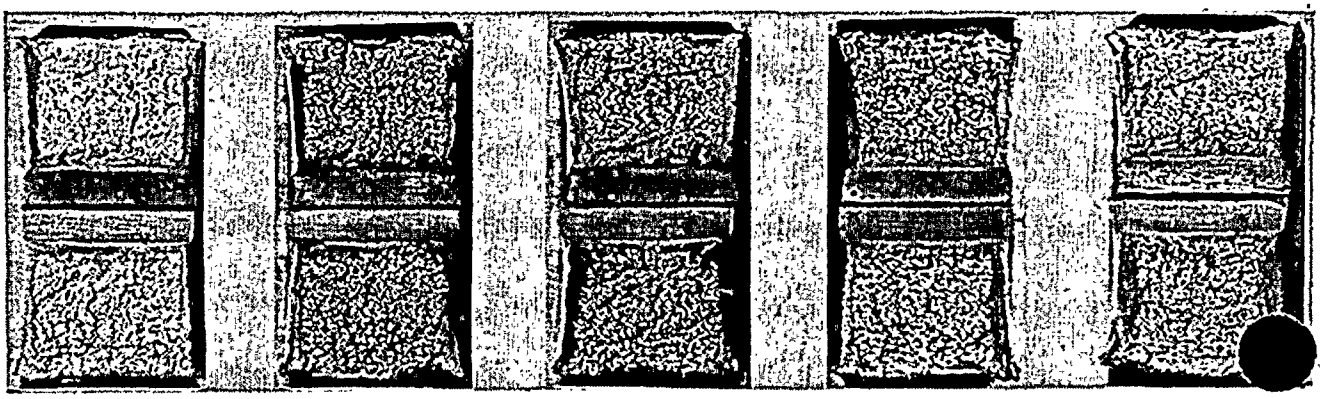

1AY53 75°F | 1AY5J 85°F | 1AY1C 100°F | 1AY2L 125°F | 1AY4U 150°F

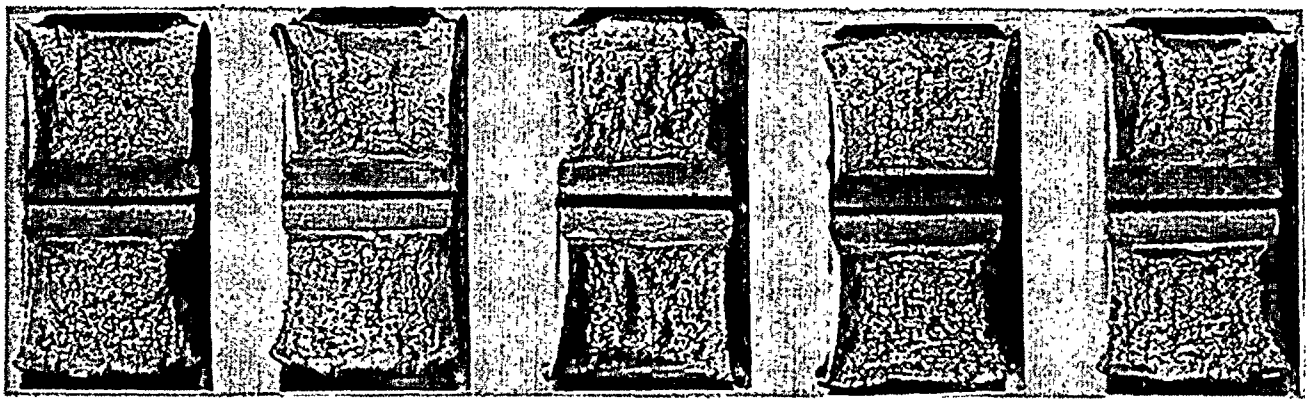

1AY4Y 185°F | 1AY32 225°F | 1AY1T 265°F | 1AY4B 300°F | 1AY1D 350°F

Figure 5-8 Charpy Impact Specimen Fracture Surfaces for Palo Verde Unit 1 Reactor Vessel Intermediate Shell Plate M-6701-2 (Transverse Orientation)

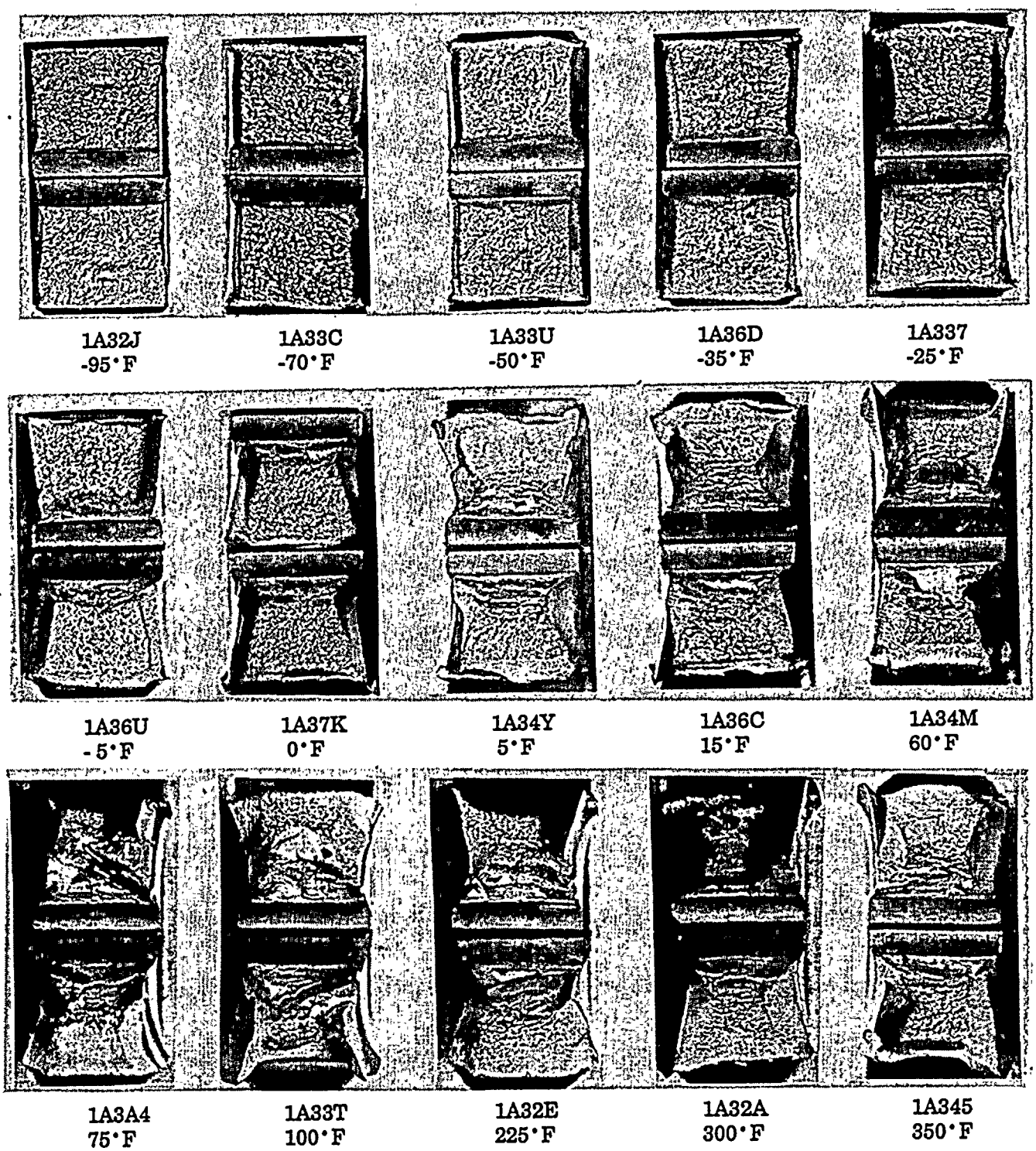

Figure 5-9 Charpy Impact Specimen Fracture Surfaces for Palo Verde Unit 1 Reactor Vessel Surveillance Weld Metal

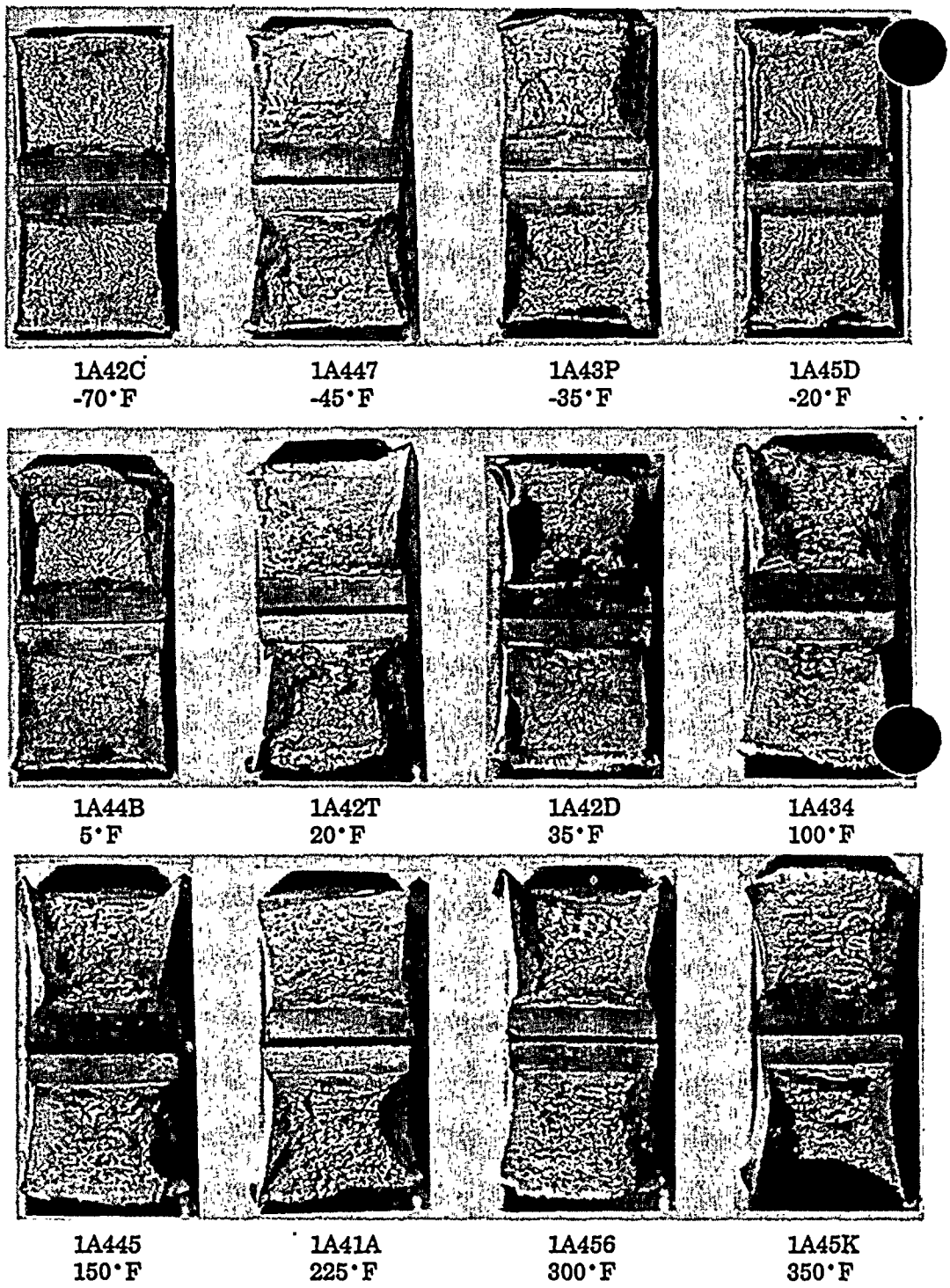

Figure 5-10 Charpy Impact Specimen Fracture Surfaces for Palo Verde Unit 1 Reactor Vessel Heat-Affected-Zone Metal

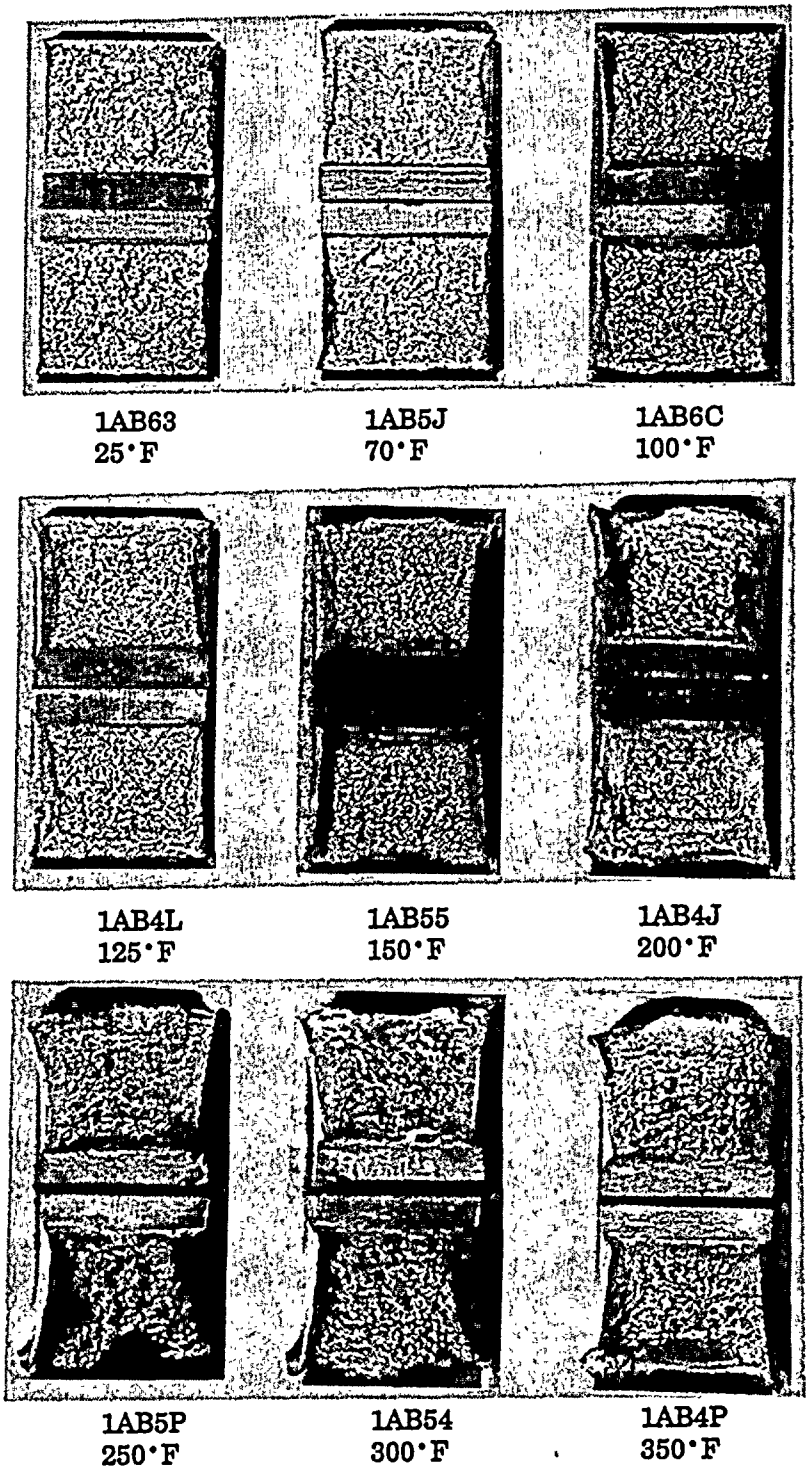

Figure 5-11 Charpy Impact Specimen Fracture Surfaces for Palo Verde Unit 1 SRM HSST 01MY (Longitudinal Orientation)

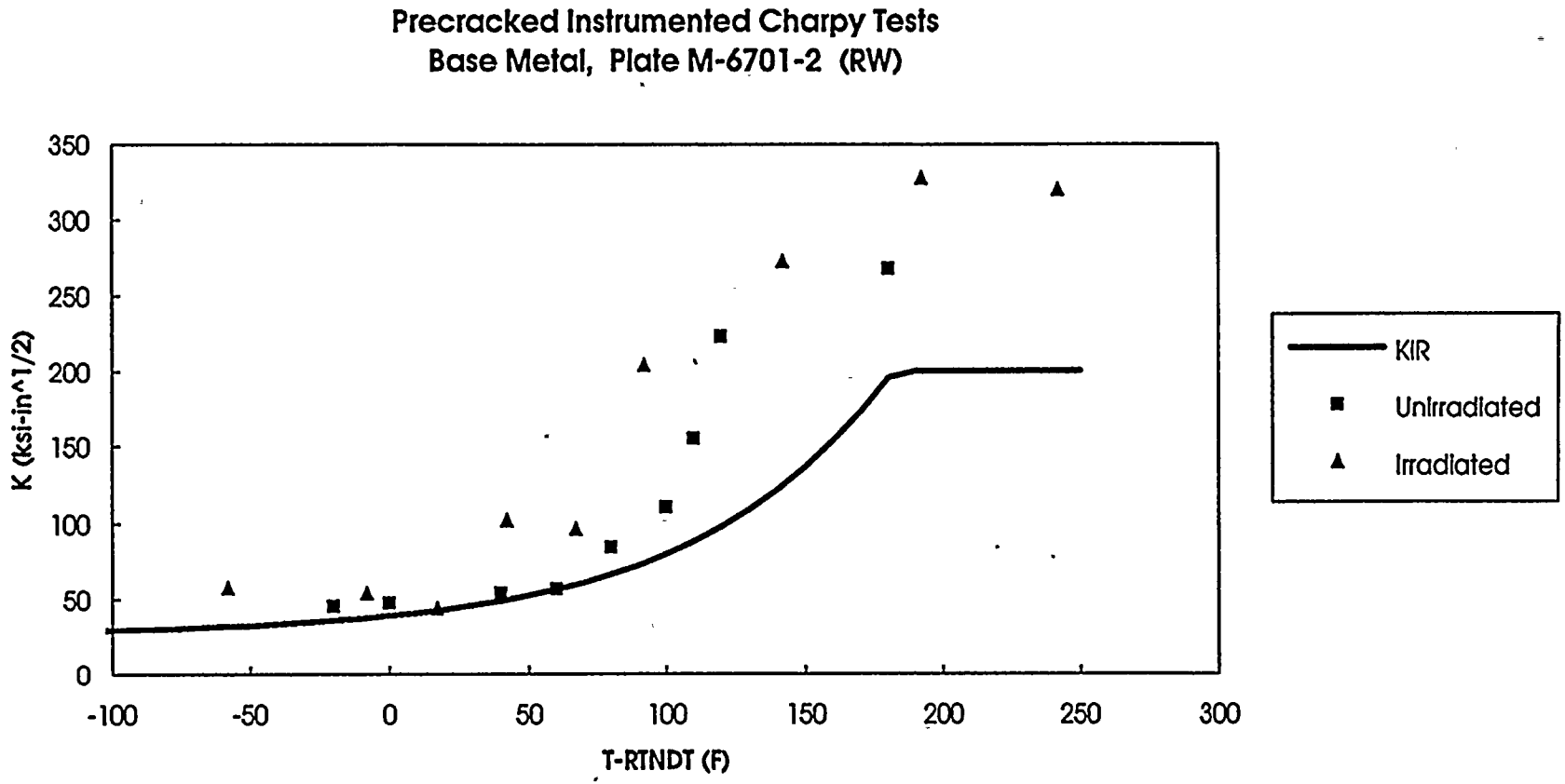

Figure 5-12 Comparison of Unirradiated and Irradiated Dynamic Fracture Toughness Values Determined by Testing of Precracked Charpy Specimens from Interm[redacted]Shell Plate M-6701-2 (Longitudinal Orientation)

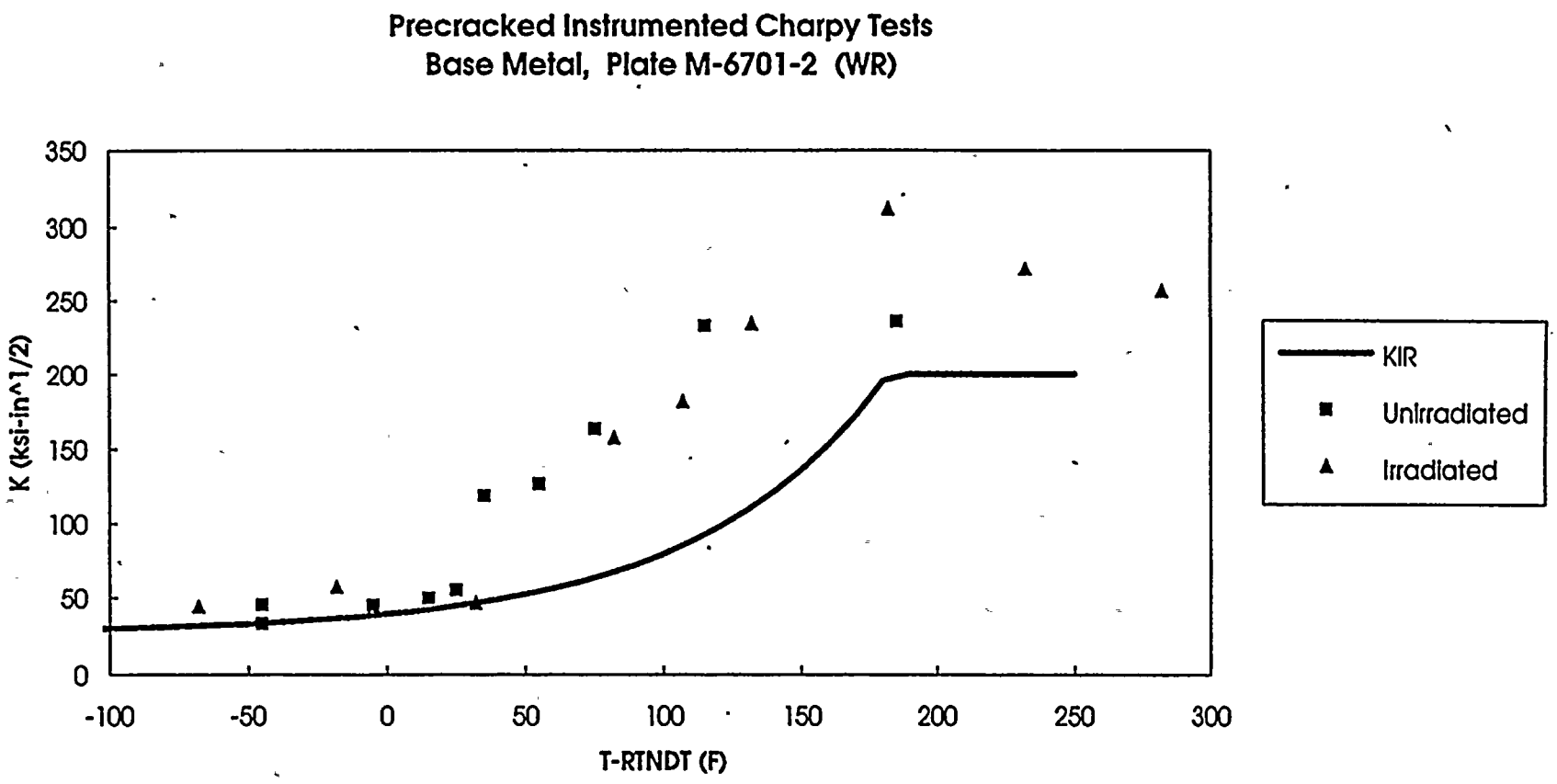

Figure 5-13 Comparison of Unirradiated and Irradiated Dynamic Fracture Toughness Values Determined by Testing of Precracked Charpy Specimens from Intermediate Shell Plate M-6701-2 (Transverse Orientation)

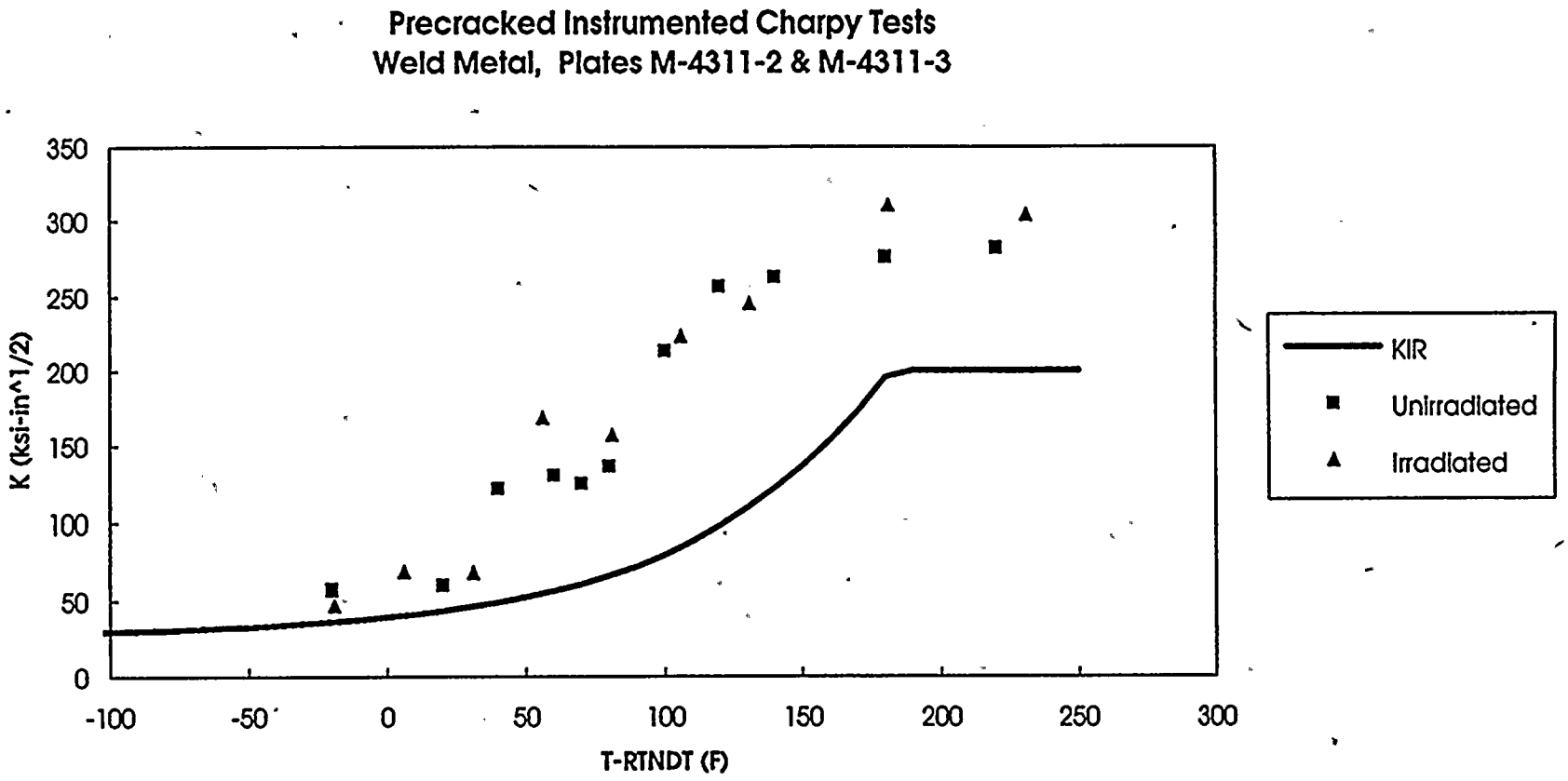

Figure 5-14 Comparison of Unirradiated and Irradiated Dynamic Fracture Toughness Values Determined by Testing of Precracked Charpy Specimens from the Pal[illegible]e Unit 1 Surveillance Weld Metal

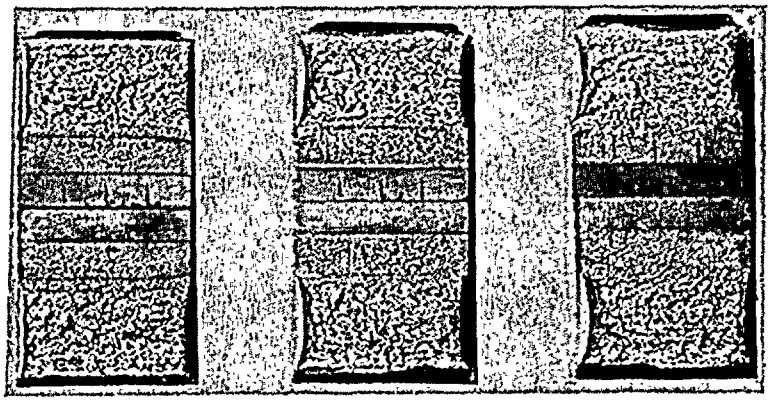

1AU3P
-25°F

1AU2Y
25°F

1AU3Y
50°F

1AU26
75°F

1AU2E
100°F

1AU4P
125°F

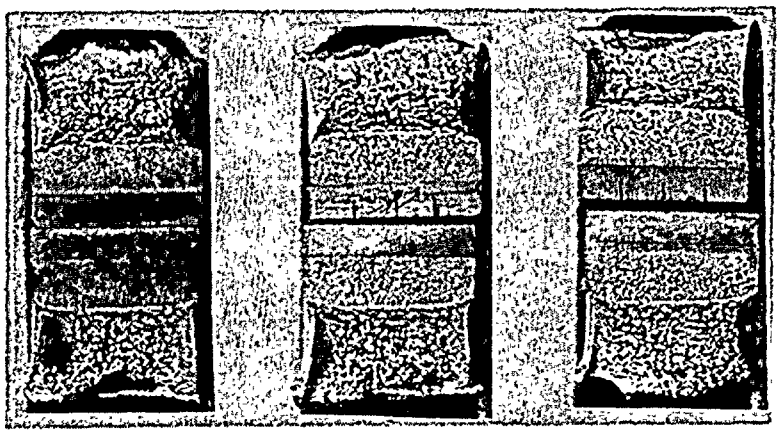

1AU2B
175°F

1AU2P
225°F

1AU24
275°F

Figure 5-15 Precracked Charpy Impact Specimen Fracture Surfaces for Palo Verde Unit 1 Intermediate Shell Plate M-6701-2 (Longitudinal Orientation)

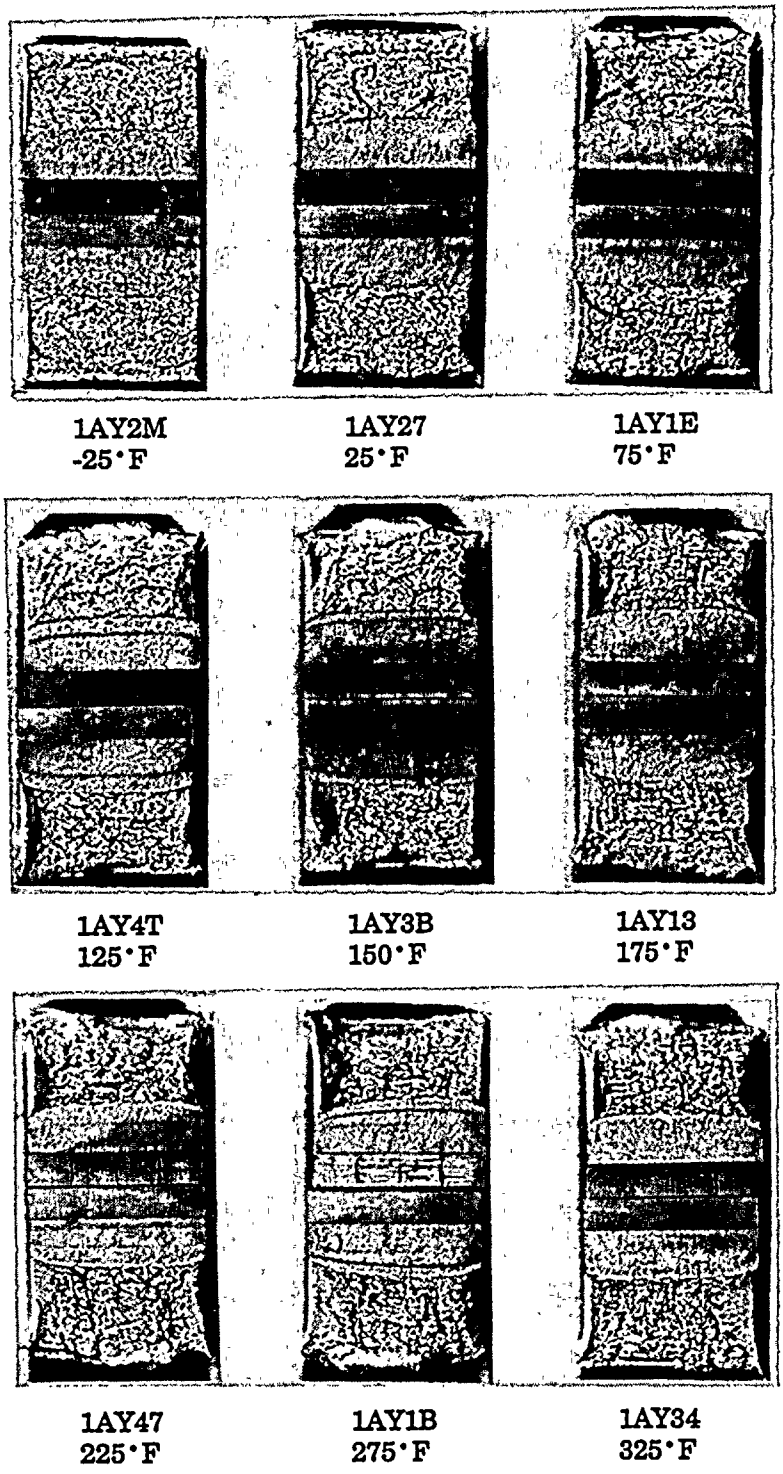

Figure 5-16 Precracked Charpy Impact Specimen Fracture Surfaces for Palo Verde Unit 1 Intermediate Shell Plate M-6701-2 (Transverse Orientation)

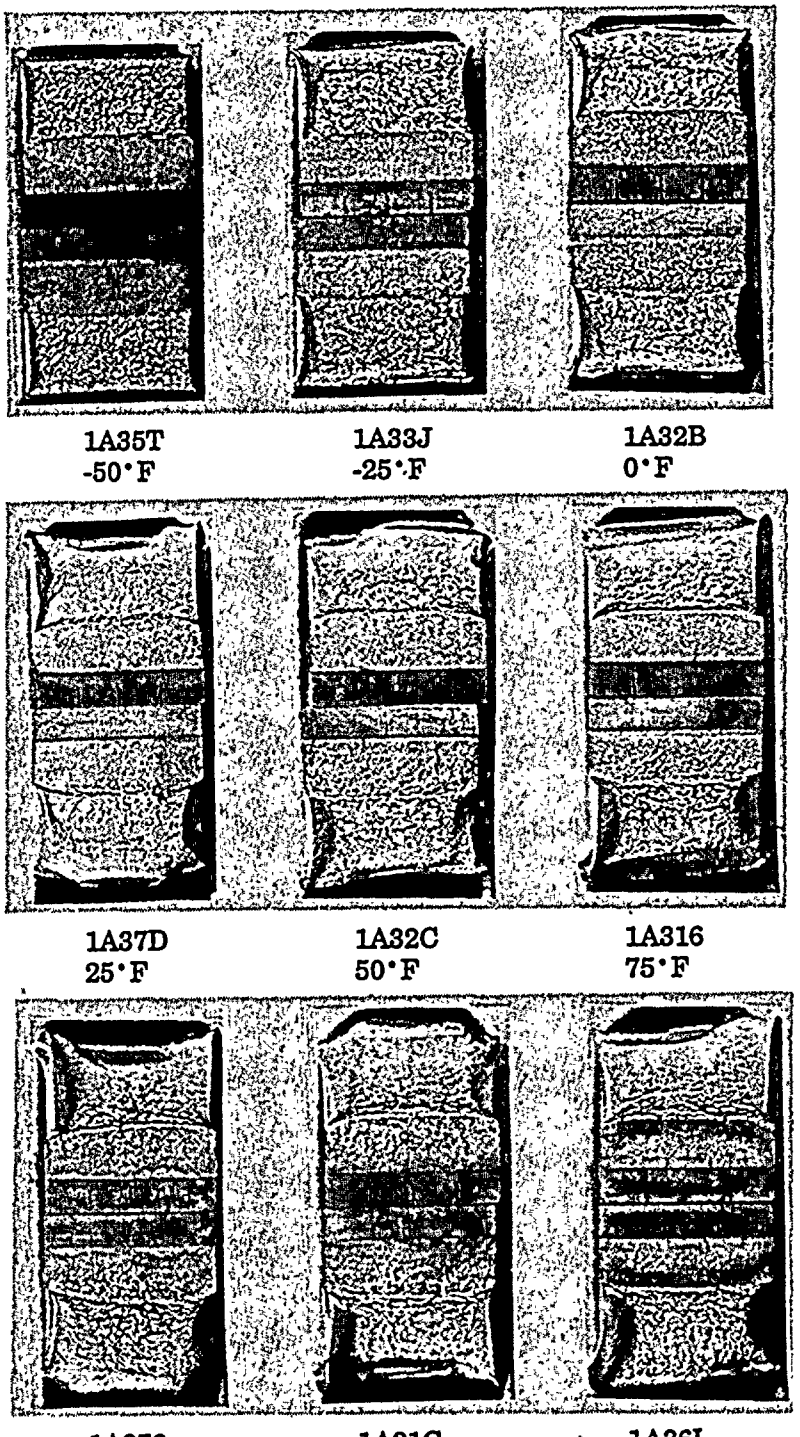

Figure 5-17 Precracked Charpy Impact Specimen Fracture Surfaces for Palo Verde Unit 1 Reactor Vessel Surveillance Weld Metal

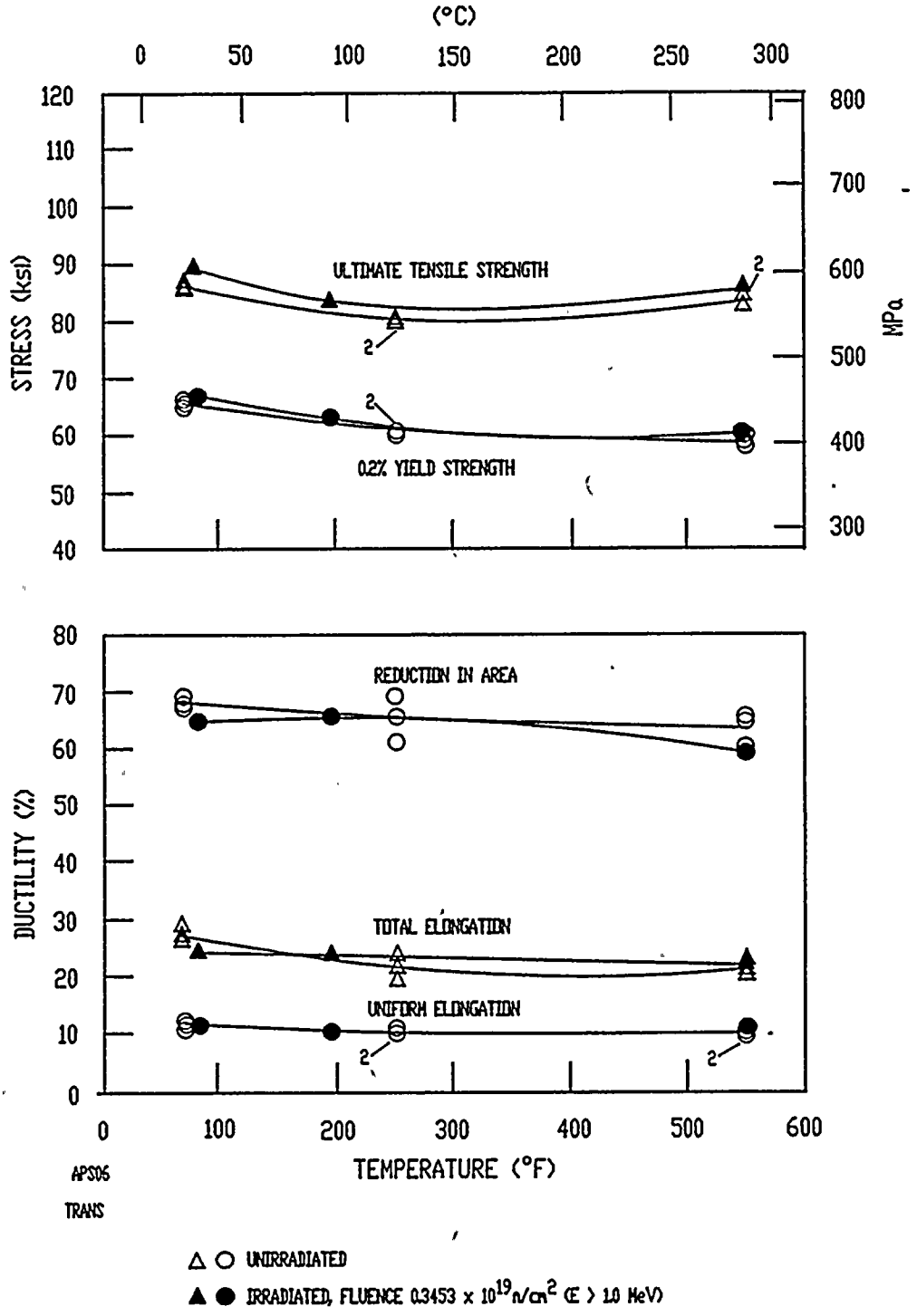

Figure 5-18 Tensile Properties for Palo Verde Unit 1 Reactor Vessel Intermediate Shell Plate M-6701-2 (Transverse Orientation)

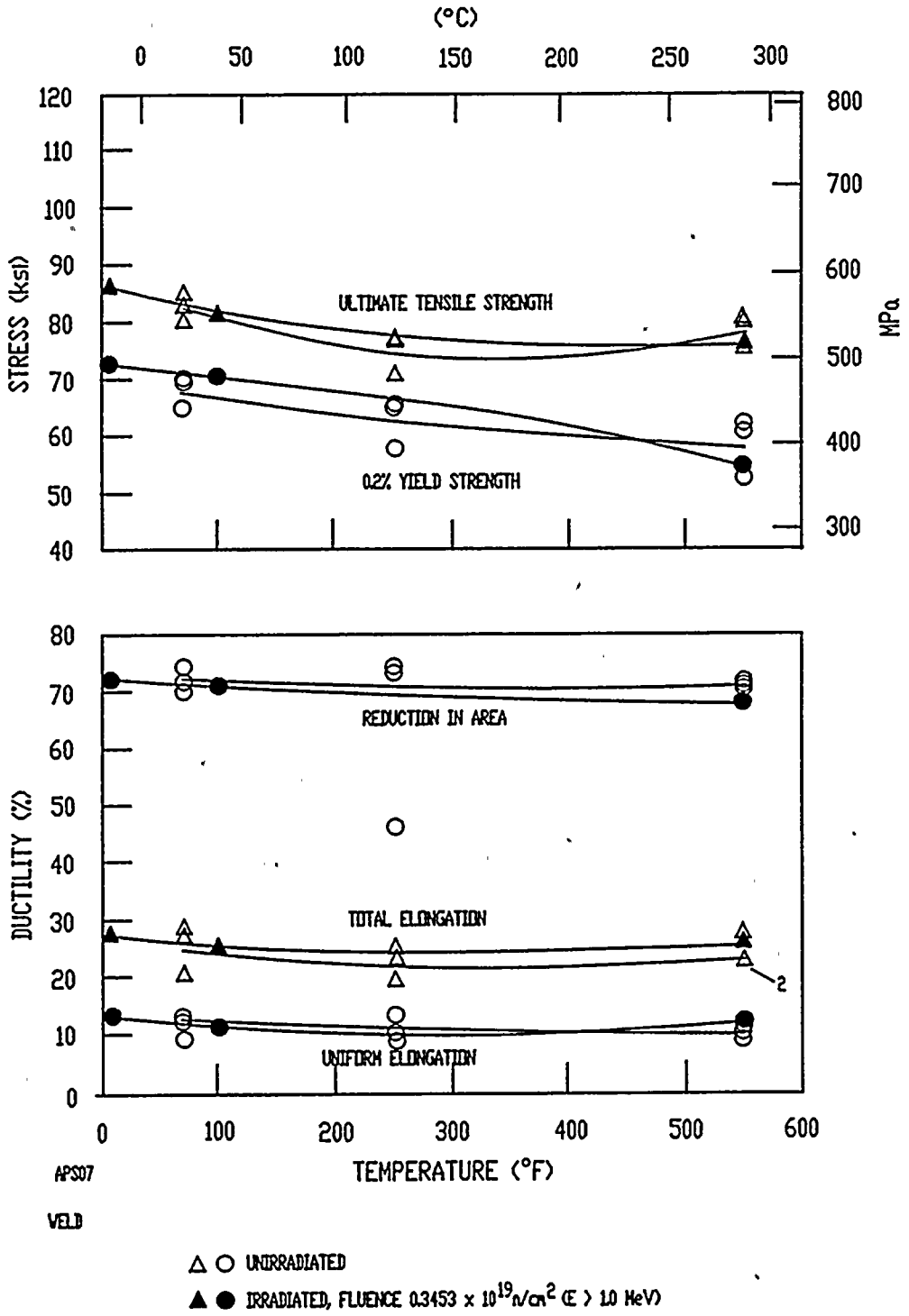

Figure 5-19 Tensile Properties for Palo Verde Unit 1 Reactor Vessel Surveillance Weld Metal

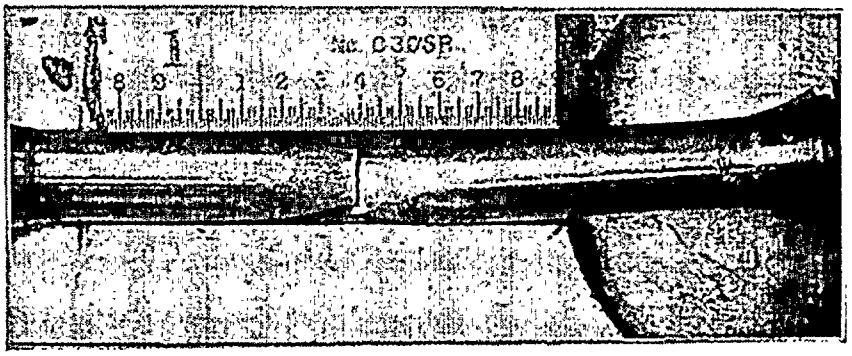

Specimen 1AYJ1 85°F

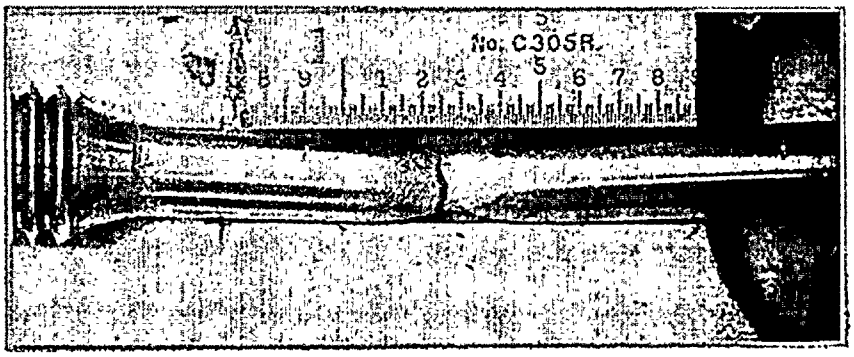

Specimen 1AYJD 190°F

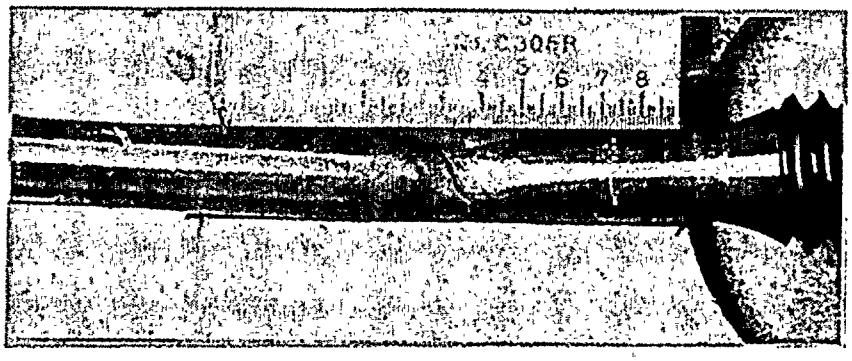

Specimen 1AYJ3 550°F

Figure 5-20 Fractured Tensile Specimens from Palo Verde Unit 1 Reactor Vessel Intermediate Shell Plate M-6701-2 (Transverse Orientation)

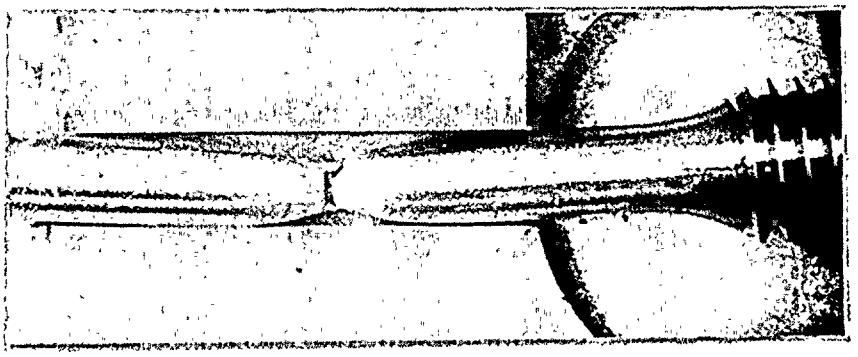

Specimen 1A3JA 10°F

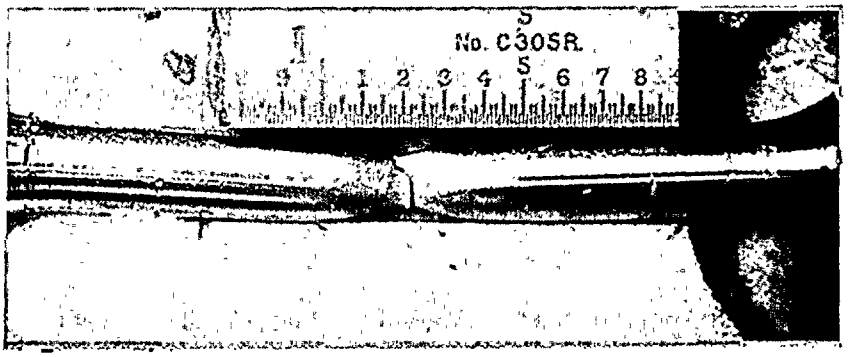

Specimen 1A3J1 100°F

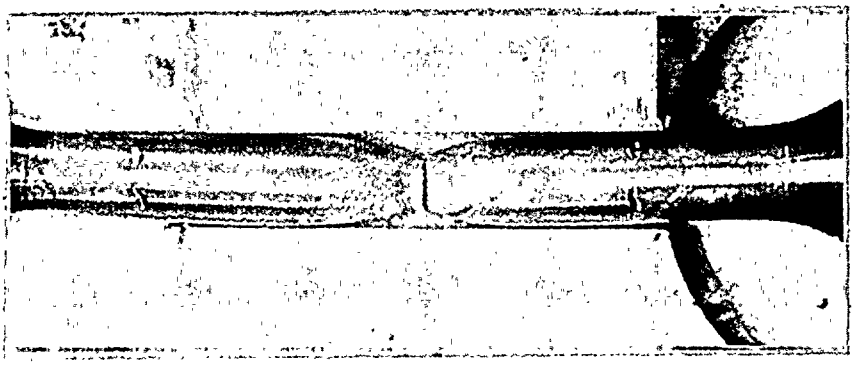

Specimen 1A3JD 550°F

Figure 5-21 Fractured Tensile Specimens from Palo Verde Unit 1 Reactor Vessel Surveillance Weld Metal

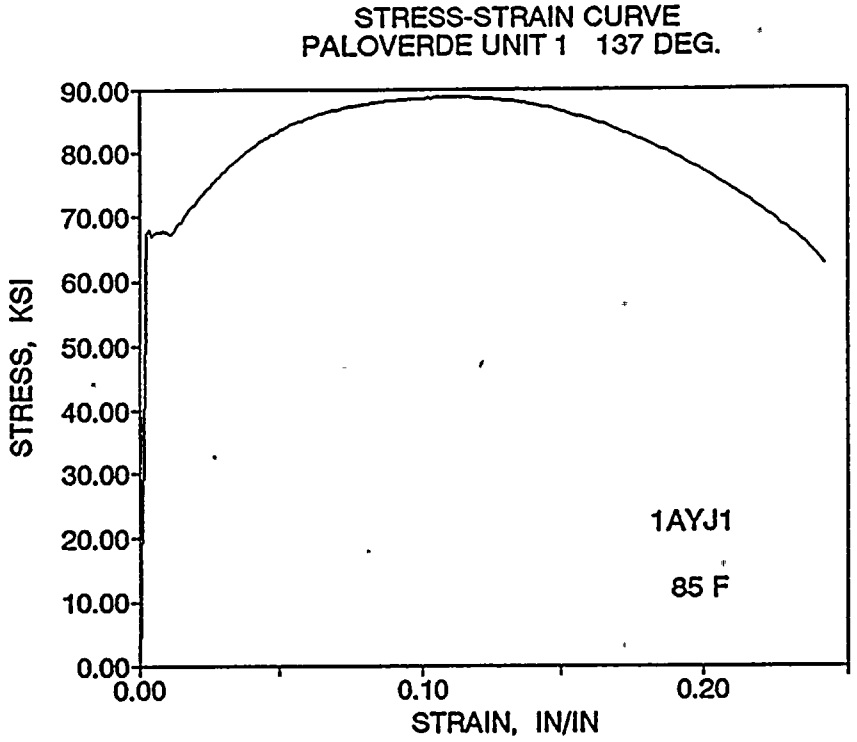

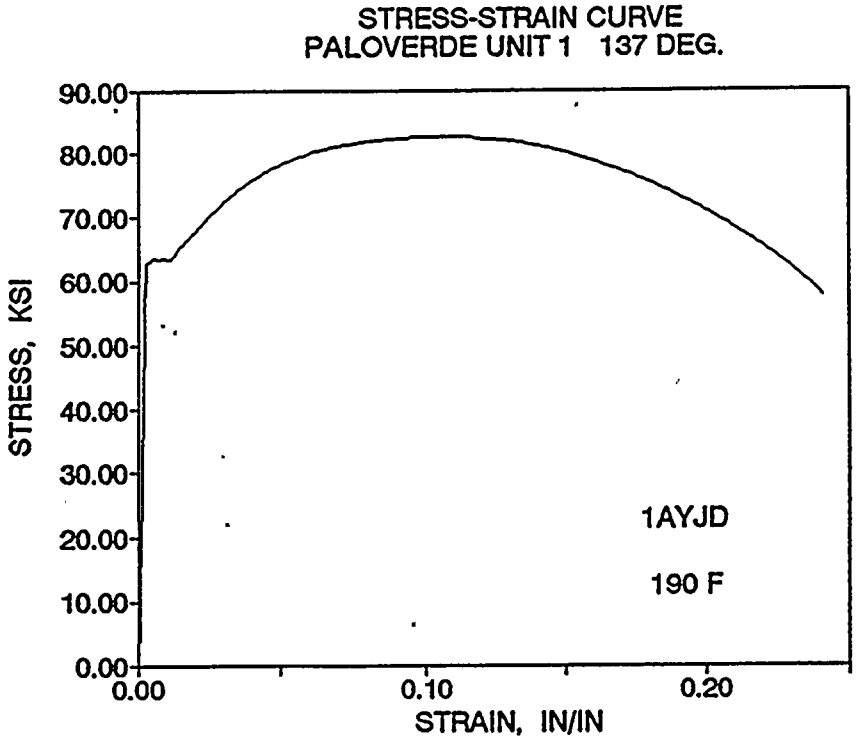

Figure 5-22 Engineering Stress-Strain Curves for Intermediate Shell Plate M-6701-2 Tensile Specimens 1AYJ1 and 1AYJD (Transverse Orientation)

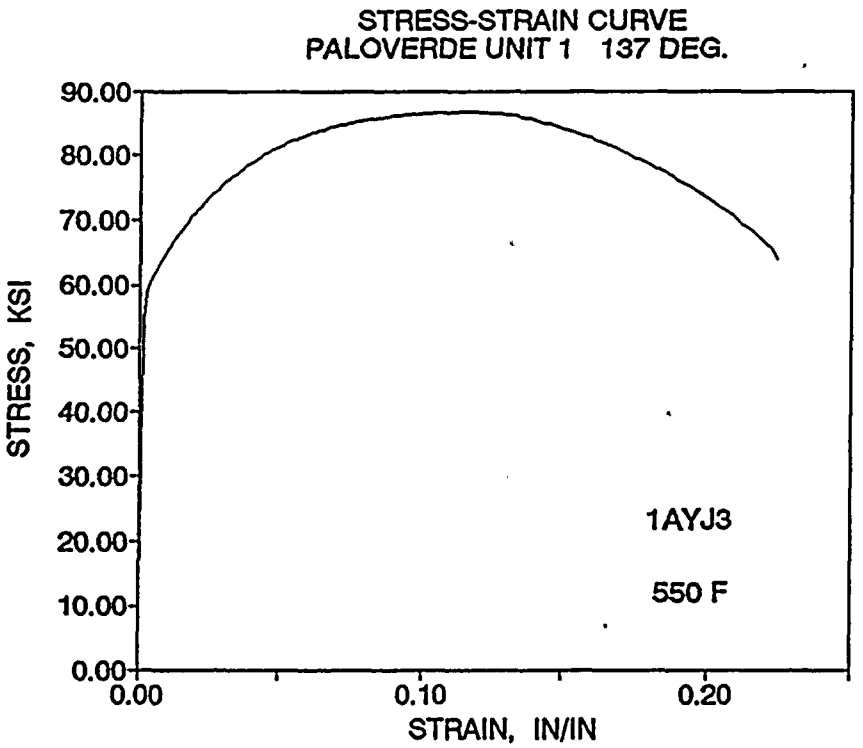

Figure 5-23 Engineering Stress-Strain Curve for Intermediate Shell Plate M-6701-2 Tensile Specimen 1AYJ3 (Transverse Orientation)

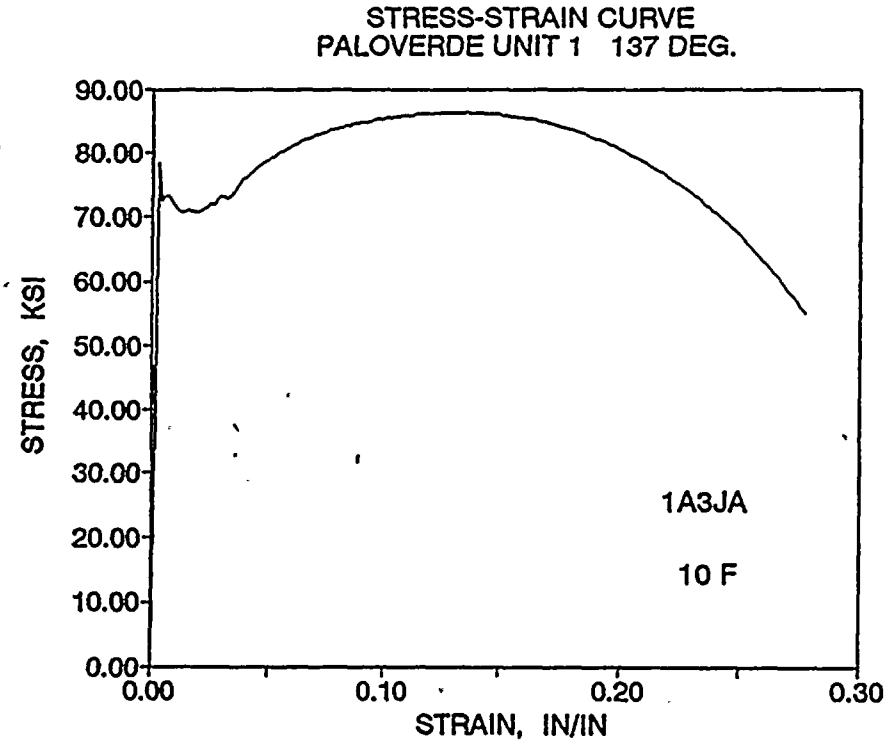

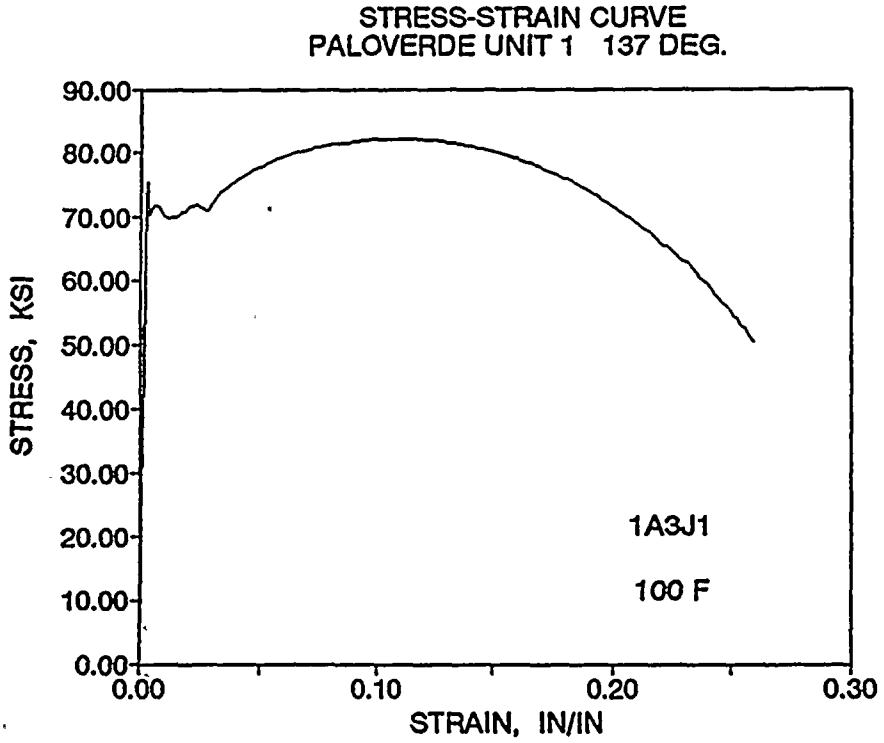

Figure 5-24 Engineering Stress-Strain Curves for Weld Metal Tensile Specimens 1A3JA and 1A3J1

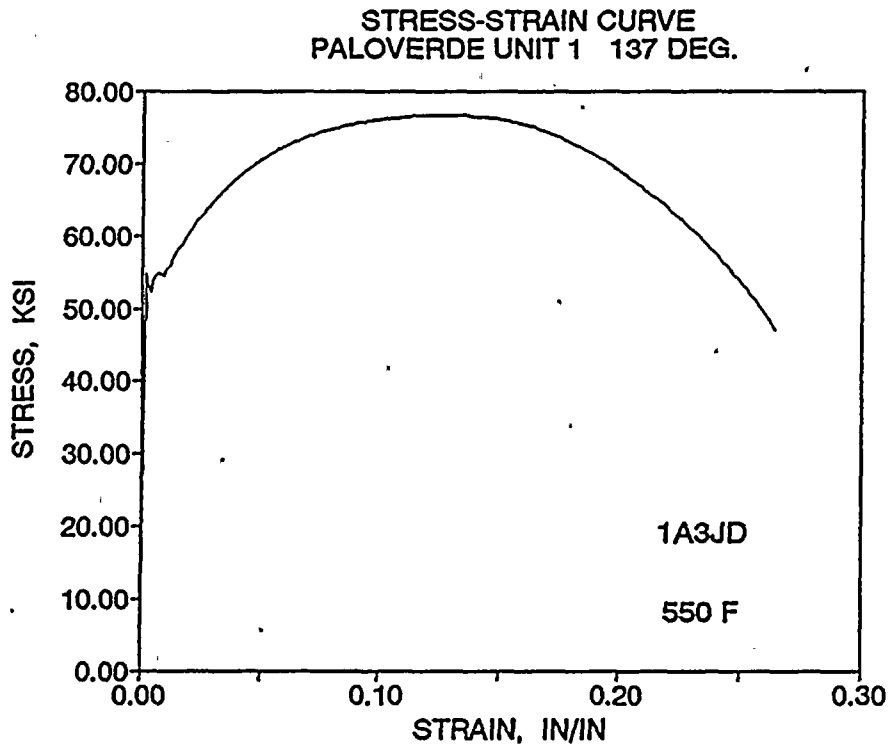

Figure 5-25 Engineering Stress-Strain Curve for Weld Metal Tensile Specimen 1A3JD

SECTION 6.0
RADIATION ANALYSIS AND NEUTRON DOSIMETRY

6.1 Introduction

Knowledge of the neutron environment within the reactor pressure vessel and surveillance capsule geometry is required as an integral part of LWR reactor pressure vessel surveillance programs for two reasons. First, in order to interpret the neutron radiation induced material property changes observed in the test specimens, the neutron environment (energy spectrum, flux, fluence) to which the test specimens were exposed must be known. Second, in order to relate the changes observed in the test specimens to the present and future condition of the reactor vessel, a relationship must be established between the neutron environment at various positions within the pressure vessel and that experienced by the test specimens. The former requirement is normally met by employing a combination of rigorous analytical techniques and measurements obtained with passive neutron flux monitors contained in each of the surveillance capsules. The latter information is generally derived solely from analysis.

The use of fast neutron fluence (E > 1.0 MeV) to correlate measured material property changes to the neutron exposure of the material has traditionally been accepted for development of damage trend curves as well as for the implementation of trend curve data to assess vessel condition. In recent years, however, it has been suggested that an exposure model that accounts for differences in neutron energy spectra between surveillance capsule locations and positions within the vessel wall could lead to an improvement in the uncertainties associated with damage trend curves as well as to a more accurate evaluation of damage gradients through the pressure vessel wall.

Because of this potential shift away from a threshold fluence toward an energy dependent damage function for data correlation, ASTM Standard Practice E853, "Analysis and Interpretation of Light Water Reactor Surveillance Results,"[13] recommends reporting displacements per iron atom (dpa) along with fluence (E > 1.0 MeV) to provide a data base for future reference. The energy dependent dpa function to be used for this evaluation is specified in ASTM Standard Practice E693, "Characterizing Neutron Exposures in Ferritic Steels in Terms of Displacements per Atom."[14] The application of the dpa parameter to the assessment of embrittlement gradients through the thickness of the pressure vessel wall has already been promulgated in Revision 2 to Regulatory Guide 1.99, "Radiation Damage to Reactor Vessel Materials."

This section provides the results of the neutron dosimetry evaluations performed in conjunction with the analysis of test specimens contained in surveillance capsule W137, withdrawn at the end of the fourth fuel cycle. This analysis is based on current state-of-the-art methodology and nuclear data, and is carried out in accordance with applicable ASTM standards[13 through 19]. The results provide a consistent fluence evaluation for use in determining the material properties of the Palo Verde Unit 1 reactor vessel.

In the dosimetry evaluation, fast neutron exposure parameters in terms of neutron fluence (E > 1.0 MeV), neutron fluence (E > 0.1 MeV), and iron atom displacements (dpa) are established for the capsule irradiation history. The analytical formalism relating the measured capsule exposure to the exposure of the vessel wall is described and used to project the integrated exposure of the vessel wall. Also, uncertainties associated with the derived exposure parameters at the surveillance capsules and with the projected exposure of the pressure vessel are provided.

6.2 Discrete Ordinates Analysis

A plan view of the reactor geometry at the core midplane is shown in Figure 4-1. Six irradiation capsules attached to the reactor vessel wall are included in the reactor design to constitute the reactor vessel surveillance program. The capsules are located at azimuthal angles of 38°, 43°, 137°, 142°, 230°, and 310° relative to the core cardinal axis as shown in Figure 4-1. A view of a surveillance capsule is shown in Figure 4-2. The stainless steel specimen containers are 1.5 by 0.75-inch and approximately 96 inches in height. The containers are positioned axially such that the test specimens are centered on the core midplane, thus spanning the central 8 feet of the 12.5 foot high reactor core.

From a neutronic standpoint, the surveillance capsules and associated support structures are significant. The presence of these materials has a marked effect on both the spatial distribution of neutron flux and the neutron energy spectrum in the region near the location of each capsule. In order to determine the neutron environment at the test specimen location, the capsules themselves must therefore be included in the analytical model. A plan view of the 1/8 core model used for the capsule fluence calculations is shown in Figure 6-1.

In performing the fast neutron exposure evaluations for the surveillance capsules and reactor vessel, two distinct sets of transport calculations were carried out. The first set, a computation in the

conventional forward mode, was used primarily to obtain relative neutron energy distributions throughout the reactor geometry as well as to establish relative radial distributions of exposure parameters {$\phi(E > 1.0$ MeV), $\phi(E > 0.1$ MeV), and dpa/sec} through the vessel wall. The neutron spectral information was required for the interpretation of neutron dosimetry withdrawn from the surveillance capsules as well as for the determination of exposure parameter ratios; i.e., [dpa/sec]/[$\phi(E > 1.0$ MeV)], within the pressure vessel geometry. The relative radial gradient information was required to permit the projection of measured exposure parameters to locations interior to the pressure vessel wall; i.e., the 1/4T, 1/2T, and 3/4T locations.

As shown in Figure 4-1, Palo Verde has four 45 degree octants with no surveillance capsules, two with one surveillance capsule at 40°, and two with two surveillance capsules at 38° and 43°. The forward calculational model is for the octant geometry with two surveillance capsules. Since the capsules are located adjacent to the vessel wall near the azimuthal maximum flux points, it was necessary to calculate the maximum vessel exposure using a second model with no surveillance capsules present. A comparison of the flux level at the reactor vessel inner radius with and without the surveillance capsules present at 38 and 43 degrees is shown in Figure 6-2. The calculation indicates that the maximum vessel fluence occurs near an angle of 40 degrees.

The second set of calculations consisted of a series of adjoint analyses relating the fast neutron flux, $\phi(E > 1.0$ MeV), at surveillance capsule positions and at several azimuthal locations on the pressure vessel inner radius to neutron source distributions within the reactor core. These calculations used separate models for each of the three octant types as appropriate to determine the fluence in each surveillance capsule position and at vessel positions without capsules. The source importance functions generated from these adjoint analyses provided the basis for all absolute exposure calculations and comparison with measurement. These importance functions, when combined with fuel cycle specific neutron source distributions, yielded absolute predictions of neutron exposure at the locations of interest for each cycle of irradiation. They also established the means to perform similar predictions and dosimetry evaluations for all subsequent fuel cycles. It is important to note that the cycle specific neutron source distributions utilized in these analyses included not only spatial variations of fission rates within the reactor core but also accounted for the effects of varying neutron yield per fission and fission spectrum introduced by the build-up of plutonium as the burnup of individual fuel assemblies increased.

The absolute cycle specific data from the adjoint evaluations together with the relative neutron energy spectra and radial distribution information from the reference forward calculation provided the means to:

1 - Evaluate neutron dosimetry obtained from surveillance capsules.
2 - Extrapolate dosimetry results to key locations at the inner radius and through the thickness of the pressure vessel wall.
3 - Enable a direct comparison of analytical prediction with measurement.
4 - Establish a mechanism for projection of pressure vessel exposure as the design of each new fuel cycle evolves.

The forward transport calculation for the reactor model summarized in Figure 6-1 was carried out in R,θ geometry using the DOT two-dimensional discrete ordinates code[20] and the SAILOR cross-section library[21]. The SAILOR library is a 47 energy group ENDF/B-IV based data set produced specifically for light water reactor applications. In these analyses anisotropic scattering was treated with a P_3 expansion of the scattering cross-sections and the angular discretization was modeled with an S_8 order of angular quadrature.

The core power distribution utilized in the forward transport calculations was taken as an average of the first four cycles of operation for Palo Verde Unit 1. This average distribution is considered to be close enough to that for typical cycles for all the Palo Verde units that it can be used generically for determination of the neutron spectra in the capsules and reactor vessel. The source neutron spectrum used was based on the burnup of the outer assemblies and utilized ENDF/B-V fission spectra for the contributing uranium and plutonium isotopes. The fuel power distributions were supplied by the Palo Verde staff in the form of beginning-of-cycle and end-of-cycle fuel pin and assembly burnups, and axial power shapes.

All adjoint calculations were also carried out using an S_8 order of angular quadrature and the P_3 cross-section approximation from the SAILOR library. Adjoint source locations were chosen at four azimuthal locations along the pressure vessel inner radius (0, 15, 30, and 45 degrees) as well as at the geometric center of each surveillance capsule. Again, these calculations were run in R,θ geometry to provide neutron source distribution importance functions for the exposure parameter of interest, in this case $\phi(E > 1.0\ MeV)$.

Having the importance functions and appropriate core source distributions, the response of interest is calculated as:

$$R(r,\theta) = \int_{r'} \int_{\theta'} \int_{E} I_{r,\theta}(r',\theta',E)\ S(r',\theta',E)\ r'\ dr'\ d\theta'\ dE$$

where:

$R(r,\theta)$	=	$\phi(E > 1.0$ MeV) at radius r and azimuthal angle θ.
$I_{r,\theta}(r',\theta',E)$	=	Adjoint source importance function at radius r', azimuthal angle θ', and neutron source energy E.
$S(r',\theta',E)$	=	Neutron source strength at core location r',θ' and energy E.

Although the adjoint importance functions used in this analysis were based on a response function defined by the threshold neutron flux $\phi(E > 1.0$ MeV), prior calculations[22] have shown that, while the variation in fuel loading patterns significantly impacts both the magnitude and spatial distribution of the neutron field, changes in the relative neutron energy spectrum are of second order. Thus, for a given location the ratio of [dpa/sec]/[$\phi(E > 1.0$ MeV)] is insensitive to changing core source distributions. In the application of these adjoint importance functions to the Palo Verde Unit 1 reactor, therefore, the iron atom displacement rates (dpa/sec) and the neutron flux $\phi(E > 0.1$ MeV) were computed on a cycle specific basis by using [dpa/sec]/[$\phi(E > 1.0$ MeV)] and [$\phi(E > 0.1$ MeV)]/[$\phi(E > 1.0$ MeV)] ratios from the forward analysis in conjunction with the cycle specific $\phi(E > 1.0$ MeV) solutions from the individual adjoint evaluations.

The reactor core power distributions used in the plant specific adjoint calculations were taken from the fuel cycle design data supplied for the first four operating cycles of Palo Verde Unit 1 .

Selected results from the neutron transport analyses are provided in Tables 6-1 through 6-5. The data listed in these tables establish the means for absolute comparisons of analysis and measurement for the capsule irradiation periods and provide the means to correlate dosimetry results with the corresponding exposure of the pressure vessel wall.

In Table 6-1, the calculated exposure parameters [$\phi(E > 1.0$ MeV), $\phi(E > 0.1$ MeV), and dpa/sec] are given at the geometric center of the three surveillance capsule positions for the plant specific core power distributions. The plant specific data, based on the adjoint transport analysis, are meant to

establish the absolute comparison of measurement with analysis. Similar data are given in Table 6-2 for the pressure vessel inner radius. Again, the three pertinent exposure parameters are listed for the cycle one through four plant specific power distributions. It is important to note that the data for the vessel inner radius were taken at the clad/base metal interface; and, thus, represent the maximum predicted exposure levels of the vessel wall itself at the axial midplane.

Radial gradient information applicable to $\phi(E > 1.0\ MeV)$, $\phi(E > 0.1\ MeV)$, and dpa/sec is given in Tables 6-3, 6-4, and 6-5, respectively. The data, obtained from the forward neutron transport calculation, are presented on a relative basis for each exposure parameter at several azimuthal locations. Exposure distributions through the vessel wall may be obtained by normalizing the calculated or projected exposure at the vessel inner radius to the gradient data listed in Tables 6-3 through 6-5. Note that these distributions are developed for the case with no surveillance capsules present. The effect of the capsules is to slightly reduce the relative flux at the inside of the vessel at angles within about $\pm$ 2 degrees of the capsule location.

An example of the derivation of the neutron flux $\phi(E > 1.0\ MeV)$ at the 1/4T depth in the pressure vessel wall along the 45° azimuth is given by:

$$\phi_{1/4T}(45°) = \phi(233.756,\ 45°)\ F(239.511,\ 45°)$$

where: $\phi_{1/4T}(45°)$ = Projected neutron flux at the 1/4T position on the 45° azimuth.

$\phi(233.756,45°)$ = Projected or calculated neutron flux at the vessel inner radius on the 45° azimuth.

$F(239.511,45°)$ = Ratio of the neutron flux at the 1/4T position to the flux at the vessel inner radius for the 45° azimuth. This ratio is obtained by interpolation from Table 6-3.

Similar expressions apply for exposure parameters expressed in terms of $\phi(E > 0.1\ MeV)$ and dpa/sec where the attenuation function F is obtained from Tables 6-4 and 6-5, respectively.

6.3 Neutron Dosimetry

The passive neutron sensors included in the Palo Verde Unit 1 surveillance program are listed in Table 6-6. Also given in Table 6-6 are the primary nuclear reactions and associated nuclear constants that were used in the evaluation of the neutron energy spectrum within the surveillance capsules and in the

subsequent determination of the various exposure parameters of interest [$\phi(E > 1.0$ MeV), $\phi(E > 0.1$ MeV), dpa/sec]. The relative locations of the neutron sensors within the capsules are shown in Figure 4-2. Since the dosimeters are all located very close to the same distance from the core at the radial center of the capsule, no gradient corrections were necessary. The iron, copper, titanium, and uranium (bare and covered) were each placed at three axial locations in the capsule near the top, middle, and bottom, respectively. The cobalt-aluminum monitors (bare and covered), as well as the nickel and sulfur, were only placed in the middle location in space provided by an extra dosimetry holder.

The use of passive monitors such as those listed in Table 6-6 does not yield a direct measure of the energy dependent neutron flux at the point of interest. Rather, the activation or fission process is a measure of the integrated effect that the time and energy dependent neutron flux has on the target material over the course of the irradiation period. An accurate assessment of the average neutron flux level incident on the various monitors may be derived from the activation measurements only if the irradiation parameters are well known. In particular, the following variables are of interest:

- The measured specific activity of each monitor.
- The physical characteristics of each monitor.
- The operating history of the reactor.
- The energy response of each monitor.
- The neutron energy spectrum at the monitor location.

The specific activity of each of the neutron monitors was determined using established ASTM procedures[23 through 29]. Following sample preparation and weighing, the activity of each monitor was determined by means of a lithium-drifted germanium, Ge(Li), gamma spectrometer. The irradiation history of the Palo Verde Unit 1 reactor during cycles one through four was supplied by NUREG-0020, "Licensed Operating Reactors Status Summary Report," for the applicable period. The irradiation history applicable to capsule W137 is given in Table 6-7.

Having the measured specific activities, the physical characteristics of the sensors, and the operating history of the reactor, reaction rates referenced to full power operation were determined from the following equation:

$$R = \frac{A}{N_0 \, F \, Y \sum \frac{P_j}{P_{ref}} \, C_j \, [1-e^{-\lambda t_j}] \, [e^{-\lambda t_d}]}$$

where:

R	=	Reaction rate averaged over the irradiation period and referenced to operation at a core power level of P_{ref} (rps/nucleus).
A	=	Measured specific activity (dps/gm).
N_0	=	Number of target element atoms per gram of sensor.
F	=	Weight fraction of the target isotope in the sensor material.
Y	=	Number of product atoms produced per reaction.
P_j	=	Average core power level during irradiation period j (MW).
P_{ref}	=	Maximum or reference power level of the reactor (MW).
C_j	=	Calculated ratio of $\phi(E > 1.0$ MeV) during irradiation period j to the time weighted average $\phi(E > 1.0$ MeV) over the entire irradiation period.
λ	=	Decay constant of the product isotope (1/sec).
t_j	=	Length of irradiation period j (sec).
t_d	=	Decay time following irradiation period j (sec).

and the summation is carried out over the total number of monthly intervals comprising the irradiation period.

In the equation describing the reaction rate calculation, the ratio $[P_j]/[P_{ref}]$ accounts for month by month variation of reactor core power level within any given fuel cycle as well as over multiple fuel cycles. The ratio C_j, which was calculated for each fuel cycle using the adjoint transport technology discussed in Section 6.2, accounts for the change in sensor reaction rates caused by variations in flux level induced by changes in core spatial power distributions from fuel cycle to fuel cycle. For a single cycle irradiation C_j is normally taken to be 1.0. However, for multiple cycle irradiations, particularly those employing low leakage fuel management, the additional C_j term can be a significant correction.

For the irradiation history of capsule W137, the flux level term in the reaction rate calculations was developed from the plant specific analysis provided in Table 6-1. Measured and saturated reaction product specific activities as well as the derived full power reaction rates are listed in Table 6-8 for capsule W137. Reactions that are cadmium shielded are denoted in this table by an asterisk (*).

Measured activities are given as corrected to 3/16/94. The table contains average saturated reaction rates (reactions per second) for each dosimeter. The average values were used to derive a average value of flux for the capsule since the variation with axial position was found to be small and showed no correlation with the calculated axial shape (Figure 6-3). The cadmium covered U-238 measurements were found to exhibit inconsistencies, which most likely derive from uncertainty in the amount of uranium present. This uncertainty is large due to fusion of the cadmium with the uranium which prevents an accurate weight determination. The bare U-238 measurements also exhibit scatter which may be due to varying contributions from U-235 and Pu-239 fissions caused by shielding variations. Neither the bare nor the covered U-238 results were used in the fluence analysis.

Values of key fast neutron exposure parameters were derived from the measured reaction rates using the FERRET least squares adjustment code[30]. The FERRET approach used the measured reaction rate data, sensor reaction cross-sections, and a calculated trial spectrum as input and proceeded to adjust the group fluxes from the trial spectrum to produce a best fit (in a least squares sense) to the measured reaction rate data. The "measured" exposure parameters along with the associated uncertainties were then obtained from the adjusted spectrum.

In the FERRET evaluations, a log-normal least squares algorithm weights both the a priori values and the measured data in accordance with the assigned uncertainties and correlations. In general, the measured values f are linearly related to the flux ϕ by some response matrix A:

$$f_i^{(s,\alpha)} = \sum_g A_{ig}^{(s)} \phi_g^{(\alpha)}$$

where i indexes the measured values belonging to a single data set s, g designates the energy group, and α delineates spectra that may be simultaneously adjusted. For example,

$$R_i = \sum_g \sigma_{ig} \phi_g$$

relates a set of measured reaction rates R_i to a single spectrum ϕ_g by the multigroup reaction cross-section σ_{ig}. The log-normal approach automatically accounts for the physical constraint of positive fluxes, even with large assigned uncertainties.

In the least squares adjustment, the continuous quantities (i.e., neutron spectra and cross-sections) were approximated in a multi-group format consisting of 53 energy groups. The trial input spectrum was converted to the FERRET 53 group structure using the SAND-II code[31]. This procedure was carried out by first expanding the 47 group calculated spectrum into the SAND-II 620 group structure using a

SPLINE interpolation procedure in regions where group boundaries do not coincide. The 620 point spectrum was then re-collapsed into the group structure used in FERRET.

The sensor set reaction cross-sections, obtained from the ENDF/B-V dosimetry file, were also collapsed into the 53 energy group structure using the SAND-II code. In this instance, the trial spectrum, as expanded to 620 groups, was employed as a weighting function in the cross-section collapsing procedure. Reaction cross-section uncertainties in the form of a 53 x 53 covariance matrix for each sensor reaction were also constructed from the information contained on the ENDF/B-V data files. These matrices included energy group to energy group uncertainty correlations for each of the individual reactions. However, correlations between cross-sections for different sensor reactions were not included. The omission of this additional uncertainty information does not significantly impact the results of the adjustment.

Due to the importance of providing a trial spectrum that exhibits a relative energy distribution close to the actual spectrum at the sensor set locations, the neutron spectrum input to the FERRET evaluation was taken from the center of the surveillance capsule modeled in the forward transport calculation with a source distribution averaged over the first four cycles. While the 53 x 53 group covariance matrices applicable to the sensor reaction cross-sections were developed from the ENDF/B-V data files, the covariance matrix for the input trial spectrum was constructed from the following relation:

$$M_{gg'} = R_n^2 + R_g \, R_{g'} \, P_{gg'}$$

where R_n specifies an overall fractional normalization uncertainty (i.e., complete correlation) for the set of values. The fractional uncertainties R_g specify additional random uncertainties for group g that are correlated with a correlation matrix given by:

$$P_{gg'} = [1-\theta] \, \delta_{gg'} + \theta \, e^{-H}$$

where:

$$H = \frac{(g-g')^2}{2 \, \gamma^2}$$

The first term in the correlation matrix equation specifies purely random uncertainties, while the second term describes short range correlations over a group range γ (θ specifies the strength of the latter term). The value of δ is 1 when $g = g'$ and 0 otherwise. For the trial spectrum used in the current evaluations, a short range correlation of $\gamma = 6$ groups was used. This choice implies that neighboring groups are strongly correlated when θ is close to 1. Strong long range correlations (or

anti-correlations) were justified based on information presented by R. E. Maerker[32]. Maerker's results are closely duplicated when $\gamma = 6$.

The uncertainties associated with the measured reaction rates included both statistical (counting) and systematic components. The systematic component of the overall uncertainty accounts for counter efficiency, counter calibrations, irradiation history corrections, and corrections for competing reactions in the individual sensors. Uncertainty estimates for the non-fission dosimeter results were taken to be 5% (10% for the cobalt monitors) based on consistency studies of capsule dosimetry[33].

Results of the FERRET evaluations of the capsule W137 dosimetry are given in Tables 6-9 through 6-12. The data summarized in Table 6-9 include fast neutron exposure evaluations in terms of $\Phi(E > 1.0$ MeV), $\Phi(E > 0.1$ MeV), and dpa. In general good results were achieved in the fits of the adjusted spectra to the individual measured reaction rates (except for the U-238 which was assigned a large uncertainty as discussed above) as shown in Table 6-10. The adjusted spectra from the least squares evaluations are given in Table 6-11 in the FERRET 53 energy group structure. Table 6-12 compares the flux and fluence results derived from the dosimeter measurements (Table 6-9) with the calculated values (Table 6-1). The results for capsule W137 are the first results for a capsule from Palo Verde Unit 1 and thus cannot be compared with other similar Unit 1 capsules to check for consistency. However, a similar capsule was recently analyzed for Unit 2 and similar results were obtained (Unit 1 C/M values are about 10-12% above those for Unit 2).[34] In addition, the good agreement between calculated and measured values supports the adequacy of the analysis.

6.4 Projections of Pressure Vessel Exposure

Neutron exposure projections at key locations on the pressure vessel inner radius are given in Table 6-13. Along with the current (4.53 EFPY) exposure, projections are also provided for exposure periods of 15 EFPY and 32 EFPY. In computing these vessel exposures, the calculated values from Table 6-2 were scaled by the average measurement/calculation ratios (M/C) observed from the evaluations of dosimetry from capsule W137 for each fast neutron exposure parameter. This procedure resulted in bias factors of 1.07, 1.16, and 1.14 being applied to the calculated values of $\Phi(E > 1.0$ MeV), $\Phi(E > 0.1$ MeV), and dpa, respectively. Projections for future operation were based on the assumption that the average exposure rates characteristic of the cycle one through four irradiation would continue to be applicable throughout plant life. This is expected to be conservative since the fuel loading patterns employed since the first cycle have led to lower fluence than this average.

The overall uncertainty associated with the best estimate exposure projections at the pressure vessel wall depends on the individual uncertainties in the measurement process, the uncertainty in the dosimetry location, and on the uncertainty in the extrapolation of results from the measurement point to the point(s) of interest in the vessel wall. For Palo Verde Unit 1, the estimated extrapolation uncertainty is 5% and the uncertainty in the plant specific measurement/calculation bias factor derived from the surveillance capsule measurement is 12% as derived by the least squares process. These uncertainties are independent and so the total uncertainty is 13% as calculated by the square root of the sum of the squares of the individual uncertainty contributors. This 13% uncertainty in the projected exposure of the pressure vessel wall is a 1σ estimate for $\Phi(E > 1.0\ MeV)$.

Exposure projections through the vessel at 15 EFPY and 32 EFPY are provided in Table 6-14 for use in the development of heatup and cooldown curves for Palo Verde Unit 1. Data are calculated based on both a $\Phi(E > 1.0\ MeV)$ slope and a plant specific dpa slope through the vessel wall. The dpa equivalent fast neutron fluence levels for the 1/4T and 3/4T positions are defined by the relations:

$$\phi(1/4T) = \phi(0T)\ \frac{dpa(1/4T)}{dpa(0T)}$$

and

$$\phi(3/4T) = \phi(0T)\ \frac{dpa(3/4T)}{dpa(0T)}\ .$$

In Table 6-15 updated lead factors are listed for each of the Palo Verde Unit 1 surveillance capsules. Lead factor data based on the accumulated fluence through cycle four are provided for each capsule.

TABLE 6-1

CALCULATED FAST NEUTRON EXPOSURE RATES AT THE SURVEILLANCE CAPSULE CENTER

	Capsule Location		
	38°	40°	43°
	ϕ(E >1.0 MeV) [n/cm^2-sec]		
Cycle 1	3.549E+10	3.589E+10	3.507E+10
Cycle 2	1.753E+10	1.761E+10	1.726E+10
Cycle 3	2.114E+10	2.133E+10	2.104E+10
Cycle 4	2.301E+10	2.318E+10	2.263E+10
Average	2.563E+10	2.585E+10	2.533E+10
	ϕ(E > 0.1 MeV) [n/cm^2-sec]		
Cycle 1	6.430E+10	6.493E+10	6.334E+10
Cycle 2	3.175E+10	3.185E+10	3.117E+10
Cycle 3	3.829E+10	3.859E+10	3.801E+10
Cycle 4	4.168E+10	4.194E+10	4.087E+10
Average	4.643E+10	4.677E+10	4.575E+10
	Iron Atom Displacement Rate [dpa/sec]		
Cycle 1	5.160E-11	5.219E-11	5.100E-11
Cycle 2	2.548E-11	2.560E-11	2.510E-11
Cycle 3	3.073E-11	3.102E-11	3.060E-11
Cycle 4	3.345E-11	3.371E-11	3.291E-11
Average	3.726E-11	3.759E-11	3.684E-11

TABLE 6-2

CALCULATED AZIMUTHAL VARIATION OF FAST NEUTRON EXPOSURE RATES AT THE PRESSURE VESSEL CLAD/BASE METAL INTERFACE

	0°	15°	30°	40° [a]	45°
			ϕ(E >1.0 MeV) [n/cm^2-sec]		
Cycle 1	1.488E+10	2.116E+10	2.118E+10	2.455E+10	2.398E+10
Cycle 2	9.855E+09	1.033E+10	1.136E+10	1.224E+10	1.196E+10
Cycle 3	1.475E+10	1.644E+10	1.413E+10	1.494E+10	1.459E+10
Cycle 4	1.170E+10	1.624E+10	1.510E+10	1.598E+10	1.561E+10
Average	1.366E+10	1.708E+10	1.633E+10	1.787E+10	1.745E+10
			ϕ(E > 0.1 MeV) [n/cm^2-sec]		
Cycle 1	3.075E+10	4.430E+10	4.437E+10	5.145E+10	5.056E+10
Cycle 2	2.037E+10	2.163E+10	2.380E+10	2.566E+10	2.522E+10
Cycle 3	3.048E+10	3.442E+10	2.960E+10	3.130E+10	3.076E+10
Cycle 4	2.418E+10	3.399E+10	3.162E+10	3.349E+10	3.292E+10
Average	2.823E+10	3.575E+10	3.420E+10	3.745E+10	3.680E+10
			Iron Atom Displacement Rate [dpa/sec]		
Cycle 1	2.303E-11	3.263E-11	3.254E-11	3.757E-11	3.676E-11
Cycle 2	1.525E-11	1.593E-11	1.746E-11	1.874E-11	1.834E-11
Cycle 3	2.282E-11	2.535E-11	2.171E-11	2.286E-11	2.237E-11
Cycle 4	1.811E-11	2.503E-11	2.319E-11	2.446E-11	2.393E-11
Average	2.114E-11	2.633E-11	2.508E-11	2.735E-11	2.676E-11

a. Values at 40° are obtained by interpolation using the azimuthal shape obtained from the forward calculation.

TABLE 6-3

RELATIVE RADIAL DISTRIBUTION OF $\phi(E > 1.0$ MeV)
WITHIN THE PRESSURE VESSEL WALL

Radius (cm)	0°	15°	30°	40°	45°
233.756[1]	1.0000	1.0000	1.0000	1.0000	1.0000
234.006	0.9854	0.9851	0.9853	0.9856	0.9854
234.631	0.9368	0.9365	0.9369	0.9366	0.9370
235.506	0.8595	0.8580	0.8587	0.8572	0.8591
236.631	0.7571	0.7549	0.7560	0.7529	0.7554
237.923	0.6460	0.6430	0.6445	0.6405	0.6434
239.409	0.5335	0.5292	0.5310	0.5273	0.5303
241.196	0.4203	0.4159	0.4178	0.4143	0.4171
243.204	0.3194	0.3154	0.3173	0.3143	0.3164
245.062	0.2460	0.2431	0.2450	0.2425	0.2433
246.477	0.2003	0.1974	0.1992	0.1976	0.1981
247.78	0.1656	0.1619	0.1635	0.1631	0.1640
249.191	0.1346	0.1311	0.1326	0.1322	0.1333
250.715	0.1076	0.1041	0.1054	0.1049	0.1062
252.055	0.0877	0.0848	0.0860	0.0854	0.0861
253.098	0.0744	0.0713	0.0723	0.0720	0.0727
254.181	0.0625	0.0592	0.0601	0.0599	0.0604
255.181	0.0527	0.0494	0.0501	0.0497	0.0502
255.994	0.0452	0.0416	0.0422	0.0416	0.0421
256.775[2]	0.0391	0.0353	0.0358	0.0351	0.0356

NOTES:
1) Base Metal Inner Radius
2) Base Metal Outer Radius

TABLE 6-4

RELATIVE RADIAL DISTRIBUTION OF $\phi(E > 0.1$ MeV) WITHIN THE PRESSURE VESSEL WALL

Radius (cm)	0°	15°	30°	40°	45°
233.756[1]	1.000	1.000	1.000	1.000	1.000
234.006	1.009	1.008	1.009	1.008	1.009
234.631	1.014	1.011	1.013	1.011	1.012
235.506	1.004	0.997	1.000	0.996	1.000
236.631	0.974	0.962	0.967	0.961	0.966
237.923	0.927	0.912	0.918	0.910	0.917
239.409	0.867	0.848	0.856	0.846	0.854
241.196	0.792	0.769	0.778	0.768	0.776
243.204	0.708	0.683	0.693	0.682	0.690
245.062	0.632	0.606	0.616	0.605	0.612
246.477	0.575	0.547	0.557	0.547	0.554
247.780	0.523	0.495	0.504	0.495	0.502
249.191	0.470	0.441	0.450	0.441	0.447
250.715	0.414	0.385	0.393	0.384	0.390
252.055	0.367	0.338	0.345	0.336	0.341
253.098	0.330	0.300	0.307	0.299	0.303
254.181	0.293	0.262	0.268	0.260	0.264
255.181	0.258	0.227	0.232	0.223	0.227
255.994	0.228	0.196	0.199	0.191	0.194
256.775[2]	0.203	0.171	0.173	0.164	0.167

NOTES:
1) Base Metal Inner Radius
2) Base Metal Outer Radius

TABLE 6-5

RELATIVE RADIAL DISTRIBUTION OF dpa/sec
WITHIN THE PRESSURE VESSEL WALL

Radius (cm)	0°	15°	30°	40°	45°
233.756[1]	1.0000	1.0000	1.0000	1.0000	1.0000
234.006	0.9868	0.9865	0.9869	0.9867	0.9870
234.631	0.9455	0.9449	0.9459	0.9450	0.9461
235.506	0.8816	0.8797	0.8816	0.8796	0.8822
236.631	0.7981	0.7951	0.7978	0.7944	0.7980
237.923	0.7073	0.7030	0.7066	0.7024	0.7065
239.409	0.6141	0.6080	0.6124	0.6080	0.6127
241.196	0.5179	0.5106	0.5156	0.5109	0.5159
243.204	0.4283	0.4203	0.4257	0.4209	0.4255
245.062	0.3592	0.3513	0.3567	0.3520	0.3557
246.477	0.3134	0.3047	0.3100	0.3062	0.3095
247.780	0.2761	0.2662	0.2712	0.2682	0.2718
249.191	0.2403	0.2301	0.2348	0.2317	0.2354
250.715	0.2061	0.1955	0.1998	0.1967	0.2000
252.055	0.1788	0.1684	0.1721	0.1689	0.1716
253.098	0.1588	0.1478	0.1511	0.1482	0.1507
254.181	0.1394	0.1278	0.1307	0.1278	0.1299
255.181	0.1223	0.1103	0.1125	0.1094	0.1112
255.994	0.1087	0.0956	0.0973	0.0939	0.0955
256.775[2]	0.0971	0.0834	0.0847	0.0812	0.0826

NOTES: 1) Base Metal Inner Radius
2) Base Metal Outer Radius

TABLE 6-6

NUCLEAR PARAMETERS USED IN THE EVALUATION OF NEUTRON SENSORS

Monitor Material	Reaction of Interest	Target Weight Fraction	Response Range	Product Half-Life	Fission Yield (%)
Copper*	$Cu^{63}(n,\alpha)Co^{60}$	0.6917	E > 5 MeV	5.271 yrs	
Iron	$Fe^{54}(n,p)Mn^{54}$	0.0580	E > 2 MeV	312.5 days	
Nickel*	$Ni^{58}(n,p)Co^{58}$	0.6827	E > 2 MeV	70.78 days	
Titanium	$Ti^{46}(n,p)Sc^{46}$	0.0810	E > 2 MeV	83.83 days	
Uranium-238*	$U^{238}(n,f)Cs^{137}$	1.0	E > 1 MeV	30.17 yrs	6.00
	$U^{238}(n,f)Ru^{103}$	1.0	E > 1 MeV	39.26 days	6.23
	$U^{238}(n,f)Zr^{95}$	1.0	E > 1 MeV	64.02 days	5.10
Cobalt-Aluminum*	$Co^{59}(n,\gamma)Co^{60}$	0.0017	0.4ev>E> 0.015 MeV	5.271 yrs	
Cobalt-Aluminum	$Co^{59}(n,\gamma)Co^{60}$	0.0017	E < 0.015 MeV	5.271 yrs	

*Denotes that monitor is cadmium shielded. Both bare and cadmium shielded U-238 monitors were included.

Note: The capsule also contained a sulfur dosimeter but this could not be analyzed due to decay of the P-32 which has a 14.28 day half-life.

TABLE 6-7

MONTHLY THERMAL GENERATION DURING THE FIRST FOUR FUEL CYCLES OF THE PALO VERDE UNIT 1 REACTOR

Year	Month	Thermal Generation (MW-hr)
1985	6	328821
	7	488786
	8	83645
	9	1069383
	10	962630
	11	194
	12	1460729
1986	1	1265571
	2	1446400
	3	566400
	4	0
	5	597004
	6	2473534
	7	1814285
	8	1746682
	9	1929290
	10	2413152
	11	2440676
	12	2768558
1987	1	1462574
	2	0
	3	1861757
	4	2705174
	5	2615160
	6	2387981
	7	29941
	8	2431392
	9	2502710
	10	144005
	11	0
	12	0
1988	1	0
	2	0
	3	1667501
	4	2300328
	5	2371300
	6	2698106
	7	503771
	8	69686
	9	2565055
	10	2659128
	11	2708768
	12	2789443
1989	1	2775471
	2	2385008
	3	0
	4	0
	5	0
	6	0
	7	0
	8	0
	9	0
	10	0
	11	0
	12	0
1990	1	0
	2	0
	3	0
	4	0
	5	0
	6	10825
	7	2146547
	8	2337547
	9	1652836
	10	2797086
	11	2704935
	12	2813104
1991	1	996506
	2	1084003
	3	2822719
	4	2731759
	5	2824227
	6	2725393
	7	2825868
	8	2824884
	9	1725887
	10	2386029
	11	2700441
	12	2822439
1992	1	1430983
	2	1248802
	3	0
	4	0
	5	389734
	6	2726926
	7	2825923
	8	2825394
	9	2545283
	10	2610331
	11	2734833
	12	2576546
1993	1	2645967
	2	2461534
	3	2806238
	4	2735243
	5	2606624
	6	2730282
	7	2487672
	8	2019059
	9	174976
(Shutdown 9/3/93)		

TABLE 6-8

MEASURED SENSOR ACTIVITIES AND REACTION RATES
SURVEILLANCE CAPSULE W137

MONITOR AND AXIAL LOCATION	MEASURED ACTIVITY (dis/sec-gm)	SATURATED ACTIVITY (dis/sec-gm)	REACTION RATE (rps/nucleus)
Cu-63 (n,α) Co-60*			
1A31Y TOP	1.04E+05	2.90E+05	
1A34B MID	9.81E+04	2.73E+05	
1A353 BOT	9.89E+04	2.75E+05	
Averages	1.00E+05	2.79E+05	4.26E- 17
FE-54 (n,p) Mn-54			
1A31Y TOP	9.79E+05	2.05E+06	
1A34B MID	9.09E+05	1.91E+06	
1A353 BOT	9.21E+05	1.93E+06	
Averages	9.36E+05	1.96E+06	3.14E-15
Ni-58 (n,p) Co-58*			
1A34B MID	3.36E+06	2.73E+07	3.90E-15
Ti-46 (n,p) Sc-46			
1A31Y TOP	1.09E+05	6.56E+05	
1A34B MID	1.03E+05	6.20E+05	
1A353 BOT	1.03E+05	6.20E+05	
Averages	1.05E+05	6.32E+05	5.95E-16
Co-59 (n,γ) Co-60			
1A34B MID	5.24E+07	1.46E+08	9.52E-12
Co-59 (n,γ) Co-60*			
1A34B MID	6.35E+06	1.77E+07	1.15E-12

* Indicates cadmium covered monitor.

TABLE 6-8 (Continued)

MEASURED SENSOR ACTIVITIES AND REACTION RATES
SURVEILLANCE CAPSULE W137

MONITOR AND AXIAL LOCATION	MEASURED ACTIVITY (dis/sec-gm)	SATURATED ACTIVITY (dis/sec-gm)	REACTION RATE (rps/nucleus)
U-238 (n,f) Cs-137*			
1A31Y TOP	4.12E+04	4.27E+05	
1A34B MID	1.00E+05	1.04E+06	
1A353 BOT	7.56E+04	7.84E+05	
Averages	7.23E+04	7.50E+05	4.94E-15
U-238 (n,f) Ru-103*			
1A31Y TOP	4.08E+04	4.07E+05	
1A34B MID	8.72E+04	8.71E+05	
1A353 BOT	6.54E+04	6.53E+05	
Averages	6.45E+04	6.44E+05	4.99E-15
U-238 (n,f) Zr-95*			
1A31Y TOP	1.37E+04	5.37E+05	
1A34B MID	2.70E+05	1.06E+07	
1A353 BOT	1.94E+04	7.60E+05	
Averages	1.01E+05	3.96E+06	2.51E-14
U-238 (n,f) Cs-137			
1A31Y TOP	2.06E+05	2.14E+06	
1A34B MID	3.68E+05	3.82E+06	
1A353 BOT	2.87E+05	2.98E+06	
Averages	2.87E+05	2.98E+06	1.96E-14
U-238 (n,f) Ru-103			
1A31Y TOP	2.34E+05	2.34E+06	
1A34B MID	4.18E+05	4.17E+06	
1A353 BOT	3.03E+05	3.03E+06	
Averages	3.18E+05	3.18E+06	2.46E-14
U-238 (n,f) Zr-95			
1A31Y TOP	6.27E+04	2.46E+06	
1A34B MID	1.08E+05	4.23E+06	
1A353 BOT	7.09E+04	2.78E+06	
Averages	8.05E+04	3.15E+06	2.00E-14

* Indicates cadmium covered monitor.

TABLE 6-9

SUMMARY OF NEUTRON DOSIMETRY RESULTS
SURVEILLANCE CAPSULE W137

Calculation of Measured Fluence	Flux	Time	Fluence	Uncertainty
Meas Fluence < 0.414 ev	2.736E+11	1.431E+08	3.914E+19	±22%
Meas Fluence > 0.1 Mev	4.806E+10	1.431E+08	6.875E+18	±19%
Meas Fluence > 1.0 Mev	2.414E+10	1.431E+08	3.453E+18	±12%
dpa	3.475E-11	1.431E+08	5.357E-03	±11%

TABLE 6-10

COMPARISON OF MEASURED AND FERRET CALCULATED
REACTION RATES AT THE SURVEILLANCE CAPSULE CENTER
SURVEILLANCE CAPSULE W137

REACTION	MEASURED	ADJUSTED CALCULATION	C/M
Cu-63 (n,α) Co-60	4.26E-17	4.56E-17	1.00
Fe-54 (n,p) Mn-54	3.14E-15	3.12E-15	1.00
Ni-58 (n,p) Co-58	3.90E-15	3.99E-15	1.02
Ti-46 (n,p) Sc-46	5.95E-16	5.99E-16	1.01
Co-59 (n,γ) Co-60	9.52E-12	8.57E-12	0.90
Co-59 (n,γ) Co-60 (Cd)	1.15E-12	9.88E-13	0.86

TABLE 6-11

ADJUSTED NEUTRON ENERGY SPECTRUM AT THE CENTER OF SURVEILLANCE CAPSULE W137

GROUP	ENERGY (MeV)	ADJUSTED FLUX (n/cm²-sec)	GROUP	ENERGY (MeV)	ADJUSTED FLUX (n/cm²-sec)
1	17.33	4.99E+06	28	9.119E-03	2.17E+09
2	14.92	1.16E+07	29	5.531E-03	2.44E+09
3	13.50	4.83E+07	30	3.355E-03	8.22E+08
4	11.62	1.13E+08	31	2.839E-03	8.41E+08
5	10.00	2.56E+08	32	2.404E-03	8.85E+08
6	8.607	4.36E+08	33	2.035E-03	2.85E+09
7	7.408	1.04E+09	34	1.234E-03	3.13E+09
8	6.065	1.44E+09	35	7.485E-04	3.51E+09
9	4.966	2.48E+09	36	4.540E-04	3.93E+09
10	3.679	2.39E+09	37	2.754E-04	4.49E+09
11	2.865	3.96E+09	38	1.670E-04	8.21E+09
12	2.231	3.76E+09	39	1.013E-04	4.76E+09
13	1.738	3.84E+09	40	6.144E-05	4.40E+09
14	1.353	2.97E+09	41	3.727E-05	3.95E+09
15	1.108	4.16E+09	42	2.260E-05	3.51E+09
16	8.208E-01	3.83E+09	43	1.371E-05	3.16E+09
17	6.393E-01	3.43E+09	44	8.315E-06	2.92E+09
18	4.979E-01	2.51E+09	45	5.043E-06	2.75E+09
19	3.877E-01	2.85E+09	46	3.059E-06	2.62E+09
20	3.020E-01	4.27E+09	47	1.855E-06	2.49E+09
21	1.832E-01	3.64E+09	48	1.125E-06	2.32E+09
22	1.111E-01	3.00E+09	49	6.826E-07	2.78E+09
23	6.738E-02	2.52E+09	50	4.140E-07	3.62E+09
24	4.087E-02	1.90E+09	51	2.511E-07	1.41E+10
25	2.554E-02	1.32E+09	52	1.523E-07	3.41E+10
26	1.989E-02	1.10E+09	53	9.237E-08	2.22E+11
27	1.503E-02	2.01E+09			

Note: Tabulated energy levels represent the upper energy in each group.

TABLE 6-12

COMPARISON OF CALCULATED AND MEASURED NEUTRON EXPOSURE LEVELS FOR PALO VERDE UNIT 1 SURVEILLANCE CAPSULE W137

Comparison of Calculated and Measured INTEGRATED Neutron EXPOSURE for Capsule W137

	Calculated	Measured	C / M
Fluence (E > 1.0 Mev) [n/cm2]	3.623E+18	3.453E+18	1.049
Fluence (E > 0.1 Mev) [n/cm2]	6.544E+18	6.875E+18	0.952
dpa	5.270E-03	5.357E-03	0.984

Comparison of Calculated and Measured Neutron EXPOSURE RATE for Capsule W137

	Calculated	Measured	C / M
Flux (E > 1.0 Mev) [n/cm2-sec]	2.533E+10	2.414E+10	1.049
Flux (E > 0.1 Mev) [n/cm2-sec]	4.575E+10	4.806E+10	0.952
dpa/s	3.684E-11	3.745E-11	0.984

TABLE 6-13

NEUTRON EXPOSURE PROJECTIONS AT KEY LOCATIONS
ON THE PRESSURE VESSEL CLAD/BASE METAL INTERFACE

BEST ESTIMATE EXPOSURE (4.533 EFPY) AT THE PRESSURE VESSEL INNER RADIUS

	0 DEG[a]	15 DEG	30 DEG[b]	40 DEG[c]	45 DEG
E > 1.0	1.868E+18	2.335E+18	2.232E+18	2.443E+18	2.386E+18
E > 0.1	4.254E+18	5.387E+18	5.154E+18	5.643E+18	5.546E+18
dpa	3.083E-03	3.840E-03	3.658E-03	3.988E-03	3.902E-03

BEST ESTIMATE FLUENCE RATE AT THE PRESSURE VESSEL INNER RADIUS

	0 DEG[a]	15 DEG	30 DEG[b]	40 DEG[c]	45 DEG
E > 1.0	1.306E+10	1.632E+10	1.561E+10	1.708E+10	1.668E+10
E > 0.1	2.974E+10	3.766E+10	3.603E+10	3.945E+10	3.877E+10
dpa	2.155E-11	2.684E-11	2.557E-11	2.788E-11	2.728E-11

BEST ESTIMATE EXPOSURE (15.0 EFPY) AT THE PRESSURE VESSEL INNER RADIUS

	0 DEG[a]	15 DEG	30 DEG[b]	40 DEG[c]	45 DEG
E > 1.0	6.180E+18	7.725E+18	7.387E+18	8.084E+18	7.895E+18
E > 0.1	1.408E+19	1.783E+19	1.706E+19	1.867E+19	1.835E+19
dpa	1.020E-02	1.271E-02	1.210E-02	1.320E-02	1.291E-02

BEST ESTIMATE EXPOSURE (32.0 EFPY) AT THE PRESSURE VESSEL INNER RADIUS

	0 DEG[a]	15 DEG	30 DEG[b]	40 DEG[c]	45 DEG
E > 1.0	1.318E+19	1.648E+19	1.576E+19	1.725E+19	1.684E+19
E > 0.1	3.003E+19	3.803E+19	3.639E+19	3.984E+19	3.915E+19
dpa	2.176E-02	2.711E-02	2.582E-02	2.815E-02	2.755E-02

(a) Applies to axial weld at 90° location.
(b) Applies to axial weld at 210° and 330° locations.
(c) Maximum fluence point.

TABLE 6-14

NEUTRON EXPOSURE VALUES

FLUENCE BASED ON E > 1.0 MeV SLOPE

	0 DEG[a]	15 DEG	30 DEG[b]	40 DEG[c]	45 DEG
			15 EFPY FLUENCE		
SURFACE	6.180E+18	7.725E+18	7.387E+18	8.084E+18	7.895E+18
1/4T	3.252E+18	4.033E+18	3.869E+18	4.234E+18	4.106E+18
3/4T	6.345E+17	7.678E+17	7.435E+17	8.136E+17	7.906E+17
			32 EFPY FLUENCE		
SURFACE	1.318E+19	1.648E+19	1.576E+19	1.725E+19	1.684E+19
1/4T	6.938E+18	8.603E+18	8.254E+18	9.032E+18	8.760E+18
3/4T	1.354E+18	1.638E+18	1.586E+18	1.736E+18	1.687E+18

FLUENCE BASED ON dpa SLOPE

	0 DEG[a]	15 DEG	30 DEG[b]	40 DEG[c]	45 DEG
			15 EFPY FLUENCE		
SURFACE	6.180E+18	7.725E+18	7.387E+18	8.084E+18	7.895E+18
1/4T	3.758E+18	4.650E+18	4.480E+18	4.866E+18	4.752E+18
3/4T	1.233E+18	1.460E+18	1.426E+18	1.536E+18	1.500E+18
			32 EFPY FLUENCE		
SURFACE	1.318E+19	1.648E+19	1.576E+19	1.725E+19	1.684E+19
1/4T	8.018E+18	9.920E+18	9.556E+18	1.038E+19	1.014E+19
3/4T	2.631E+18	3.115E+18	3.043E+18	3.276E+18	3.200E+18

(a) Applies to axial weld at 90° location.

(b) Applies to axial weld at 210° and 330° locations.

(c) Maximum fluence point.

TABLE 6-15

UPDATED LEAD FACTORS FOR PALO VERDE UNIT 1
SURVEILLANCE CAPSULES

CAPSULE	LEAD FACTOR
W38	1.43
W43	1.41
W137	1.41*
W142	1.43
W230	1.44
W310	1.44

* WITHDRAWN EOC 4, BASIS FOR THIS ANALYSIS

FIGURE 6-1

PALO VERDE REACTOR MODEL SHOWING A 45 DEGREE (R,Θ) SECTOR

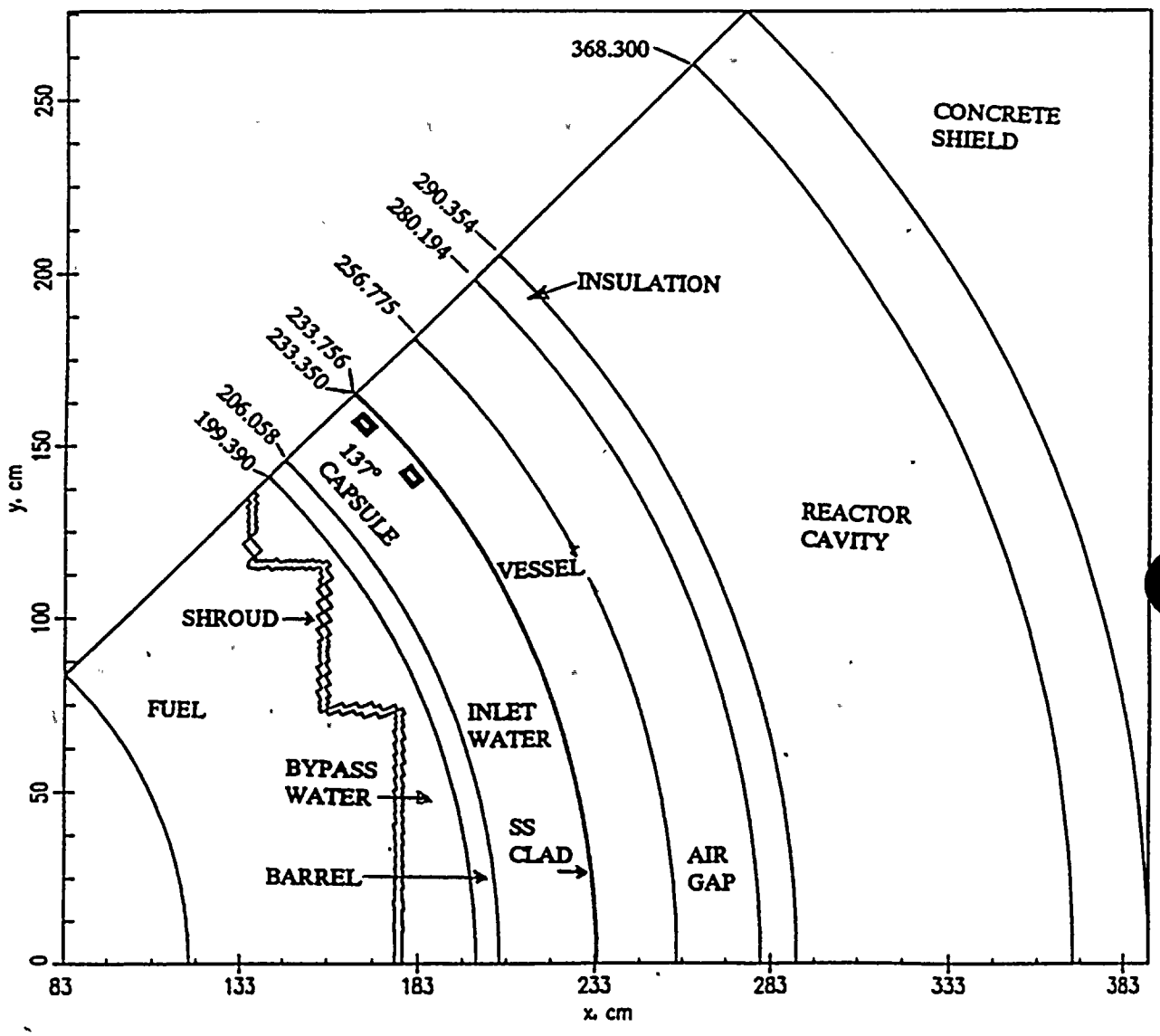

FIGURE 6-2

AZIMUTHAL VARIATION OF NEUTRON FLUX (E > 1.0 MEV)
AT THE REACTOR VESSEL INNER RADIUS

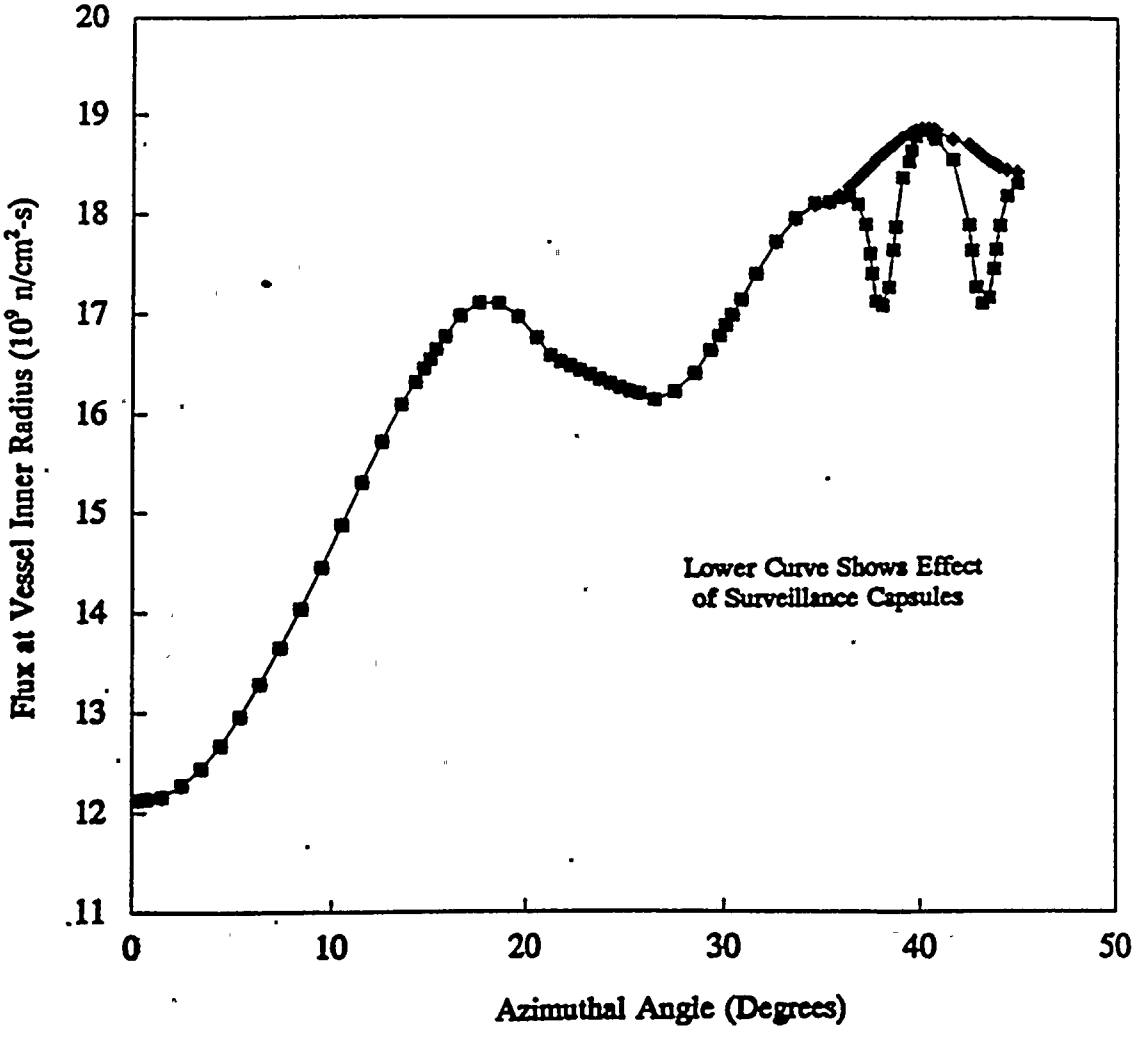

FIGURE 6-3

AXIAL DISTRIBUTION OF REACTOR POWER

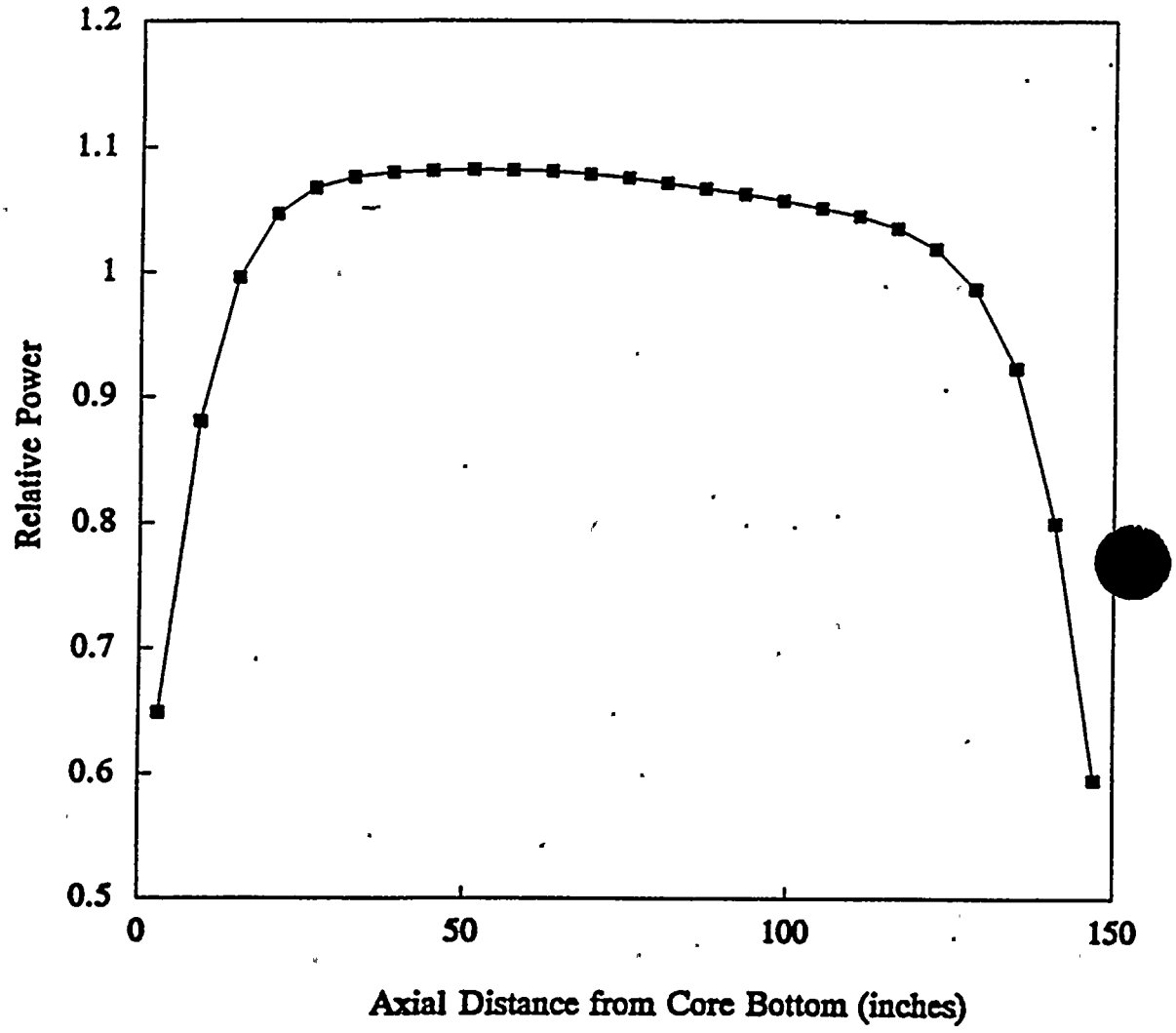

SECTION 7.0
SURVEILLANCE CAPSULE REMOVAL SCHEDULE

The following surveillance capsule removal schedule meets the requirements of ASTM E185-82 and is recommended for future capsules to be removed from the Palo Verde Unit 1 reactor vessel:

Table 7-1

Palo Verde Unit 1 Reactor Vessel Surveillance Capsule Withdraw Schedule

Location	Lead Factor	Removal Time (EFPY)[a]	Fluence (n/cm^2)
137°	1.41	4.533	3.453×10^{18} [b]
230°	1.44	15	1.17×10^{19}
310°	1.44	EOL	2.49×10^{19}
38°	1.43	Stand-by	- -
43°	1.41	Stand-by	- -
142°	1.43	Stand-By	- -

(a) Effective Full Power Years (EFPY) from plant startup.

(b) Actual measured neutron fluence

SECTION 8.0
REFERENCES

1. Regulatory Guide 1.99, Revision 2, *Radiation Embrittlement of Reactor Vessel Materials*, U.S. Nuclear Regulatory Commission, May, 1988.

2. Chang, B.C., *Arizona Public Service Company Palo Verde Unit 1 Evaluation of Baseline Specimens Reactor Vessel Materials Irradiation Surveillance Program*, ABB Combustion Engineering Report TR-V-MCM-012, Issue Date 1-31-87.

3. Section III of the ASME Boiler and Pressure Vessel Code, Appendix G, *Protection Against Nonductile Failure.*

4. ASTM E208, *Standard Test Method for Conducting Drop-Weight Test to Determine Nil-Ductility Transition Temperature of Ferritic Steels*, in ASTM Standards, Section 3, American Society for Testing and Materials, Philadelphia, PA.

5. Data package supplied to Westinghouse by the Arizona Public Service Company (File APS-106/13 Capsule W137)).

6. Code of Federal Regulations, 10CFR50, Appendix G, *Fracture Toughness Requirements*, and Appendix H, *Reactor Vessel Material Surveillance Program Requirements*, U.S. Nuclear Regulatory Commission, Washington, D.C.

7. ASTM E185-82, *Standard Practice for Conducting Surveillance Tests for Light-Water Cooled Nuclear Power Reactor Vessels, E706 (IF)*, in ASTM Standards, Section 3, American Society for Testing Materials, Philadelphia, PA, 1993.

8. ASTM E23-92, *Standard Test Methods for Notched Bar Impact Testing of Metallic Materials*, in ASTM Standards, Section 3, American Society for Testing and Materials, Philadelphia, PA, 1992.

9. ASTM A370-92, *Standard Test Methods and Definitions for Mechanical Testing of Steel Products*, in ASTM Standards, Section 3, American Society for Testing Materials, Philadelphia, PA, 1993.

10. ASTM E8-93, *Standard Test Methods of Tension Testing of Metallic Materials*, in ASTM Standards, Section 3, American Society for Testing Materials, Philadelphia, PA, 1991.

11. ASTM E21-92, *Standard Practice for Elevated Temperature Tension Tests of Metallic Materials*, in ASTM Standards, Section 3, American Society for Testing Materials, Philadelphia, PA, 1989.

12. ASTM E83-93, *Standard Practice for Verification and Classification of Extensometers*, in ASTM Standards, Section 3, American Society for Testing Materials, Philadelphia, PA, 1992.

13. ASTM Designation E853-87, *Standard Practice for Analysis and Interpretation of Light-Water Reactor Surveillance Results*, in ASTM Standards, Section 12, American Society for Testing and Materials, Philadelphia, PA, 1993.

14. ASTM Designation E693-79, *Standard Practice for Characterizing Neutron Exposures in Ferritic Steels in Terms of Displacements per Atom (dpa)*, in ASTM Standards, Section 12, American Society for Testing and Materials, Philadelphia, PA, 1993.

15. ASTM Designation E706-87, *Standard Master Matrix for Light-Water Reactor Pressure Vessel Surveillance Standard*, in ASTM Standards, Section 12, American Society for Testing and Materials, Philadelphia, PA, 1993.

16. ASTM Designation E482-89, *Standard Guide for Application of Neutron Transport Methods for Reactor Vessel Surveillance*, in ASTM Standards, Section 12, American Society for Testing and Materials, Philadelphia, PA, 1993.

17. ASTM Designation E560-84, *Standard Recommended Practice for Extrapolating Reactor Vessel Surveillance Dosimetry Results*, in ASTM Standards, Section 12, American Society for Testing and Materials, Philadelphia, PA, 1993.

18. ASTM Designation E261-90, *Standard Method for Determining Neutron Flux, Fluence, and Spectra by Radioactivation Techniques*, in ASTM Standards, Section 12, American Society for Testing and Materials, Philadelphia, PA, 1993.

19. ASTM Designation E262-86, *Standard Method for Measuring Thermal Neutron Flux by Radioactivation Techniques*, in ASTM Standards, Section 12, American Society for Testing and Materials, Philadelphia, PA, 1993.

20. R. G. Soltesz, R. K. Disney, J. Jedruch, and S. L. Ziegler, *Nuclear Rocket Shielding Methods, Modification, Updating and Input Data Preparation. Vol. 5--Two-Dimensional Discrete Ordinates Transport Technique*, WANL-PR(LL)-034, Vol. 5, August 1970.

21. *ORNL RSCI Data Library Collection DLC-76 SAILOR Coupled Self-Shielded, 47 Neutron, 20 Gamma-Ray, P3, Cross Section Library for Light Water Reactors.*

22. R. E. Maerker, et al, *Accounting for Changing Source Distributions in Light Water Reactor Surveillance Dosimetry Analysis*, Nuclear Science and Engineering, Volume 94, Pages 291-308, 1986.

23. ASTM Designation E1005-84, *Standard Method for Application and Analysis of Radiometric Monitors for Reactor Vessel Surveillance*, in ASTM Standards, Section 12, American Society for Testing and Materials, Philadelphia, PA, 1993.

24. ASTM Designation E263-88, *Standard Method for Determining Fast-Neutron Reaction Rates by Radioactivation of Iron*, in ASTM Standards, Section 12, American Society for Testing and Materials, Philadelphia, PA, 1993.

25. ASTM Designation E264-92, *Standard Method for Determining Fast-Neutron Reaction Rates by Radioactivation of Nickel*, in ASTM Standards, Section 12, American Society for Testing and Materials, Philadelphia, PA, 1993.

26. ASTM Designation E481-86, *Standard Method for Measuring Neutron Fluence Rate by Radioactivation of Cobalt and Silver*, in ASTM Standards, Section 12, American Society for Testing and Materials, Philadelphia, PA, 1993.

27. ASTM Designation E523-92, *Standard Method for Determining Fast-Neutron Reaction Rates by Radioactivation of Copper*, in ASTM Standards, Section 12, American Society for Testing and Materials, Philadelphia, PA, 1993.

28. ASTM Designation E526-92, *Standard Method for Determining Fast-Neutron Reaction Rates by Radioactivation of Titanium*, in ASTM Standards, Section 12, American Society for Testing and Materials, Philadelphia, PA, 1993.

29. ASTM Designation E704-90, *Standard Method for Measuring Reaction Rates by Radioactivation of Uranium-238*, in ASTM Standards, Section 12, American Society for Testing and Materials, Philadelphia, PA, 1993.

30. F. A. Schmittroth, *FERRET Data Analysis Core*, HEDL-TME 79-40, Hanford Engineering Development Laboratory, Richland, WA, September 1979.

31. W. N. McElroy, S. Berg and T. Crocket, *A Computer-Automated Iterative Method of Neutron Flux Spectra Determined by Foil Activation*, AFWL-TR-7-41, Vol. I-IV, Air Force Weapons Laboratory, Kirkland AFB, NM, July 1967.

32. EPRI-NP-2188, *Development and Demonstration of an Advanced Methodology for LWR Dosimetry Applications*, R. E. Maerker, et al., 1981.

33. WCAP-13390, *Westinghouse Fast Neutron Exposure Methodology for Pressure Vessel Fluence Determination and Dosimetry Evaluation*, S. L. Anderson, May 1992.

34. WCAP-13935, *Analysis of the 137° Capsule from the Arizona Public Service Company Palo Verde Unit No. 2 Reactor Vessel Radiation Surveillance Program*, E. Terek, E. P. Lippincott, and A. Madeyski, February 1994.

APPENDIX

LOAD-TIME RECORDS FOR CHARPY IMPACT TESTS AND COMPARISONS OF DATA FOR UNIRRADIATED AND IRRADIATED PRECRACKED CHARPY SPECIMENS

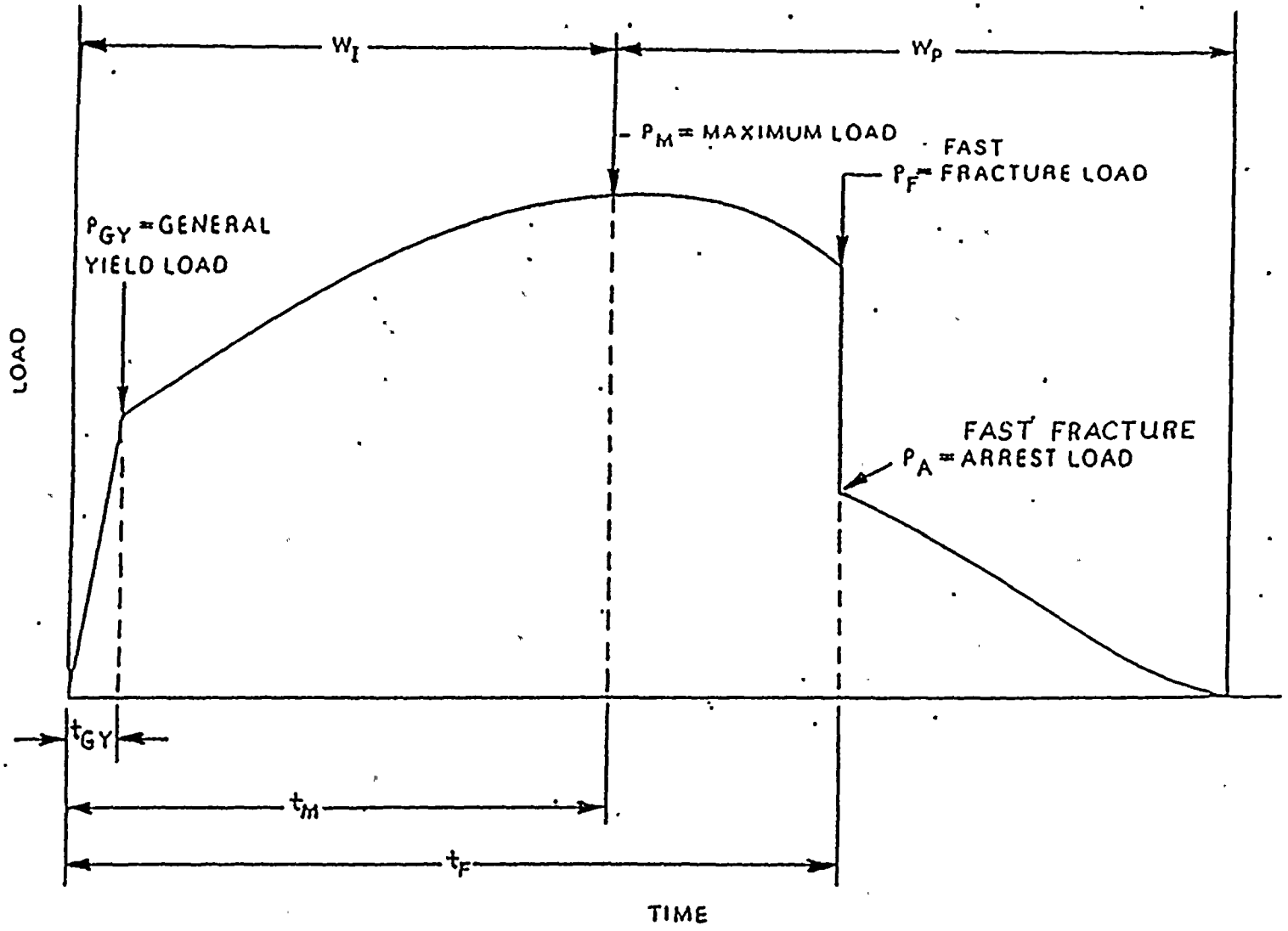

W_I = Fracture initiation region

W_p = Fracture propagation region

t_{GY} = Time to general yielding

t_M = Time to maximum load

t_F = Time to fast (brittle) fracture start

Figure A-1. Idealized load-time record

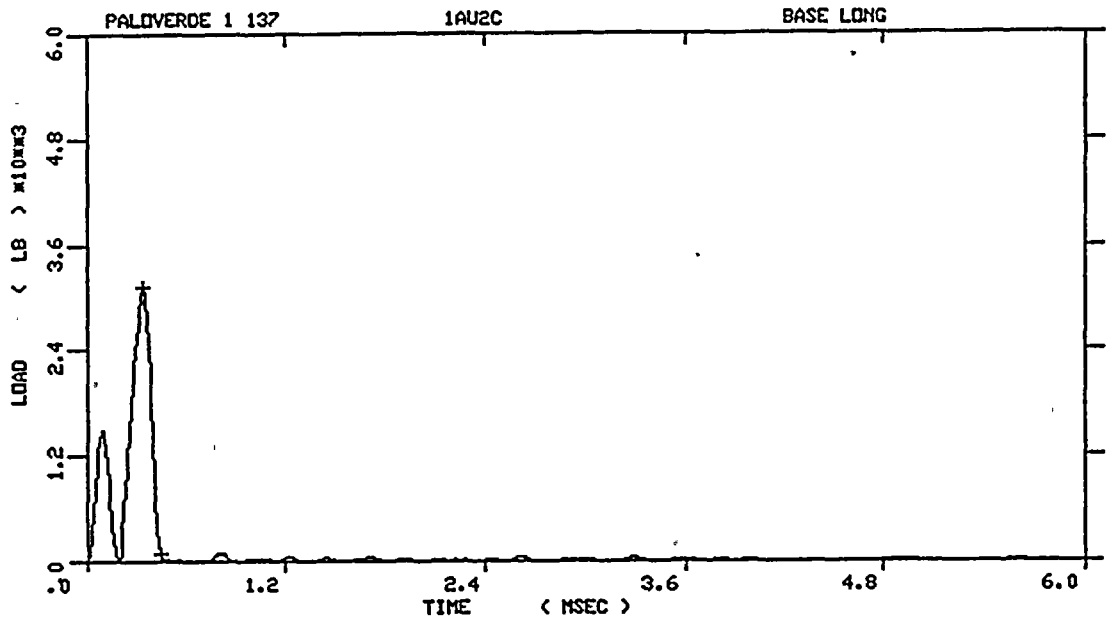

PALOVERDE 1 137
SPECIMEN NUMBER :1AU2C
MATERIAL :BASE LONG
CAPSULE :PALOVERDE #1 137
:

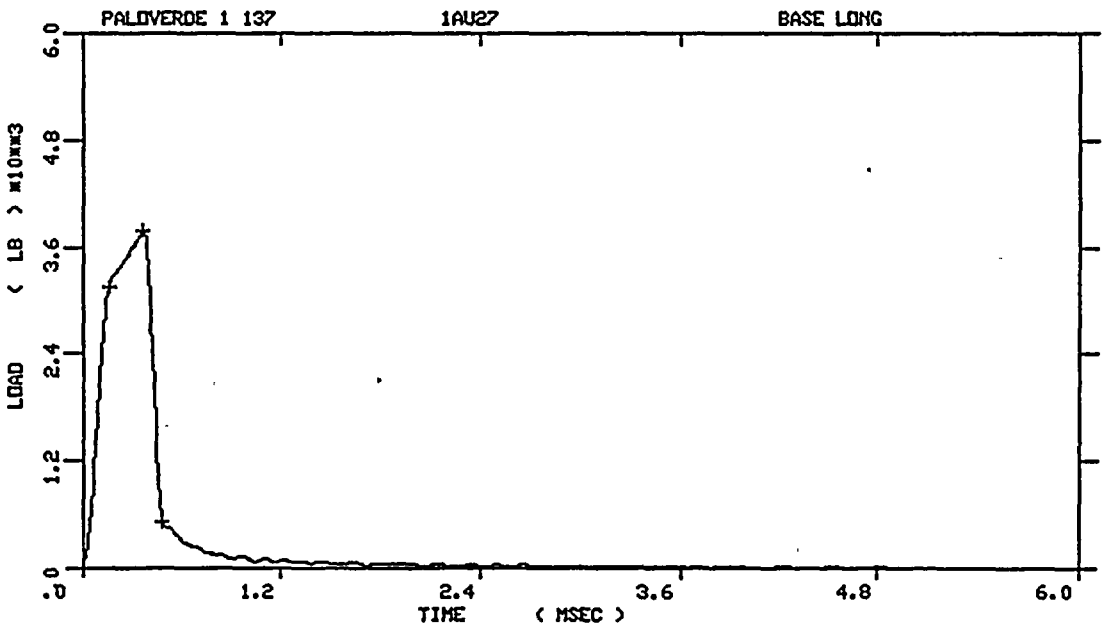

PALOVERDE 1 137
SPECIMEN NUMBER :1AU27
MATERIAL :BASE LONG
CAPSULE :PALOVERDE #1 137
:

Figure A-2. Load-time records for Specimens 1AU2C and 1AU27

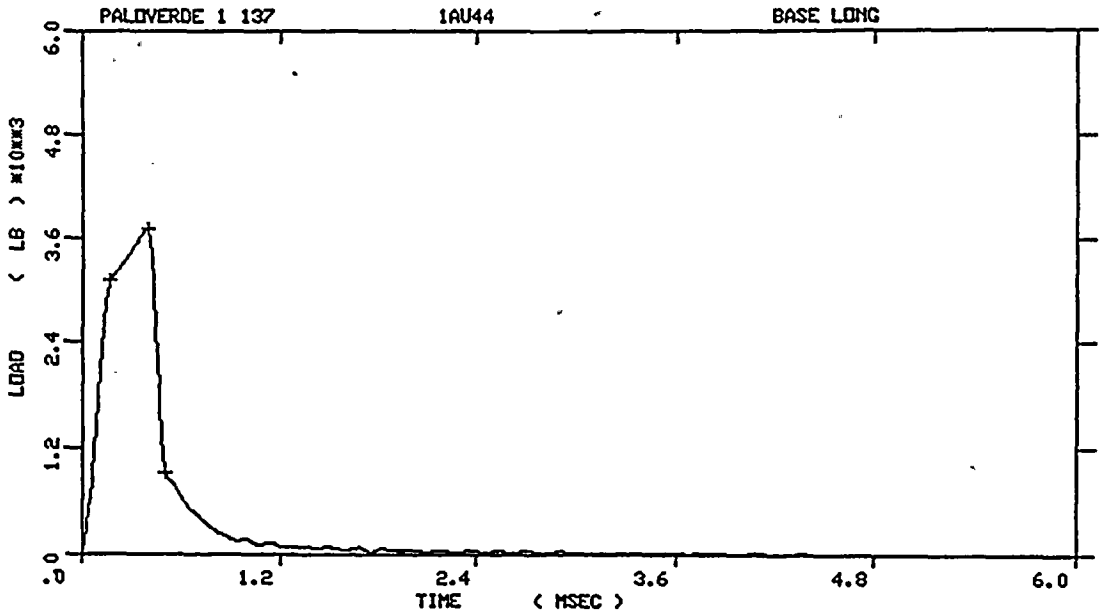

PALOVERDE 1 137
SPECIMEN NUMBER : 1AU44
MATERIAL :BASE LONG
CAPSULE :PALOVERDE #1 137
:

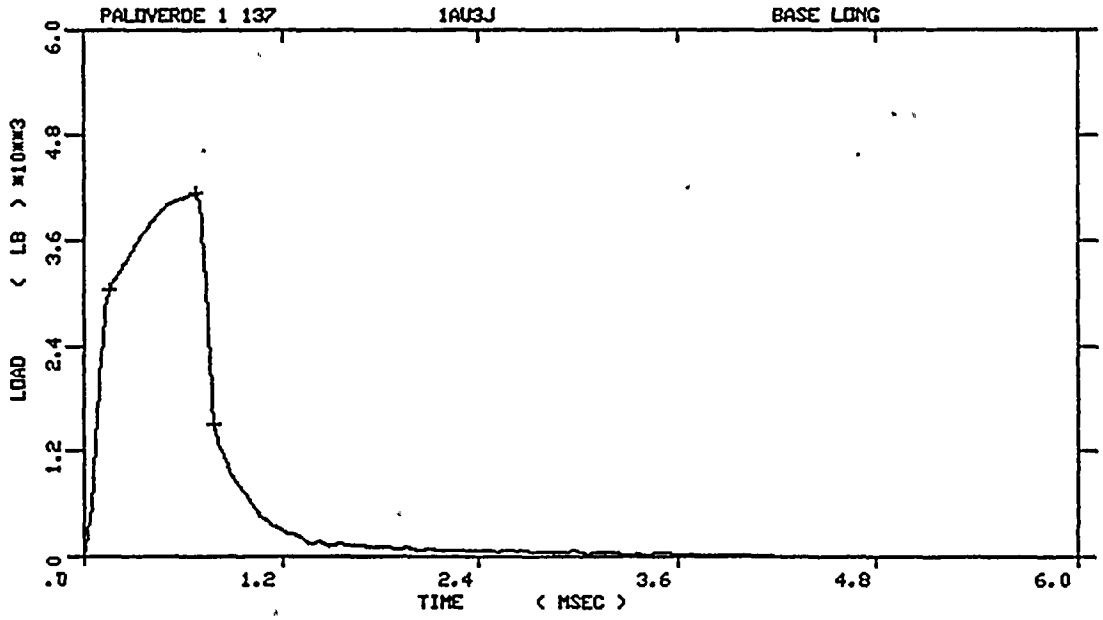

PALOVERDE 1 137
SPECIMEN NUMBER :1AU3J
MATERIAL :BASE LONG
CAPSULE :PALOVERDE #1 137
:

Figure A-3. Load-time records for Specimens 1AU44 and 1AU3J

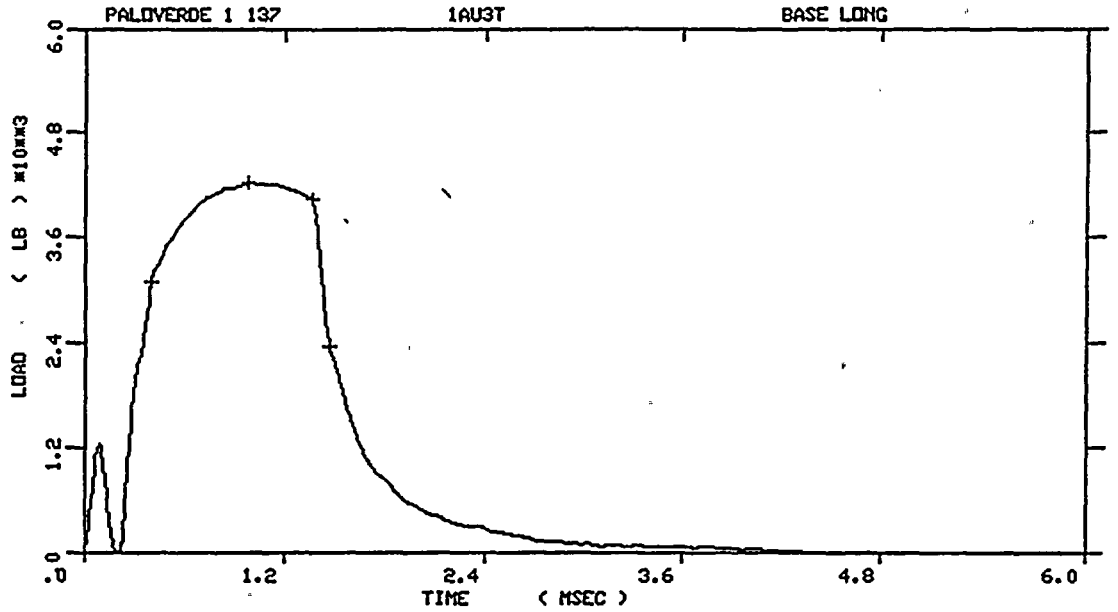

PALOVERDE 1 137
SPECIMEN NUMBER :1AU3T
MATERIAL :BASE LONG
CAPSULE :PALOVERDE #1 137
:

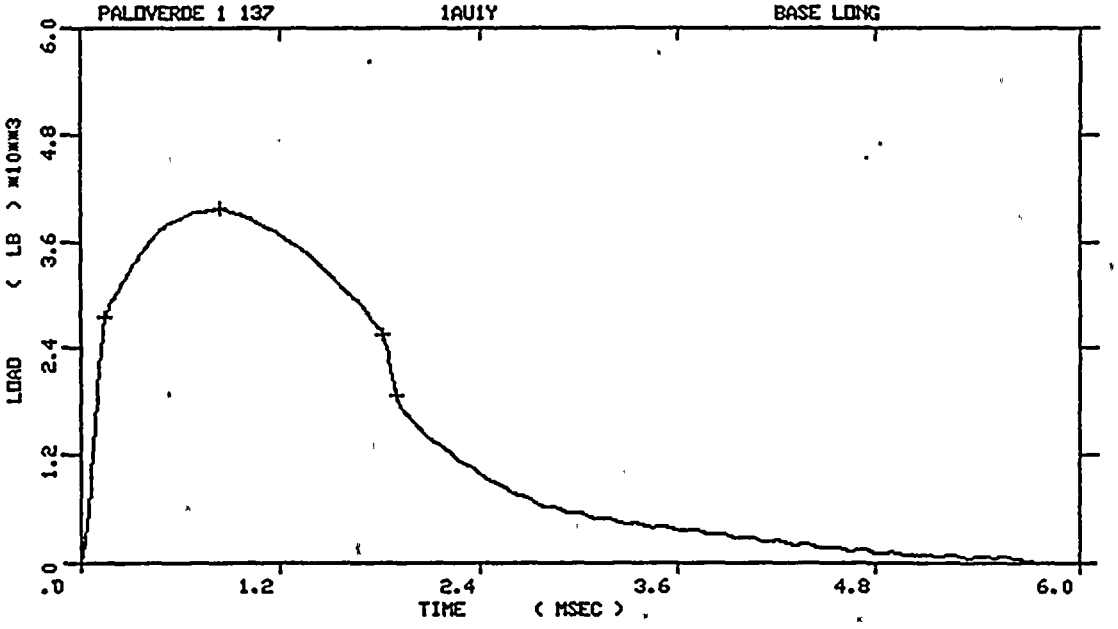

PALOVERDE 1 137
SPECIMEN NUMBER :1AU1Y
MATERIAL :BASE LONG
CAPSULE :PALOVERDE #1 137
:

Figure A-4. Load-time records for Specimens 1AU3T and 1AU1Y

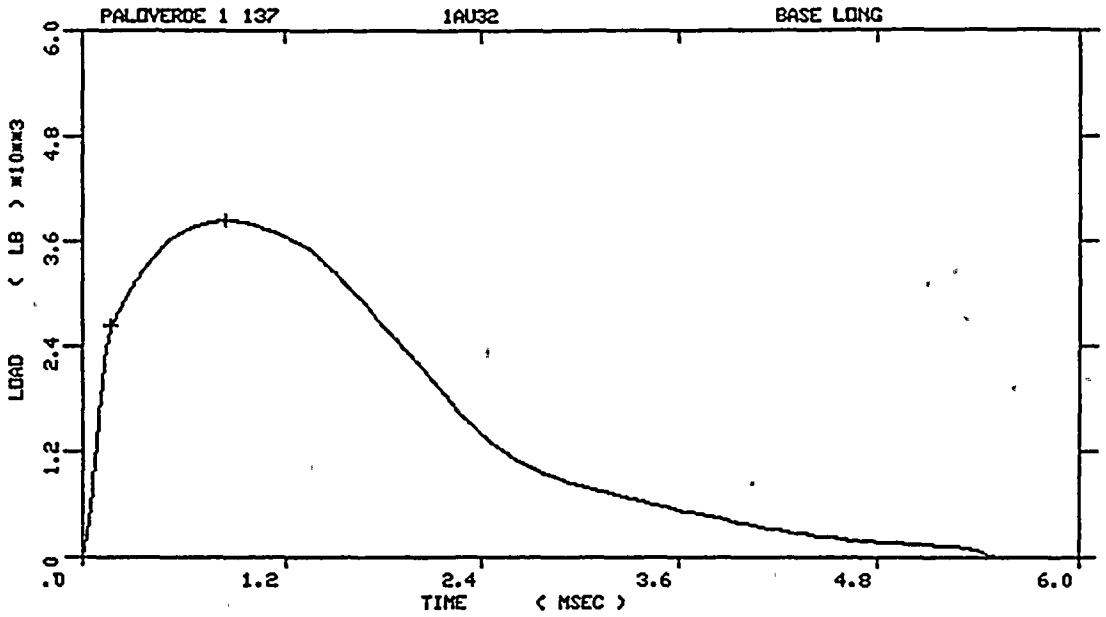

PALOVERDE 1 137
SPECIMEN NUMBER :1AU32
MATERIAL :BASE LONG
CAPSULE :PALOVERDE #1 137
:

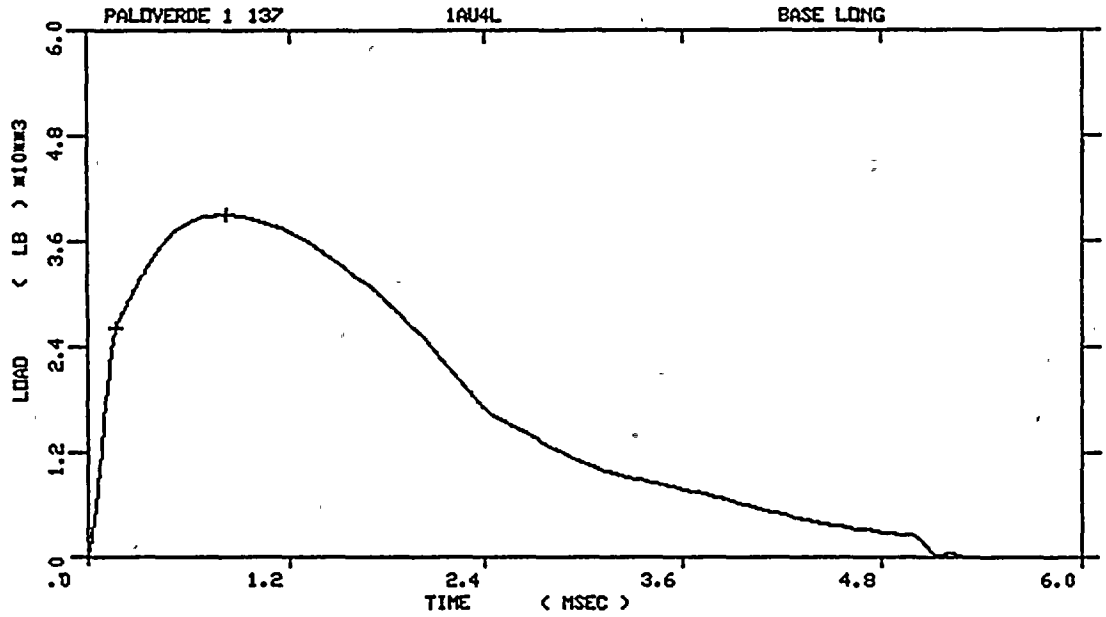

PALOVERDE 1 137
SPECIMEN NUMBER :1AU4L
MATERIAL :BASE LONG
CAPSULE :PALOVERDE #1 137
:

Figure A-5. Load-time records for Specimens 1AU32 and 1AU4L

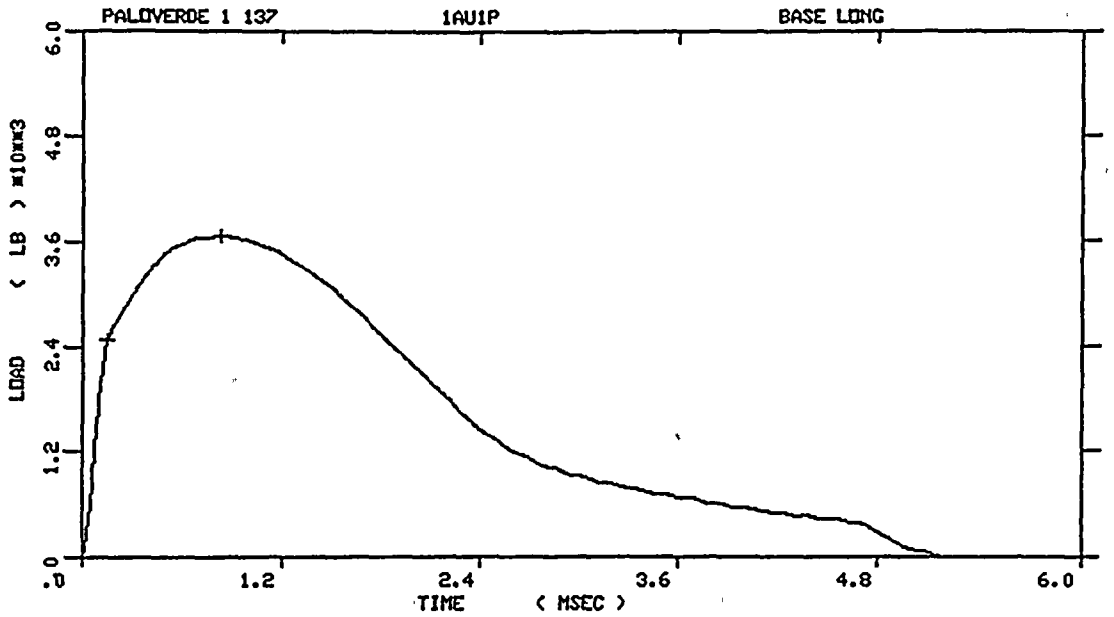

PALOVERDE 1 137
SPECIMEN NUMBER :1AU1P
MATERIAL :BASE LONG
CAPSULE :PALOVERDE #1
:137

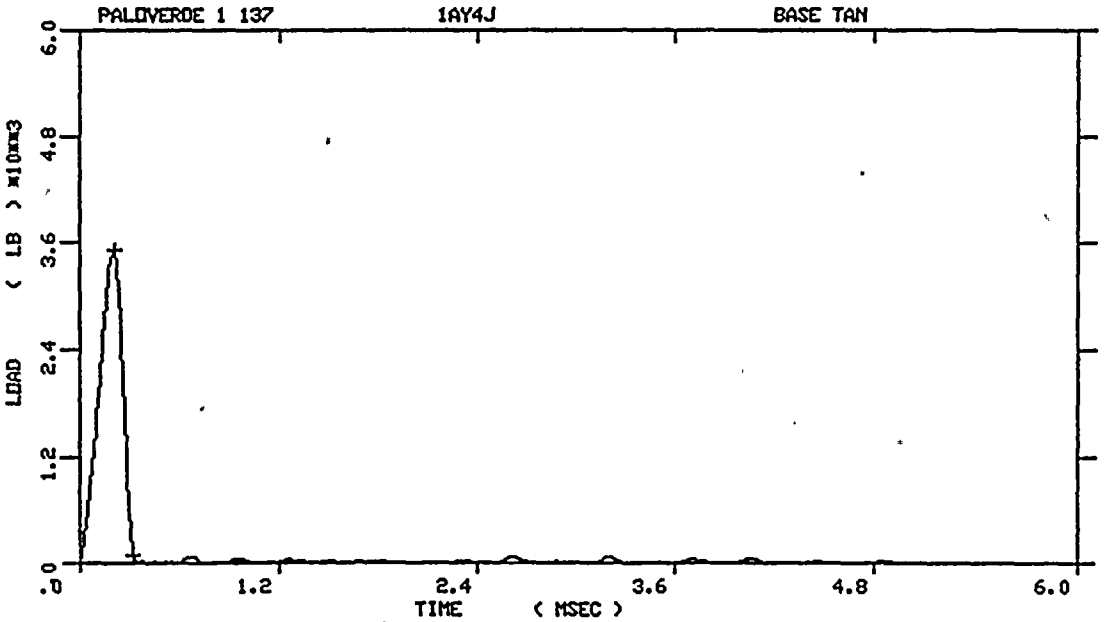

PALOVERDE 1 137
SPECIMEN NUMBER :1AY4J
MATERIAL :BASE TAN
CAPSULE :PALOVERDE #1, 137
:

Figure A-6. Load-time records for Specimens 1AU1P and 1AY4J

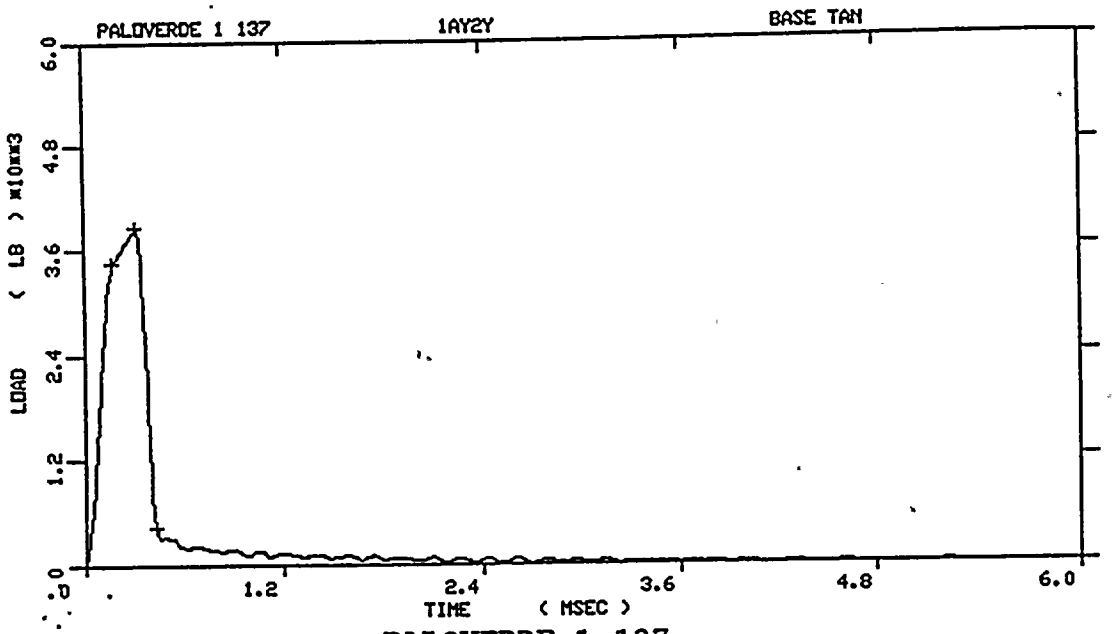

PALOVERDE 1 137
SPECIMEN NUMBER :1AY2Y
MATERIAL :BASE TAN
CAPSULE :PALOVERDE #1 137
:

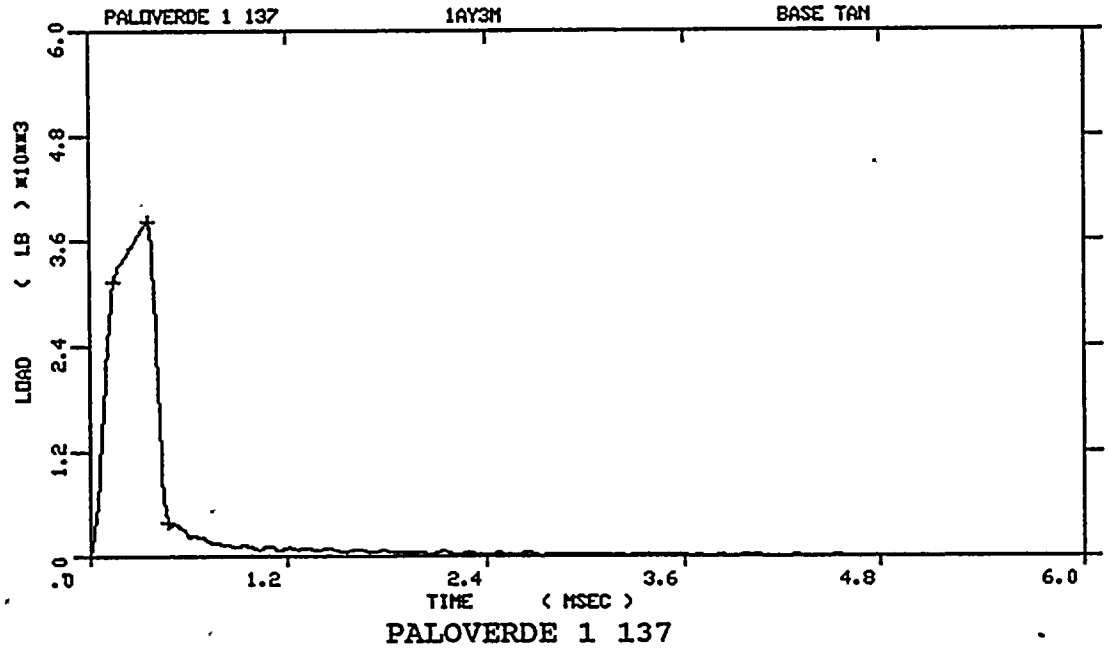

PALOVERDE 1 137
SPECIMEN NUMBER :1AY3M
MATERIAL :BASE TAN
CAPSULE :PALOVERDE #1 137
:

Figure A-7. Load-time records for Specimens 1AY2Y and 1AY3M

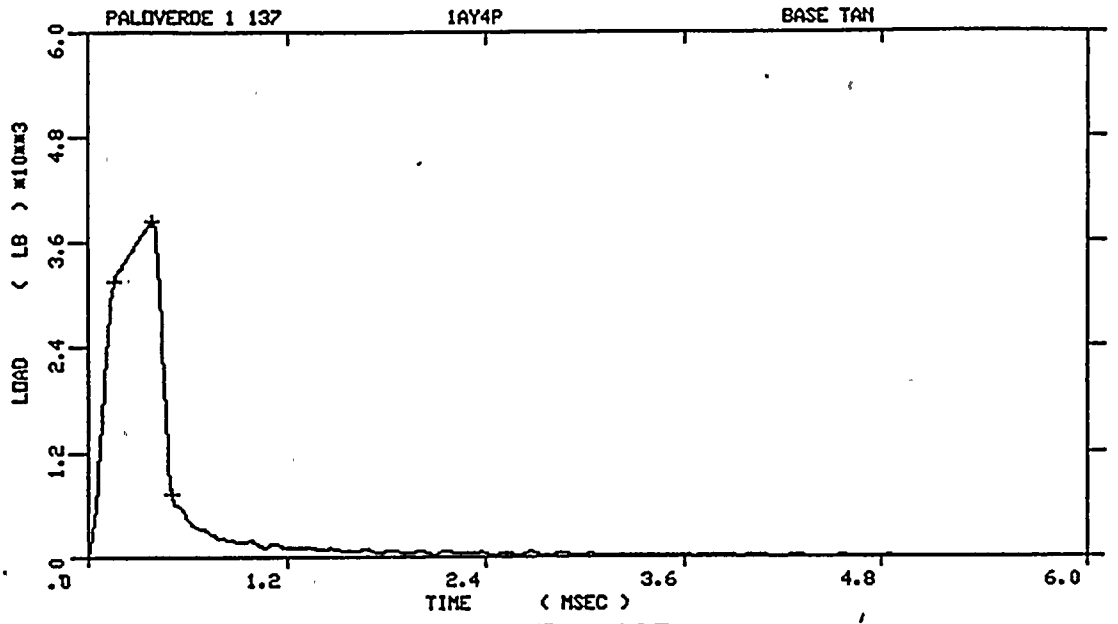

PALOVERDE 1 137
SPECIMEN NUMBER :1AY4P
MATERIAL :BASE TAN
CAPSULE :PALOVERDE #1 137
:

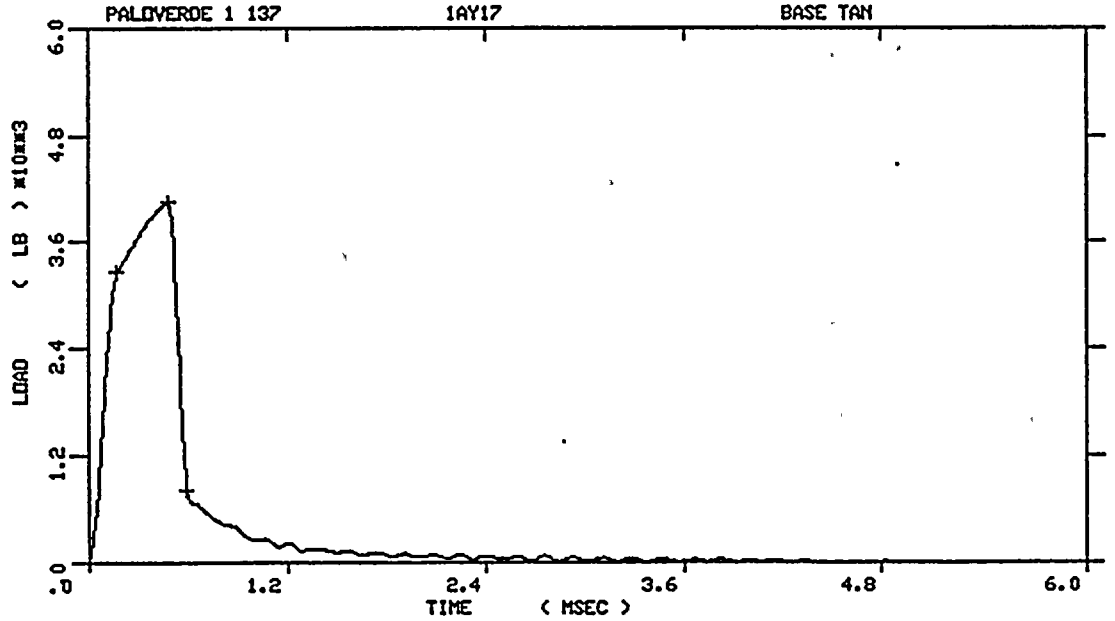

PALOVERDE 1 137
SPECIMEN NUMBER :1AY17
MATERIAL :BASE TAN
CAPSULE :PALOVERDE #1 137
:

Figure A-8. Load-time records for Specimens 1AY4P and 1AY17

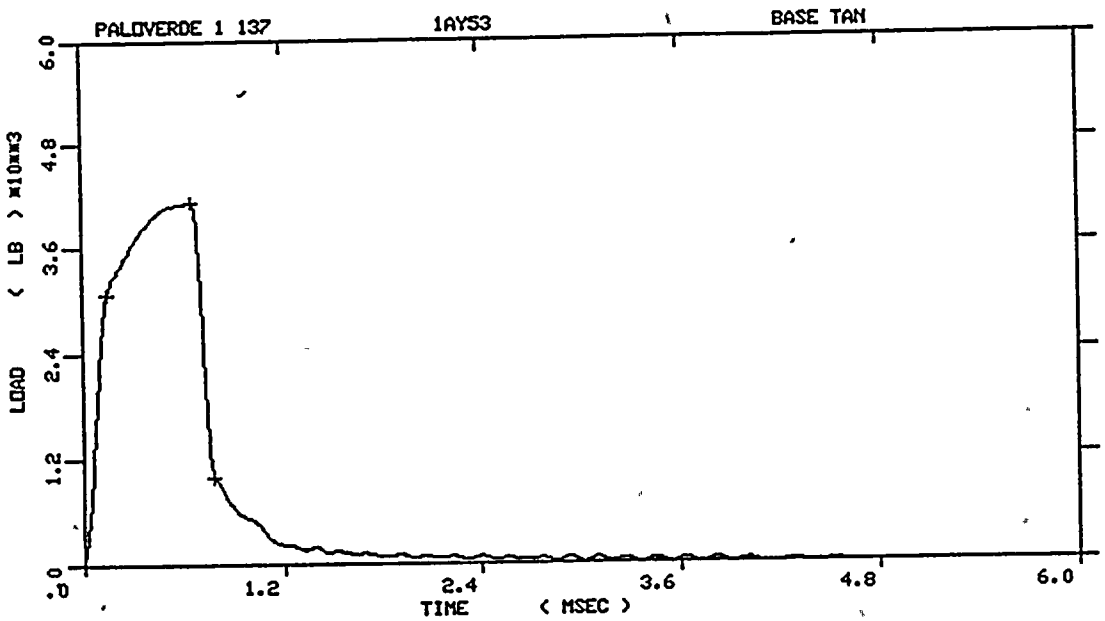

PALOVERDE 1 137
SPECIMEN NUMBER :1AY53
MATERIAL :BASE TAN
CAPSULE :PALOVERDE #1 137
:

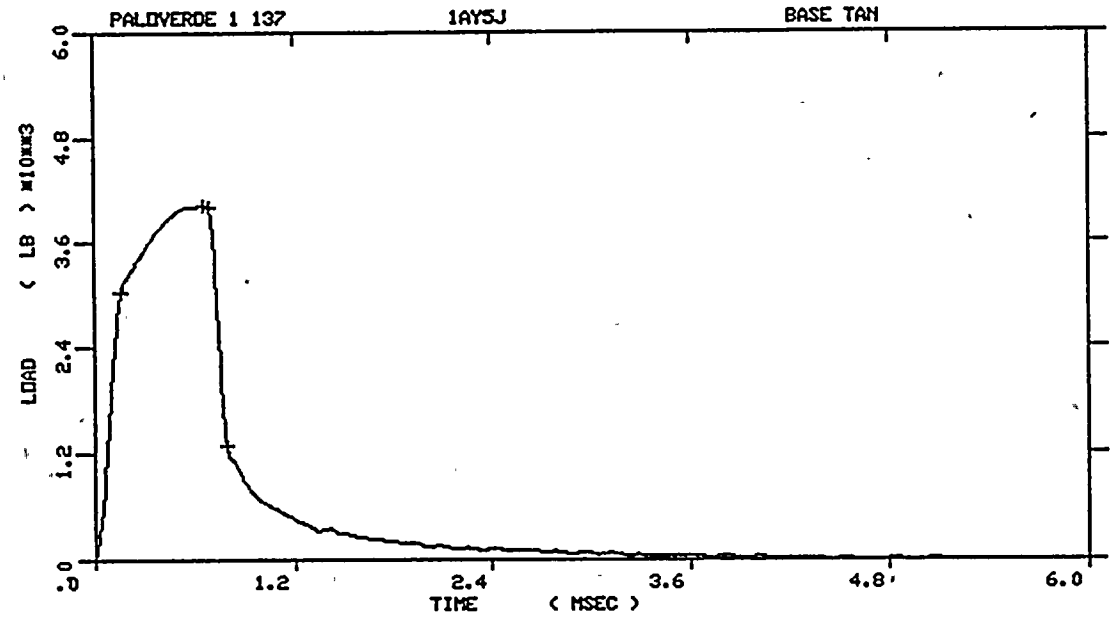

PALOVERDE 1 137
SPECIMEN NUMBER :1AY5J
MATERIAL :BASE TAN
CAPSULE :PALOVERDE #1 137
:

Figure A-9. Load-time records for Specimens 1AY53 and 1AY5J

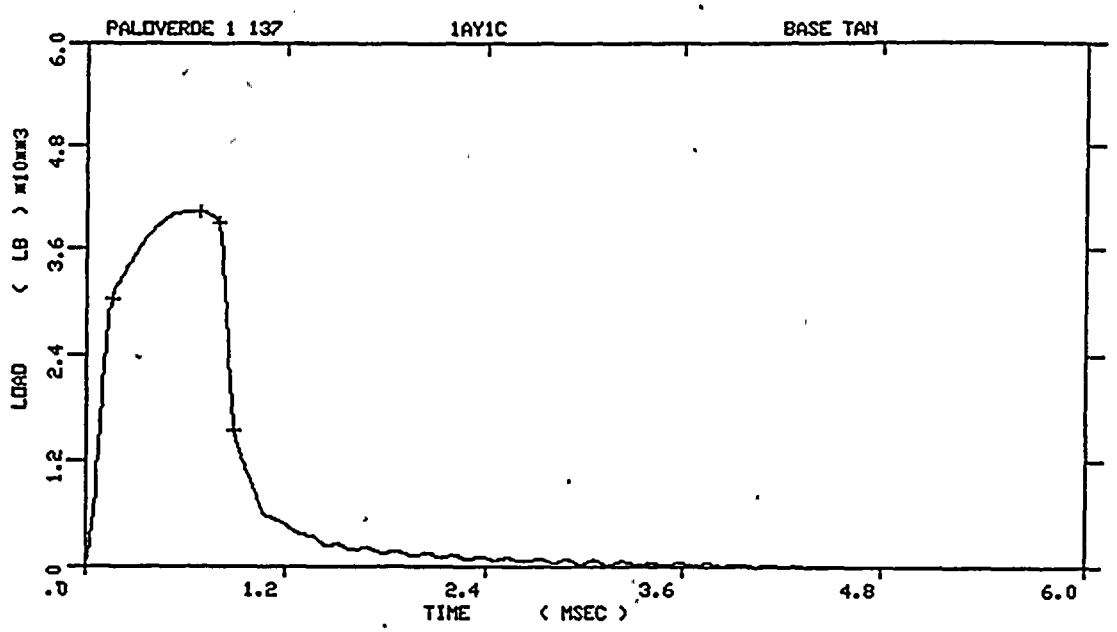

PALOVERDE 1 137
SPECIMEN NUMBER :1AY1C
MATERIAL :BASE TAN
CAPSULE :PALOVERDE #1 137
:

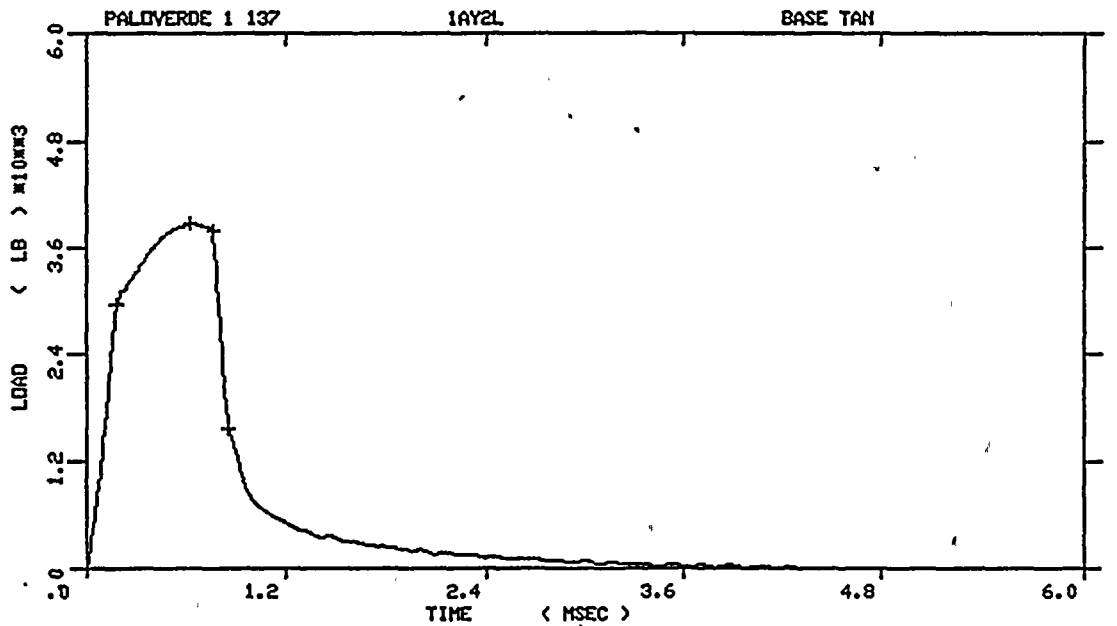

PALOVERDE 1 137
SPECIMEN NUMBER :1AY2L
MATERIAL :BASE TAN
CAPSULE :PALOVERDE #1
:137

Figure A-10. Load-time records for Specimens 1AY1C and 1AY2L

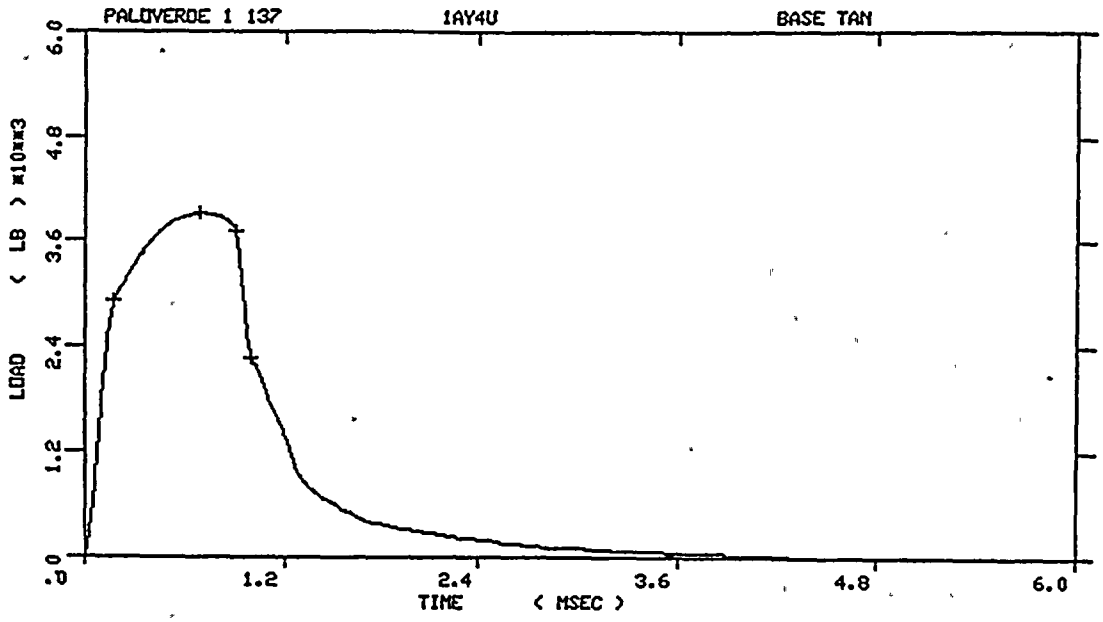

PALOVERDE 1 137
SPECIMEN NUMBER :1AY4U
MATERIAL :BASE TAN
CAPSULE :PALOVERDE #1 137
:

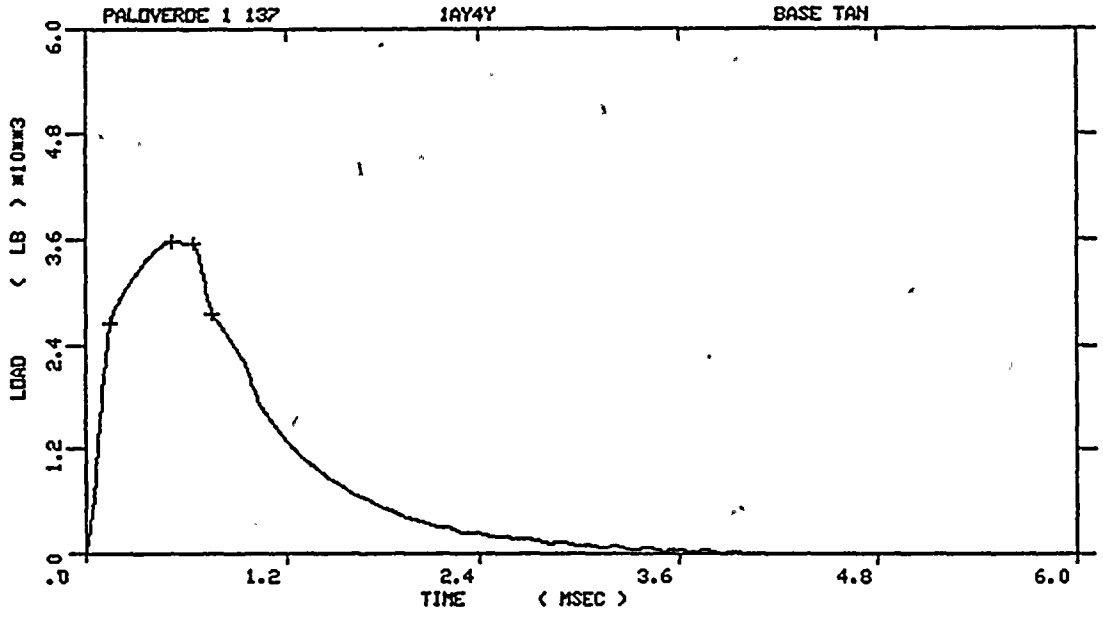

PALOVERDE 1 137
SPECIMEN NUMBER :1AY4Y
MATERIAL :BASE TAN
CAPSULE :PALOVERDE #1 137
:

Figure A-11. Load-time records for Specimens 1AY4U and 1AY4Y

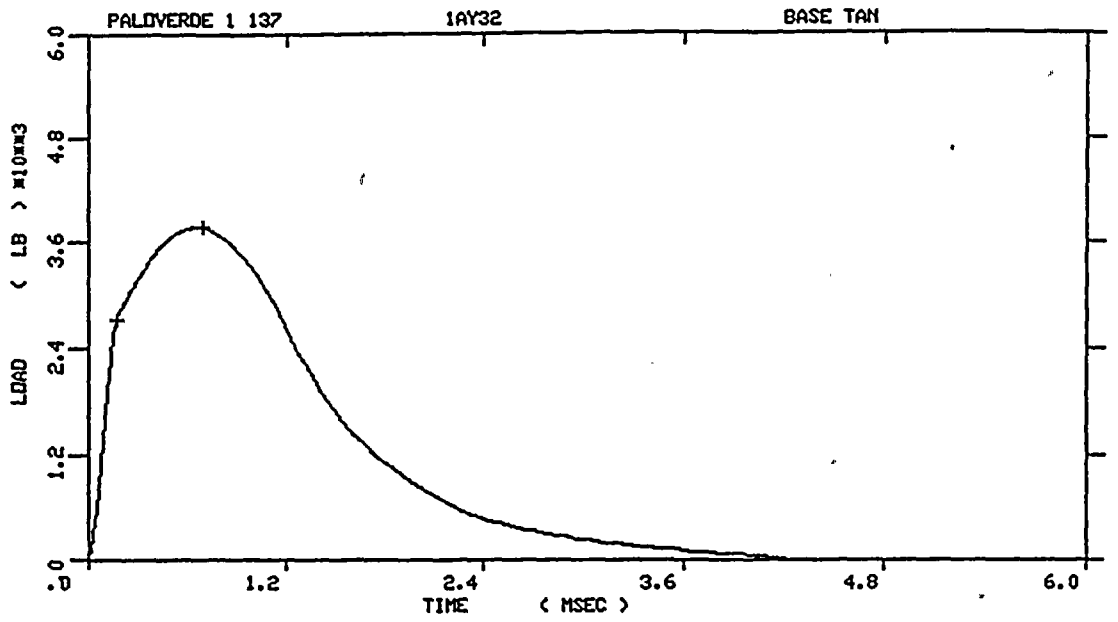

PALOVERDE 1 137
SPECIMEN NUMBER :1AY32
MATERIAL :BASE TAN
CAPSULE :PALOVERDE #1 137
:

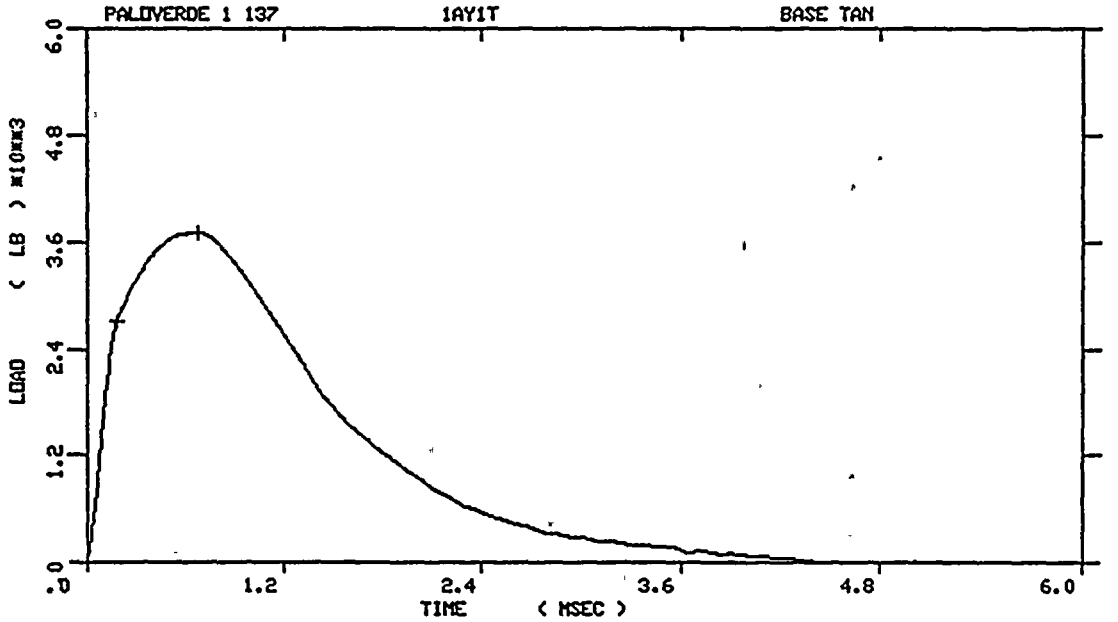

PALOVERDE 1 137
SPECIMEN NUMBER :1AY1T
MATERIAL :BASE TAN
CAPSULE :PALOVERDE #1 137
:

Figure A-12. Load-time records for Specimens 1AY32 and 1AY1T

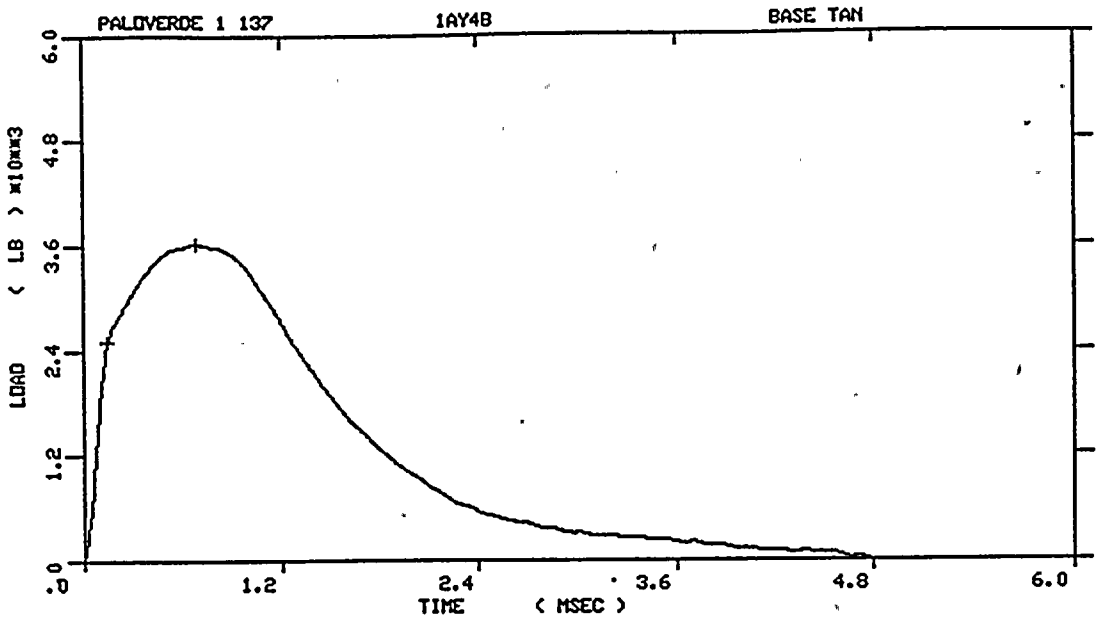

PALOVERDE 1 137
SPECIMEN NUMBER :1AY4B
MATERIAL :BASE TAN
CAPSULE :PALOVERDE #1
:137

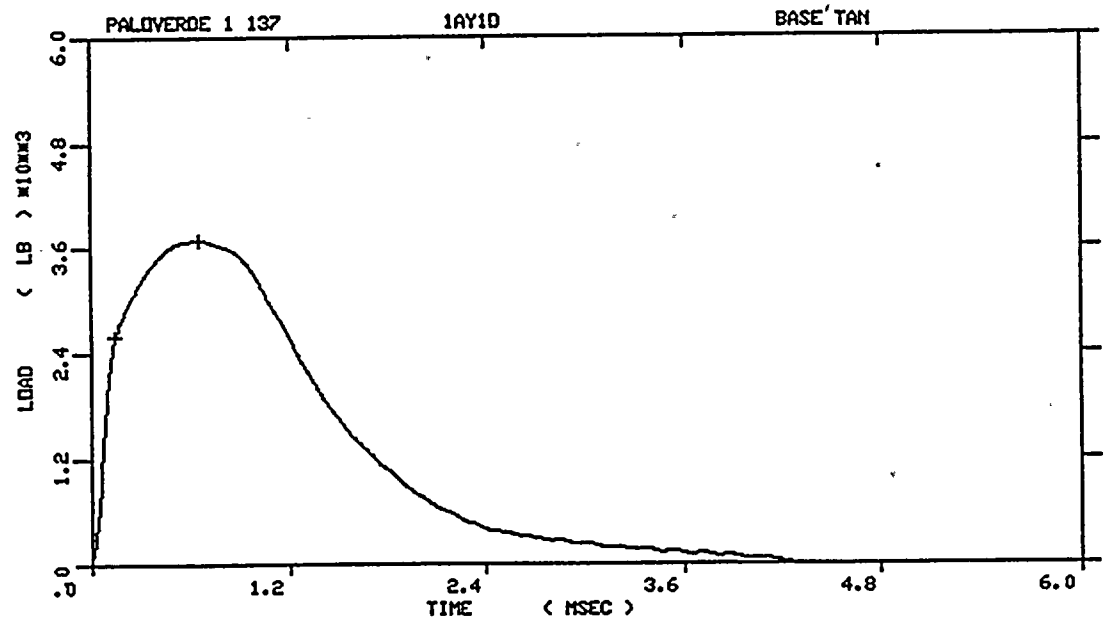

PALOVERDE 1 137
SPECIMEN NUMBER :1AY1D
MATERIAL :BASE TAN
CAPSULE :PALOVERDE #1 137
:

Figure A-13. Load-time records for Specimens 1AY4B and 1AY1D

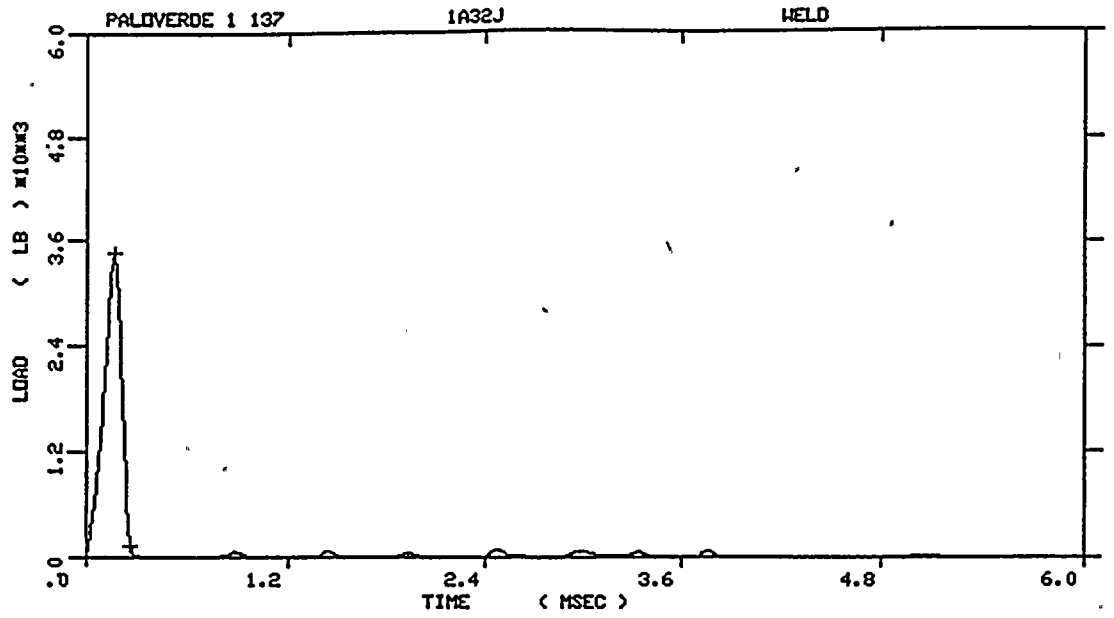

PALOVERDE 1 137
SPECIMEN NUMBER :1A32J
MATERIAL :WELD
CAPSULE :PALOVERDE #1 137
:

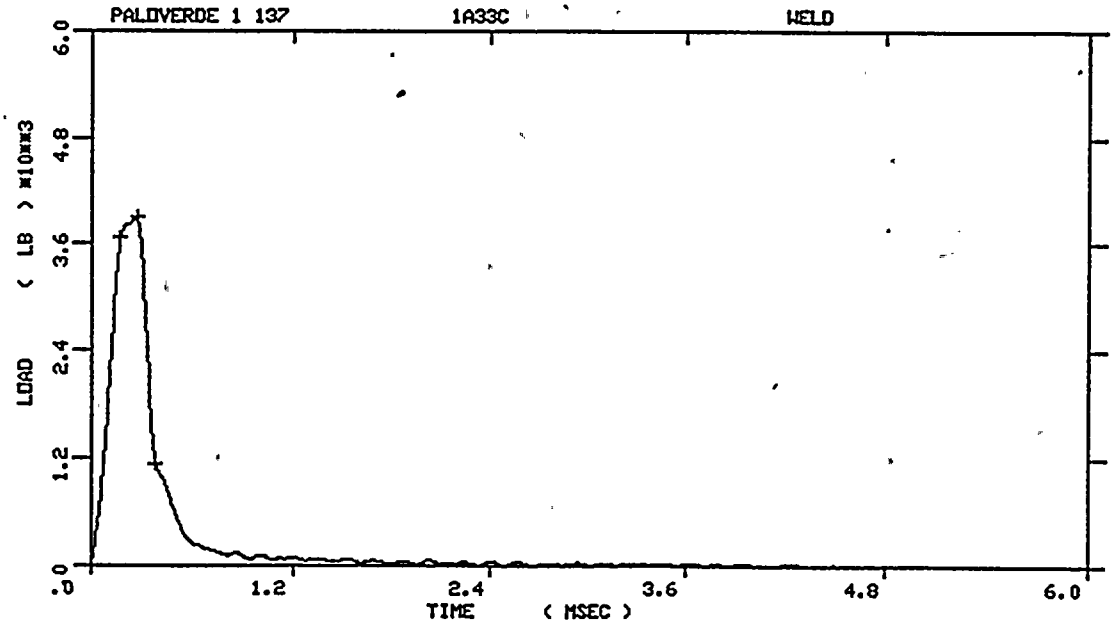

PALOVERDE 1 137
SPECIMEN NUMBER :1A33C
MATERIAL :WELD
CAPSULE :PALOVERDE #1
:137

Figure A-14. Load-time records for Specimens 1A32J and 1A33C

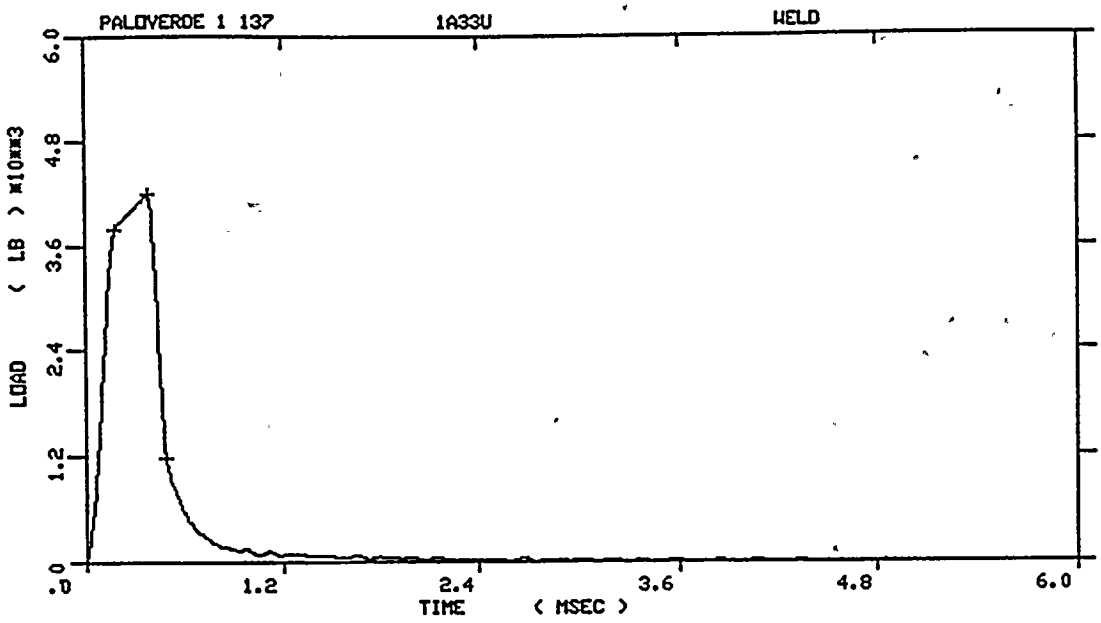

PALOVERDE 1 137
SPECIMEN NUMBER :1A33U
MATERIAL :WELD
CAPSULE :PALOVERDE #1 137
:

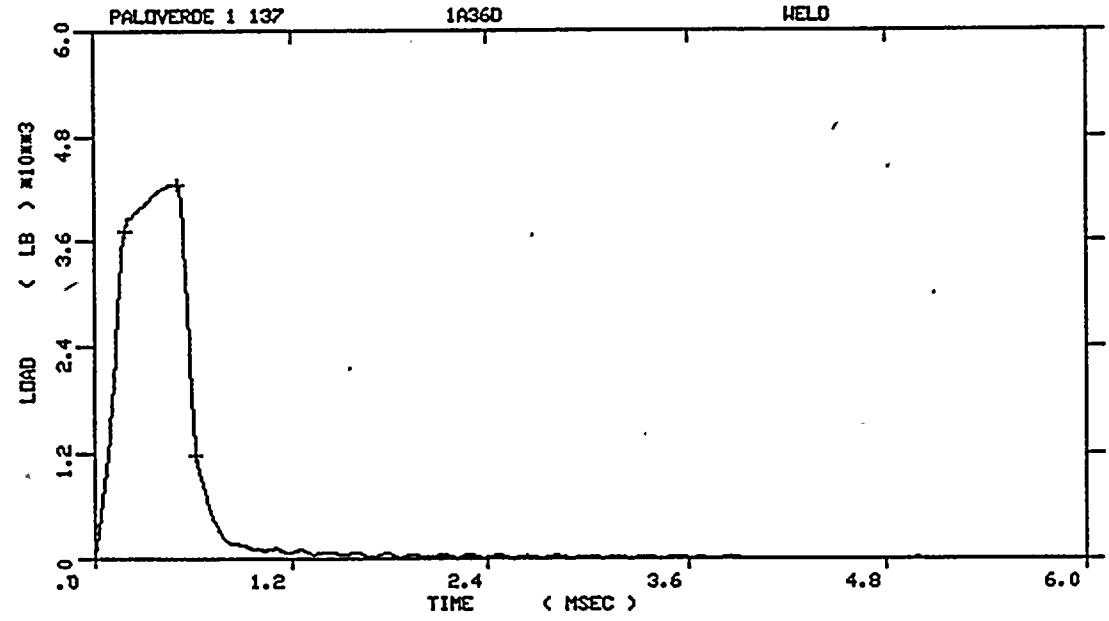

PALOVERDE 1 137
SPECIMEN NUMBER :1A36D
MATERIAL :WELD
CAPSULE :PALOVERDE #1 137
:

Figure A-15. Load-time records for Specimens 1A33U and 1A36D

The load-time record for Specimen 1A337 is not available because of computer system malfunction

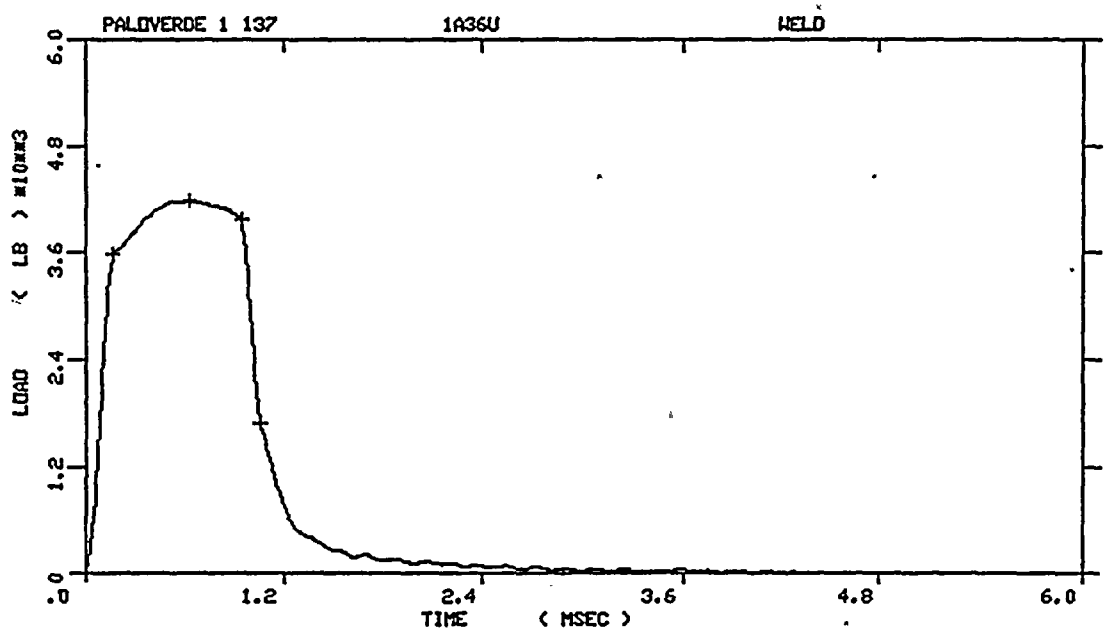

Figure A-16. Load-time records for Specimens 1A337 and 1A36U

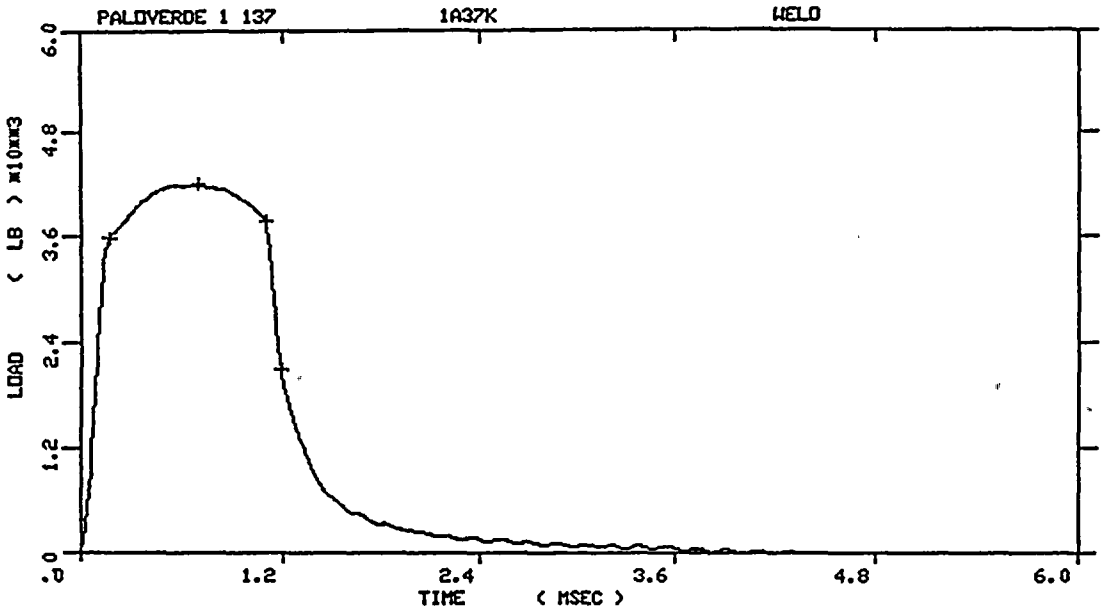

PALOVERDE 1 137
SPECIMEN NUMBER :1A37K
MATERIAL :WELD
CAPSULE :PALOVERDE #1 137
:

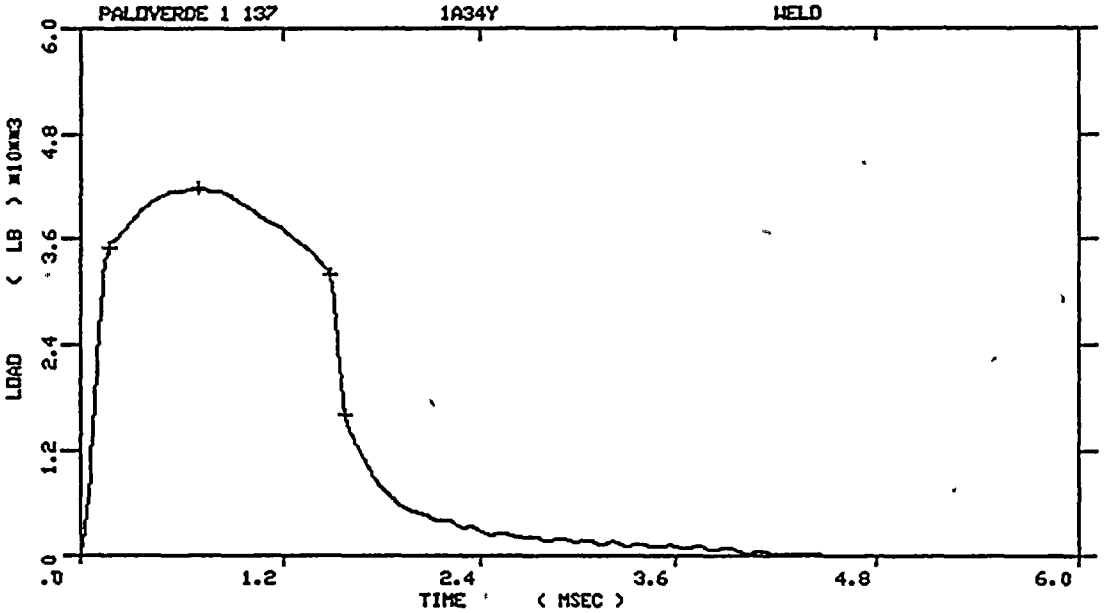

PALOVERDE 1 137
SPECIMEN NUMBER :1A34Y
MATERIAL :WELD
CAPSULE :PALOVERDE #1 137
:

Figure A-17. Load-time records for Specimens 1A37K and 1A34Y

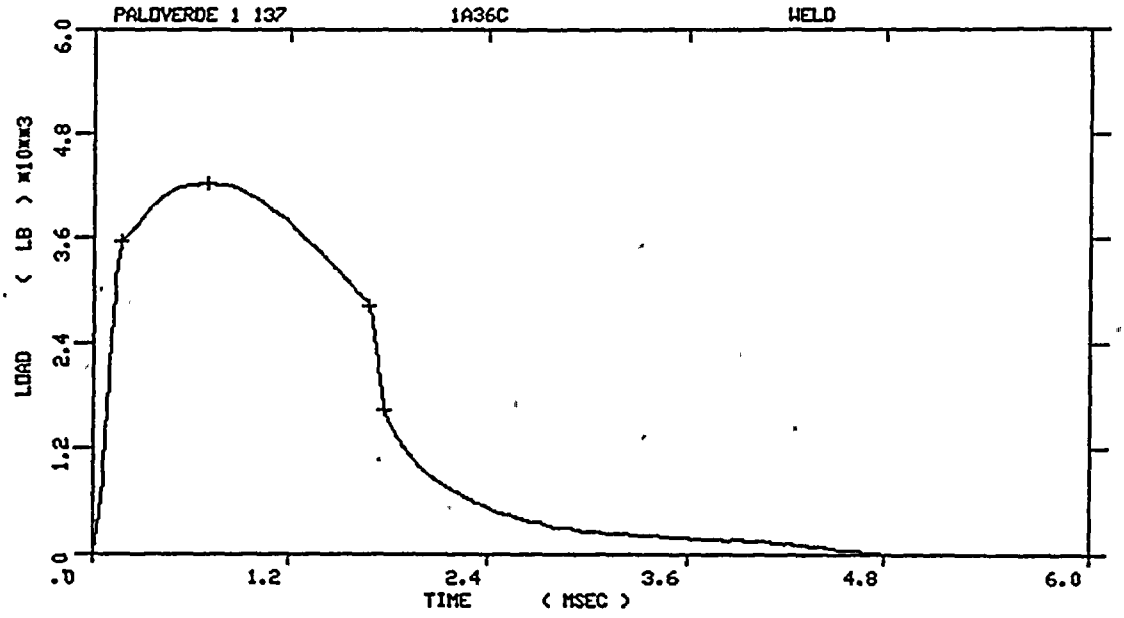

PALOVERDE 1 137
SPECIMEN NUMBER :1A36C
MATERIAL :WELD
CAPSULE :PALOVERDE #1 137
:

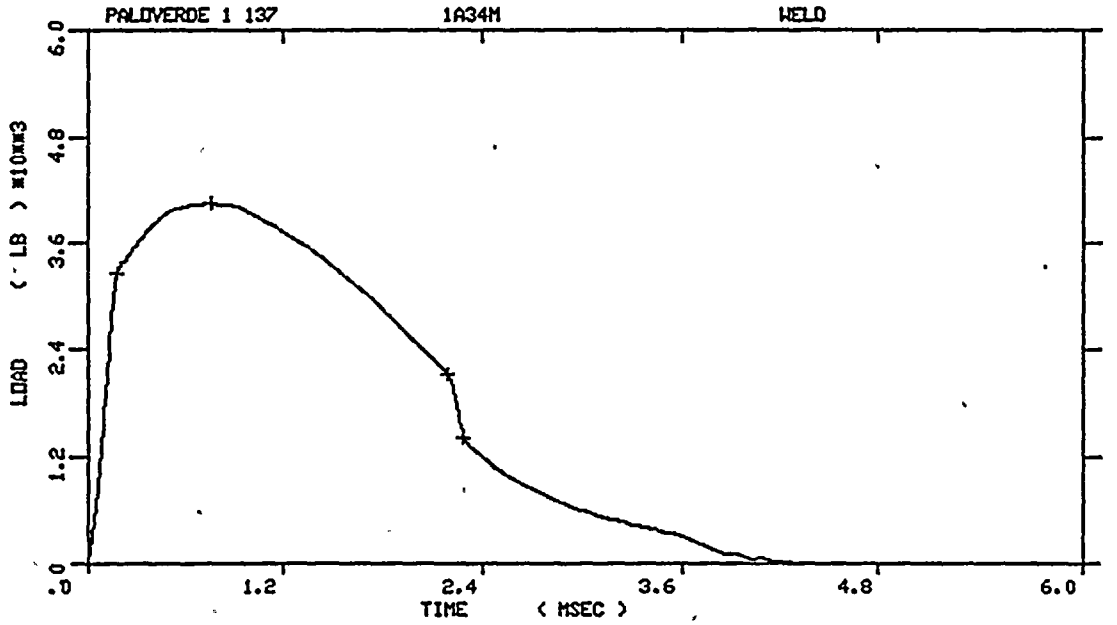

PALOVERDE 1 137
SPECIMEN NUMBER :1A34M
MATERIAL :WELD
CAPSULE :PALOVERDE #1 137
:

Figure A-18. Load-time records for Specimens 1A36C and 1A34M

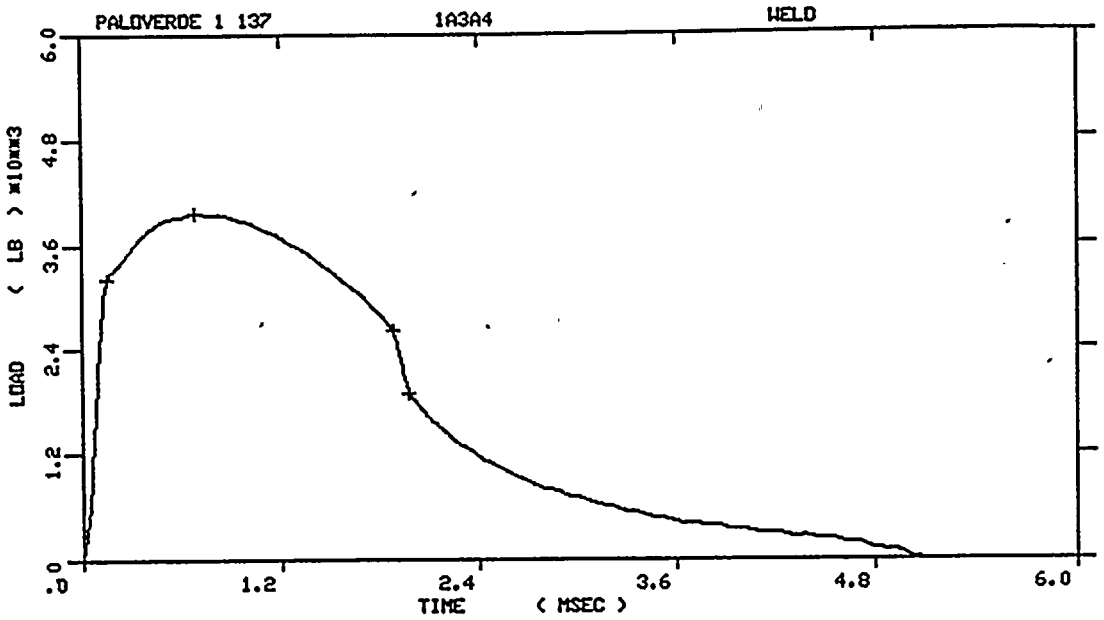

PALOVERDE 1 137

SPECIMEN NUMBER :1A3A4
MATERIAL :WELD
CAPSULE :PALOVERDE #1 137
:

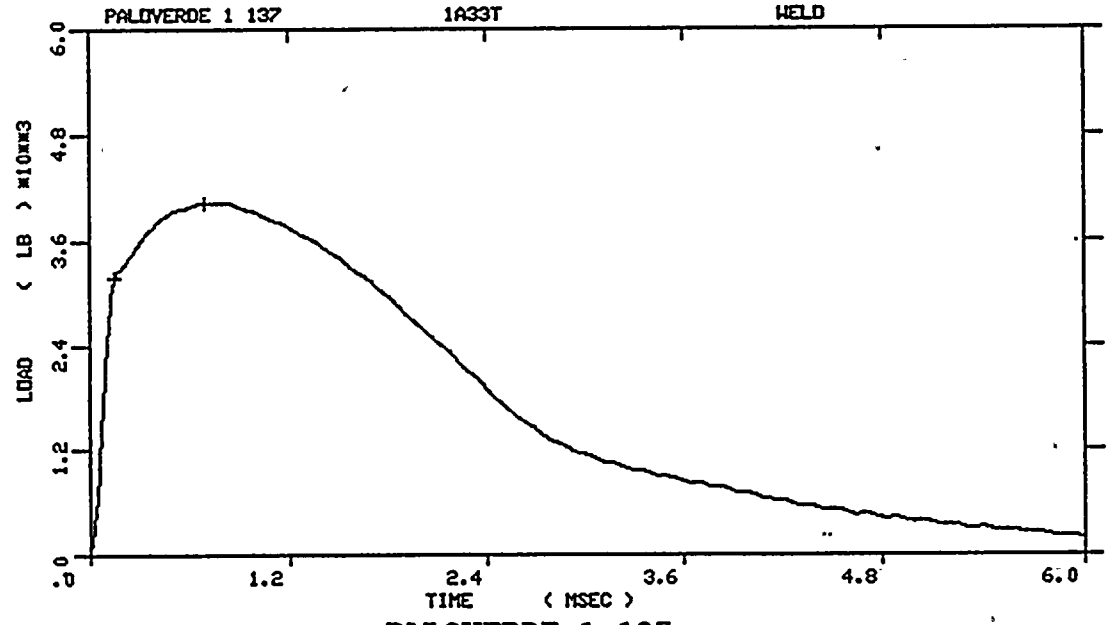

PALOVERDE 1 137

SPECIMEN NUMBER :1A33T
MATERIAL :WELD
CAPSULE :PALOVERDE #1 137
:

Figure A-19. Load-time records for Specimens 1A3A4 and 1A33T

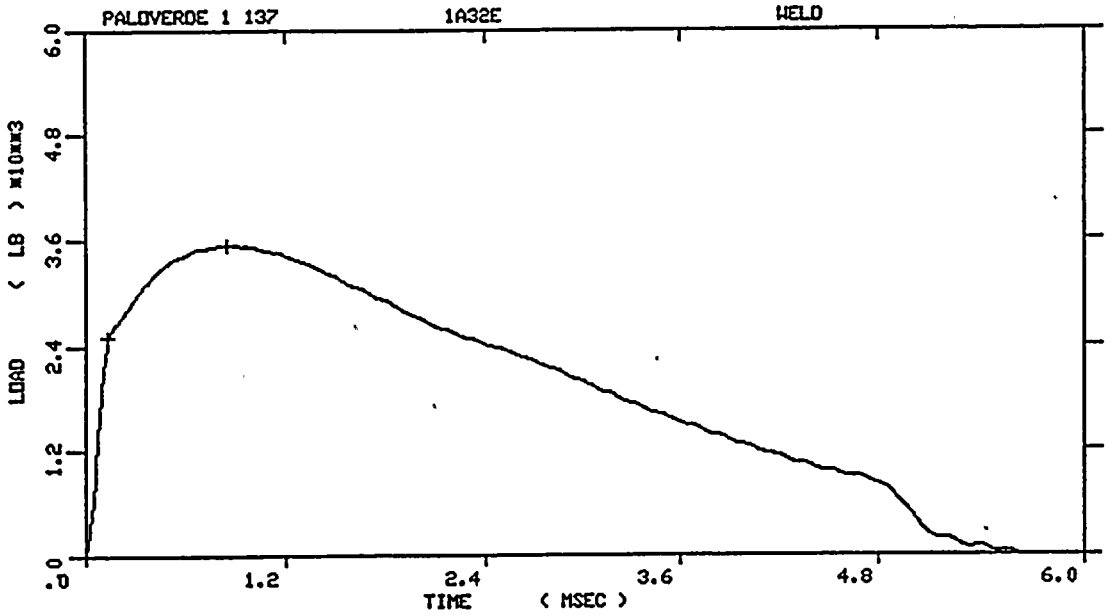

PALOVERDE 1 137
SPECIMEN NUMBER :1A32E
MATERIAL :WELD
CAPSULE :PALOVERDE #1 137
:

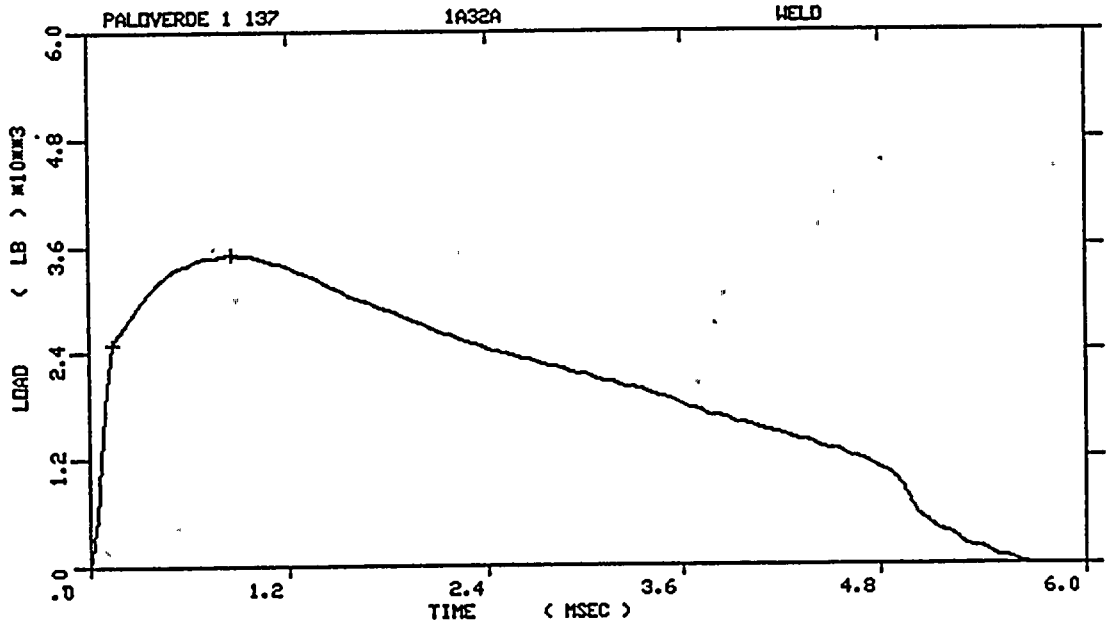

PALOVERDE 1 137
SPECIMEN NUMBER :1A32A
MATERIAL :WELD
CAPSULE :PALOVERDE #1
:137

Figure A-20. Load-time records for Specimens 1A32E and 1A32A

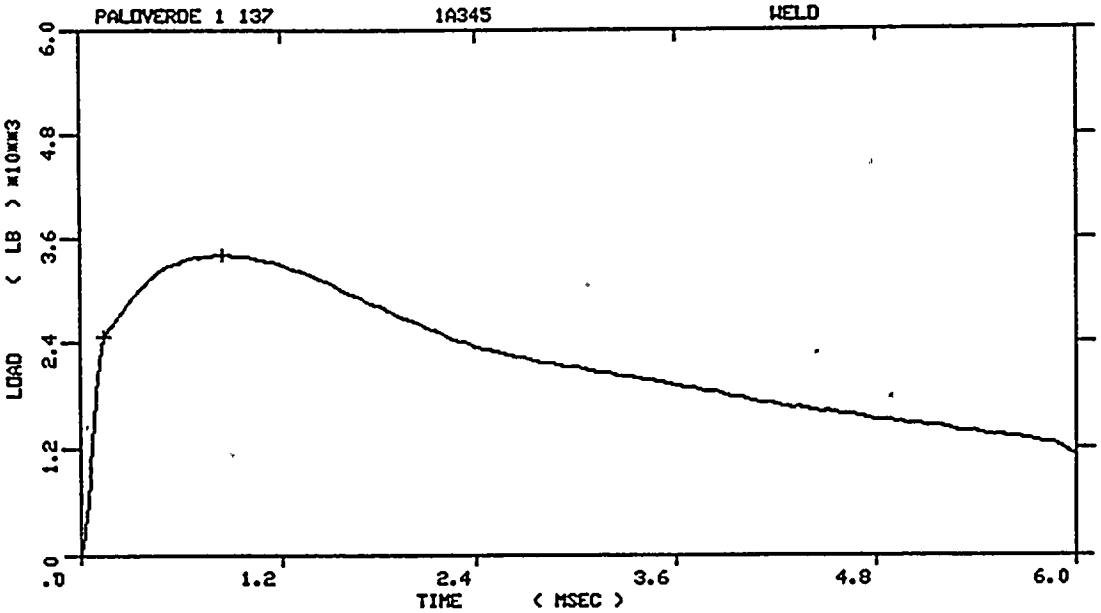

PALOVERDE 1 137
SPECIMEN NUMBER :1A345
MATERIAL :WELD
CAPSULE :PALOVERDE #1 137
:

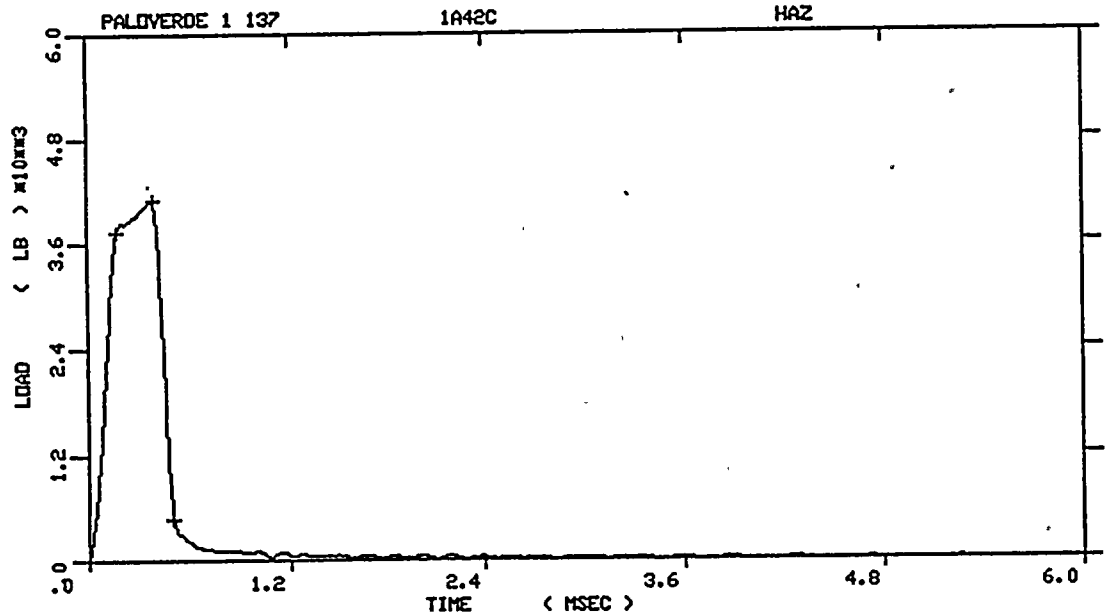

PALOVERDE 1 137
SPECIMEN NUMBER :1A42C
MATERIAL :HAZ
CAPSULE :PALOVERDE #1
:137

Figure A-21. Load-time records for Specimens 1A345 and 1A42C

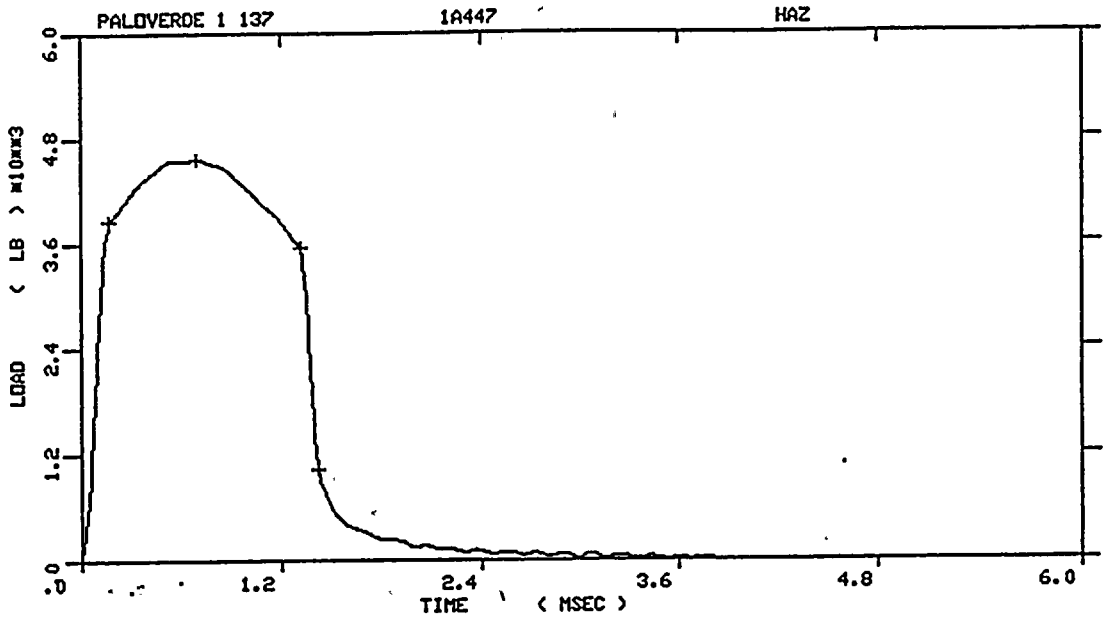

PALOVERDE 1 137
SPECIMEN NUMBER :1A447
MATERIAL :HAZ
CAPSULE :PALOVERDE #1 137
:

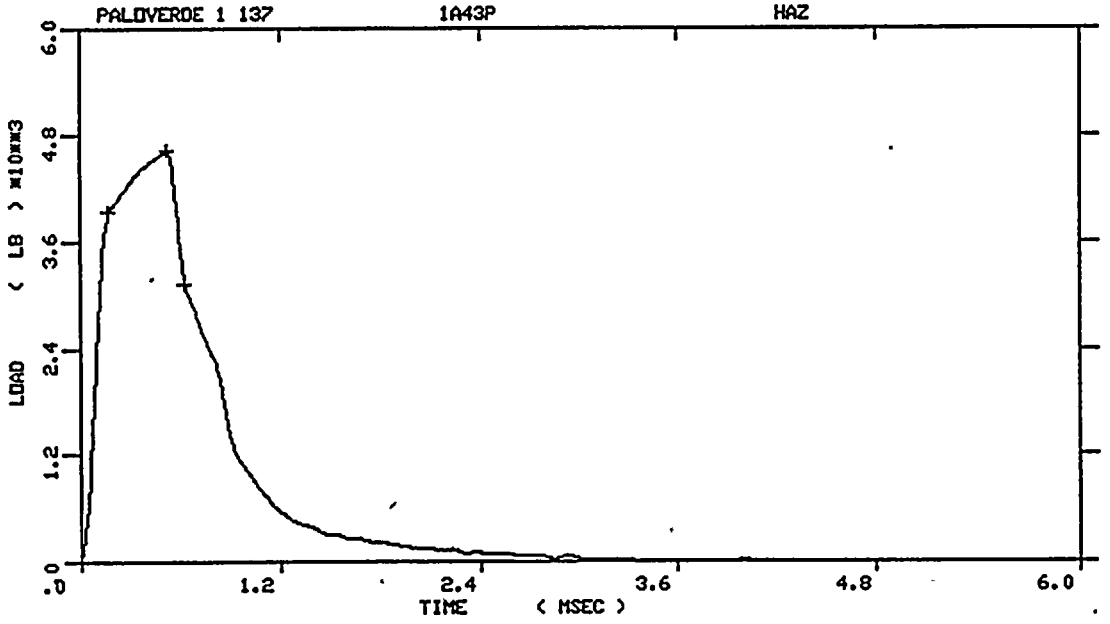

PALOVERDE 1 137
SPECIMEN NUMBER :1A43P
MATERIAL :HAZ
CAPSULE :PALOVERDE #1 137
:

Figure A-22. Load-time records for Specimens 1A447 and 1A43P

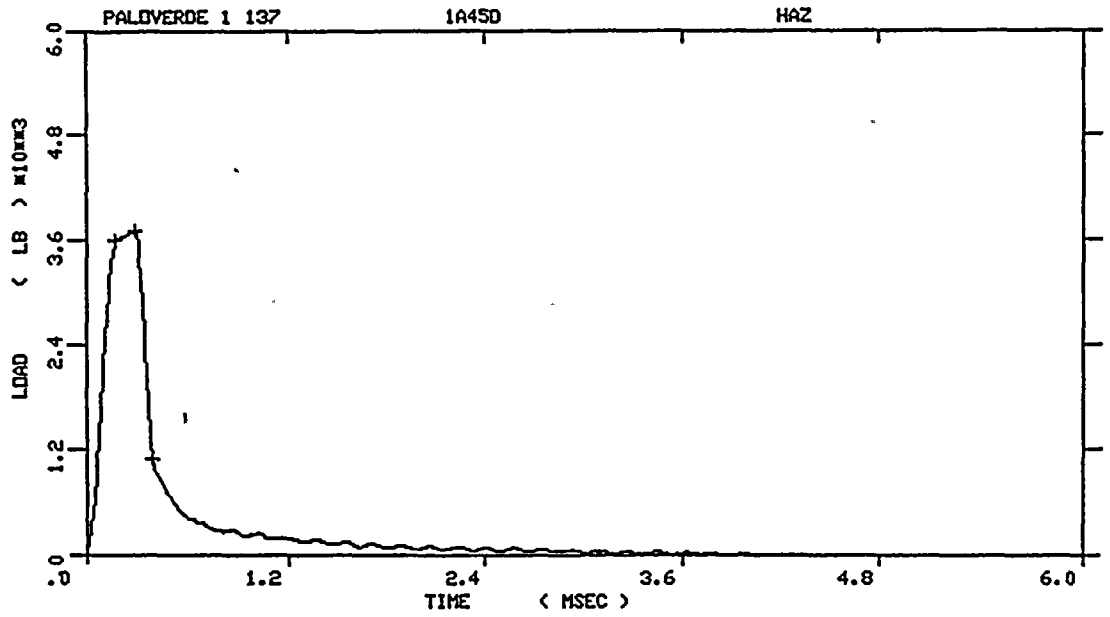

PALOVERDE 1 137
SPECIMEN NUMBER :1A45D
MATERIAL :HAZ
CAPSULE :PALOVERDE #1 137
:

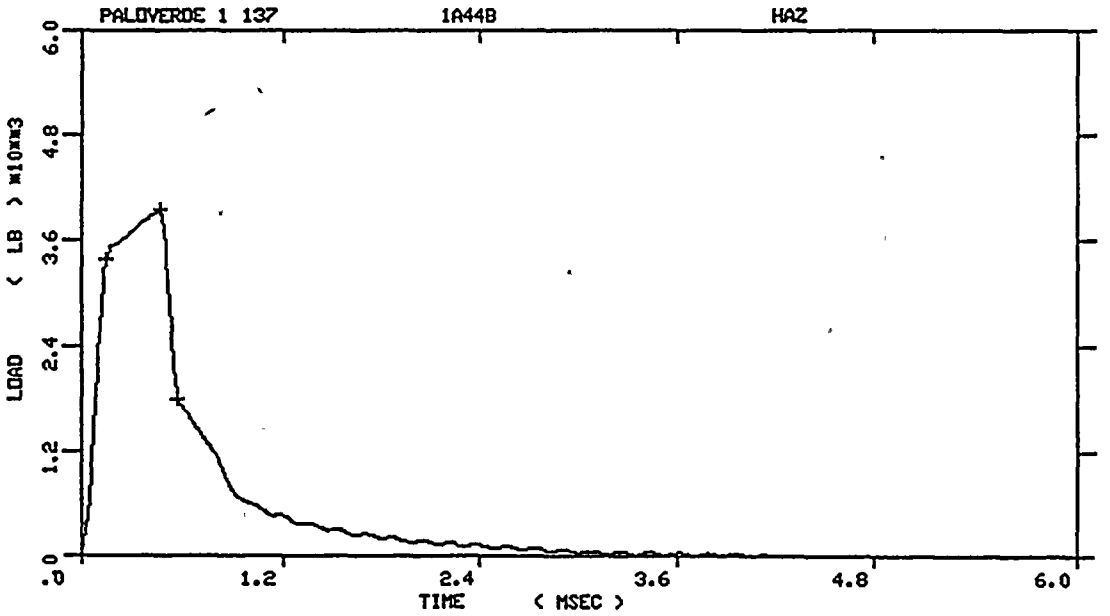

PALOVERDE 1 137
SPECIMEN NUMBER :1A44B
MATERIAL :HAZ
CAPSULE :PALOVERDE #1 137
:

Figure A-23. Load-time records for Specimens 1A45D and 1A44B

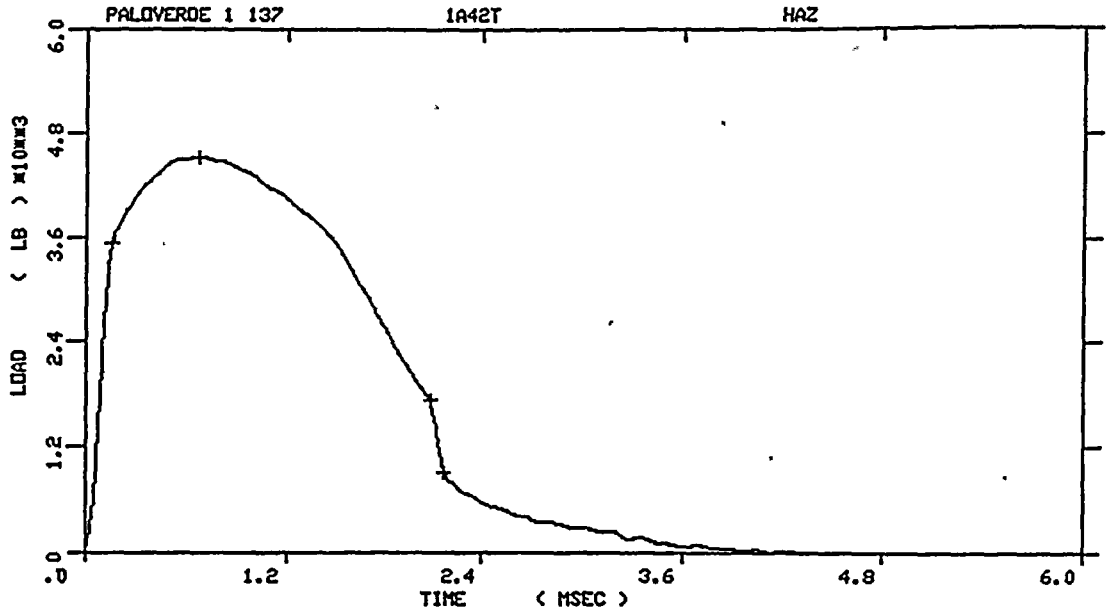

PALOVERDE 1 137
SPECIMEN NUMBER :1A42T
MATERIAL :HAZ
CAPSULE :PALOVERDE #1 137
:

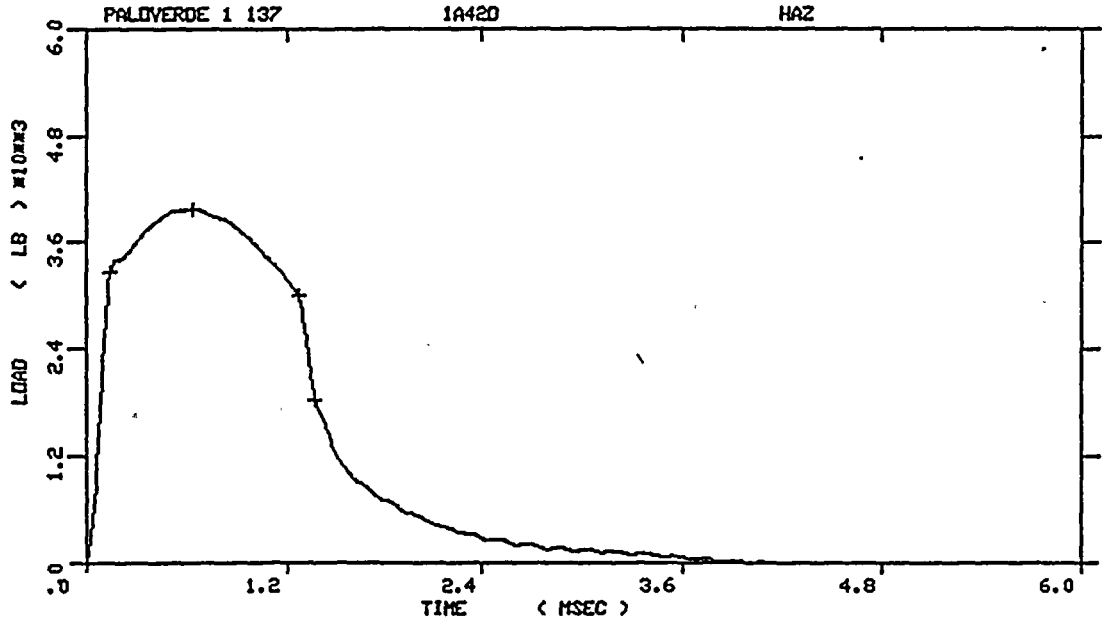

PALOVERDE 1 137
SPECIMEN NUMBER :1A42D
MATERIAL :HAZ
CAPSULE :PALOVERDE #1 137
:

Figure A-24. Load-time records for Specimens 1A42T and 1A42D

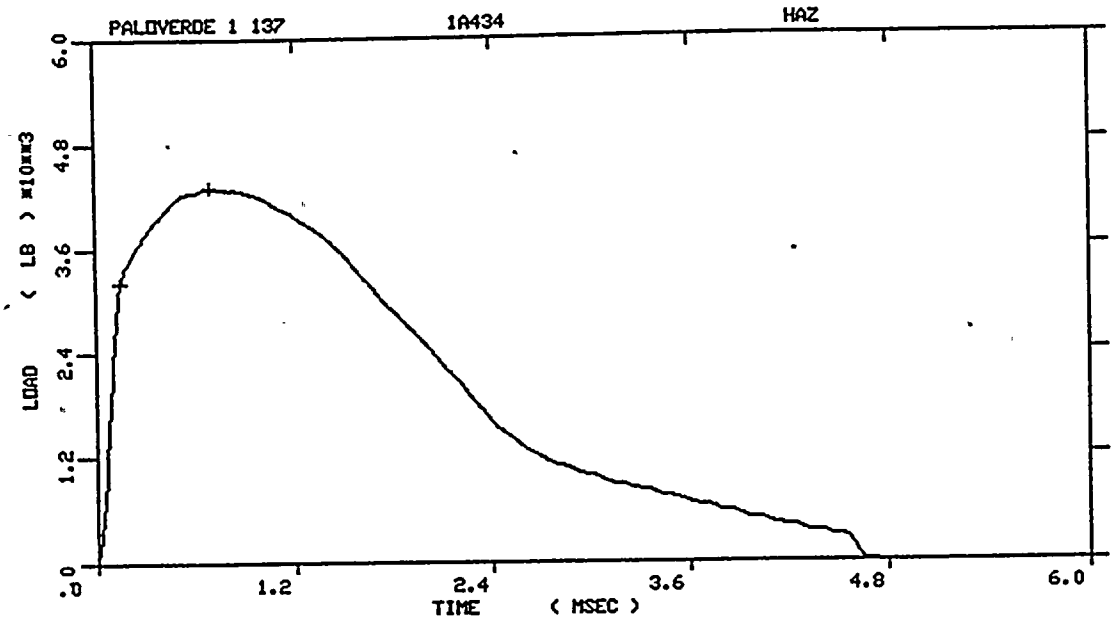

PALOVERDE 1 137
SPECIMEN NUMBER :1A434
MATERIAL :HAZ
CAPSULE :PALOVERDE #1 137
:

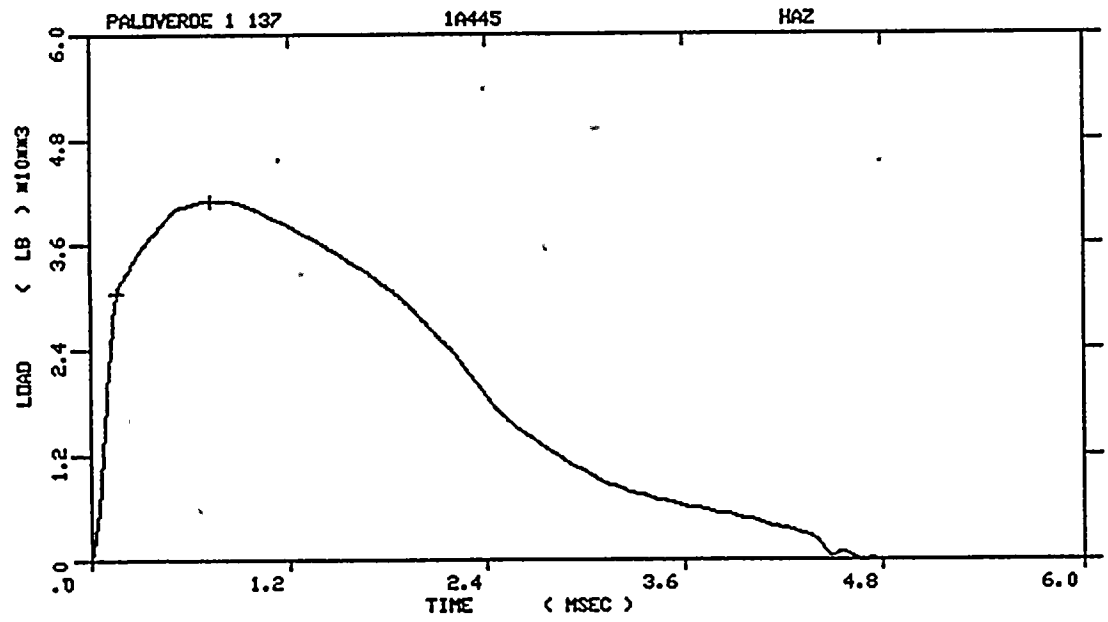

PALOVERDE 1 137
SPECIMEN NUMBER :1A445
MATERIAL :HAZ
CAPSULE :PALOVERDE #1 137
:

Figure A-25. Load-time records for Specimens 1A434 and 1A445

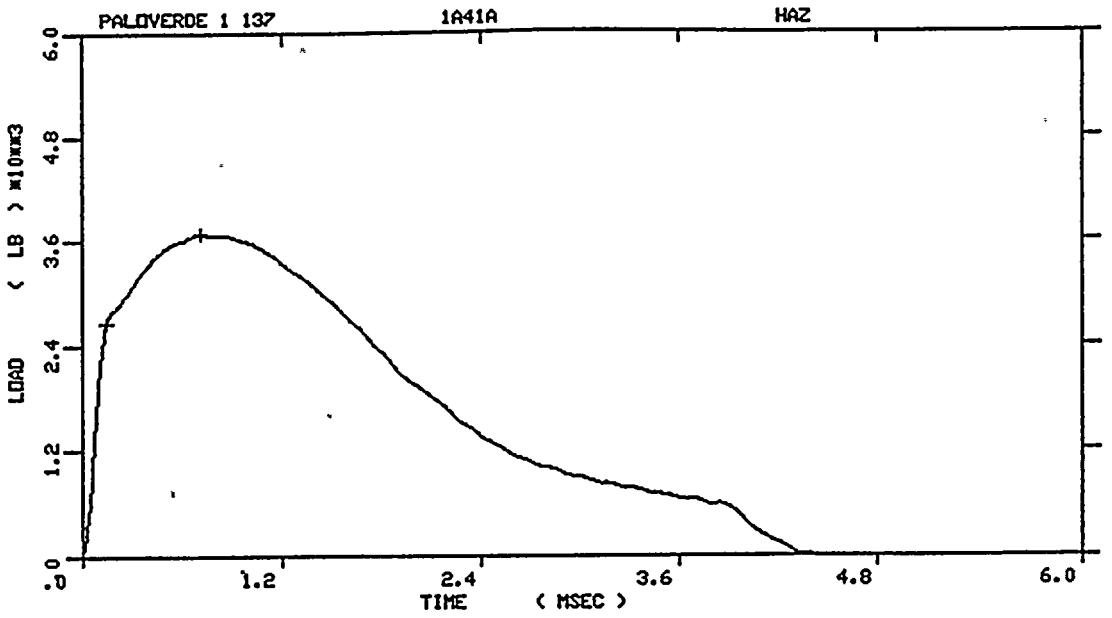

PALOVERDE 1 137
SPECIMEN NUMBER :1A41A
MATERIAL :HAZ
CAPSULE :PALOVERDE #1 137
:

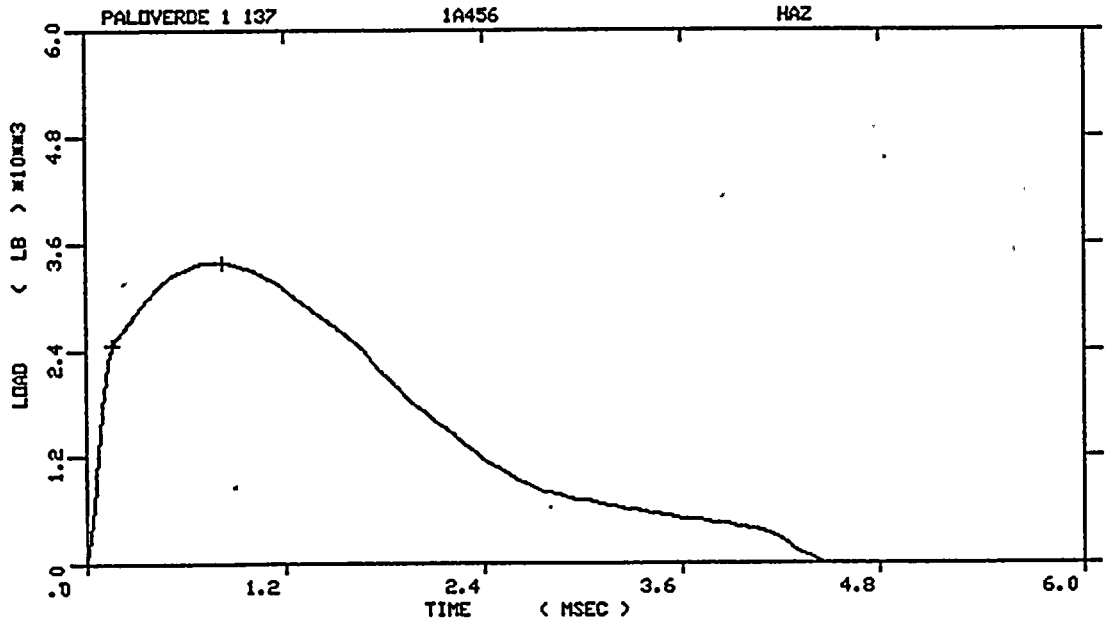

PALOVERDE 1 137
SPECIMEN NUMBER :1A456
MATERIAL :HAZ
CAPSULE :PALOVERDE #1
:137

Figure A-26. Load-time records for Specimens 1A41A and 1A456

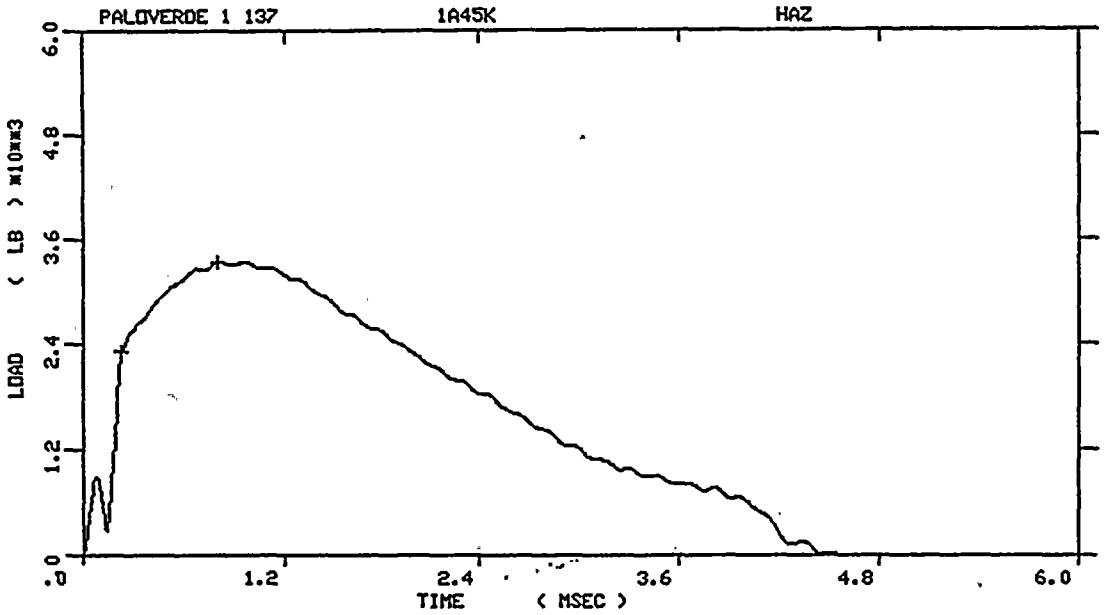

PALOVERDE 1 137

SPECIMEN NUMBER	:1A45K
MATERIAL	:HAZ
CAPSULE	:PALOVERDE #1 137
	:

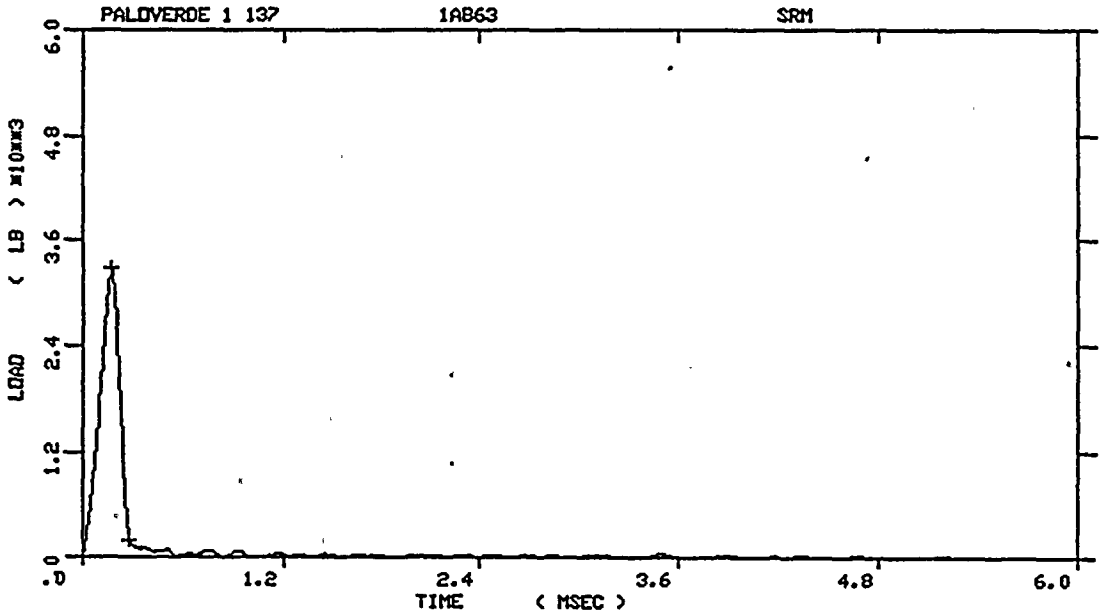

PALOVERDE 1 137

SPECIMEN NUMBER	:1AB63
MATERIAL	:SRM
CAPSULE	:PALOVERDE #1 137
	:

Figure A-27. Load-time records for Specimens 1A45K and 1AB63

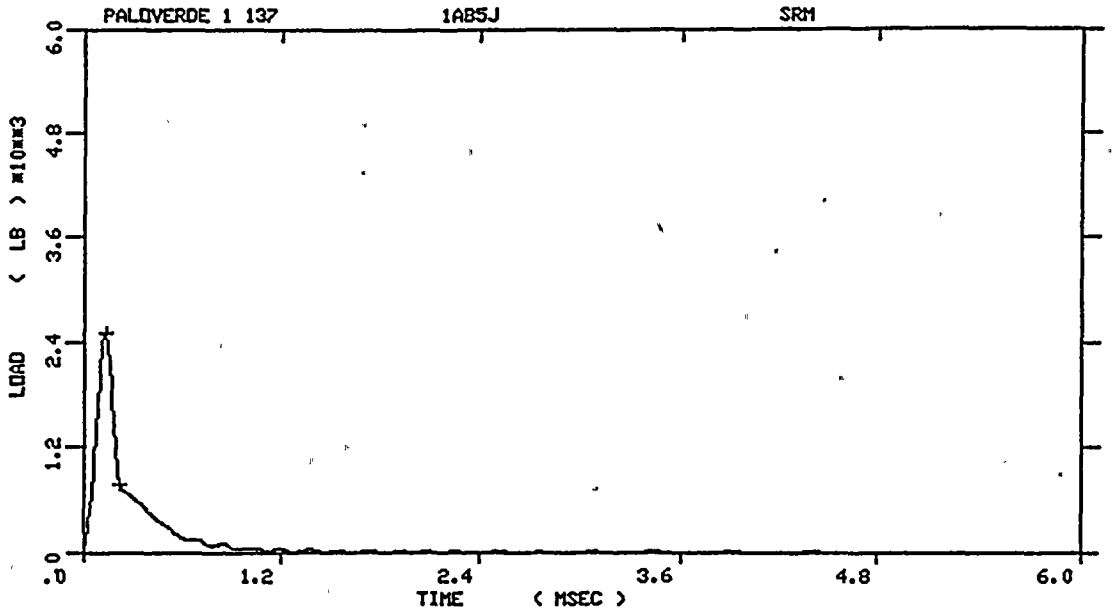

PALOVERDE 1 137
SPECIMEN NUMBER :1AB5J
MATERIAL :SRM
CAPSULE :PALOVERDE #1 137
:

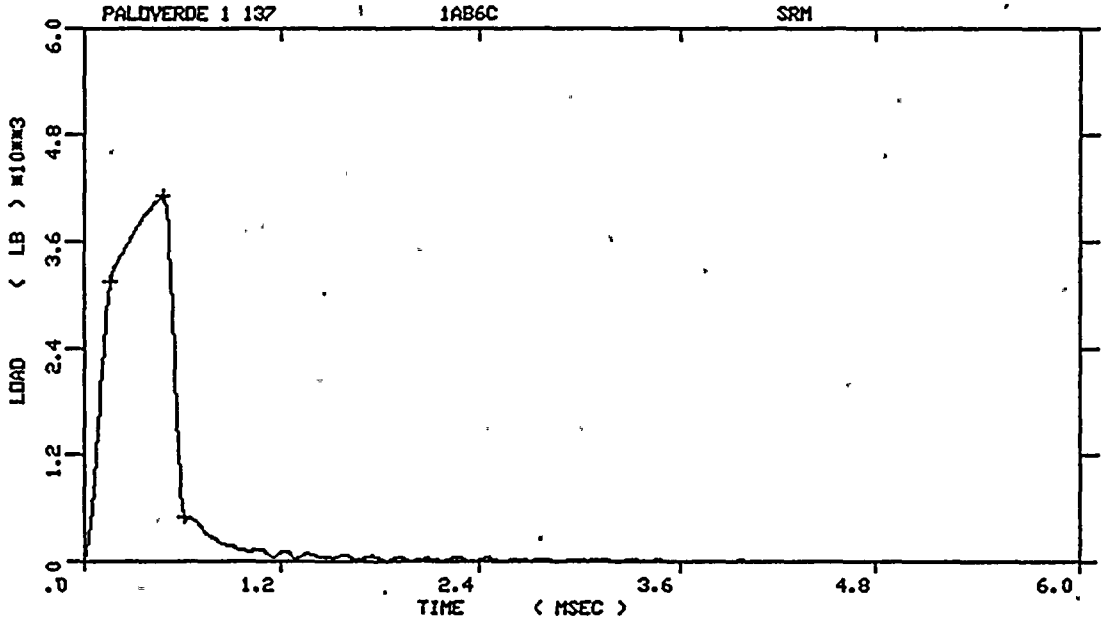

PALOVERDE 1 137
SPECIMEN NUMBER :1AB6C
MATERIAL :SRM
CAPSULE :PALOVERDE #1
:137

Figure A-28. Load-time records for Specimens 1AB5J and 1AB6C

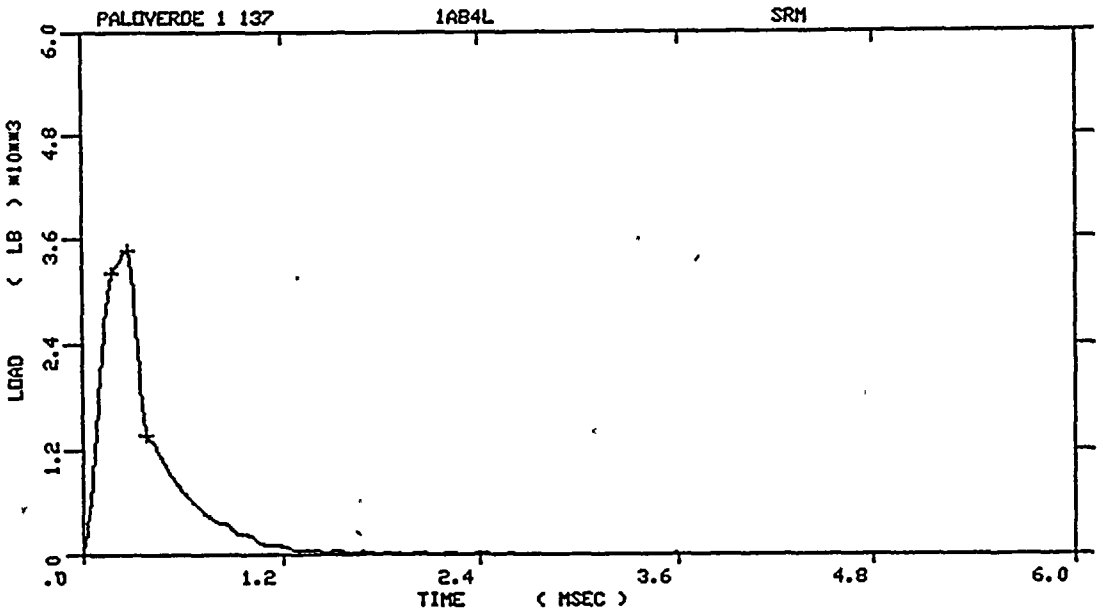

PALOVERDE 1 137
SPECIMEN NUMBER :1AB4L
MATERIAL :SRM
CAPSULE :PALOVERDE #1 137
:

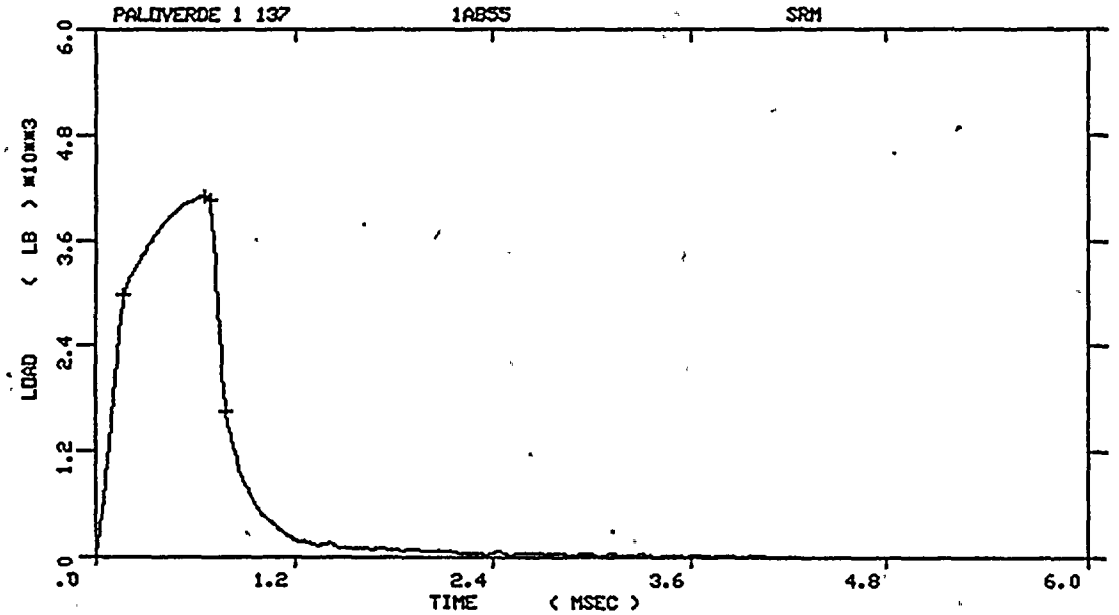

PALOVERDE 1 137
SPECIMEN NUMBER :1AB55
MATERIAL :SRM
CAPSULE :PALOVERDE #1 137
:

Figure A-29. Load-time records for Specimens 1AB4L and 1AB55

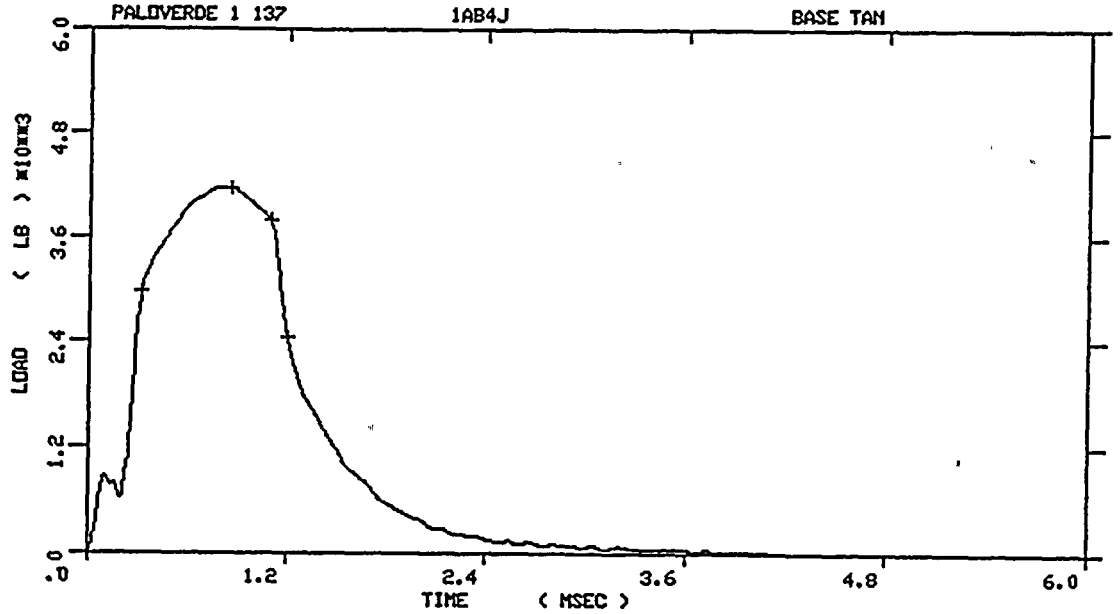

PALOVERDE 1 137
SPECIMEN NUMBER :1AB4J
MATERIAL :SRM
CAPSULE :PALOVERDE #1
:137

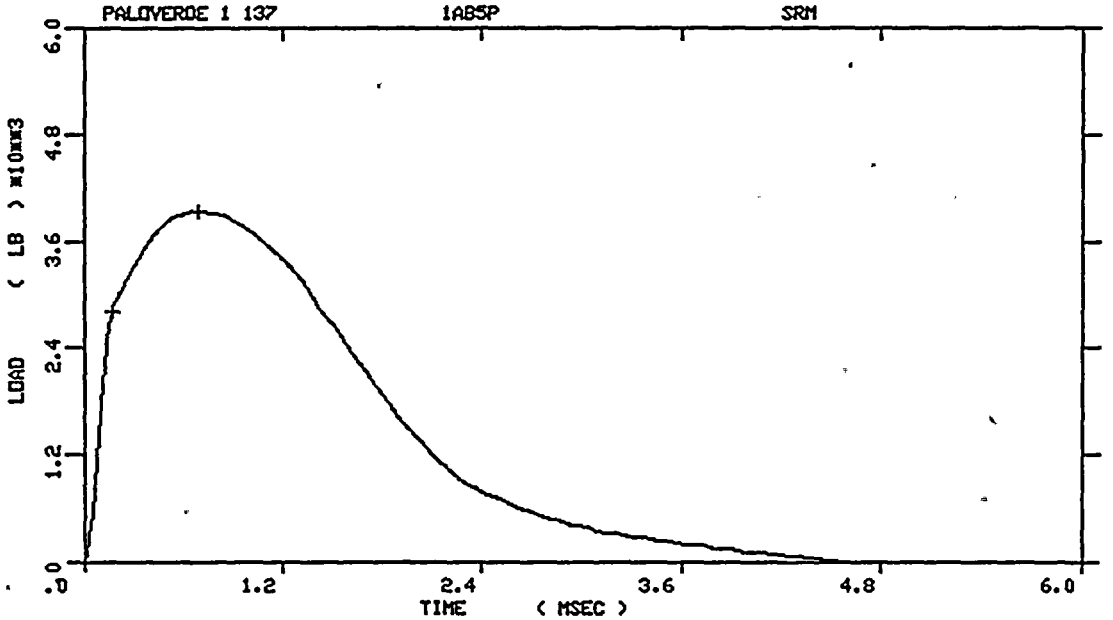

PALOVERDE 1 137
SPECIMEN NUMBER :1AB5P
MATERIAL :SRM
CAPSULE :PALOVERDE #1 137
:

Figure A-30. Load-time records for Specimens 1AB4J and 1AB5P

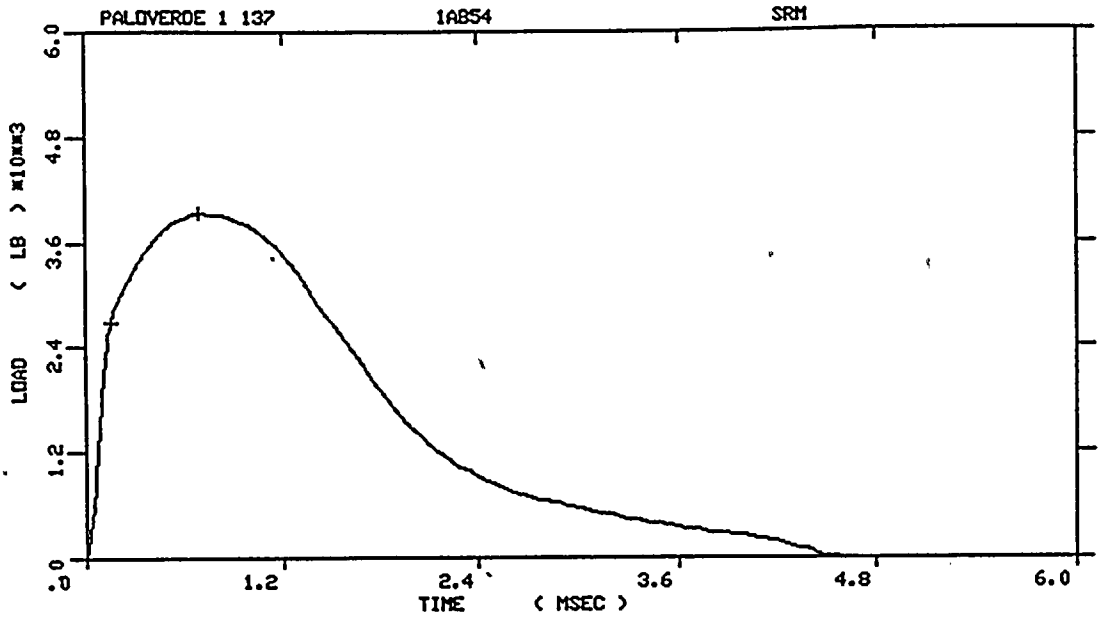

PALOVERDE 1 137
SPECIMEN NUMBER :1AB54
MATERIAL :SRM
CAPSULE :PALOVERDE #1
:137

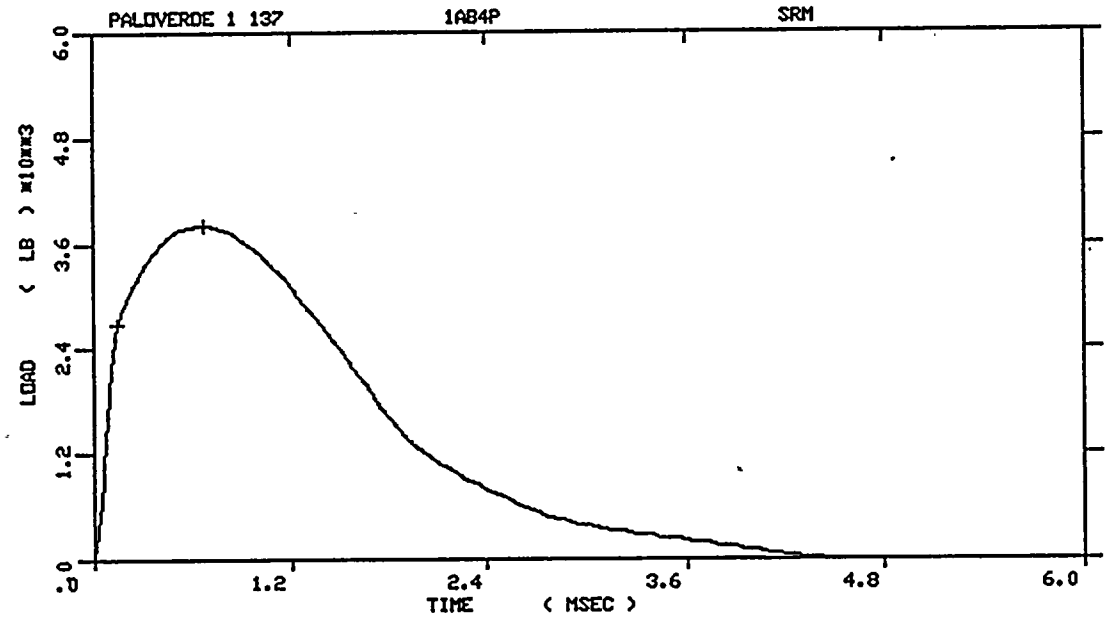

PALOVERDE 1 137
SPECIMEN NUMBER :1AB4P
MATERIAL :SRM
CAPSULE :PALOVERDE #1 137
:

Figure A-31. Load-time records for Specimens 1AB54 and 1AB4P

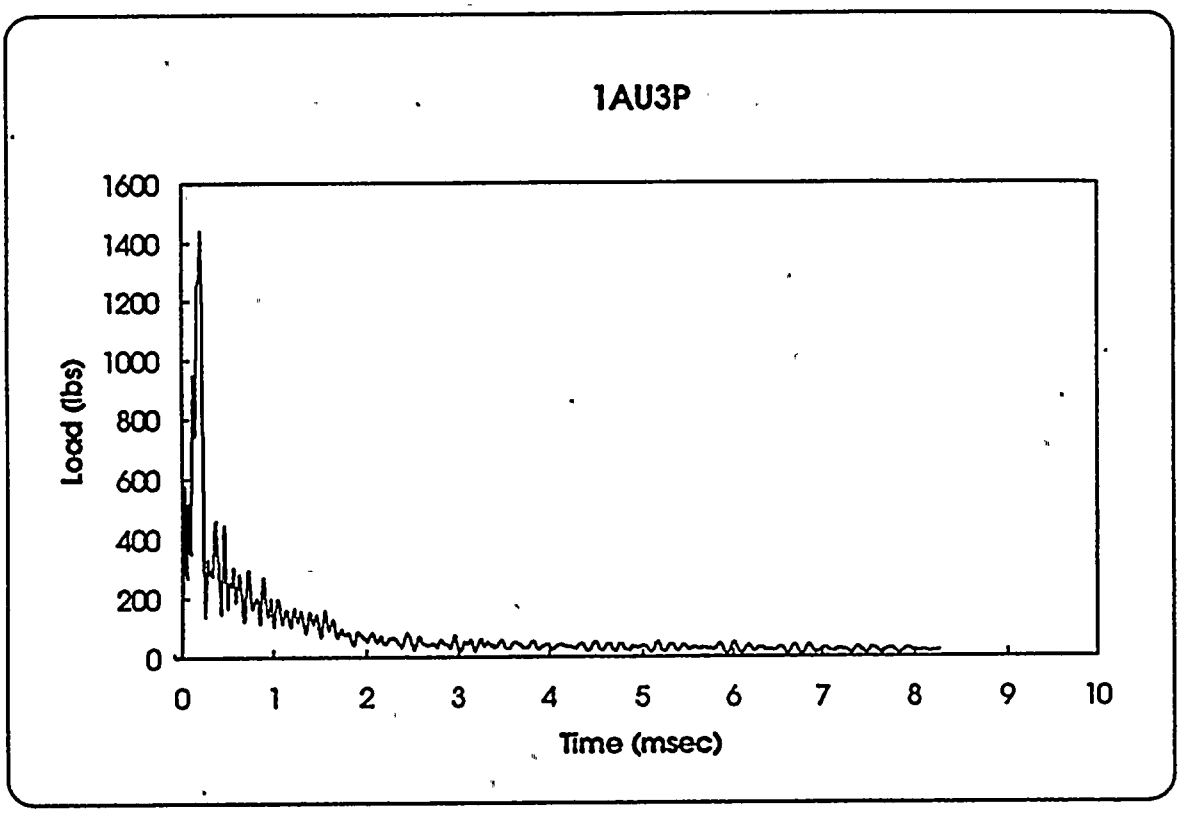

Specimen	1AU3P
Temperature	-25 F
Available Energy	289 in-lbs
Initial Velocity	61.0 in/sec

Time to Yield	0.210 mSec *
Yield Load	1440 lbs *
Time to Maximum	0.210 mSec
Maximum Load	1440 lbs
Energy at Max. Load	10.1 in-lbs

Crack Length	0.188 in
a/W	0.477
Specimen Compliance	51.1
Machine Compliance	55.1

KID	57.5 ksi-in^1/2
Yield Stress	112.0 ksi *

* No General Yielding

Figure A-32. Load-time record and data for precracked specimen 1AU3P

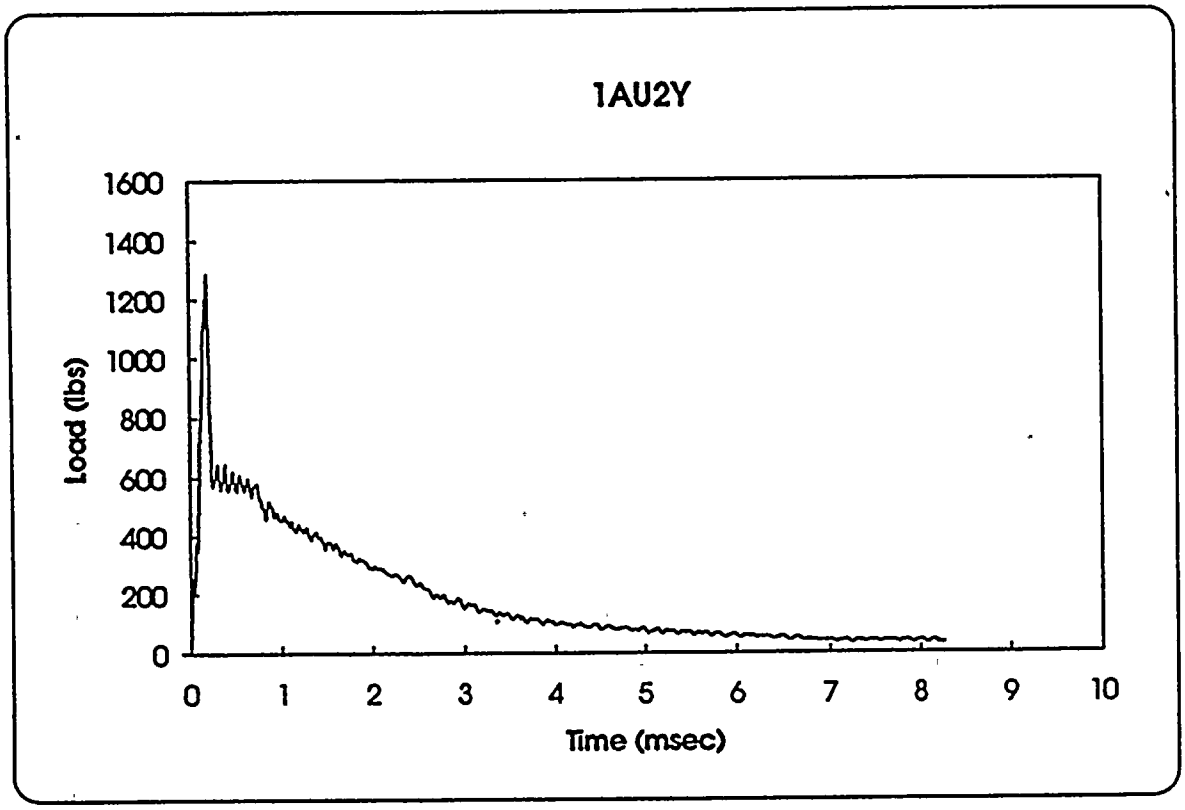

Specimen	1AU2Y
Temperature	25 F
Available Energy	291 in-lbs
Initial Velocity	61.3 in/sec

Time to Yield	0.185 mSec *
Yield Load	1286 lbs *
Time to Maximum	0.185 mSec
Maximum Load	1286 lbs
Energy at Max. Load	6.4 in-lbs

Crack Length	0.195 in
a/W	0.495
Specimen Compliance	54.8
Machine Compliance	49.7

KID	54.3 ksi-in^1/2
Yield Stress	107.2 ksi *

* No General Yielding

Figure A-33. Load-time record and data for precracked specimen 1AU2Y

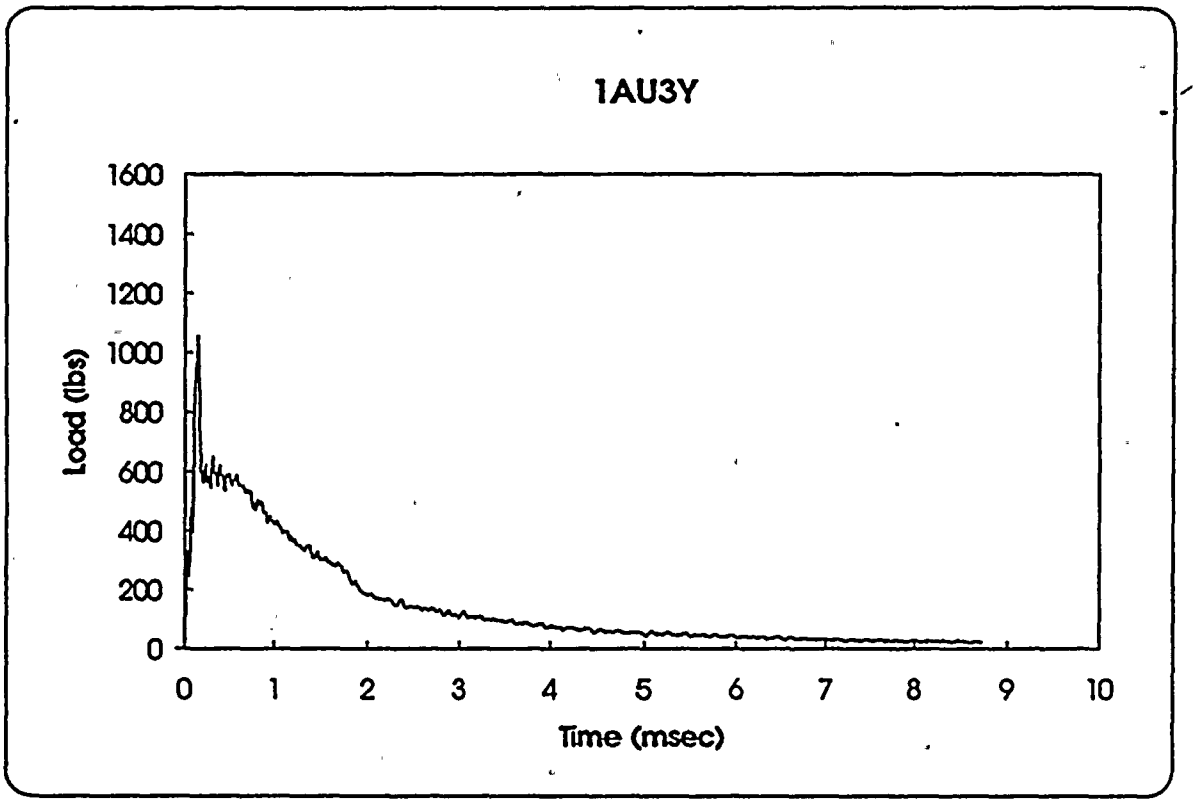

Specimen	1AU3Y
Temperature	50 F
Available Energy	504 in-lbs
Initial Velocity	80.6 in/sec

Time to Yield	0.140 mSec *
Yield Load	1055 lbs *
Time to Maximum	0.140 mSec
Maximum Load	1056 lbs
Energy at Max. Load	5.0 in-lbs

Crack Length	0.194 in
a/W	0.492
Specimen Compliance	54.2
Machine Compliance	72.0

KID	44.2 ksi-in^1/2
Yield Stress	87.0 ksi *

* No General Yielding

Figure A-34. Load-time record and data for precracked specimen 1AU3Y

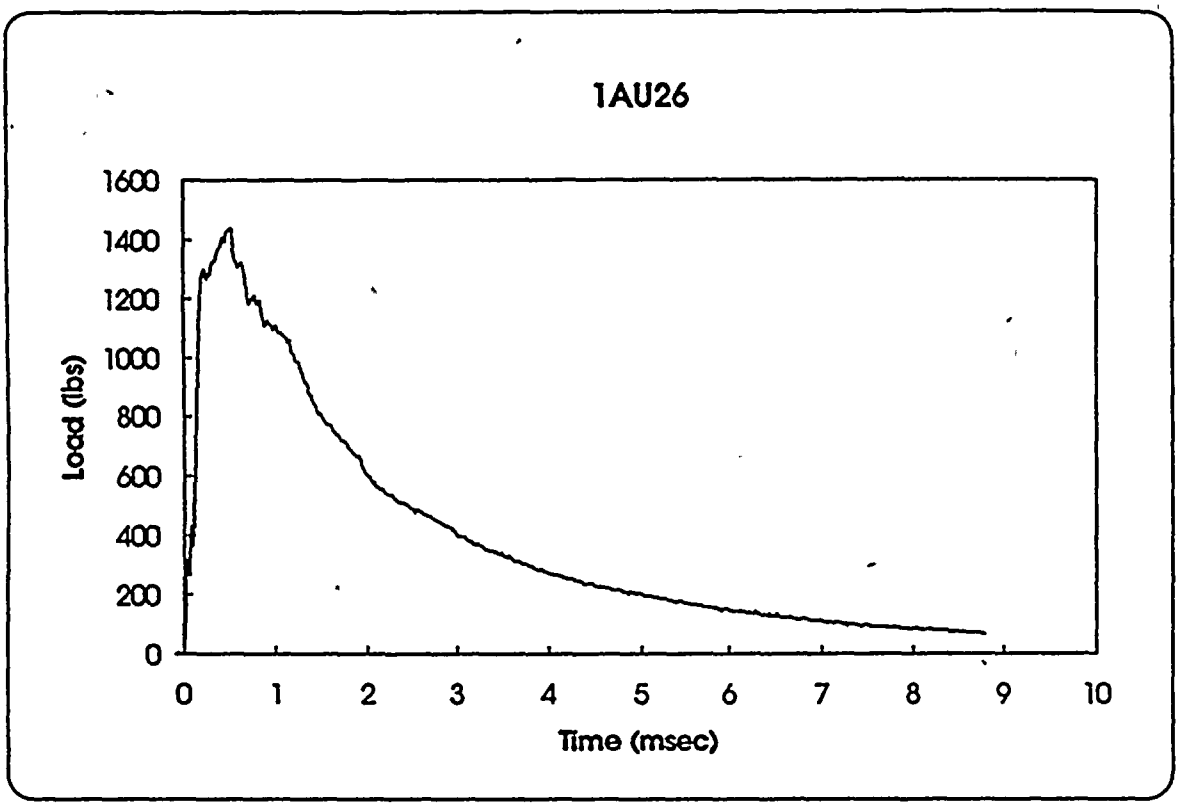

Specimen	1AU26
Temperature	75 F
Available Energy	499 in-lbs
Initial Velocity	80.2 in/sec

Time to Yield	0.190 mSec
Yield Load	1285 lbs
Time to Maximum	0.505 mSec
Maximum Load	1439 lbs
Energy at Max. Load	41.3 in-lbs

Crack Length	0.190 in
a/W	0.482
Specimen Compliance	52.1
Machine Compliance	87.3

KJD	158.0 ksi-in^1/2
Yield Stress	101.9 ksi

Figure A-35. Load-time record and data for precracked specimen 1AU26

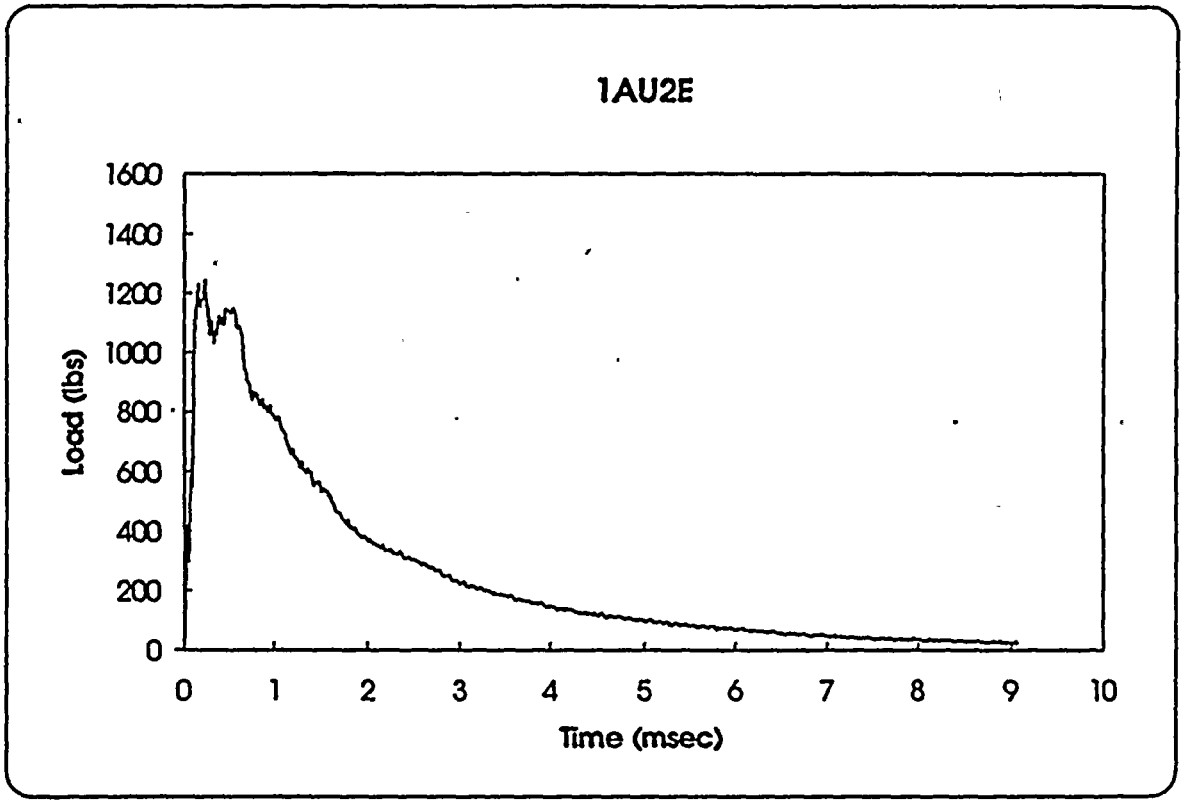

Specimen	1AU2E
Temperature	100 F.
Available Energy	781 in-lbs
Initial Velocity	100.3 in/sec

Time to Yield	0.140	mSec
Yield Load	1225	lbs
Time to Maximum	0.225	mSec
Maximum Load	1244	lbs
Energy at Max. Load	17.6	in-lbs

Crack Length	0.194 in
a/W	0.492
Specimen Compliance	54.2
Machine Compliance	80.1

KJD	96.4	ksi-in^1/2
Yield Stress	101.1	ksi

Figure A-36. Load-time record and data for precracked specimen 1AU2E

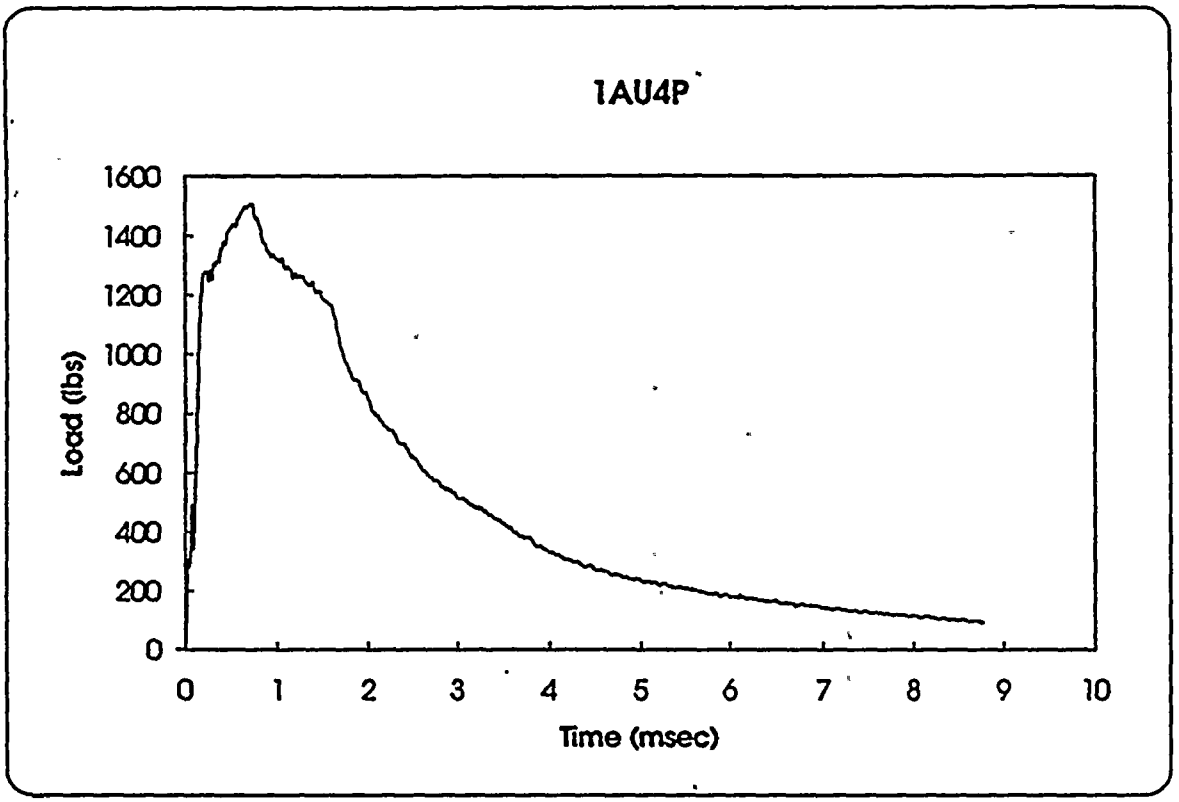

Specimen	1AU4P
Temperature	125 F
Available Energy	507 in-lbs
Initial Velocity	80.8 in/sec

Time to Yield	0.170	mSec
Yield Load	1250	lbs
Time to Maximum	0.715	mSec
Maximum Load	1508	lbs
Energy at Max. Load	65.4	in-lbs

Crack Length	0.185 in
a/W	0.470
Specimen Compliance	49.6
Machine Compliance	78.6

KJD	203.8	ksi-in^1/2
Yield Stress	94.4	ksi

Figure A-37. Load-time record and data for precracked specimen 1AU4P

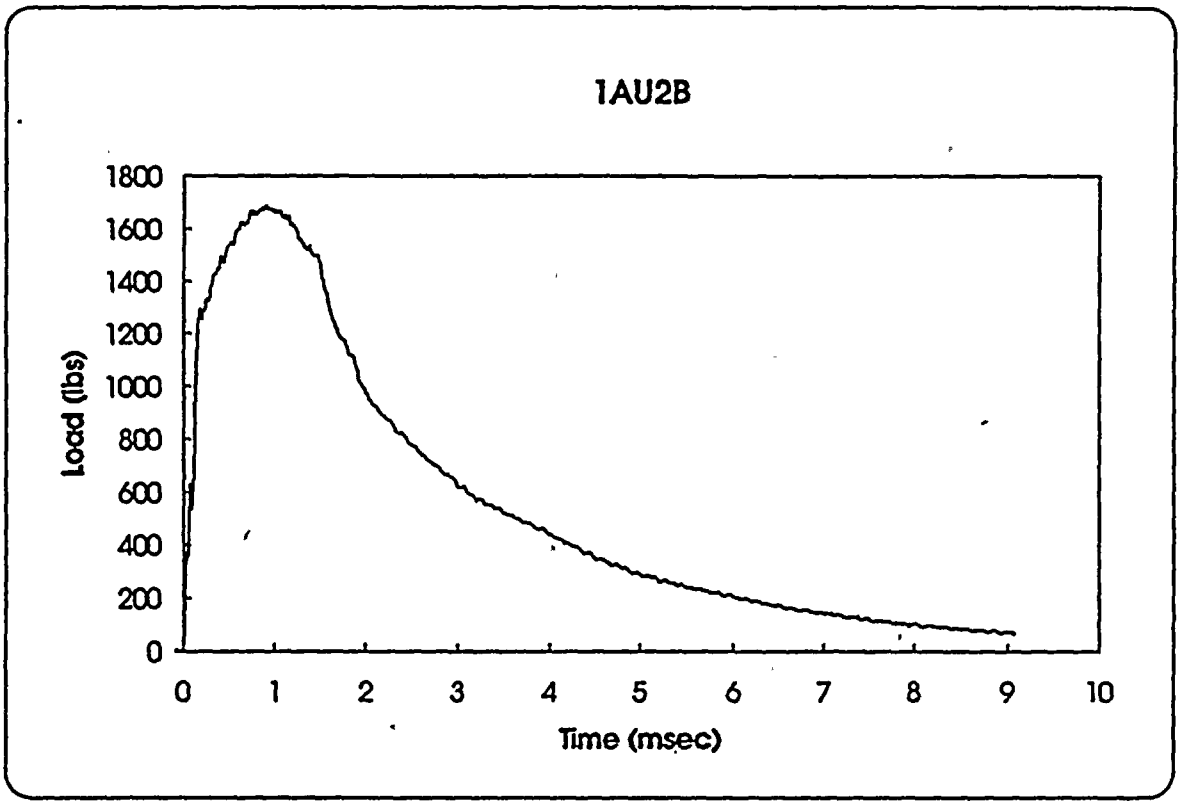

Specimen	1AU2B
Temperature	175 F
Available Energy	768 in-lbs
Initial Velocity	99.5 in/sec

Time to Yield	0.160 mSec
Yield Load	1260 lbs
Time to Maximum	0.900 mSec
Maximum Load	1689 lbs
Energy at Max. Load	115.7 in-lbs

Crack Length	0.185 in
a/W	0.470
Specimen Compliance	49.6
Machine Compliance	96.7

KJD	272.2 ksi-in^1/2
Yield Stress	95.2 ksi

Figure A-38. Load-time record and data for precracked specimen 1AU2B

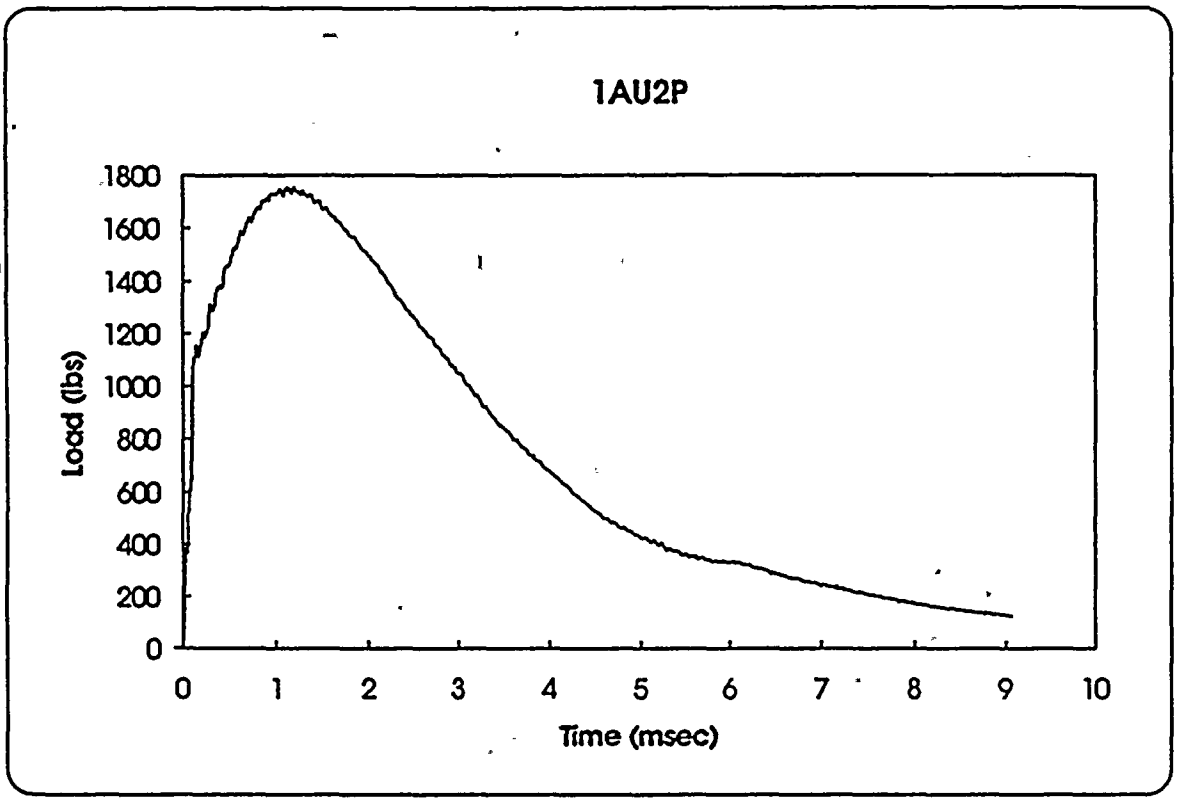

Specimen	1AU2P
Temperature	225 F
Available Energy	772 in-lbs
Initial Velocity	99.7 in/sec

Time to Yield	0.120 mSec
Yield Load	1105 lbs
Time to Maximum	1.190 mSec
Maximum Load	1755 lbs
Energy at Max. Load	158.4 in-lbs

Crack Length	0.189 in
a/W	0.480
Specimen Compliance	51.6
Machine Compliance	72.8

KJD	327.6 ksi-in^1/2
Yield Stress	86.8 ksi

Figure A-39. Load-time record and data for precracked specimen 1AU2P

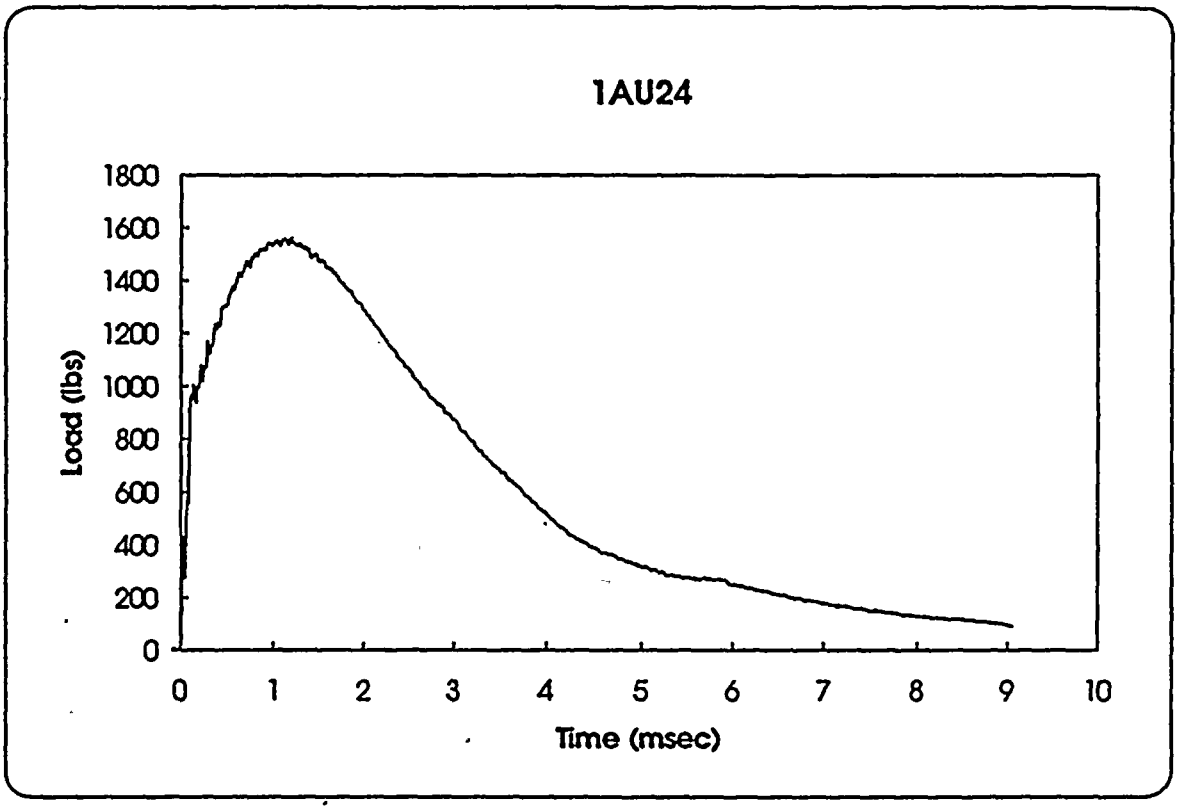

Specimen	1AU24
Temperature	275 F
Available Energy	778 in-lbs
Initial Velocity	100.1 in/sec

Time to Yield	0.110	mSec
Yield Load	960	lbs
Time to Maximum	1.185	mSec
Maximum Load	1562	lbs
Energy at Max. Load	142.4	in-lbs

Crack Length	0.201 in
a/W	0.510
Specimen Compliance	58.3
Machine Compliance	72.5

KJD	320.0	ksi-in^1/2
Yield Stress	85.0	ksi

Figure A-40. Load-time record and data for precracked specimen 1AU24

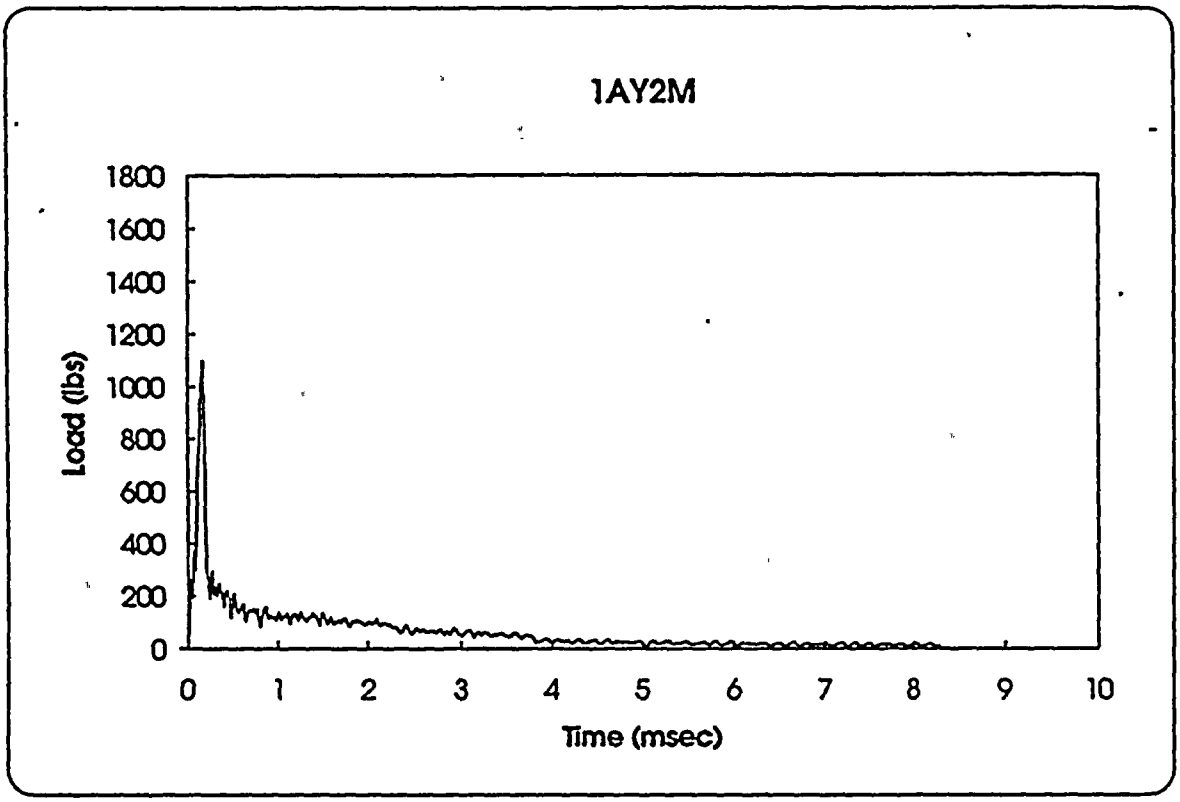

Specimen	1AY2M
Temperature	-25 F
Available Energy	288 in-lbs
Initial Velocity	60.9 in/sec

Time to Yield	0.160	mSec *
Yield Load	1098	lbs *
Time to Maximum	0.165	mSec
Maximum Load	1098	lbs
Energy at Max. Load	4.5	in-lbs

Crack Length	0.189 in
a/W	0.480
Specimen Compliance	51.6
Machine Compliance	54.4

KID	44.2	ksi-in^1/2
Yield Stress	86.2	ksi *

* No General Yielding

Figure A-41. Load-time record and data for precracked specimen 1AY2M

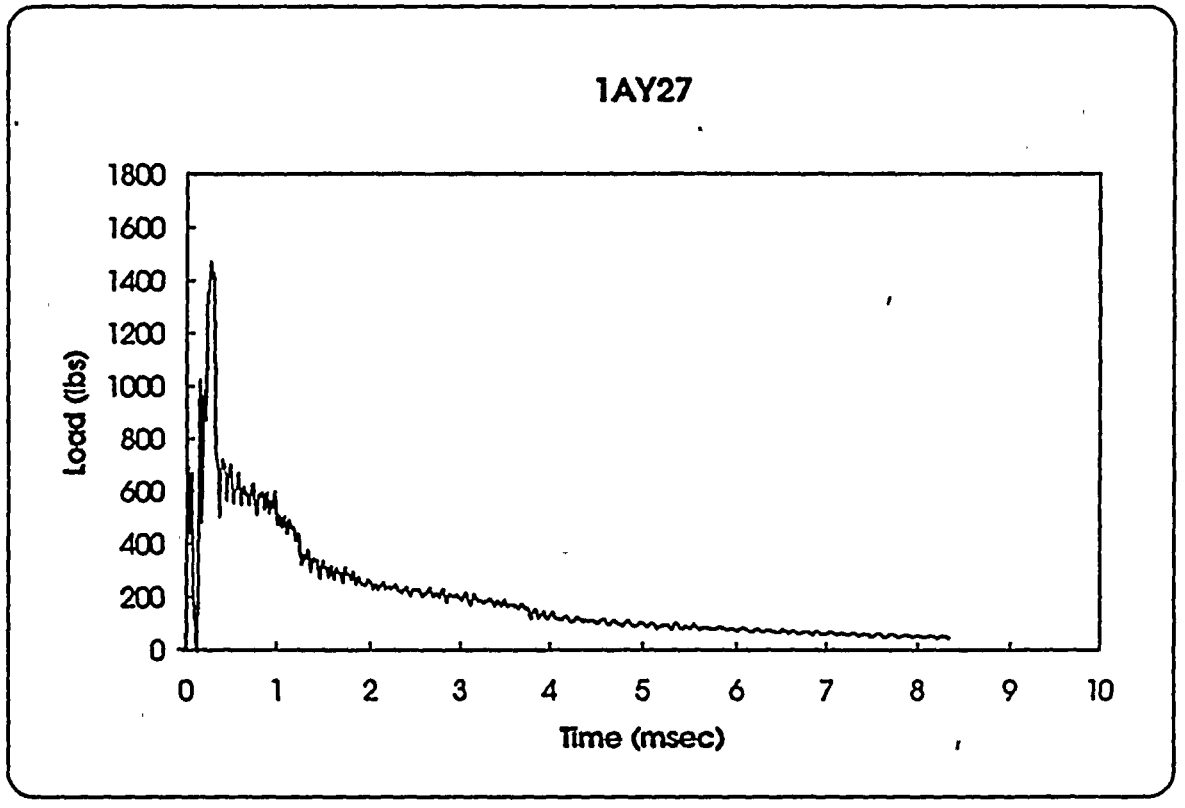

Specimen	1AY27
Temperature	25 F
Available Energy	291 in-lbs
Initial Velocity	61.3 in/sec

Time to Yield	0.265 mSec *
Yield Load	1467 lbs *
Time to Maximum	0.275 mSec
Maximum Load	1468 lbs
Energy at Max. Load	12.3 in-lbs

Crack Length	0.185 in
a/W	0.470
Specimen Compliance	49.6
Machine Compliance	81.5

KID	57.3 ksi-in^1/2
Yield Stress	110.8 ksi *

* No General Yielding

Figure A-42. Load-time record and data for precracked specimen 1AY27

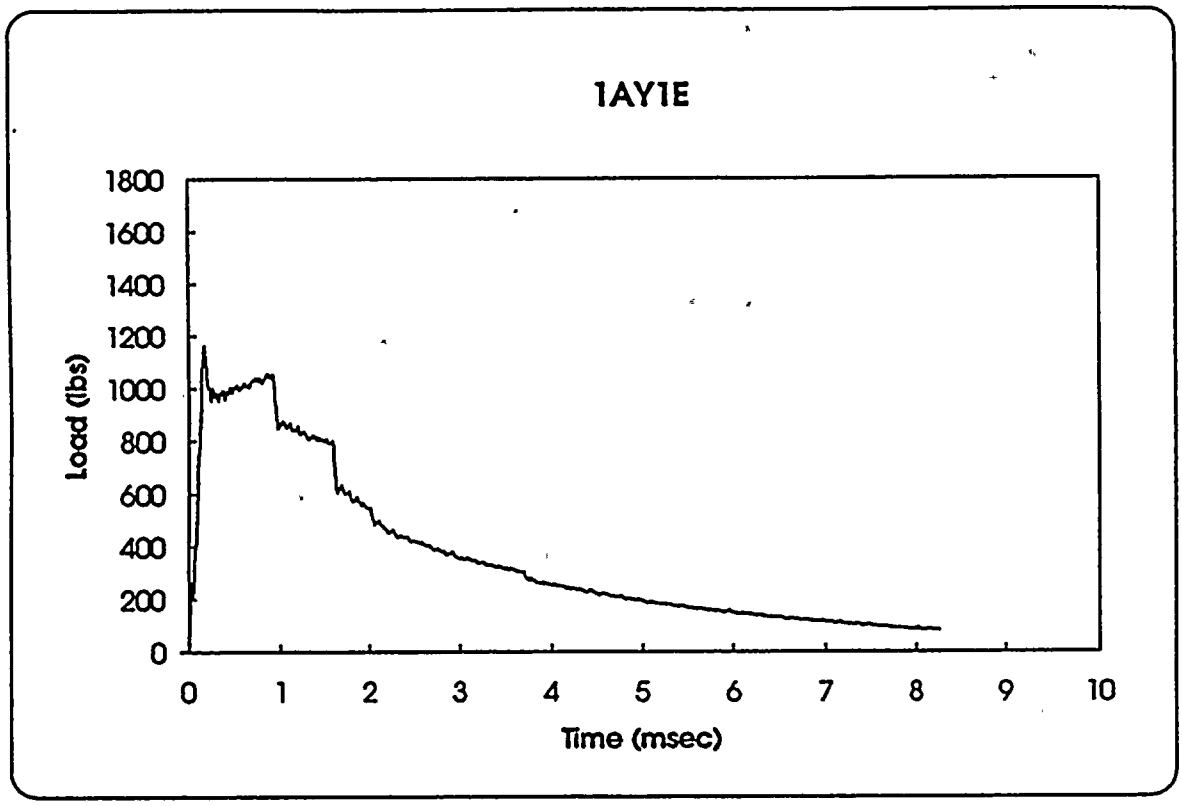

Specimen	1AY1E
Temperature	75 F
Available Energy	295 in-lbs
Initial Velocity	61.6 in/sec

Time to Yield	0.165 mSec *
Yield Load	1160 lbs *
Time to Maximum	0.170 mSec
Maximum Load	1163 lbs
Energy at Max. Load	5.3 in-lbs

Crack Length	0.188 in
a/W	0.477
Specimen Compliance	51.1
Machine Compliance	52.0

KID	46.4 ksi-in^1/2
Yield Stress	90.2 ksi *

* No General Yielding

Figure A-43. Load-time record and data for precracked specimen 1AY1E

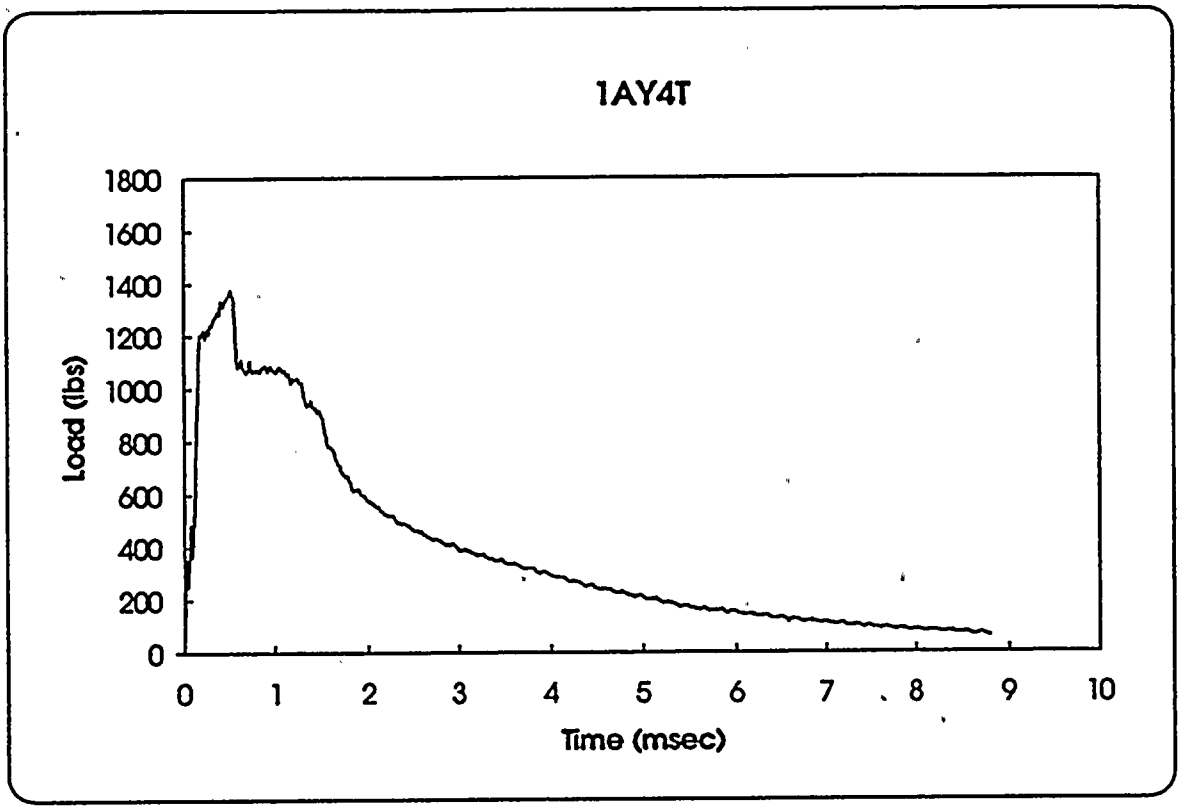

Specimen	1AY4T
Temperature	125 F
Available Energy	500 in-lbs
Initial Velocity	80.2 in/sec

Time to Yield	0.170 mSec
Yield Load	1205 lbs
Time to Maximum	0.510 mSec
Maximum Load	1374 lbs
Energy at Max. Load	40.2 in-lbs

Crack Length	0.190 in
a/W	0.482
Specimen Compliance	52.1
Machine Compliance	80.0

KJD	157.6 ksi-in^1/2
Yield Stress	95.6 ksi

Figure A-44. Load-time record and data for precracked specimen 1AY4T

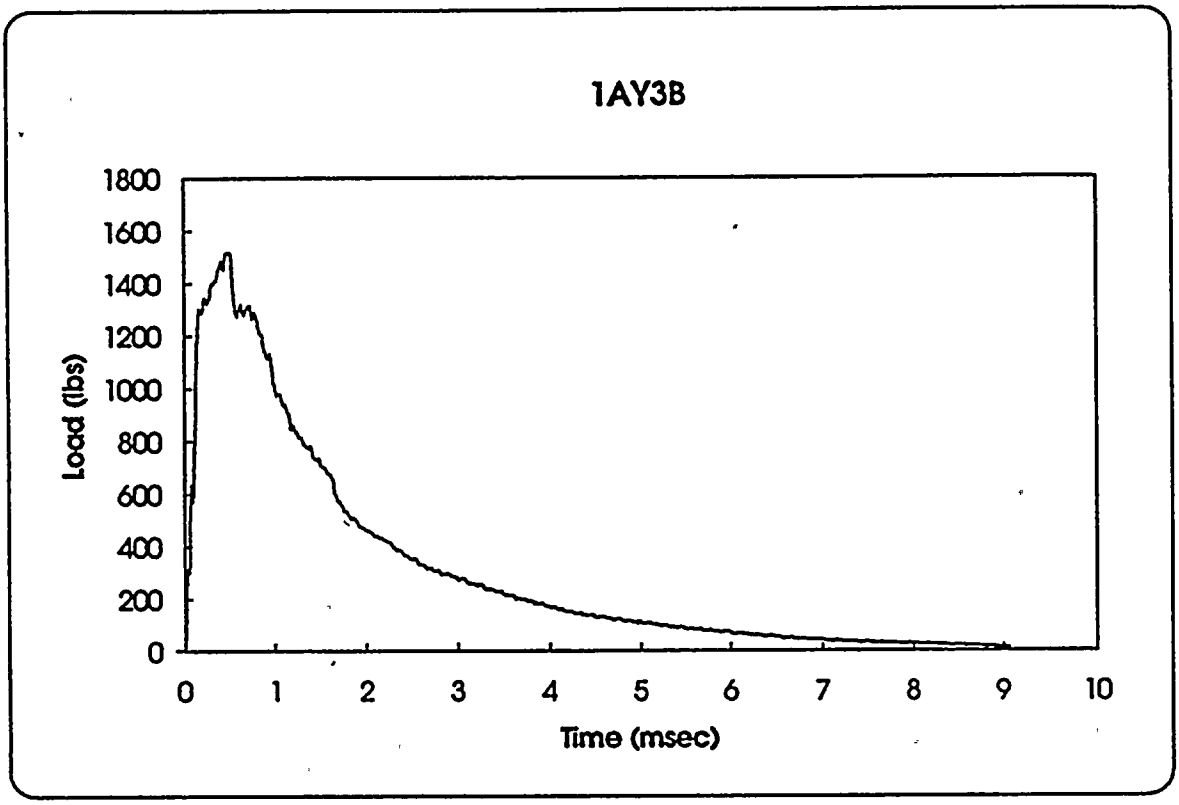

Specimen	1AY3B
Temperature	150 F
Available Energy	785 in-lbs
Initial Velocity	100.5 in/sec

Time to Yield	0.155 mSec
Yield Load	1295 lbs
Time to Maximum	0.480 mSec
Maximum Load	1519 lbs
Energy at Max. Load	52.8 in-lbs

Crack Length	0.193 in
a/W	0.490
Specimen Compliance	53.7
Machine Compliance	86.2

KJD	181.5 ksi-in^1/2
Yield Stress	105.8 ksi

Figure A-45. Load-time record and data for precracked specimen 1AY3B

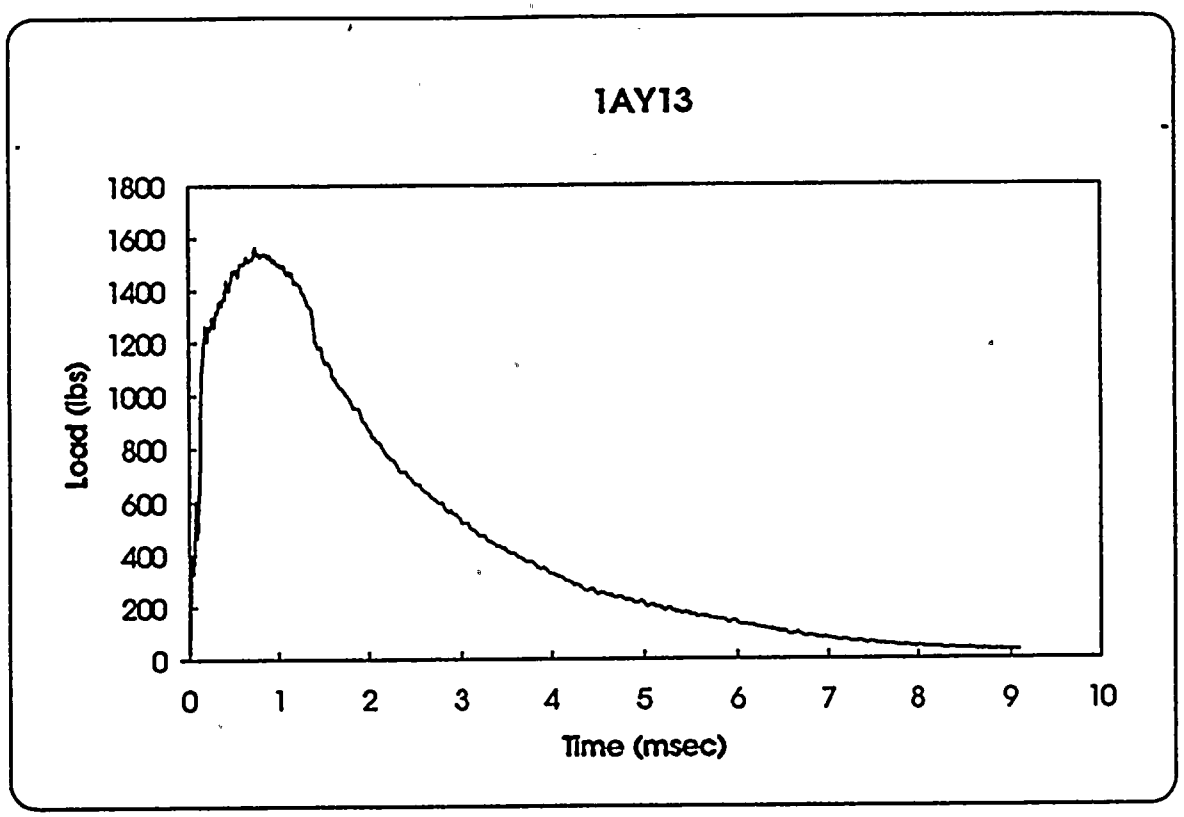

Specimen	1AY13
Temperature	175 F
Available Energy	773 in-lbs
Initial Velocity	99.8 in/sec

Time to Yield	0.165 mSec
Yield Load	1230 lbs
Time to Maximum	0.730 mSec
Maximum Load	1563 lbs
Energy at Max. Load	85.5 in-lbs

Crack Length	0.191 in
a/W	0.485
Specimen Compliance	52.6
Machine Compliance	102.4

KJD	234.3 ksi-in^1/2
Yield Stress	98.5 ksi

Figure A-46. Load-time record and data for precracked specimen 1AY13

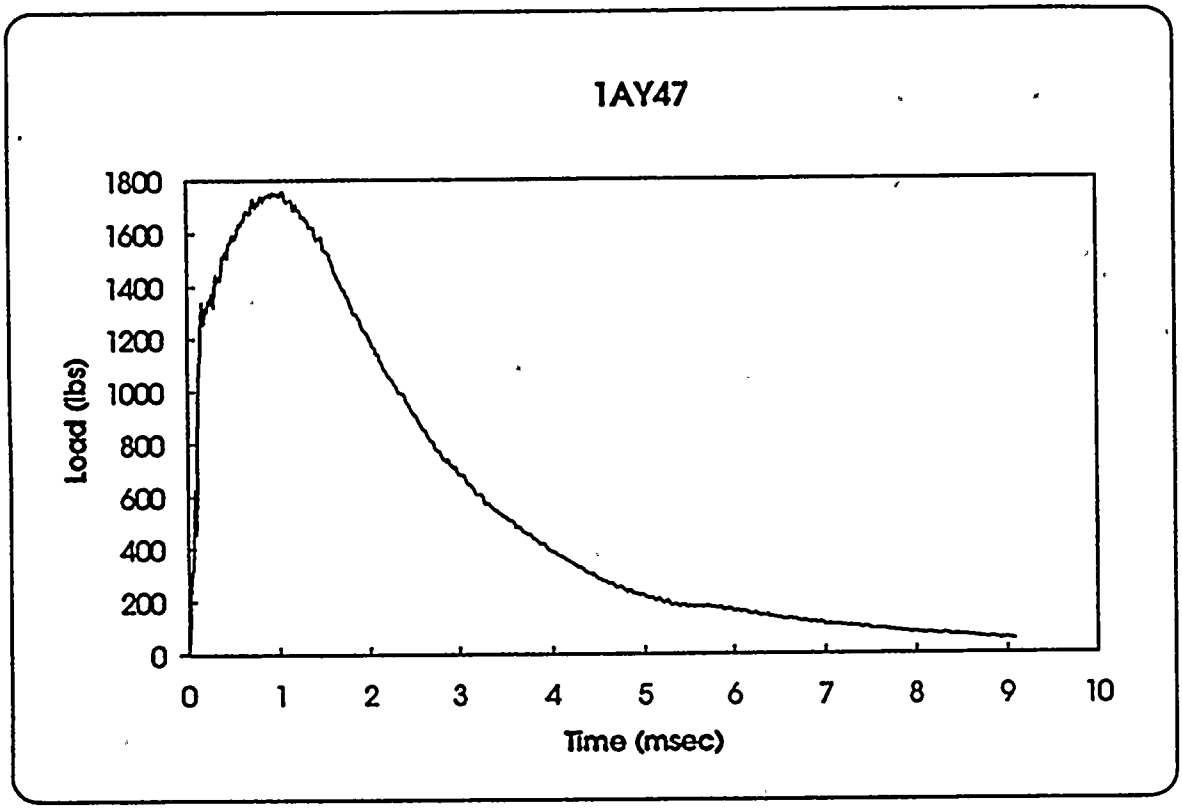

Specimen	1AY47
Temperature	225 F
Available Energy	777 in-lbs
Initial Velocity	100.0 in/sec

Time to Yield	0.140 mSec
Yield Load	1300 lbs
Time to Maximum	1.050 mSec
Maximum Load	1758 lbs
Energy at Max. Load	143.9 in-lbs

Crack Length	0.190 in
a/W	0.482
Specimen Compliance	52.1
Machine Compliance	71.7

KJD	312.1 ksi-in^1/2
Yield Stress	103.1 ksi

Figure A-47. Load-time record and data for precracked specimen 1AY47

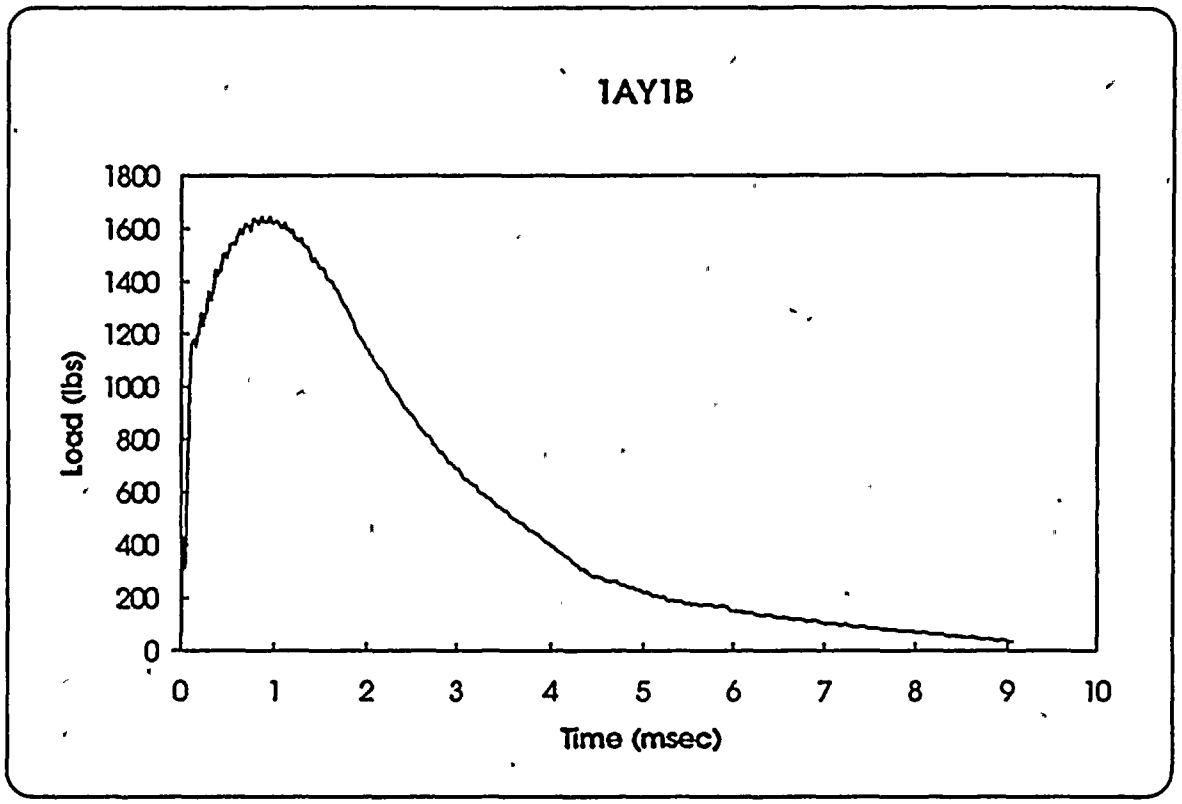

Specimen	1AY1B
Temperature	275 F
Available Energy	782 in-lbs
Initial Velocity	100.4 in/sec

Time to Yield	0.110 mSec
Yield Load	1160 lbs
Time to Maximum	0.860 mSec
Maximum Load	1643 lbs
Energy at Max. Load	110.6 in-lbs

Crack Length	0.191 in
a/W	0.485
Specimen Compliance	52.6
Machine Compliance	74.8

KJD	271.4 ksi-in^1/2
Yield Stress	92.9 ksi

Figure A-48. Load-time record and data for precracked specimen 1AY1B

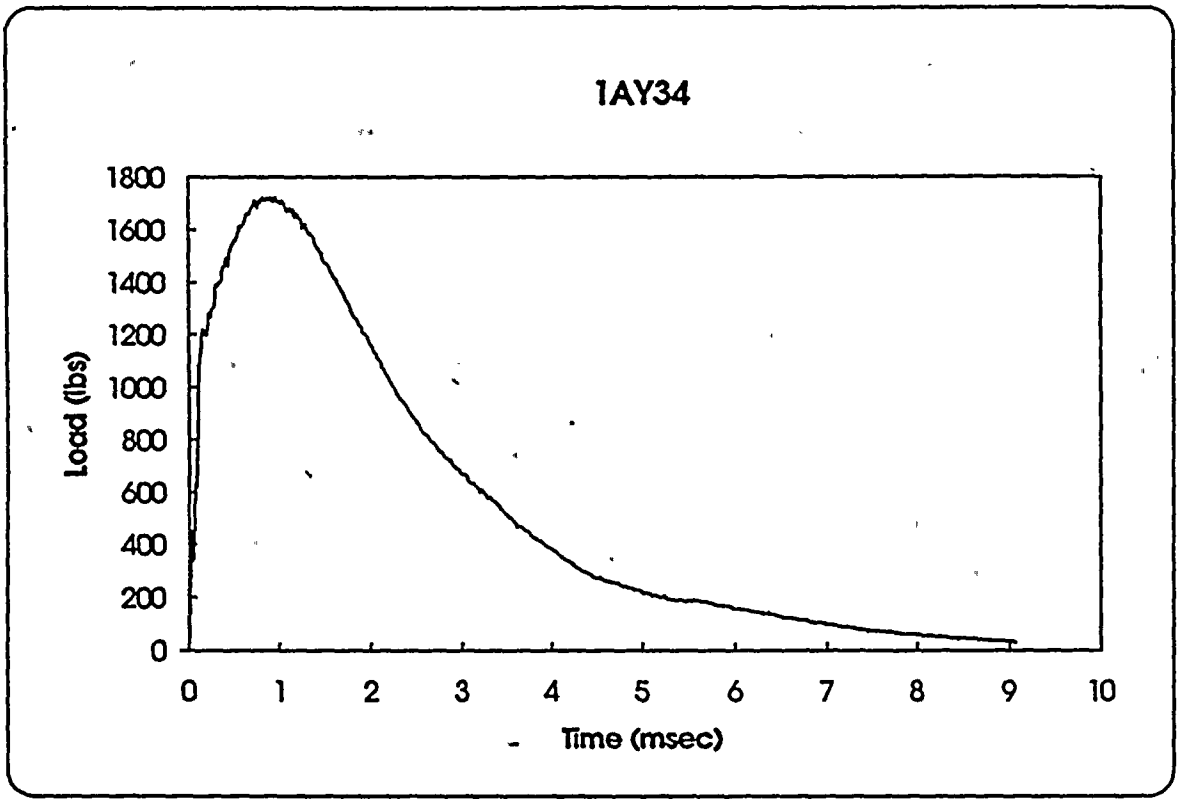

Specimen	1AY34
Temperature	325 F
Available Energy	780 in-lbs
Initial Velocity	100.2 in/sec

Time to Yield	0.110 mSec
Yield Load	1120 lbs
Time to Maximum	0.805 mSec
Maximum Load	1722 lbs
Energy at Max. Load	104.3 in-lbs

Crack Length	0.181 in
a/W	0.459
Specimen Compliance	47.8
Machine Compliance	63.5

KJD	256.3 ksi-in^1/2
Yield Stress	81.5 ksi

Figure A-49. Load-time record and data for precracked specimen 1AY34

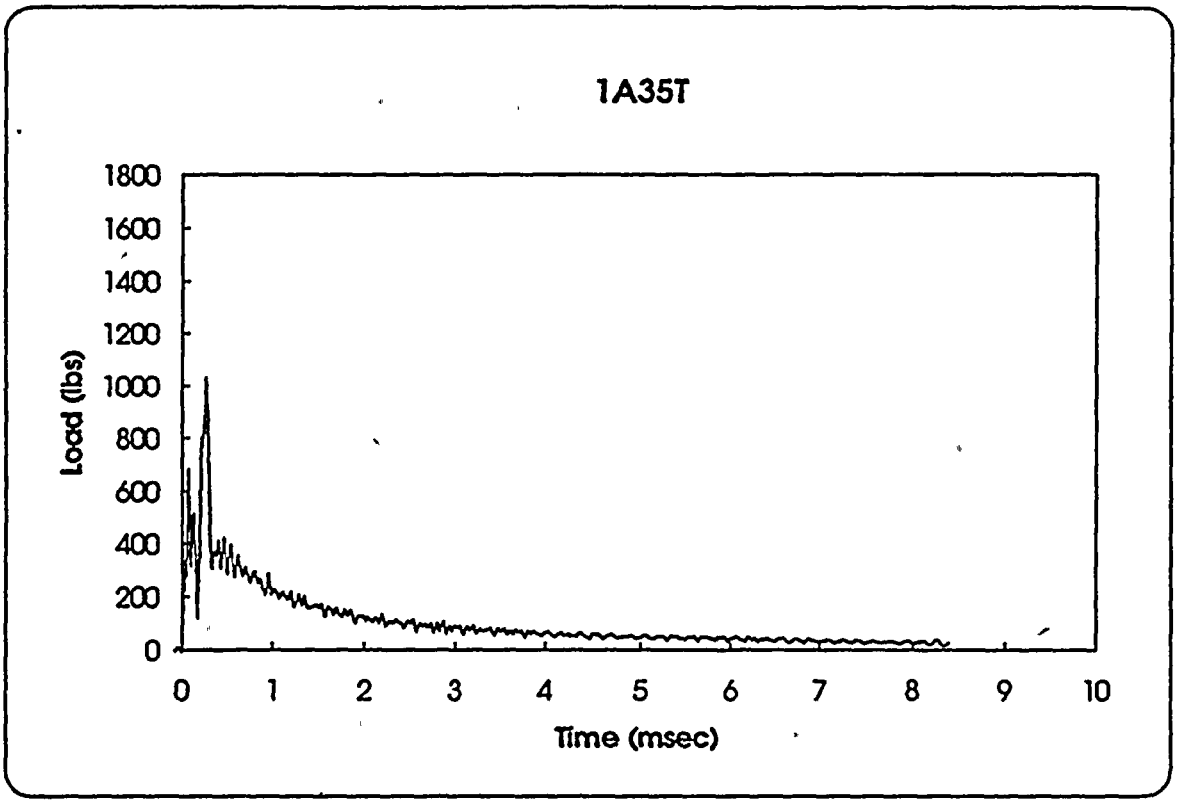

Specimen	1A35T
Temperature	-50 F
Available Energy	287 in-lbs
Initial Velocity	60.8 in/sec

Time to Yield	0.265 mSec *
Yield Load	1030 lbs *
Time to Maximum	0.265 mSec
Maximum Load	1030 lbs
Energy at Max. Load	9.4 in-lbs

Crack Length	0.204 in
a/W	0.518
Specimen Compliance	60.2
Machine Compliance	127.5

KID	46.8 ksi-in^1/2
Yield Stress	94.2 ksi *

* No General Yielding

Figure A-50. . Load-time record and data for precracked specimen 1A35T

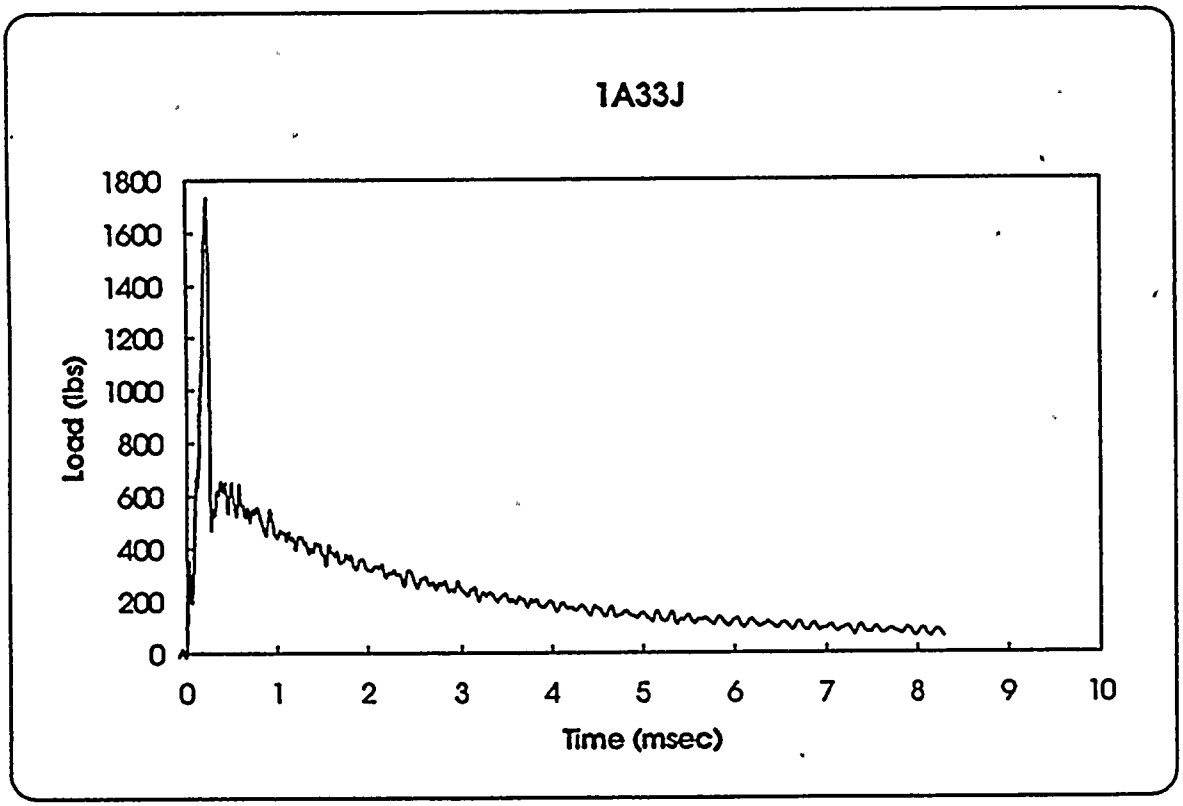

Specimen	1A33J
Temperature	-25 F
Available Energy	289 in-lbs
Initial Velocity	61.0 in/sec

Time to Yield	0.220 mSec *
Yield Load	1735 lbs *
Time to Maximum	0.225 mSec
Maximum Load	1738 lbs
Energy at Max. Load	10.9 in-lbs

Crack Length	0.188 in
a/W	0.477
Specimen Compliance	51.1
Machine Compliance	41.3

KID	69.4 ksi-in^1/2
Yield Stress	134.9 ksi *

* No General Yielding

Figure A-51. Load-time record and data for precracked specimen 1A33J

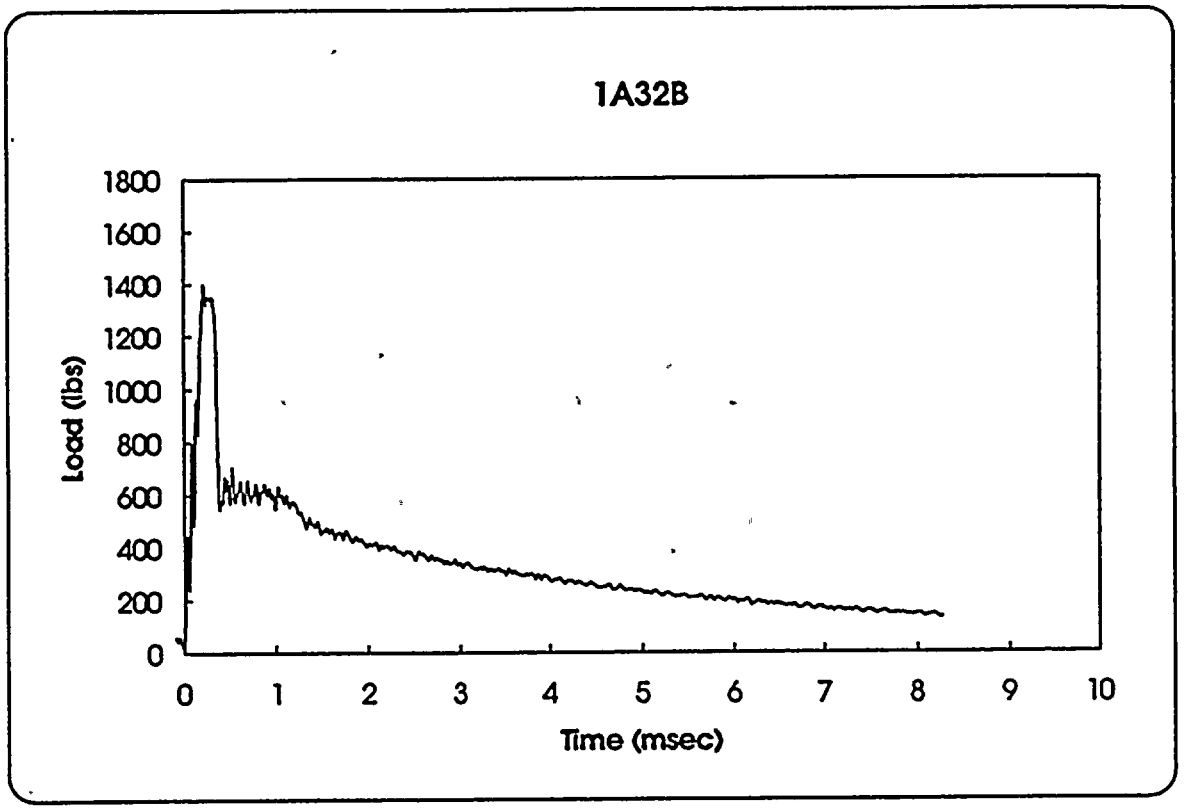

Specimen	1A32B
Temperature	0 F
Available Energy	289 in-lbs
Initial Velocity	61.0 in/sec

Time to Yield	0.210 mSec
Yield Load	1395 lbs
Time to Maximum	0.215 mSec
Maximum Load	1398 lbs
Energy at Max. Load	10.1 in-lbs

Crack Length	0.200 in
a/W	0.508
Specimen Compliance	57.7
Machine Compliance	51.1

KJD	68.4 ksi-in^1/2
Yield Stress	122.3 ksi

Figure A-52. Load-time record and data for precracked specimen 1A32B

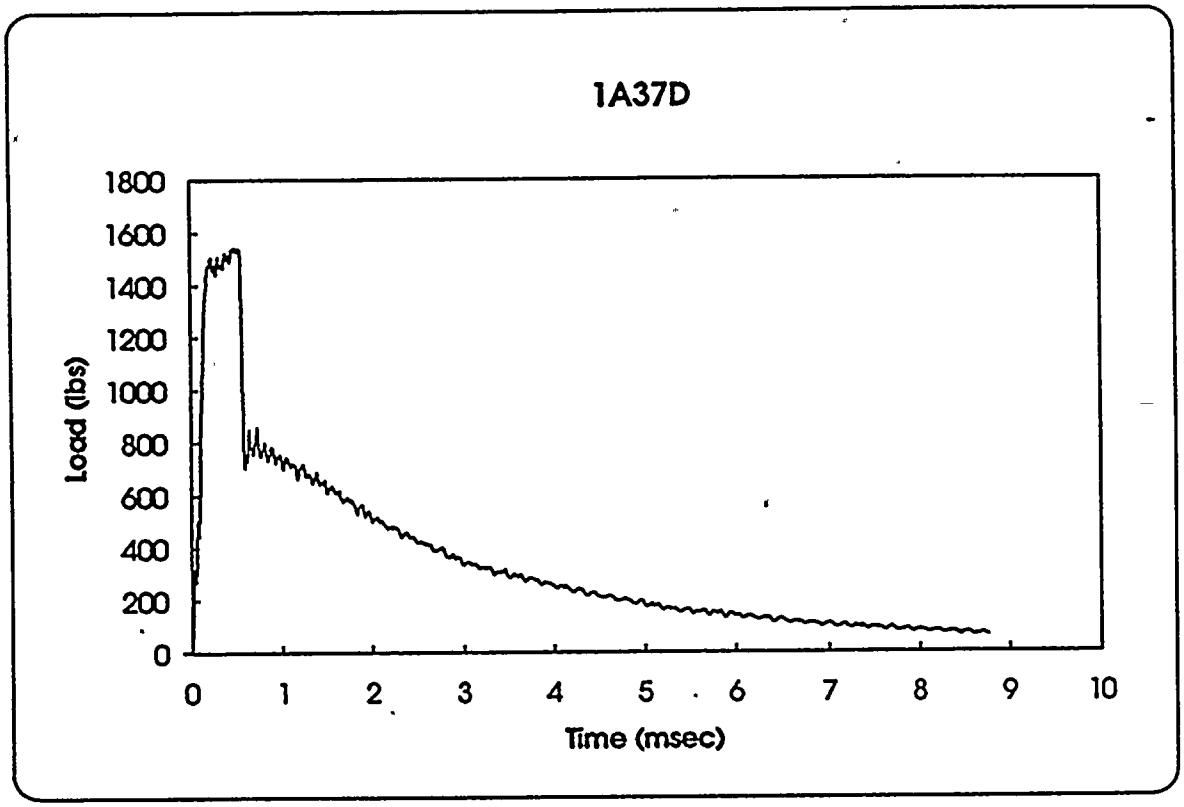

Specimen	1A37D
Temperature	25 F
Available Energy	504 in-lbs
Initial Velocity	80.6 in/sec

Time to Yield	0.180 mSec
Yield Load	1475 lbs
Time to Maximum	0.485 mSec
Maximum Load	1542 lbs
Energy at Max. Load	44.9 in-lbs

Crack Length	0.188 in
a/W	0.477
Specimen Compliance	51.1
Machine Compliance	65.4

KJD	168.7 ksi-in^1/2
Yield Stress	114.7 ksi

Figure A-53. Load-time record and data for precracked specimen 1A37D

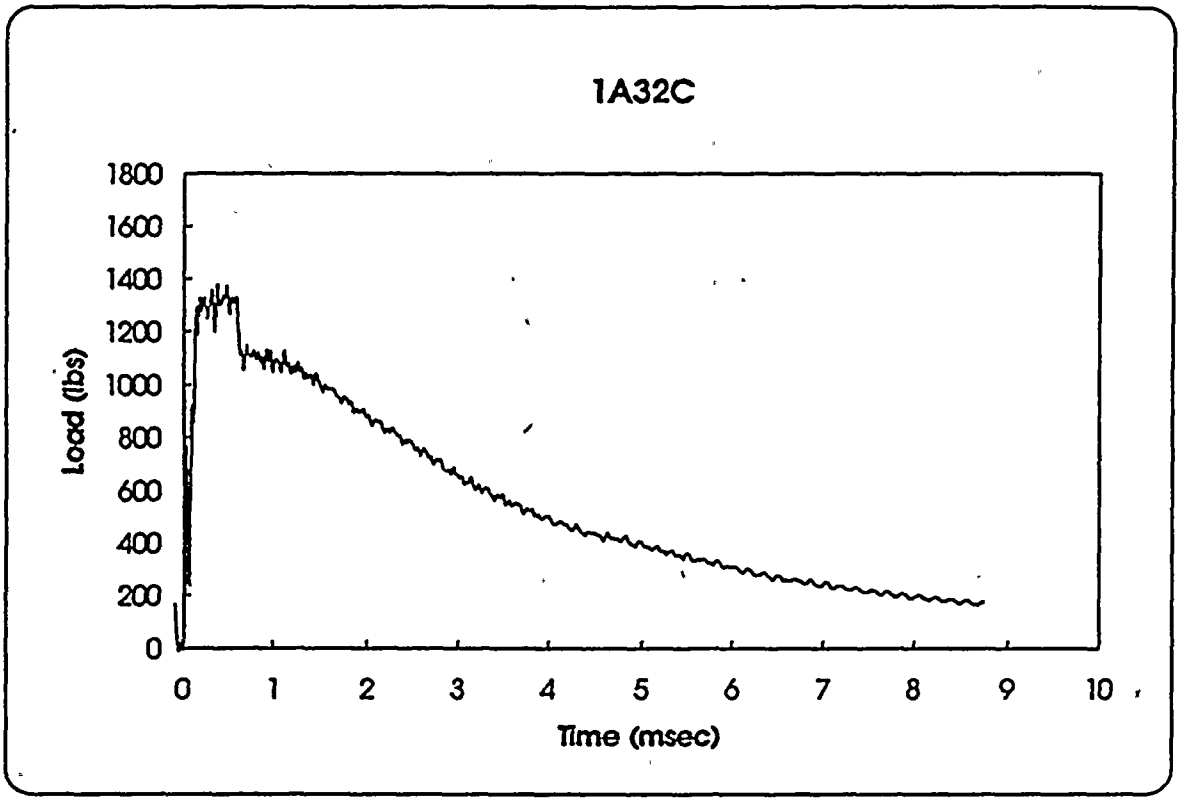

Specimen	1A32C
Temperature	50 F
Available Energy	495 in-lbs
Initial Velocity	79.8 in/sec

Time to Yield	0.135 mSec
Yield Load	1285 lbs
Time to Maximum	0.370 mSec
Maximum Load	1377 lbs
Energy at Max. Load	33.0 in-lbs

Crack Length	0.208 in
a/W	0.528
Specimen Compliance	62.8
Machine Compliance	36.2

KJD	157.0 ksi-in^1/2
Yield Stress	122.6 ksi

Figure A-54. Load-time record and data for precracked specimen 1A32C

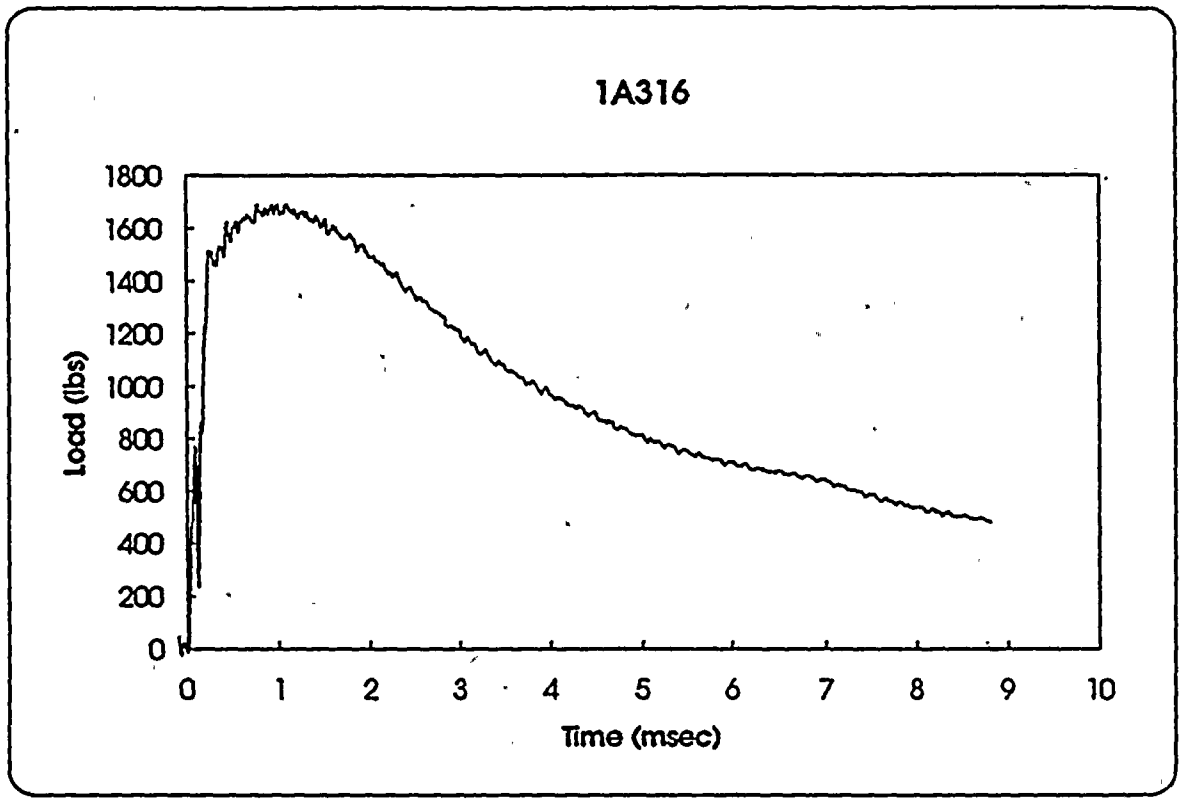

Specimen	1A316
Temperature	75 F
Available Energy	495 in-lbs
Initial Velocity	79.9 in/sec

Time to Yield	0.225 mSec
Yield Load	1500 lbs
Time to Maximum	0.755 mSec
Maximum Load	1689 lbs
Energy at Max. Load	78.0 in-lbs

Crack Length	0.189 in
a/W	0.480
Specimen Compliance	51.6
Machine Compliance	89.3

KJD	222.7 ksi-in^1/2
Yield Stress	117.8 ksi

Figure A-55. Load-time record and data for precracked specimen 1A316

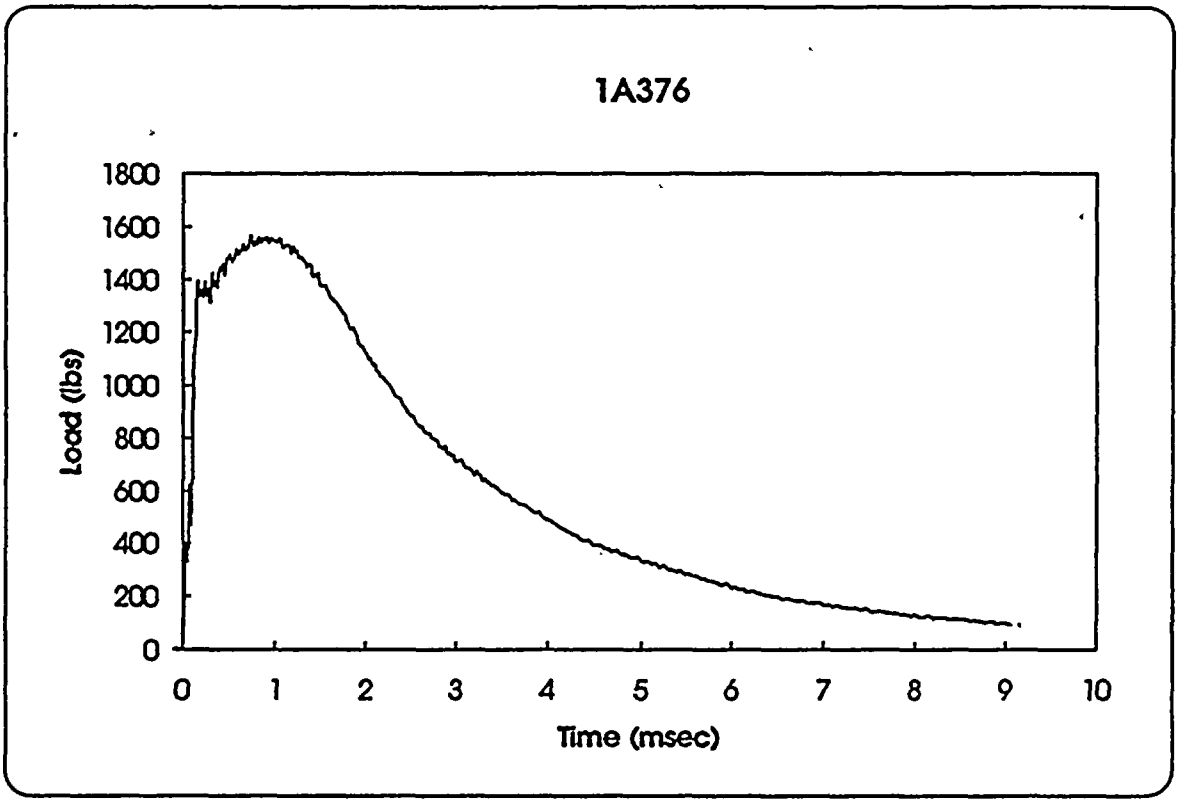

Specimen	1A376
Temperature	100 F
Available Energy	767 in-lbs
Initial Velocity	99.4 in/sec

Time to Yield	0.150 mSec
Yield Load	1360 lbs
Time to Maximum	0.720 mSec
Maximum Load	1568 lbs
Energy at Max. Load	87.5 in-lbs

Crack Length	0.193 in
a/W	0.490
Specimen Compliance	53.7
Machine Compliance	74.8

KJD	244.6 ksi-in^1/2
Yield Stress	111.1 ksi

Figure A-56. Load-time record and data for precracked specimen 1A376

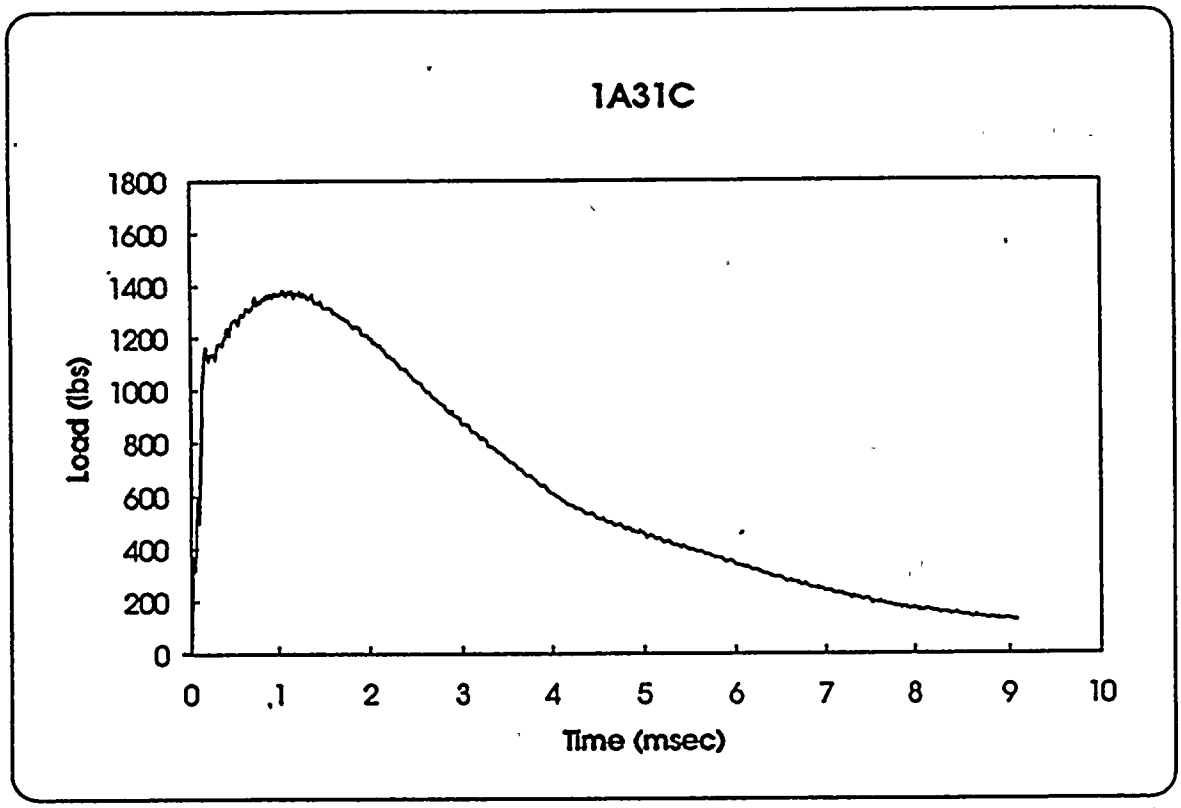

Specimen	1A31C
Temperature	150 F
Available Energy	777 in-lbs
Initial Velocity	100.0 in/sec

Time to Yield	0.160	mSec
Yield Load	1150	lbs
Time to Maximum	1.150	mSec
Maximum Load	1383	lbs
Energy at Max. Load	129.7	in-lbs

Crack Length	0.205 in
a/W	0.520
Specimen Compliance	60.8
Machine Compliance	101.0

KJD	310.1	ksi-in^1/2
Yield Stress	106.2	ksi

Figure A-57. Load-time record and data for precracked specimen 1A31C

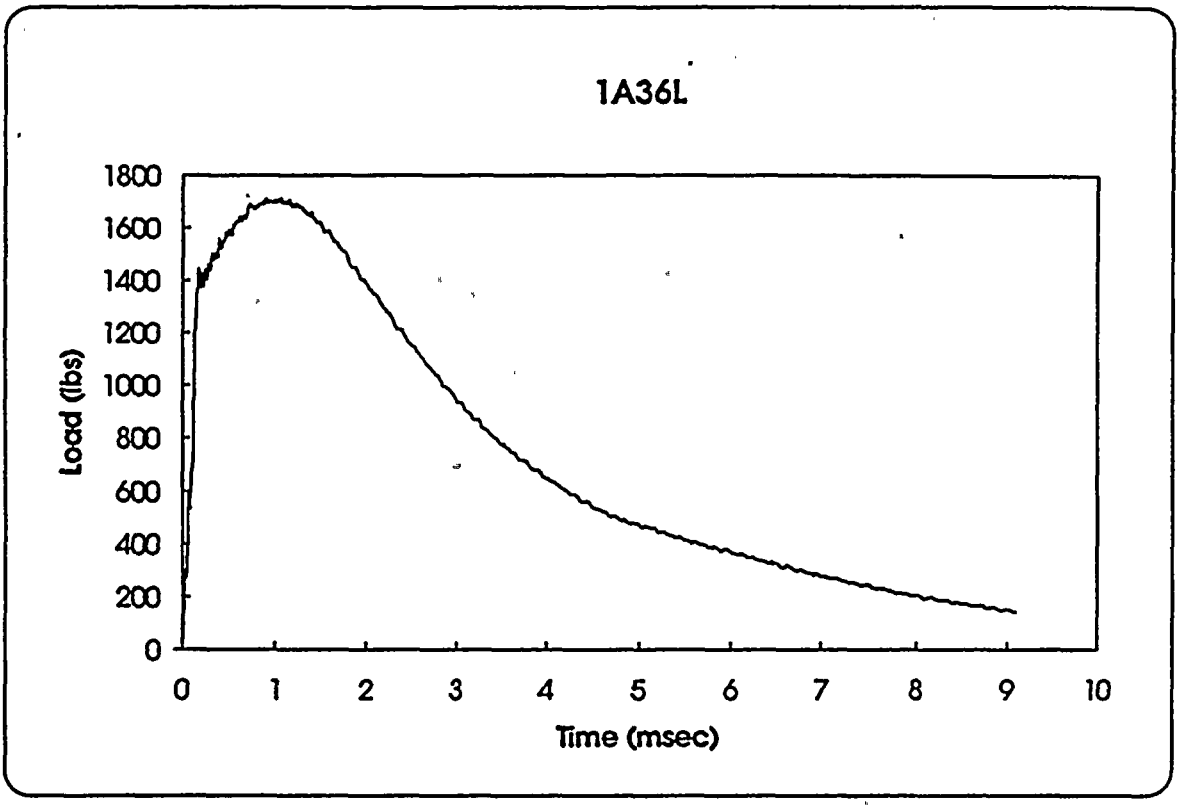

Specimen	1A36L
Temperature	200 F
Available Energy	773 in-lbs
Initial Velocity	99.8 in/sec

Time to Yield	0.180 mSec
Yield Load	1420 lbs
Time to Maximum	1.055 mSec
Maximum Load	1712 lbs
Energy at Max. Load	143.3 in-lbs

Crack Length	0.183 in
a/W	0.464
Specimen Compliance	48.7
Machine Compliance	97.2

KJD	303.7 ksi-in^1/2
Yield Stress	105.3 ksi

Figure A-58. Load-time record and data for precracked specimen 1A36L